Methodology for Enhancing Solar Energy Utilization in Solaria and Greenhouses

Diane Bastien

A Thesis
In the Department
of
Building, Civil, and Environmental Engineering

Presented in Partial Fulfillment of the Requirements
For the Degree of
Doctor of Philosophy (Building Engineering) at
Concordia University
Montréal, Québec, Canada

December 2015

CONCORDIA UNIVERSITY
SCHOOL OF GRADUATE STUDIES

This is to certify that the thesis prepared

By: Diane Bastien

Entitled: Methodology for Enhancing Solar Energy Utilization in Solaria and Greenhouses

and submitted in partial fulfillment of the requirements for the degree of

Ph.D. Building Engineering

complies with the regulations of the University and meets the accepted standards with respect to originality and quality.

Signed by the final examining committee:

Dr. G. Gouw — Chair

Dr. M. Kummert — External Examiner

Dr. M. Paraschivoiu — External to Program

Dr. H. Ge — Examiner

Dr. R. Zmeureanu — Examiner

Dr. A. Athienitis — Thesis Supervisor

Approved by

Chair of Department or Graduate Program Director

22/12/2015

Dean of Faculty

Abstract

Methodology for Enhancing Solar Energy Utilization in Solaria and Greenhouses

Diane Bastien, Ph.D.

Concordia University, 2015

Solaria and greenhouses may provide many benefits, such as collecting solar heat and providing an environment where people and plants can thrive. The aim of this work is to enhance the solar energy utilization in solaria and greenhouses by improving the design and control of their fenestration and thermal energy storage (TES) systems.

This work is focusing on two aspects: first, to maximize the solar radiation collection, and secondly, to make effective use of the collected heat by designing appropriate TES systems. These two aspects are inherently linked and must be considered together, since improving only one of them in isolation cannot satisfactorily improve the overall performance.

Designing energy efficient fenestration systems in heating dominated climates calls for a high solar transmittance and thermal resistance. However, increasing the thermal resistance generally happens to the detriment of the solar transmittance, which complicates the design process. To address this issue, a methodology has been developed, which allows the comparison of different fenestration systems (including exterior and/or interior shades) on a diagram that shows their annual net energy gains for a given façade and climate.

A new strategy for improving the control of shades has been developed, based on maximizing the total heat flow through fenestration systems. This control algorithm was shown to reduce heating requirements and improve thermal comfort. By following the proposed methodology and control method for fenestration systems, the indoor operative temperature can be significantly increased; TES systems are thus essential for reducing temperature fluctuations. The design of passive TES systems in solaria and greenhouses has been studied with two complementary modelling approaches: frequency response (FR) and finite difference (FD). The FR model is used during typical short design periods for analyzing the TES sensitivity to different design variables. The FD model is used for annual performance evaluation using real weather data for two Canadian cities and years. A methodology based on the FR model is proposed and design recommendations are provided. If was found that increasing the TES thickness from 0.1 m to 1 m can raise the minimum operative temperature by 3 to 5 °C in unheated solaria and it is recommended to select a TES with a minimal thickness of 0.2 m for reducing temperature swings.

Acknowledgement

Throughout my graduate studies at Concordia, I had the privilege to be surrounded by many exceptional persons who have made this journey not only possible, but also highly enjoyable.

I want first to thank my parents. Maman, ton amour et support inconditionnel m'ont donné une solide confiance en moi qui me permet de croire que j'ai la force d'atteindre les ambitieux objectifs qui me trottent souvent en tête. Papa, en plus de me transmettre ton intérêt pour la recherche, ton soucis des détails et ton esprit logique, tu m'a surtout appris que finalement, rien n'est compliqué quand on prends son temps.

I also want to thank my supervisor, Andreas, for trusting me and giving so much freedom in my research. I've learned so much more that what is contained in this thesis, thanks to the various conferences and workshops I had the privilege to attend. The knowledge I've gained and contacts I've made during these events are invaluable. Also, thank you for your continuing support when I had my first child and soon after moved away in Denmark; I am really grateful for your support and flexibility during these life changing events.

Having a supervisor involved in many research activities and groups obviously keeps him very busy; this is why the students team around him is highly important. When in doubt, we first start discussing with each other and very often are able to solve our problems ourselves. The students in the solar lab have always been invaluable for helping recruits to progress quickly in their research and creating a friendly atmosphere which made my experience at Concordia extremely enjoyable. To all the students who have been part of the solar lab and to our neighboring friends from the CZEBS group, thank you.

Tingting Yang, thank you for choosing us. I could truly know you only by sharing my house with you. I opened my door, and you opened your heart. I am especially grateful for the moments we shared during my pregnancy and with tiny Léo. I will never forget you, nor to put ginger in my tea when I get sick.

When stuck in a mist of confusion, I often turned out to my friend José Candanedo, a former solar lab PhD student. José, thank you so much for always being so open and available, and for your great suggestions about my chapter on thermal mass. And to my partner, Costa Kapsis, thank you for being at my sides for so many years and for loving windows and shades

as much as I do. José and Costa, you two are very gifted for teaching science and having inspiring discussions around a beer or a campfire.

A special thanks goes to Vasken Dermardiros for being in the lab setting up and carrying out my experiments while I was in Denmark. Thank you for your conscientious work and our fruitful discussions.

To late professor Paul Fazio, I am extremely grateful for the questions you've asked me and the discussions we've had. Your vision of highly performant buildings, which goes beyond low energy consumption and encompass countless issues from water management to envelop durability, has inspired hundreds of students.

To my husband, Yannick Dupont, you were right: writing a thesis is like running a marathon. And with a baby around, it's more like a relay race. Thank you for running your part. For your pep post-it. For believing in me. And for being a truly awesome father. And to little Léo, thank you for making me smile so many times per day. For being so enthusiastic about sunrises. For always looking for the moon in the sky. I love you.

Finally, I am extremely grateful for the numerous financial awards I received. Pursuing graduate studies without worrying about daily subsistence is tremendously helpful for keeping the focus on research and an intact motivation. I want to thank the Natural Sciences and Engineering Research Council of Canada (NSERC) for an Alexander Graham Bell Canada Graduate Scholarship, le Fond de recherche Nature et technologies (FQRNT) for a doctoral research scholarship, Concordia University for a Scholarship for New High-Calibre Ph.D. Student and other scholarships and the Smart Net-zero Energy Buildings strategic Research Network (SNEBRN).

Table of Contents

List of Figures

List of Tables

Nomenclature

Symbols

A_i	Area of surface i [m^2]
c_{eff}	Effective specific heat capacity [J/kg-K]
c_p	Specific heat capacity [J/kg-K]
C	Capacitance [J/K]
C_i	Indoor CO_2 concentration [kg_{CO_2}/kg_{air}]
C_g	CO_2 enrichment flux [kg_{CO_2}/m^2-s]
C_v	CO_2 exchanged by ventilation [kg_{CO_2}/m^2-s]
D	Yearly heat load [kKh]
D_h	Hydraulic diameter [m]
DHR	Diffuse horizontal radiation [W/m^2]
DNR	Direct normal radiation [W/m^2]
E	Ratio of evaporation to solar radiation
f_j	Correction factor for diffuse radiation
f_s	Solid fraction in the two-phase region at the solidus front
$f_{w,i}$	Portion of window area illuminating directly surface i [m^2]
f_x	Average absorbed beam fraction
F	Portion of floor covered by plants
F_{ij}	View factor between surface i and j
F_{ij}^d	Transfer factor
F_s	Shading factor
g	Gravitational constant [m^2/s]
g_j	Angular profile
g_s	Leaf conductance to CO_2 [kg_{air}/m^2-s]
G	CO_2 uptake by plants [kg_{CO_2}/m^2-s]
G_a	Incoming solar radiation absorbed by glazing, W/m^2
G_b	Transmitted beam solar radiation [W/m^2]
G_d	Transmitted diffuse solar radiation [W/m^2]
G_{ij}	Gebhart coefficient
GHR	Global horizontal radiation [W/m^2]
h	Effective height [m]
h_c	Convective heat transfer coefficient [W/m^2-K]
h_{ext}	Combined exterior heat transfer coefficient [W/m^2-K]
h_{int}	Combined interior heat transfer coefficient [W/m^2-K]

h_{ExtS}	Combined coefficient in ext shade/window cavity [W/m^2-K]
h_{IntS}	Combined coefficient in int shade/window cavity [W/m^2-K]
h_r	Linearized radiative coefficient [W/m^2-K]
H	Hour angle [°]
H_g	Height of glazing [m]
I	Solar intensity [W/m^2]
I_b	Incident beam solar radiation [W/m^2]
I_d	Total incident diffuse solar radiation [W/m^2]
$I_{b,ho}$	Horizontal beam solar radiation [W/m^2]
I_{dg}	Incident ground diffuse solar radiation [W/m^2]
I_{ds}	Incident sky diffuse solar radiation [W/m^2]
$I_{ds,ho}$	Horizontal sky diffuse solar radiation [W/m^2]
I_{on}	Extraterrestrial solar radiation [W/m^2]
I_{PAR}	Photosynthetically active radiation [W/m^2]
I_{sc}	Solar constant [1367 W/m^2]
$\bar{I}$	Corrected incident radiation [kWh/m^2]
j	$\sqrt{-1}$
k	Thermal conductivity [W/m-K]
K	Light extinction coefficient in the canopy [m^2_{ground}/m^2_{leaf}]
l_Ψ	Vision area perimeter [m]
L	Length, thickness or characteristic length [m]
LAR	Leaf area ratio [$m^2_{\text{leaf}}/kg_{\text{crop}}$]
m	Mass [kg]
M_{water}	Moisture removal rate [kg_{water}/s]
M_{crop}	Dry weight of the crop [kg/m^2]
n	Number of surfaces
n_{day}	Day of the year, where January 1st=1
N	Frequency number
N_{oc}	Number of occupants
Nu	Nusselt number
OP	Openness factor
P	Perimeter of the heat exchanger [m]
q	Radiative heat flux [W]
Q	Heat flux or heat source [W]
Q_f	Volumetric flow rate [m^3/s]
$\dot{Q}$	Energy [J]
$\bar{Q}$	Net energy gain (or loss) [kWh/m^2]
$\bar{Q}'_t$	Energy gain (or loss) at time t [kWh/m^2]
R_{ExtS}	Thermal resistance of exterior shade [m^{2}K/W]
R_{IntS}	Thermal resistance of interior shade [m^{2}K/W]
$R_{i,j}$	Thermal resistance beween nodes i and j [K/W]
R_r	Respiration rate [$kg_{CO_2}/kg_{crop\,CO_2}$-s]
Ra	Rayleigh number
s	Laplace transform variable, $s = \sqrt{-1}\,\omega$
S	Solar radiation transmitted and absorbed by interior surfaces [W]

$S_{b,i}$	Total beam solar radiation absorbed by surface i [W]
$S_{d,i}$	Total diffuse solar radiation absorbed by surface i [W]
SHGC_g	Solar heat gain coefficient of glazing
SHGC_{gS}	Solar heat gain coefficient of covered glazing
SHGC_w	Solar heat gain coefficient of window
SHGC_{wS}	Solar heat gain coefficient of covered window
SHGC_{igIntS}	SHGC of a i pane(s) glazing with interior shade
$\mathrm{SHGC}_{igIntExtS}$	SHGC of a i pane(s) glazing with interior and exterior shade
SHGC_{igExtS}	SHGC of i pane(s) glazing with exterior shade
t	Time [s]
t'	Time [h]
T	Temperature [K]
T_b	Balance temperature [K]
T_i	Temperature of surface i [K]
T_{in}	Interior air temperature [K]
T_{in}^*	Standard interior temperature [K]
T_{met}	Mean radiant temperature [K]
T_o	Exterior air temperature [K]
T_{op}	Operative temperature [K]
T_o^*	Standard exterior temperature [K]
T_r	Environmental temperature [K]
$T_{s,i}$	Temperature of the interior surface of the shade [K]
$T_{s,o}$	Temperature of the exterior surface of the shade [K]
$T_{w,i}$	Temperature of the innermost glazing [K]
$T_{w,o}$	Temperature of the outermost glazing [K]
T_x	Temperature at which the gross photosynthesis is maximal [K]
u_i	Conductance of surface i multiplied by its area [W/K]
U	Conductance [W/m^2-K]
U_t'	U-value of fenestration system at a time t [W/m^2-K]
U_{eff}	Effective U-value [W/m$^2-$K]
U_{ExtS}	Overall U-value of glazing with exterior shade [W/m^2-K]
U_f	Frame U-value [W/m^2-K]
U_g	Glazing U-value [W/m^2-K]
U_{gs}	Shaded glazing U-value [W/m^2-K]
U_{IntS}	Overall U-value of glazing with interior shade [W/m^2-K]
$U_{IntExtS}$	Overall U-value of glazing with int and ext shade [W/m^2-K]
U_w	Window U-value [W/m^2-K]
U_{wS}	Shaded window U-value [W/m^2-K]
$U'_{\mathrm{øh}_{ext}}$	Glazing U-value without h_{ext} [W/m^2-K]
$U'_{\mathrm{øh}_{int}}$	Glazing U-value without h_{int} [W/m^2-K]
$U'_{\mathrm{øh}_{ext}\&\mathrm{h}_{int}}$	Glazing U-value without h_{ext} and h_{int} [W/m^2-K]
v	Specific volume [m^3/kg $_{\text{dry air}}$]
v_{air}	Air velocity [m/s]
v_{mean}	Mean air velocity in a cavity [m/s]
v_w	Wind speed [m/s]

W	Humidity ratio [$\mathrm{kg_{water}/kg_{\ dry\ air}}$]
Y_s	Self admittance [W/K]
Y_t	Transfer admittance [W/K]
Z	Zenith angle [°]
Z_{in}	Inlet pressure drop factor
Z_{out}	Outlet pressure drop factor

Greek Symbols

α	Solar altitude [°]
α_{gi}	Absorptance of ith pane of glass
α_i	Absorbtance of surface i
α_s	Shade absorptance
α_{th}	Thermal diffusivity [$\mathrm{m^2/s}$]
β	Angle between a surface and the horizontal [°]
β_{th}	Thermal expansion coefficient [1/K]
δ	Declination angle
δ_P	Photosynthesis temperature response [$\mathrm{K^{-2}}$]
Δ_B	Sky brightness
ϵ	Photosynthesis efficiency [$\mathrm{kg_{CO_2}/J_{PAR}}$]
ϵ_{sky}	Sky clearness index
$\epsilon_{s,i}$	Emissivity of the interior surface of the shade
$\epsilon_{s,o}$	Emissivity of the exterior surface of the shade
$\epsilon_{w,i}$	Emissivity of the innermost glazing
$\epsilon_{w,o}$	Emissivity of the outermost glazing
ϵ_i	Emitance of surface i
γ	Solar surface azimuth [°]
γ_r	Radiative fraction
λ	Latitude [°]
λ_f	Latent heat of fusion [J/kg]
λ_{fg}	Latent heat of vaporization of water [J/kg]
Λ_{nm}	Conductance of the nm glass cavity [$\mathrm{W/m^2}$-K]
μ	Stability coefficient
η	Utilization factor
θ	Incidence angle [°]
ϕ	Solar azimuth angle [°]
Φ	$1 - e^{-K\,LAR\,M_{\mathrm{crop}}}$
ν	Kinematic viscosity [$\mathrm{m^2/s}$]
ν_r	Respiration exponent [$\mathrm{K^{-}1}$]
ω	Frequency [$\mathrm{s^{-1}}$]
ρ	Density [$\mathrm{kg/m^3}$]
ρ_i	Reflectivity of surface i
ρ_{gr}	Ground reflectivity
ρ_g	Glazing reflectivity of outer pane

ρ'_g	Glazing reflectivity of inner pane
ρ_s	Shade reflectivity of exterior surface
ρ'_s	Shade reflectivity of interior surface
ψ	Surface azimuth angle [°]
Ψ	Linear thermal transmittance, W/(mK)
σ	Stefan-Boltzmann constant [W/m^2-K^4]
τ	Transmittance
$\tau_{[Q_a - T_s]}$	Solar radiation - storage temperature time lag [h]
τ_g	Glazing transmittance
τ_s	Shade transmittance
τ_{ExtS}	Transmittance of glazing with exterior shade
τ_{IntS}	Transmittance of glazing with interior shade
$\tau_{IntExtS}$	Transmittance of glazing with interior and exterior shades
ζ	Ratio of PAR to solar radiation

Chapter 1

Introduction

1.1 Motivations

Buildings are now required to provide more services to their occupants than merely protecting them from weather conditions: they have to be energy efficient, durable, adaptable and comfortable. Buildings that produce as much energy as they consume over the course of a year, also known as Net-Zero Energy Buildings (NZEB), are becoming a medium-term objective sought by many states and organizations, like European Union Member States (EU, 2009) and the American Society of Heating, Refrigerating and Air-Conditionning Engineers (ASHRAE, 2008). One step further is the evolution towards a more holistic approach, in which the building provides the resources not only for itself, but also for its occupants (Droege et al., 2009). This is done by bringing agriculture into the built environment – so-called building-integrated agriculture. Producing food in cities can play a positive role by enhancing food security, creating urban jobs, transforming urban organic waste into useful nutrient sources and improving access to fresh food (van Vennhuizen, 2006). However, in cold countries like Canada where field cultivation is possible only a few months per year, protected cultivation structures like greenhouses are needed for year-round cultivation. Greenhouses do not only allow a near continuous production, they can also produce food using up to 10 times less water and 20 times less land area than farm fields (Vogel, 2008).

Although usually not seen as such, highly glazed spaces such as solaria are actually solar collectors which can collect useful heat with efficiencies of the same order of magnitude as solar thermal collectors (Bastien and Athienitis, 2013). In addition, greenhouses or solaria may provide other benefits: besides being used as a solar collector, they allow the cultivation

of plants and vegetables and provide an enjoyable living space for their occupants. While it is possible to design a sunspace that allows these three functions (solar collection – living space – plants production), it is not possible to fully optimize the space to fulfill these functions simultaneously because of conflictive objectives and needs. Therefore, when designing a solarium or a greenhouse, it is necessary to identify the most desired functions of the space since this will affect important decisions regarding its design and operation.

A solarium or a greenhouse and a building can both benefit from their integration by experiencing reduced heating and cooling loads than when separated. Growing food in buildings reduces transportation costs, saves energy within the building envelope and may improve the well being of building occupants (Droege et al., 2009). The addition of vegetation on otherwise dark rooftops can mitigate the urban heat island effect (Wong and Yu, 2005; Alexandri and Jones, 2007; Takebayashi and Moriyama, 2007) while greenhouses can benefit from a warmer environment by having reduced heating loads. With aging building stock, solaria/greenhouses can be retrofitted to existing buildings and increase their energy performance while providing additional space. Therefore, there are many symbiotic relationships to be exploited to the advantage of both a building and a greenhouse.

Figure 1.1: Urban rooftop greenhouse and attached solaria in the countryside

With rising energy demand, high environmental risks linked to non conventional fossil fuels, climate change and increasing interest for local vegetable production, there are plenty of reasons for integrating solaria and greenhouses to buildings. However, there is a lack of awareness about their potential benefits and how to optimize their design and the control of their systems.

This work aims to facilitate the integration of solaria and greenhouses with the built environment to help buildings reaching net-zero energy consumption. With buildings accounting for 29% of greenhouse gas emissions and 31% of total energy consumption in Canada (Nat-

ural Resources Canada, 2015), designing NZEB is an objective which will play a significant role in alleviating environmental issues related to atmospheric pollution and climate change. Integrating solaria and greenhouses to buildings can help them in achieving net-zero energy consumption by producing additional heat and/or electricity.

1.2 Problem statement

The idea of using solaria as a heat collecting device for houses dates back from the 80's when research about their potential got started. Prototypes have been built and some jurisdictions offered tax incentives for building attached solaria. However, when fossil fuels became inexpensive after the resolution of the oil crisis, enthusiasm – and support – about attached solaria vanished.

With the advent of new technologies like advanced glazings and shading devices, phase change materials, solar dehumidification and advanced climate control models, the performance of solaria and greenhouses can be significantly improved. These advances offer new opportunities, but also introduce new challenges regarding the selection of the most appropriate technologies and how to implement them efficiently.

For instance, increasing the solar radiation collection of a solarium by adopting an optimized geometry and improved glazing material without appropriate TES would quickly lead to overheating. On the other hand, many studies reported little energy savings attributed to TES (Bojic and Loveday, 1997; Aste et al., 2009; Ozel, 2014; Navarro et al., 2015); thus, improving TES systems in isolation yield little performance improvements. These two aspects – increasing solar radiation collection and improving TES systems – are the key elements tackled in this thesis for enhancing the solar energy utilization in solaria and greenhouses.

Since the type of glazing and shading devices has a significant impact on the energy consumption of greenhouses (Dieleman and Kempkes, 2006; Hemming et al., 2007; Tantau et al., 2011), the design of these elements is a critical factor. Many tools already exist to help selecting windows and their shading devices. Programs such as WINDOW (and its companion software THERM and RESFEN) (LBNL, 2014, 2005), WIS (WinDat, 2004) and ParaSol (Lund University, 2010) are stand-alone tools that calculate the solar and thermal properties of windows, which may be accompanied with some types of shading devices. There are also whole building energy simulation software with the capability of carrying detailed heat trans-

fer calculations through windows and fenestration systems like EnergyPlus (U.S. Department of Energy, 2013), TRNSYS (Klein and al., 2010) and ESP-r (ESR U, 2011).

After reviewing the existing tools, it was found that there is a need to develop a simple tool to be used at the early design stages allowing the comparison of the net energy gains of various fenestration systems, where the influence of the shades on the SHGC and U-value of the fenestration system is accounted for in the energy balance.

In addition, the type of control of movable shading devices may significantly impact the indoor conditions inside a greenhouse. While it is recognized that the use of multiple shades is an efficient way for reducing heat losses in greenhouses (Tantau et al., 2011), there is a need for a new control method to improve their performance. Calculating the heat transfer through multiple-layers fenestration systems requires detailed models characterizing the convective and radiative heat transfers. In particular, calculating the convective heat transfer in a ventilated cavity, represented by $h_{c,2}$ and $h_{c,4}$ in figure 1.2, requires detailed iterative calculations. A detailed control method for the operation of shades, based on performing an energy balance on the fenestration system, has not been reported in the scientific literature.

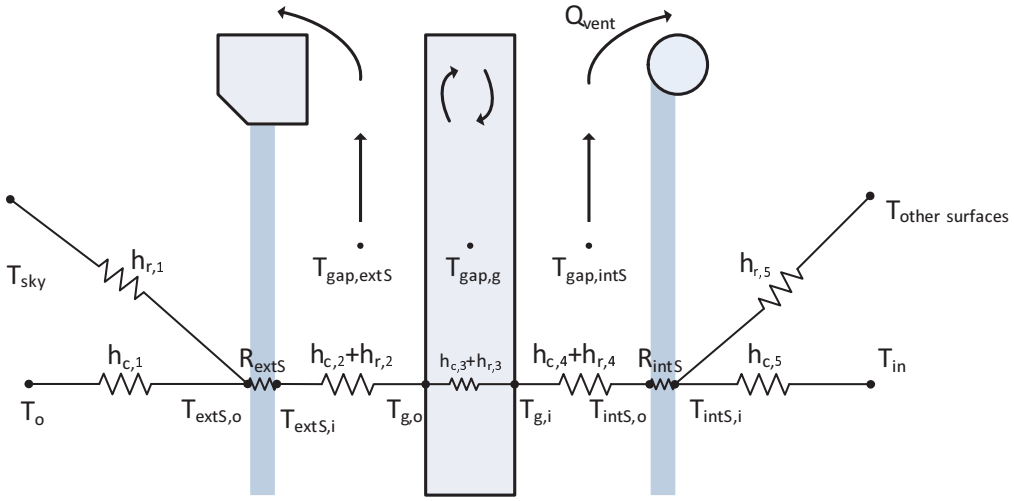

Figure 1.2: Thermal network of a fenestration system

Different design approaches have been considered for capturing solar radiation in buildings: 1) massive exterior walls; 2) Trombe walls; 3) direct-gain spaces; 4) isolated-gain spaces. Trombe walls consist of massive exterior walls where a glazing layer was introduced for reducing heat losses. Direct-gain spaces admit solar radiation directly in living spaces through windows and use interior massive elements for storing heat. Isolated-gain spaces are similar to direct-gain spaces but they are free of the requirement of maintaining thermal comfort for people at all times.

TES systems are included in buildings to answer various needs, such as reducing energy consumption, temperature fluctuations and delaying effects from peak solar gains. While recommendations have been provided to meet some design targets for some applications, for instances for reducing temperature fluctuations in direct-gain spaces, a systematic review of the possible design targets along with appropriate design metrics to analyze them is still lacking. In addition, a methodology and design recommendations for sizing TES systems specifically for isolated-gain applications such as solaria and greenhouses are needed.

The simplest configuration is depicted in figure 1.3a for an all glazed solarium/greenhouse. In this case, there are only three main nodes: T_{in} for the indoor air, T_g for the glazing and T_s for the storage mass on the floor. The heat stored in the thermal mass can be simulated by dividing the mass into control volumes and lumping the mass, or by distributing the mass equally without introducing spatial discretization (as shown in figure 1.3b); the first resolution method involves a finite difference model while the latter involves a frequency response model. The selection of a model type depends on the simulation objectives; since the two models provide valuable insight more adapted for different design stages, both modelling approaches are employed in this work.

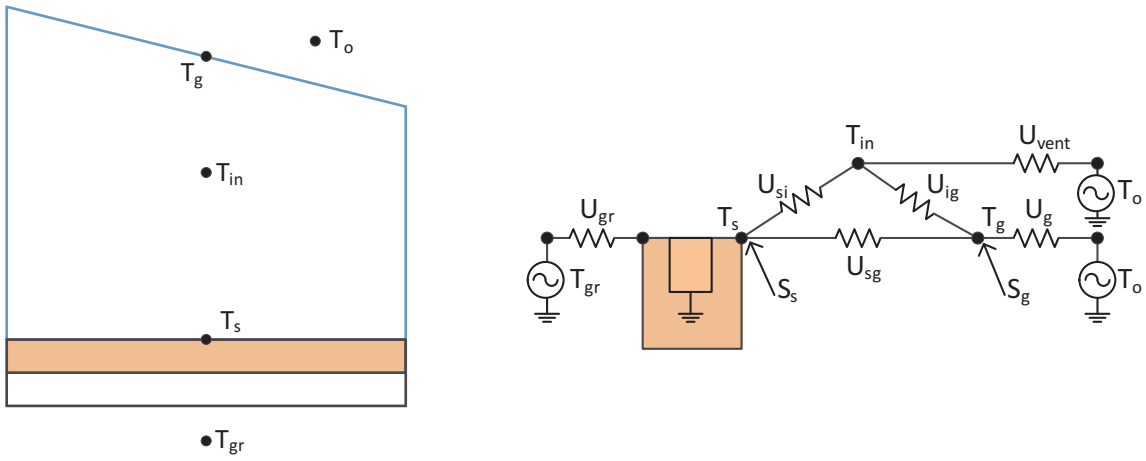

Figure 1.3: Configuration F0 and its thermal network

The most important design variables for solaria and greenhouses are the geometrical parameters and orientation, glazing and shading materials, thermal energy storage elements and auxiliary heating systems. The main variables affecting the indoor conditions in greenhouses are the air temperature, humidity, CO_2 concentration and solar radiation level. These parameters can be controlled via various systems such as heating systems, ventilation systems, dehumidification or evaporative cooling systems, artificial lights, CO_2 injection equipment

and thermal/solar screens. The state of these variables will determine crop yields, energy consumption and thermal comfort. The modification of one system element often impacts more than one variable and sometimes, modifying a system will improve some variables while adversely affecting others. It it thus necessary to have a global understanding of the various physical processes occurring in solaria and greenhouses.

1.3 Scope of thesis

This work aims to improve the performance of solaria and greenhouses by enhancing their solar energy utilization. This is best seen as a two fold process: solar radiation collection should be first maximized and then used efficiently, where TES should be used for improving the thermal conditions in the space. This thesis is focused on the design and control of glazing and shading materials along with passive TES systems. Considerations related to the integration of solaria and greenhouses in buildings are also discussed in this work, where there are many symbiotic relationships that can be optimized to the advantage of both a building and a greenhouse.

This thesis is providing guidelines to assist in the design and operation of energy efficient solaria/greenhouses. These spaces can be versatile and support different functions. Possible design targets are reviewed and suggestions for reaching them are provided. Solaria and greenhouses can be supplemented with auxiliary heat or be designed to provide satisfactorily interior conditions without any external heat; they can even collect surplus heat that can be supplied to adjacent buildings and thus become net energy providers. Conventional solaria and greenhouses, with their low insulation levels, require large amount of energy to maintain comfortable conditions. However, with careful design and efficient operation, these spaces can be converted from energy consumers to net energy providers. Indeed, the amount of solar energy received by a greenhouse exceeds by far its annual energy needs, even in a cold country like Canada.

This thesis is focused on designing solaria and greenhouses in cold climates like Canada and northern Europe and Asia. Cold climates are defined by Hutcheon and Handegord (1995) as locations having a winter design temperature of -7 °C or lower. Many recommendations are also applicable – and desirable – in more favorable climates with less severe winters. However, greenhouses in tropical climates are used for different reasons, like controlling water flows and pest management, and therefore are outside the scope of this thesis.

The aim of this work is to develop methodologies and control strategies to assist building designers for the design and control of solaria and greenhouses. Aspects specific to building-integrated solaria and greenhouses are widely discussed in this work. To be fully integrated, one must carefully consider and balance architectural, thermal, moisture and indoor air quality issues with occupant needs. Both residential and commercial scale greenhouses have a lot of potential in terms of heat and food production. With accelerated urbanization and pressing environmental issues, this work presents a lot of potential to help cities all around the world to be literally greener, more energy efficient and more sustainable while facilitating access to fresh vegetables.

1.4 Thesis overview

This introduction is followed by a broad literature review on important design and control considerations related to solaria and greenhouses. The first section is focused on the most important design variables affecting the interior conditions: the geometrical parameters and orientation, glazing and shading materials, TES systems and auxiliary heating systems. The second section reviews strategies for the control of the main variables governing the indoor climate: the indoor air temperature, relative humidity, solar radiation intensity and CO_2 concentration. A selection of greenhouse climate control models is also presented, and the concepts of closed and semi-closed greenhouses and their particular operational characteristics are introduced. The third section focuses on building-integrated solaria and greenhouses. Based on this review of the scientific literature, knowledge gaps and research opportunities are identified in the last section.

Chapter 3 presents a short study on the energy saving potential of building-integrated solaria and greenhouses. Chapter 5, 6 and 7 are using different solarium models, which varies depending on their objectives; some key common elements of the solarium models used in these chapters are presented in chapter 4. Chapter 5 presents a methodology for the design of fenestration systems, which calculates the annual performance of windows or glazings with one interior shade, one exterior shade or the combination of both. A control algorithm for improving the performance of these shading elements is presented in chapter 6. Finally, chapter 7 presents frequency domain and finite difference models for the design of TES systems in solaria and greenhouses and proposes a methodology along with design recommendations. The conclusion presented in chapter 8 summarizes the main contributions of this work and provides recommendations for future research in this field.

Appendix A presents tables for estimating the solar transmittance and absorptance of glass panes from the U-value, SHGC and gas infill of an insulated glazing unit (IGU). They can be used if this information is not available for the IGU of interest, when comparing various fenestrations systems with the methodology presented in chapter 5. The uncertainty associated with the calculation of the heat stored and released by the PCM material in the experiment presented in chapter 5 is presented in appendix B. Fundamental commonly used equations employed in the models developed in this thesis are presented in appendix C, where equations for modelling solar radiation availability and view factors are provided. Appendix D presents the thermal networks and associated energy balance equations of five solaria/greenhouses configurations, which can be used when implementing the methodology for sizing TES systems presented in chapter 7. The impact of varying glazing type and enhancing thermal coupling on the main performance parameters have been analyzed with FR models and are shown in appendix E. Detailed monthly results obtained with FD models are presented in appendix F. Finally, appendix G shows a table for estimating the absorbed beam radiation fraction by indoor surfaces for a latitude of 55°.

Chapter 2

Literature review

In desiring, through you, to point out to the London Horticultural Society, what the figure is, which will receive the greatest possible quantity of the sun's rays, at all times of the day, and at all seasons of the year, I do not presume that any of the members are ignorant of the solution of so simple a problem. [...] It must have occurred to you, that that form is to be found in the sphere [...].
Mackenzie (1815)

This chapter presents an overview of the scientific literature on important design and control considerations related to solaria and greenhouses. The first section discusses design elements that play an important role in the performance of solaria/greenhouses, such as geometrical parameters, glazing and shading materials and thermal energy storage systems. The second section covers important aspects related to the control of different systems and their impact on the main variables governing the indoor climate in greenhouses: the air temperature, relative humidity, CO_2 concentration and solar radiation level. The third section focuses on issues and opportunities of fully integrating solaria and greenhouses with buildings. The fourth and last section presents a succinct summary of the most relevant work and identify research opportunities.

2.1 Designing low energy solaria/greenhouses

2.1.1 Geometrical parameters and orientation

The geometry and orientation of a greenhouse exert a significant effect on the indoor conditions. The positioning of transparent and opaque surfaces as well as ventilation openings are important design elements that must be carefully designed. This section presents a summary of relevant studies conducted on these topics.

2.1.1.1 Solar radiation collection

Studies have been conducted as early as in the 19th century about the ideal shape a greenhouse (so-called a forcing-house or hothouse at that time) should have to receive the greatest quantity of solar radiation. In 1808, as mentioned by Knight (1808), it was known that the maximum solar transmission through glass occurs when the sun's ray fall most perpendicularly on it. From his experiments, he suggested to select a south-facing roof with an elevation of 34° under his latitude of 52°.

Reverend Wilkinson published in 1809 a rule generalizing how to determinate the best roof angle of a glass house for all climates:

«Having determined in what season, we wish to have the most powerful effects from the sun, we may construct our houses accordingly by the following rule. Make the angle contained between the back wall of the house and its roof, = to the complement of the latitude of the place, ± the sun's declination for that day on which we wish his rays to fall perpendicularly. From the vernal to the autumnal equinox, the declination is to be added, and the contrary.» Wilkinson (1809)

Mackenzie (1815) suggested a spherical shape for greenhouses as being the shape receiving the greatest quantity of rays from the sun. However, Loudon (1817) tempered his enthusiasm by noting that while it is true that the center of a sphere receives the maximum rays, points at different locations, such as the back wall or the floor, receive less radiation and such a shape induces a lack of solar radiation uniformity impinging on the crop. In addition, it was observed that young leafs were burned in spherical greenhouses due the the concavity of the glass which focused light, and that ventilation openings were insufficient – due the curvilinearity of the structure which prevents operable sashes – which caused excessive humidity (Taylor, 1995).

Many studies have analyzed the effect of the orientation on different greenhouse shapes in various locations. Studies conducted in England (Lawrence, 1963; Harnett, 1975), Japan (Kozai, 1977b), Italy (Facchini et al., 1983), Portugal (Rosa et al., 1989) and India (Gupta and Chandra, 2002) suggested/concluded that it is beneficial for greenhouses to have their longest side facing south. Harnett (1975) measured 7.4%-10.5% higher solar radiation transmission throughout the year in a east-west greenhouse compared to the same north-south oriented greenhouse, located in England. Sethi (2009) concluded that an east-west orientation should be preferred at all latitudes except near the equator because a greenhouse with this orientation receives more radiation in winter, when it is most needed.

These conclusions are consistent with passive solar design principles, which identified south façades as the most useful orientation for maximizing solar radiation transmission in winter and limiting solar penetration in summer (Butti and Perlin, 1980; Parekh et al., 1990).

An aspect ratio (the length of a building divided by its width) of 1.2 to 1.3 is often recommended for passive solar houses (Athienitis, 2007; CMHC, 1998). However, such rules of thumb are nor reported for greenhouses.

Kozai (1977b) carried simulations of single span greenhouses with different roof angles (16°, 32°, 52°) and orientations at three different latitudes. It was found that the transmissivity (i.e. the ratio of solar radiation falling onto the greenhouse glazing to the radiation falling on a horizontal plane in the greenhouse) of a east-west greenhouse in Amsterdam (latitude of 52°), Sapporo (43°) and Tokyo (35°) is higher with a roof angle of 52° at the winter solstice. However, the difference between 52° and 32° is very small for the three cities.

Kozai (1977a) also conducted simulations of multispan greenhouses of infinite length and no structural members with a ratio of the height of the side walls to the width of one span of 0.8 (roof angle of 20°). He found that the transmissivity of a north-south greenhouse was barely affected by the number of span while a est-west greenhouse is significantly affected. In Osaka, (latitude of 34°), the average transmissivity of a span is about 90% for the first two spans but it decreases smoothly to reach a constant transmissivity of about 75% from spans 5-8 (at winter solstice). However, for Amsterdam, the average transmissivity remains at about 90% for the first fourth spans but keeps decreasing until reaching about 65% at the eighth span.

Kumar et al. (1994) reported that for the same glass area, the south glass oriented at the optimum angle for a given latitude gives better thermal comfort compared to a vertical south glass or a combination of vertical and tilted glass.

Some studies found that having a reflective north wall in east-west oriented greenhouses significantly increases their transmissivity. Thomas (1978) reported that a back wall inclined at 75° increases the transmissivity the most. In addition, they noted that having a reflective north wall brings the opportunity to insulate that wall, therefore reducing heat losses. Lawand et al. (1975) judiciously noted that having a reflective north wall slope approximately equal to the maximum solar altitude at the summer solstice is ideal. Indeed, having a higher slope would not significantly enhance the amount of light reflected on the plants while having a smaller slope would decrease the amount of transmitted light in summer.

Critten (1983) conducted simulations and found that an infinitely long multispan greenhouse with a roof slope of 56° has an average transmissivity 3% higer than with a roof slope of 26° (at a latitude of 52°). He also conducted simulations of different greenhouse designs with symmetrical and vertical south roofs under diffuse and direct light (Critten, 1984). He found that under some circumstances, a double glazed greenhouse with a vertical south roof may have an 8% increase in transmissivity compared to a single glazed symmetrical roof greenhouse. He noticed that for vertical south roofs, all first reflections are directed downward, which is not the case for symmetrical roofs (as shown in figure 2.1). Double glazing a symmetrical roof induces a 9% transmissivity loss while double glazing a vertical south roof induces only a 3% transmissivity loss. In a subsequent study from the same author, he concluded that a single glazed vertical south roof multispan greenhouse transmits 5% more light than a symmetrical greenhouse during winter, and 1.5% more during summer (Critten, 1985).

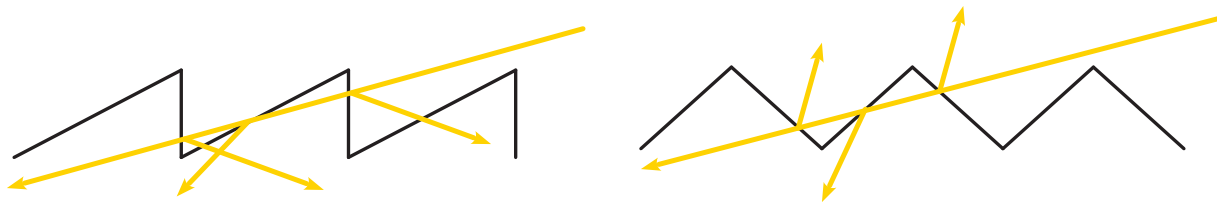

Figure 2.1: 1^{st} reflections through a vertical south roof (left) and a symmetrical roof (right)

Tiwari and Gupta (2002) studied different greenhouse shapes and their effect on thermal load levelling in winter. They classified the following greenhouse shapes in descending order in terms of thermal load levelling enhancement as: vinery, uneven span, even span, modified arc and modified IARI (Indian Agricultural Research Institute). Some typical greenhouse shapes are illustrated in Figures 2.2a-2.2f. Therefore, vinery (with roof angles of 68° and 37°) and uneven (with a roof angle of 18°) greenhouse shapes were shown to have a better performance in winter (for New Delhi, at a latitude of 28.7°).

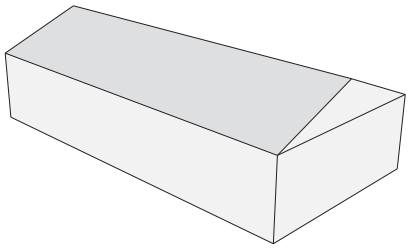

(a) Gable or evenspan greenhouse

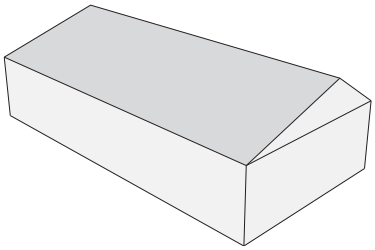

(b) Uneven greenhouse

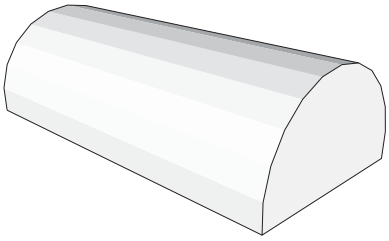

(c) Quonset greenhouse

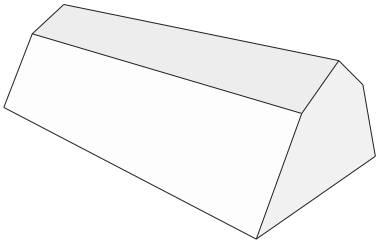

(d) Vinery greenhouse

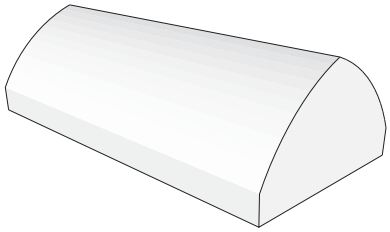

(e) Gothic arch greenhouse

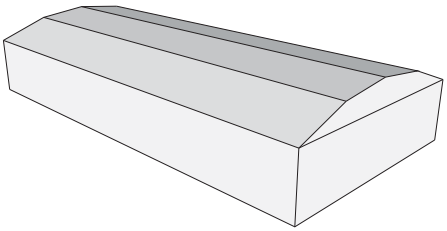

(f) Modified arch greenhouse

Figure 2.2: Common greenhouse shapes

In another study, Gupta and Chandra (2002) analyzed three different shapes of greenhouses in their simulations: quonset, gable and gothic arch. They found that a gothic arch greenhouse consumed 2.6% and 4.2% less heat than a gable and quonset greenhouse, respectively (located in northern India, latitude of 28.3°). Gupta (2004) also analyzed the effect of different greenhouse shapes on the weighted solar fraction of the north partition wall. Their results showed that the weighted solar fraction was higher for an even span shape than for uneven shape at latitudes of 13°-34°. However, although of some interest, the weighted solar fraction of the north wall is not the most appropriate variable to optimize; solar radiation incident on the floor is as useful as the radiation incident on the wall, contributing to photosynthesis when absorbed by plants and thermal load levelling when absorbed by the floor.

Malquori et al. (1993) have studied different single-span greenhouse shapes (oriented east-west) and found that a greenhouse with an asymmetrical profile with a south roof slope of

29° and a north roof slope of 34° could collect more solar radiation than the other greenhouse profiles studied (at a latitude of 43.5°).

Soriano et al. (2004) studied solar radiation transmission with scale greenhouse models in Granada, Spain (latitude of 37°). Their results for three spans greenhouses are summarized in Table 2.1. It can be seen that the greenhouse scale model with a symmetrical roof angle of 27° has the highest solar radiation transmission in winter while the greenhouse with a south roof angle of 18° and a north roof angle of 8° has a higher transmission at the equinox and in summer.

Roof angle (°)		Seasonal transmission		
South slope	North slope	Summer solstice	Equinox	Winter solstice
18	8	74.9	69.8	59.0
36	55	69.7	66.3	56.7
45	27	71.3	67.7	66.6
27	27	71.0	68.5	70.1

Table 2.1: Mean seasonal transmission for four scale models with different roof slopes (from Soriano et al. (2004))

Beshada and Zhang (2006) conducted simulations of a solar greenhouse design developed in northern China adapted to the winter conditions in Manitoba. As illustrated in figure 2.3, this type of greenhouse has an insulated north wall and roof as well as side walls. The back wall is filled with sand and a thermal blanket is manually unrolled at night. Their study pointed out that the slope of the north roof must be higher that 46°-60° at latitudes of 58°-43° to avoid shading of the north wall (by the north roof) until the end of April. Shading during summer might be considered as an asset to reduce ventilation loads. Simulations conducted for a latitude of 49° indicated that up to 35% of the north wall might be shaded by end walls in December for a 30 m long greenhouse (with an aspect ratio of 4.3). It is therefore suggested that greenhouses with insulated side walls should be as long as possible to reduce this effect.

Lawand et al. (1975) at the Brace Research Institute carried out simulations and experimentations of greenhouses in Québec and proposed a new design to improve the performance in winter by having a transparent sloped south roof and vertical walls with a reflective (and insulated) north wall (see figure 2.4). From simulations, they concluded that the range of values of tilt angles for near optimum design is 40-70° for the south wall and 60-75° for the north wall. By analyzing data obtained for a prototype greenhouse, they estimated that this green-

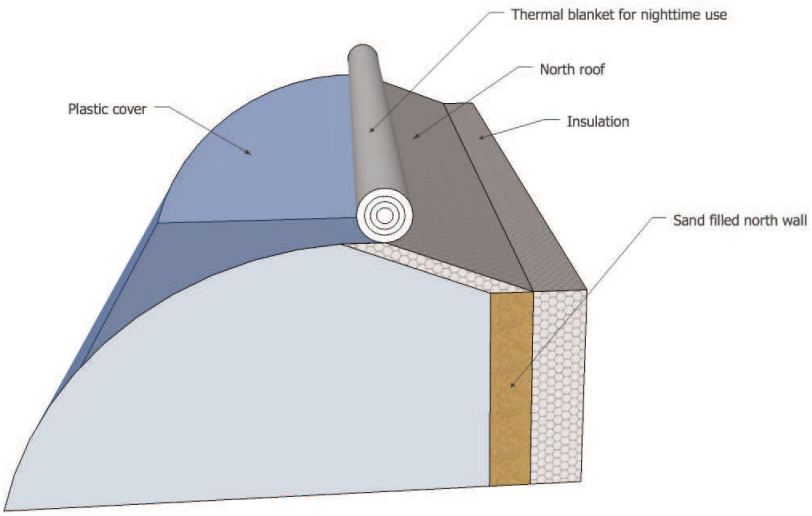

Figure 2.3: A typical chinese solar greenhouse

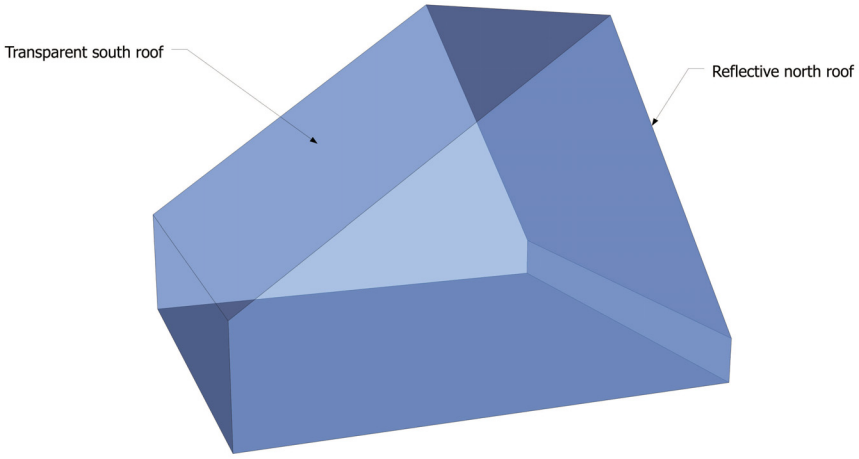

Figure 2.4: A greenhouse design developed by the Brace Research Institute

house design can lead to a 30%-40% reduction of heating requirements when compared with the most common greenhouse type (quonset shape with double polyethylene cover).

While many studies have been conducted for various types of greenhouses in different climates, some authors have noted the lack of general guidelines for optimal roof slopes (Soriano et al., 2004) and the need for a model to compare various design options (Gupta and Chandra, 2002).

2.1.1.2 Natural ventilation

Natural ventilation (and infiltration) in buildings is driven by pressure differences induced by wind and air density differences between indoor and outdoor (buoyancy, or stack effect) (ASHRAE, 2009, chapter 16). However, during warm weather, the stack effect is limited and natural ventilation depends mainly on wind forces (Bot, 1983; Zemanchik et al., 1991). Boulard and Baille (1995, Fig. 9) have shown, for a specific case, that at wind speeds of 0.5-0.7 m/s, the buoyancy and wind speed driven ventilation have about the same magnitude, but that ventilation due to wind is more than 8 times greater than buoyancy effects at a wind speed of 2 m/s. Hellickson and Walker (1983) suggested to orient the length of a building (and ventilation inlets) perpendicular to the prevailing winds to enhance natural ventilation. They also noted that it is not unusual to have prevailing winds with different directions in summer and in winter.

However, the impact of a building orientation on the natural ventilation flow may be not very significant. A study found that the average ventilation rate for a naturally vented building for the best orientation is only 13% higher than for the worst orientation (at outdoor temperatures above 20°C) (Zemanchik et al., 1991).

Ventilation flux in naturally vented greenhouses have been simulated using various theoretical and Computational Fluid Dynamics (CFD) models (Boulard and Baille, 1995; Seginer, 1997; Mistriotis et al., 1997; Boulard et al., 1999; Lee et al., 2005; Ould Khaoua et al., 2006). However, the ventilation rate depends strongly on greenhouses design characteristics like the aspect ratio and position of openings, as well as on the wind direction and intensity. Therefore, the conclusions of studies are applicable only for the specific cases investigated; generalizations are not possible (Mistriotis et al., 1997). Because of the difficulties to identify general guidelines for optimum greenhouse design for natural ventilation, this field of study is still under active development.

Greenhouses typically have ventilation openings along the longest side at the roof ridge and/or along a side wall (see figure 2.5). Bot (1983) estimated that the addition of side vents on only 10% of the side wall of a greenhouse equipped with roof vents only may increase the ventilation rate by almost 70%.

Lee et al. (2000) have shown with 2D CFD simulations that having side vents openings closer to the ground increases natural ventilation rates for a double polyethylene multi-span greenhouse. It also favors ventilation efficiency by reducing short-circuiting, i.e. air incoming by the side vents and exiting directly through the 1st roof vent without mixing. They also

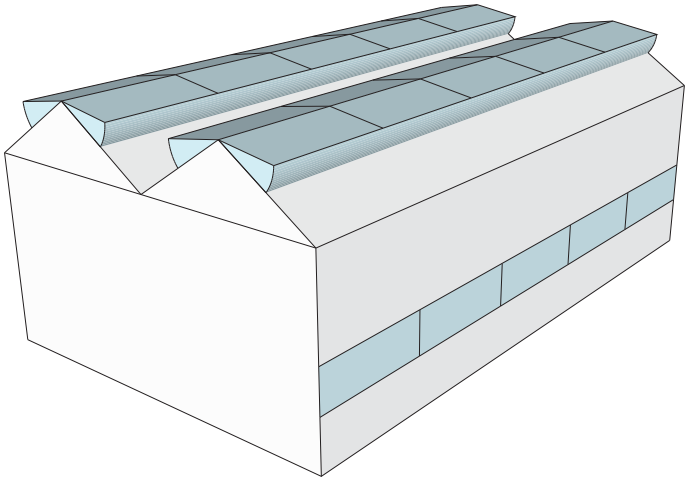

Figure 2.5: Typical ventilation openings in greenhouses with continuous roof vents and continuous side vents

found that increasing the size of the side vents can increase the ventilation rate. For instance, increasing the size of the vents from 0.9 to 2.7 m increased the ventilation rate from 12.6 to 25.8 ACH for a windward wind and from 13.8 to 18 ACH for a leeward wind, under low wind conditions (0.5 m/s).

A 3D CFD study of a twin span plastic greenhouse found that the length of a greenhouse may affect significantly the air exchange rate (Mistriotis et al., 1997). Simulation results reveal that a 32 m long greenhouse has a ventilation rate of 22.4 ACH while the same greenhouse with a length of 64 and 96 m experiences ventilation rates of 9.9 and 13.3 ACH respectively. It is mentioned that the use of internal separating wall might improve the ventilation efficiency.

A study conducted by Kacira et al. (1998) found that having windward side vents can have a significant influence on ventilation rates and airflow patterns. He observed that the closing of windward side vents can reduce the ventilation rate by 80% to 90%.

In a following study, Kacira et al. (2004) found that when neglecting buyoancy in CFD simulations, the ventilation rate increases linearly with the external wind speed for all the cases studied. The ratio of roof opening to the greenhouse floor was 9.6% in all tested cases. They found ventilation rates of 66-282 ACH at a wind speed of 3.5 m/s for 24 and 6 spans greenhouses respectively for greenhouses equipped with roof vents and fully open windward and leeward side vents while the ventilation rates were only 9.6-14.4 ACH for greenhouses equipped with roof vents only. They concluded that the opening ratio is not sufficient to ensure adequate ventilation for greenhouses with roof vents only and endorse the recommendation of having an opening ratio of 15%-25%. They found an exponential

reduction of the ventilation rate with the number of spans being increased from 6 to 24 for greenhouses with roof and side vents, while the reduction was much less pronounced for greenhouses with roof vents only.

He et al. (2015) conducted a 3D CFD study on an 11 span plastic greenhouse for analyzing the effects of varying vents openings on the interior microclimate during the summer and winter seasons. They recommend to use roof and side vents for summer cooling and roof vents only for winter dehumidification. They reported that in winter, the use of roof and side vents has the highest dehumidification potential, but also experiences the highest heat losses. The use of side vents only offers the highest dehumidification efficiency, but also provides the worst temperature and humidity homogeneity in the crop canopy, and thus suggest to use roof vents only as a good compromise between heat losses, dehumidification efficiency and microclimate homogeneity.

2.1.2 Glazing and shading materials

Many different materials can be used as greenhouse covers. Traditionally, clear glass was the only material available, but plastic materials are now widely used. Plants need solar radiation at wavelengths between 400-700 nm, which is the part of the spectrum typically called the photosynthetically active radiation (PAR) (Mccree, 1971). In cold climates, it is desirable to select materials with a high transmittance to short-wave solar radiation (0.2-3 μm) to reduce heating needs. In addition, a good greenhouse cover would ideally have a low emissivity at long-wave radiations (>3μm) and therefore a low thermal transmittance to reduce heat losses during the cold season.

This section is divided into three sub-sections which describ different greenhouse cover types: glass, rigid plastics and flexible plastic films. Typically, glass is the most durable and expensive cover material while flexible films are the least expensive and durable materials. Whereas increasing the insulation of greenhouse cover materials is indeed a good way to save energy, it also increases the relative humidity level (Bailey, 1984), and therefore humidity management becomes more important. These considerations are covered in details in section 2.2.2.

2.1.2.1 Glass

Glass is an excellent cover material that is durable, but heavy and expensive. In Germany, 90% of the total greenhouse floor area is covered by glass and 98.5% in the Netherlands, but

only 45%, 10% and 5% in France, Italy and Greece respectively (Briassoulis et al., 1997). In Canada, 34% of greenhouse floor area is covered by glass, but only 28% and 13% in the provinces of Ontario and Québec respectively (Statistics Canada, 2010). Typically, only single glass was used for greenhouses, but with rising energy prices, double glass is now sometimes being used in some countries like Germany, but still represents less than 5% of glass covered greenhouse area (Briassoulis et al., 1997). Triple glass, which is heavy and costly, is not being used in commercial greenhouses at the moment.

Table 2.2 on page 21 lists important parameters characterizing the performance of glass and plastic covers. The typical clear glass presented in this table is representative of a typical clear float glass. Low iron glass can increase the transmittance and eliminate the greenish tint of normal clear glass. Anti reflective (AR) coatings can be applied on glass to reduce the reflective component and increase the transmittance. By using these advanced technologies, manufacturers can now produce glass with a visible transmittance as high as 0.993 and solar transmittance up to 0.910 (LBNL, 2012). The three AR glass panes presented in table 2.2 are the ones with the highest visible transmittance, the highest solar transmittance and the best combination of high solar and visible transmittance available from the International Glazing Database LBNL (2012).

Low emissivity (low-e) coatings can be applied to glass to reduce radiative heat losses. These coatings can be divided into two categories: hard coatings and soft coatings. Hard coatings are based on tin oxide and use a pyrolytic process which creates a hard, durable coat. Soft coatings are usually produced in a sputtered process and have a soft finish which must be protected (Hammarberg, 2003). Only hard coatings can be used on single windows because soft coatings have to be applied on surfaces #2 or #3[1] of insulated glass units for longevity. Typically, hard low-e have a higher solar transmittance and higher emittance that soft low-e.

While the presence of a low-e coating increases the thermal resistance of a window, it also reduces its light and solar transmittance. However, applying an AR coating could reduce this effect (Rosencrantz et al., 2005). The hard low-e glass listed in table 2.2 is a typical clear glass with a pyrolytic coating. The hard low-e AR glass below is the pyrolytic low e glass with the highest visible and solar transmittance available on the market. From table 2.2, it can be seen that AR low-e single glass can offer almost the same visible transmittance as clear glass while reducing its U-value by 38%, although at the expense of a solar transmittance 10% lower. The low-e coating is on the inner pane of the glass, which gives a lower U-value

[1]Surfaces are numbered from the exterior to the interior, with the exterior surface of the exterior glass being #1, the interior surface of the exterior glass being #2, etc.

than when deposited on the outer pane, but it also reduces the temperature of the inner pane, which is even lower than for clear glass (Nijskens et al., 1984); therefore, if used in greenhouses, good humidity management is needed to avoid condensation problems.

It is possible to combine two panes of glass into a sealed unit to create an insulated glass unit (IGU). Inert gas like argon and even krypton can be used to fill the unit for reducing convection in the glass cavity and further reduce the U-value. A selection of some of the best IGU's that can be created from the best window panes available on the market are listed in table 2.2.

A study conducted in the Netherlands compared a conventional greenhouse with single glass with different greenhouse covers: single AR glass, single AR low-e glass, double AR glass and double AR low-e glass. They found that the four alternative greenhouse covers had a higher economic yield, with the single and double AR glass being the most attractive option for maximizing profit (Hemming et al., 2007).

2.1.2.2 Rigid plastics

Rigid plastics are used to cover 9% of the greenhouse area in Germany, 6% in France and less than 3% in Italy, Greece and Netherlands (Briassoulis et al., 1997). In Canada and Ontario, rigid plastics cover 7% of the total greenhouse floor area while this number rises to 9% for Québec (Statistics Canada, 2010). Rigid plastics may be used on new greenhouses or for retrofitting existing glasshouses. With their lower weight, it would be possible to remove some structural members and therefore reduce structural shading (Giacomelli and Roberts, 1993).

Polycarbonate (PC) panels are available as single layer corrugated sheet and as double or triple multilayered cross sections for improved strength and insulation. These panels are affected by UV radiation and should be protected for durability (Giacomelli and Roberts, 1993).

Acrylic or *polymethyl methacrylate* (PMMA) is better known under its commercial name, Plexiglass ®. It is available as flat or corrugated sheet and double multilayered cross sections. Its transmittance is slightly lower than glass and is characterized by a high coefficient of thermal expansion, so a careful installation is required (Papadakis et al., 2000). Acrylic panels have potential fire problems (Giacomelli and Roberts, 1993).

Polyvinyl chloride (PVC) is found in the form of corrugated sheets. Its transmittance in the PAR region is uneven: it is lower in the yellow band, but higher in the red and blue regions. This material is not totally opaque to infrared radiation (Papadakis et al., 2000).

Fiberglass reinforced polyester (FRP) panels are manufactured as rigid corrugated sheets with surface protection to reduce yellowing (like a thin Tedlar ® coating) (Papadakis et al., 2000). Like acrylic, FRP panels have potential fire problems, but are resistant to hail damage (Giacomelli and Roberts, 1993). FRP has the highest thermal transmittance from all greenhouse covers (see table 2.2).

Material	Transmittance			U-value
	Solar	PAR	Long wave	(W/m^2K)
Single glass				
Typical clear glass	84.1	89.9		5.92
AR glass 1	84.3	99.3		5.97
AR glass 2	91.0	91.6		5.92
AR glass 3	88.1	97.3		5.97
Glass - hard low-e	63.5	82.0		3.61
Glass - hard low-e - AR	74.8	88.8		3.68
Double glass				
Typical clear/x2 - Air	71.6	81.3		2.73
AR glass 3 /x2 - Argon	79.8	94.7		2.63
Typical clear/Typical low-e - Argon	63.0	76.4		1.65
AR glass 3/hard low-e - Argon	68.0	86.5		1.62
Hard low-e - AR/x2 - Argon	59.9	79.5		1.29
Rigid plastic				*Single/**Double***
Polycarbonate (PC)	77	78	3	/**3.2-3.5**
PMMA	82	86	1	/**3.0-3.4**
Rigid PVC	81	84	6	6.6/**3.3**
Fiberglass (FRP)	75-87	-	87-90	
Plastic films				
LDPE	88-89		63-65	9.0/**6.4**
PE-IR	85-86		12-28	
PVC	85-90		10-15	7.6/
EVA	90		13-25	7.8/
ETFE Cascone et al. (2005)	93-95		22-29	

Table 2.2: Important parameters for most common greenhouse coverings. Values for glass were selected from the library in Windows LBNL (2012) and optical values for rigid and flexible plastic covers are taken from Papadakis et al. (2000), unless specified otherwise. U-values of plastics materials are taken from Nijskens et al. (1984).

2.1.2.3 Plastic films

Plastic films are widely used in warm european countries: they cover 94% of greenhouse area in Greece, 87% in Italy and 49% in France, but only 1% in Germany and the Netherlands (Briassoulis et al., 1997). However, in Canada, Ontario and Québec, as much as 60%, 65% and 78% of greenhouse area is covered by plastic film respectively (Statistics Canada, 2010).

Polyethylene (PE) film is the most common greenhouse cover in the United-States. They have a lifetime of 2-4 years before being degraded by UV radiations. *Low-density polyethyelene* (LDPE) has a relatively high solar transmittance and but also the highest thermal transmittance of all cover materials (see table 2.2). It is possible to add additives to PE films to reduce thermal transmittance (Giacomelli and Roberts, 1993). These *thermal polyethylene* films (PE-IR) can bring the thermal transmittance of about 0.65 as low as 0.12 with only a small reduction of solar transmittance.

Polyvinyl chloride (PVC) films are used extensively in Japan, but their use is limited in Europe. They exhibit a high solar transmittance and a low thermal transmittance. However, their higher cost compared to PE limit their integration as well as the harmful dioxin emissions that are released when burned (Papadakis et al., 2000).

Ethylene vinyl acetate copolymer (EVA) is produced by the co-polymerization of ethylene with vinyl acetate, which reduces the thermal transmittance (Papadakis et al., 2000). It has a high solar transmittance and a relatively low thermal transmittance.

A study found that *Ethylene-tetra-fluorine-ethylene* ETFE has a significantly higher solar transmittance and lower thermal transmittance than PE and EVA, resulting in a higher mean air temperature inside a greenhouse (Cascone et al., 2005). ETFE is a very promising material, however its high cost limits its integration (Bot et al., 2005). The installation of this material is often carried out in multiple layers in combination with forced ventilation in the cavities. Such an installation requires particular care and regular maintenance to ensure the performance and air tightness of the structure is thus less adapted to small scale facilities.

Air born exposure of Bisphenol A (BPA) can occur by off-gassing of plastic products. BPA is considered as an endocrine disrupting compound which can cause adverse health effect, even at low doses. BPA is part of polycarbonate plastics and often used as an additive to other plastics such as PVC. Phthalates are also commonly used as plasticizers to impart flexibility and elasticity to polymers such as PVC. They are not monomers as BPA and are therefore more prone to leaching out of products. Phthalates can compose a major part of plastics,

sometimes up to 80% by weight. They are endocrine disrupting compounds with suspected health effects on reproductive systems. Both BPA and phthalates are commonly found in humans and even in breast milk. Other additives to plastics are also a source of concerns, like polyhalogenated flame retardants (Halden, 2010).

2.1.2.4 Shading systems

Shades can be used in greenhouses to reduce solar gains and heat losses. A shade whose main purpose is to reject near infra-red radiation (NIR) is called a solar screen while a shade whose main purpose is to allow solar heat and reduce heat losses is named a thermal screen. For both types of shades, visible and PAR radiation should not be blocked to provide daylight to occupants and plants. The ideal solar screen should therefore reject the near-infrad portion of the solar spectrum rather than the visible part. Reflection of the NIR region is preferred to absorption to reduce solar heat gains. Having a low transmittance at far-infrared wavelengths would be beneficial to reduce night heat losses (Nijskens et al., 1985).

While rejecting NIR is beneficial in summer for reducing the air temperature inside greenhouses, allowing NIR is useful for supplying heat in winter (Kempkes, 2008). Therefore, an ideal shade for the winter season would have a high solar and visible transmittance but a low thermal transmittance.

A third type of screen can also be used: a blackout screen, to be used only at night. Its thermal properties are optimized to reduce heat losses only without considering solar properties (Meyer, 2011).

The possibilities of using up to three screens is now envisioned to reduce the energy consumption of greenhouses. One shade would be a solar screen, aluminised and NIR reflective; another one would be a thermal screen, with a high PAR and solar transmittance; the third one would be a black-out screen, which should have a low U-value. Combining three screens could lead to a reduction of energy consumption of 80% (Tantau et al., 2011).

There are many different shades with different properties available on the market. Important properties of common screen materials and methods for determining screens properties can be found in Roberts et al. (1981), Nijskens et al. (1985) and Cohen and Fuchs (1999). Control strategies for the opening and closing of shades are presented in section 2.2.1.3.

2.1.2.5 Design tools for the selection of glazing and shading materials

The selection of the optimum glazing for a house or a greenhouse is a tedious task. This section discusses issues related to the design of glazing and shading elements and presents some existing tools that can be used to assist in this task. These tools have been designed primarily for the design of residential and office buildings, but could be helpful for designing solaria and greenhouses as well.

Selecting the best windows for a house is more complicated than selecting the best walls, since the performance of windows is governed by two major variables: the solar heat gain coefficient (SHGC) and the thermal resistance. In cold climates, it is desirable to have windows with both high thermal resistance and SHGC. However, these two variables usually move in opposite directions: as the thermal resistance increases, usually the SHGC decreases. In addition, windows are one the most expensive component in a house (on a unit area basis). As a result, the selection of windows is one of the the most problematic aspect of net-zero energy buildings (NZEB) (Proskiw, 2010).

Furthermore, the use of shading devices (and their operation if moveable) significantly affect the performance of windows by altering their thermal resistance and solar gains. Some tools are available to guide designers for selecting windows. RESFEN 5.0 (LBNL, 2005) calculates the heating and cooling energy use associated with windows. It also calculates cost associated with energy use and peak heating and cooling demand. RESFEN, developed by the Lawrence Berkeley National Laboratory, comes with a rather limited default set of window library, but data for other windows can be easily imported from WINDOW 6.3 (LBNL, 2014). Windows can be oriented north, east, south and west and skylights can also be simulated. However, other orientations cannot be selected. Some types of fixed shading devices, like overhangs, interior shades, exterior obstructions or a combination of these can be simulated. However, their shading capability is constant and cannot be modified nor controlled.

ParaSol (Lund University, 2010) is mainly used for the design of solar protection on windows at an early design stage. Interior, exterior and between the panes shades can be simulated simultaneously. Awnings, venetian blinds, brises-soleil, roller shades, shutters and pleated curtain can be simulated, but side fins are still not available. Default shades and windows are available in a library and it is also possible to specify custom shades and windows. Only one orientation is simulated at each run, but any orientation can be selected. The monthly solar and visible transmittance of the bare window and the window-shade system are given as outputs. It is possible to define simple controls of sunshades, based on solar radiation intensity, indoor/outdoor temperatures or a hourly schedule. Results from energy balance

calculations are the peak heating and cooling loads and annual heating and cooling demands with and without sunshades. This tool is useful for designing solar protection and visualizing its effects versus a bare window, but cannot be used to compare the performance of various windows and shades combinations for the design stage.

WIS (WinDat, 2004) is a European tool for calculating optical and thermal properties of windows and shading systems. The development of the standard ISO 15099 (2003) for calculating the thermal performance of windows was inspired by this software for calculating the solar optical properties of shading devices (Tzempelikos, 2008).

RESFEN, WINDOW, WIS and ParaSol are stand-alone tools that calculate the solar and thermal properties of windows, which may be accompanied with some types of shading devices. WINDOW and WIS are mainly used for certification purposes as they carry out simulations at fixed conditions, usually chosen to match a specific standard. RESFEN and ParaSol offer the possibility of calculating annual heating and cooling loads associated with windows. There are also whole building energy simulation software with the capability of carrying detailed heat transfer calculations through windows and fenestration systems like EnergyPlus (U.S. Department of Energy, 2013), TRNSYS (Klein and al., 2010) and ESP-r (ESR U, 2011). A more detailed description of these software can be found in Loutzenhiser et al. (2007), Tzempelikos (2008) and in Rogalsky (2011).

Nielsen et al. (2001) presented a simple method for comparing the energy performance of glazings or windows for heating dominated buildings. The net energy gain is calculated for the heating season and is equal to the solar gains minus the heat losses through the glazing. Following this method, diagrams presenting the net energy gain for different combinations of SHGC and U-values are generated for a specific orientation. Such diagrams allow a designer to quickly visualize what is the best window for a given orientation, which is needed at the design stage. Heat gains can be reduced by employing a shading coefficient to represent overhangs or obstructions, but only a fixed value for the year can be simulated and the thermal effects of including different shading devices are not accounted for.

Upon review of the existing tools, it is observed that none has been designed to perform comparisons of different window/shade systems specifically for the design stage. There is a need to develop a tool allowing the visualization of the energy performance of different window/shade combinations that takes into account the effects of a shade on the overall solar and thermal transmission of the fenestration system.

2.1.3 Thermal energy storage

Thermal energy storage (TES) is particularly needed for intermittent energy sources such as solar energy. Diurnal storage accumulates heat during the day and releases it at night, following a 24 hour cycle, while seasonal storage accumulates solar heat during summer months to provide heating during winter months, following a yearly cycle (Hadorn, 2005). Short term storage (less than a week) is the most common type. Abundant surplus heat is available in the summer but seasonal storage is limited due to economic factors (Kaygusuz, 1999).

TES are usually classified by the process which is involved in storing heat: sensible heat storage materials accumulate heat by changing temperature, latent heat storage materials accumulate heat by changing phase (Kaygusuz, 1999) and thermochemical heat storage materials accumulate heat by physico-chemical process (like adsorption or absorption) (Hadorn, 2005).

Important criteria for TES materials are (Hadorn, 2005):

- Capacity and density
- Loading and unloading rate
- Efficiency of thermal storage ($E_{\text{out}}/E_{\text{in}}$)
- Stability (mechanical, chemical)
- Reversability during a number of cycles
- Cost
- Toxicity
- Recyclability assessed through a life cycle analysis

The following sub-sections present the most commonly used materials for TES, strategies for sizing TES and examples of greenhouses with TES systems.

2.1.3.1 Materials

The most common type of thermal storage consists of *sensible heat storage*, where heat is stored by raising the temperature of the storage medium. The heat stored in a medium can be calculated from

$$Q = mc_p\Delta T \tag{2.1}$$

where m is the mass of the storage, c_p is the specific heat capacity and ΔT is the temperature difference of the storage medium. It is therefore desirable to use a material with a high specific heat capacity to enhance storage capacity. Having a high density is also desirable as a denser material would reduce the volume needed to store heat. Water is an excellent medium because it has the highest heat capacity (4.19 kJ/kg-°C) of the commonly used TES materials (ASHRAE, 2007), is inexpensive and widely available (Hasnain, 1998). In addition, stratification can be easily achieved in water tanks, which is desirable because a higher water temperature can be obtained and the efficiency of solar thermal systems is enhanced compared with fully mixed water tanks. However, water may be expensive to contain and is prone to leakage, which may limit its use in greenhouses. In contrast, the soil under a greenhouse has a large thermal mass and is readily available and inexpensive (Gauthier et al., 1997). Extensive numerical and experimental studies have been conducted about the use of soil heat exchangers in greenhouses; an overview is presented in section 2.1.3.3. Table 2.3 lists the specific heat capacity, density and the volume required to store 1850 kWh (with a ΔT of 70°C) for different sensible heat storage medium.

Material	Specific heat capacity [J/(kg°C)]	Density [kg/m^3]	Volume of material to store 1850 kWh with ΔT=70°C
Water	4190	1000	23
Concrete	1130	2400	35
Earth (dry)	800	1300	91
Earth (wet)	2000	1700	28
Cast iron	452	7900	27

Table 2.3: Physical properties of different TES materials, from Hadorn (2005).

Latent heat storage is accumulating (or releasing) heat during the phase change occurring at the phase transition temperature. The latent heat for a given mass of substance is given by

$$Q = m\lambda_f \tag{2.2}$$

where λ_f is the latent of fusion. One kilogram of water, for example, absorbs 80 times more energy when melting than by raising its temperature of 1 °C. This means that a smaller weight and volume of material is needed to store the same quantity of heat. Mainly solid-liquid phase change materials (PCM) are typically used, because liquid-gas PCM would undergo large volume transformations and therefore would not be practical (Hasnain, 1998). Heat is absorbed during the melting process whereas it is released during crystallization. Water/ice, salt hydrates, paraffin wax and some polymers are the most commonly used PCM. A good

PCM should have an appropriate phase change temperature, a high latent heat, should be inexpensive, non toxic and non flammable and have a long durability under repeated phase change (Kaygusuz, 1999). Table 2.4 list some PCM and their relevant properties. For a complete list of all PCM commercially available, one may refer to the IAE Annex 17 (IEA, 2005).

PCM name	Type	$T_{melting}$ [°C]	Latent heat [kJ/kg]
RUBITHERM ® RT 100	Latent heat paraffin	99	168
PCM 80	Erythritol/Trimethyrole-thane/ Trimethyrolpropane	80	231
TH 58	Salt Hydrate	58	226
ClimSel C 32	Salt Hydrate	32	302
RUBITHERM® PX 27	Latent heat powder	28	112
TH 25	Salt Hydrate	25	159
A22	-	22	220
ClimSel C 15	-	15	130
SN03	Salt Solution	-3	328
STL-21	Salt Solution	-21	240

Table 2.4: Physical properties of selected PCMs, from IEA (2005).

Heat transfer in PCM is usually modeled using finite difference or finite elements methods. The phase change occurring in a material has to be modeled separately because of the non linearity of the phenomenon. The two most common modeling methods are the enthalpy method and the effective heat capacity method (Lamberg et al., 2004).

The enthalpy method simulates the heat released by the PCM during freezing as a volumetric heat generation term:

$$q = \rho \lambda_f \frac{df_s}{dt} \tag{2.3}$$

where f_s is the solid fraction in the two-phase region at the solidus front. The unidimensional heat diffusion through a wall is described by the heat diffusion equation:

$$\rho c \frac{\partial T(x,t)}{\partial t} = k \frac{\partial^2 T(x,t)}{\partial x^2} + q \tag{2.4}$$

This mathematical model has shown relatively good agreement with experimental results (Athienitis et al., 1997; Lamberg et al., 2004). The effective heat capacity method allows the modeling of non-isothermal phase change in PCMs, which is frequently observed in reality. The effective heat capacity is calculated as

$$c_{\text{eff}} = \frac{\lambda_f}{T_2 - T_1} + c_p \tag{2.5}$$

where T_1 is the temperature where melting (or solidification) begins and T_2 is the temperature at which the material is totally melted (or solidified). The effective heat capacity can be calculated separately for melting and freezing processes. The energy balance equation with initial and boundary conditions can be found in Lamberg et al. (2004). After comparing numerical models with experiments, they concluded that the effective heat capacity method with a narrow temperature range ($\Delta T = 2°\text{C}$) is the most precise method.

Hed and Bellander (2006) presented a mathematical model of a PCM air heat exchanger. They defined a fictive convective heat transfer coefficient as

$$h_c^* = \frac{v_{air}\, A\, \rho\, c_p (1 - e^{\frac{P\, U\, L}{v_{air}\, A\, \rho\, c_p}})}{P\, L} \tag{2.6}$$

where A, P and L are the area, perimeter and length of the heat exchanger and U is the heat transfer coefficient between the middle of PCM and the air. The advantage of this method lies in the fact that this fictive heat transfer coefficient can be easily integrated within existing building energy simulation software.

2.1.3.2 Thermal storage sizing strategies

One existing method for sizing TES systems is based on the thermal admittance of a multilayered wall (Athienitis, 1994). The the self and transfer admittance of a wall are transfer functions particularly useful to analyze the effects of cyclic varying conditions (like solar radiation and temperature) under steady periodic conditions. In solaria and greenhouses, internal heat storage elements are absorbing and releasing heat from the same surface. In this case, we are mainly interested in the self-admittance, which relates the effect of a heat source at one surface to the temperature of the same surface. The self-admittance Y_s is given by the ratio of the heat flow at the interior surface divided by the temperature of that same surface

$$Y_s = \frac{Q_{inside}}{T_{inside}} \tag{2.7}$$

For a wall section made of an insulating and a thermally massive layer, as depicted in figure 2.6, the self-admittance is calculated with

$$Y_s = \frac{A\big[U + k\gamma_n tanh(\gamma_n L)\big]}{\frac{U}{k\gamma_n} tanh(\gamma_n L) + 1} \tag{2.8}$$

where A is the wall area, U is the conductance of the insulation layer, k is the thermal conductivity of the massive layer and L is the thickness of the massive layer. The thermal diffusivity of the massive layer α_{th} and the penetration depth γ_n are is given by

$$\alpha_{th} = \sqrt{\frac{k}{\rho c_p}} \tag{2.9}$$

$$\gamma_n = \sqrt{\frac{j\omega_n}{\alpha_{th}}} \tag{2.10}$$

where $j = \sqrt{-1}$, ω_n is the frequency and the index n represents the number of frequencies.

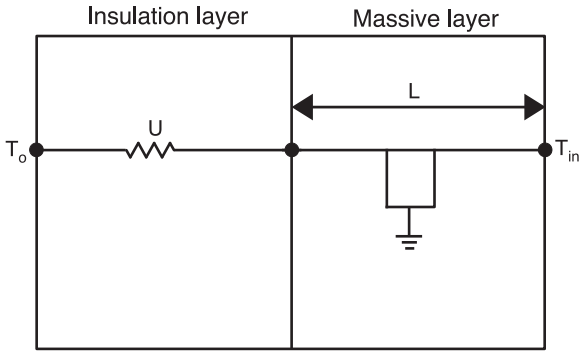

Figure 2.6: Cross section of a wall with an inner massive layer and outer insulation layer

Analyzing the self-admittance as a function of thickness for a 24 h cycle can be useful for reducing temperature fluctuations inside a room due to solar radiation. For instance, concrete has a maximum self-admittance at thickness of about 20 cm (Athienitis, 1994). However, the self-admittance remains high for thicknesses greater than 15 cm, so there is a wide range of thicknesses offering good thermal performance. Similarly, another analysis reported that the daily penetration of solar heat is limited to 14 cm for concrete Hadorn (2005).

2.1.3.3 Thermal storage in greenhouses

Santamouris et al. (1994b) published a review of heat storage systems used in 95 greenhouses around the world. Five categories of heat storage mediums are reviewed: water, latent heat materials, rock beds, buried pipes and other types of systems. Santamouris (1993) also conducted a review of 53 greenhouses using different types of solar collectors and thermal storage. He noted that there is no standard procedures for designing thermal storage systems and that special attention should be given to the selection of the storage volume and capacity.

A more recent review of heating systems for greenhouses has been carried out by Sethi and Sharma (2008). This review covers water storage systems, rock beds, PCM, earth-to-air heat exchangers (EAHE) and north walls. Correlations of storage volume of different storage media for a given greenhouse area and cover type have been generated from the collected information. The authors are suggesting that these correlations can be used at an early design stage to provide an approximate value of the required storage volume.

As mentioned is section 2.1.1, it was observed that greenhouses are more efficient when having their longest side facing south. For a fully glazed greenhouse with a south orientation, radiation entering from the south side can exit the greenhouse through the north side. This effect can have a large impact especially for narrow greenhouses. Having an opaque north wall enhances solar radiation collection in a greenhouse and can reduce heat losses if well insulated. Some studies suggested to make this wall reflective (Thomas, 1978; Lawand et al., 1975), while others promoted the idea of using this location for passive thermal storage (Tiwari et al., 1988; Singh and Tiwari, 2000; Beshada and Zhang, 2006). It was shown that having thermal storage on the north wall can significantly increase thermal load levelling (Tiwari et al., 1988). A review of the use of north walls for absorption or reflection of solar radiation revealed a 1-10°C air temperature increase and a 35-82% heating needs reduction (Sethi and Sharma, 2008).

China has a long tradition of local cultivation using so-called chinese solar greenhouses (CSG). These greenhouses have all adopted a similar design, which includes a plastic film covering the slanted south roof, a thermal blanket deployed at night and a thermally massive north wall. The exposed soil on the ground also contributes to thermal load leveling, although uninsulated. The north walls in CSG are usually made of bricks or earth; brick walls are generally 0.4-0.8 m thick while earth walls can be as thick as 5.5 m (Tong et al., 2013).

In a review of EAHE systems installed in greenhouses, reported energy savings of 28% to 62% and air temperature increase of 3-10°C have been reported. Pipes are usually made of plastic but aluminum and concrete have also been tested. Typically one or two rows of pipes are placed 0.4-2.1 m below the ground (Sethi and Sharma, 2008).

A brief overview of previous mathematical models of EAHE and their limitations is presented by Gauthier et al. (1997). They presented a new model with the capability to predict transient three dimensional heat transfer. The model can simulate non homogenous soil properties, concrete foundation and insulation as well as condensation and evaporation in the pipes. This model is then used to conduct a parametric study on the design and control of EAHE. Their results revealed that adding perimeter and under slab insulation increased the energy recovery ratio from 0.66 to 0.92.

Kurata and Takakura (1991) conducted simulations to evaluate the performance of underground seasonal thermal storage in greenhouses. They compared the same greenhouse operated in seasonal storage mode (with water-based solar thermal collectors used to charge the TES and air ducts for heat extraction) and in daily mode (with air ducts for charging/discharging the TES only). They found that the energy used for circulating air and pumping water was more then the heating energy saved when the underground TES was used in seasonal storage mode, while that the net energy savings were positive when the TES was used in daily storage mode. It should be noted that the soil under the greenhouse used for storing heat was not insulated and the energy required for operating pumps was very high.

A review of greenhouses using PCM for energy storage has been conducted by Kurklu (1998). The most commonly used PCM are $CaCl_2{\cdot}6H_2O$, $Na_2SO_2{\cdot}10H_2O$, PEG and paraffins. The amount of PCM used varied greatly from 4.8 kg/m^2 to 83 kg/m^2. Energy savings from 30% to 80% were reported. All studies under review suggested that PCM can be efficiently used for energy storage and humidity control in greenhouses.

A study conducted by Öztürk (2005) focused on characterizing the energy and exergy efficiencies of a seasonal latent heat storage system for an experimental 180 m^2 greenhouse in Turkey. They studied paraffin (with melting temperatures of 45°- 60°) coupled to a 27 m^2 solar thermal collector array. The greenhouse was filled with 6000 kg of paraffin, an equivalent of 33.33 kg/m^2. They obtained an average net energy efficiency of 40% and an average net exergy efficiency of 4%. They concluded that exergy analysis should be used to design thermal energy storage systems with high thermodynamic efficiencies.

2.1.4 Auxiliary heating systems

Even with a good passive solar design, auxiliary heating might be needed, especially if commercial crops are to be grown. In Canada, the total greenhouse operating expenses in 2010 reached 2.1 billions, from which 14% was spent for electricity, natural gas, heating oil and other fuels. Natural gas heating is the most common option in Canada and represents 61% of all expenses for heating fuels and electricity (Statistics Canada, 2010).

Some innovative and sustainable heating systems/strategies have been designed and implemented in greenhouses; the most promising options are briefly described in this section.

Introducing animals in greenhouses may be beneficial by adding sensible (and latent) heat into the system. Heat production from animals is between 1.5-21 W/kg, the former being

representative of the lower limit for dairy cows and the latter of the higher limit for young chickens (ASHRAE, 2009, chapter 10). However, indoor air quality must be monitored and noxious gas emitted by animals and their wastes, like ammonia (NH_3) and hydrogen sulfide (H_2S), must be controlled (FAO, 1994).

Additional heat can be obtained by mixing animal manure with plant waste in a tank to produce methane and heat. The methane can be used for heating or cooking in small facilities or for generating electricity in larger facilities. Such a system provides sound waste management, improves indoor air quality (by reducing toxic gases), and produces a high quality fertilizer which results from the fermentation process (FAO, 1994). Kostov (1995) observed a 48-79% yield increase of cucumber production by using composting waste as growing media compared to a control mixture. It is suggested that this effect is due to a higher nutrient content and temperature of the compost media as well from CO_2 emissions resulting from the decomposition process.

Hong et al. (1997) have composted manure with rice hulls in a greenhouse where tomatoes were grown in soil beds. The beds were located in rows surrounded by composting material and were therefore heated by direct heat transfer through the soil. The soil beds temperature was maintained between 17.5-32.5 °C while outside underground temperature was between 6-11.9 °C. The resulting composted product took 42 days to reach maturity and was suitable for use as an organic fertilizer.

Wood biomass is a renewable source that is considered carbon neutral, since the greenhouse gas (GHG) released during combustion has been absorbed from the atmosphere during growth. Therefore, no additional GHG are released into the atmosphere during their combustion (when neglecting the energy required for transportation and transformation of the biomass). According to Chau et al. (2009), the installation of a wood pellet boiler in a greenhouse to supply up to 60% of the total heat demand is economical for average or large greenhouses (7.5-15 ha) in Canada. As flue gas from natural gas boilers is often injected inside greenhouses for CO_2 enrichment (to enhance crop growth), the authors assumed that displacing 100% of natural gas with wood pellets would require buying liquid CO_2 for enrichment, which may not be economically feasible. However, many methods for CO_2 recovery from the exhaust gas of biomass heating systems exist. Dion et al. (2011) published a review of these methods for safe CO_2 enrichment in greenhouses. While they concluded that future research is needed to optimize safe and clean CO_2 enrichment from biomass heating systems, they pointed out that improving biomass boiler efficiency, using scrubbers to clean NO_x and SO_x and using membrane separation techniques to prevent fine particles are viable techniques for reducing the overall carbon footprint of greenhouse plant production.

2.1.5 Greenhouse design optimization

A research team in the Netherlands developed a model for optimizing greenhouse design for a broad range of climatic conditions (Vanthoor et al., 2012). Their model performs a modified controlled random search using parallel computing for maximizing the Net Financial Return (NFR) for growing tomatoes. This design method selects the best alternative for maximizing the NFR for eight design elements: 1) the type of greenhouse structure; 2) the cover material; 3) the type of exterior shading screen; 4) the whitewash type; 5) the type of interior shading screen; 6) the type and capacity of the heating system; 7) the type and capacity of the cooling system; 8) the type and capacity of CO_2 enrichment (the term whitewash is defined in section 2.2.1.3). Each design element is represented by an array of discrete options ranging from 3 to 12. Most design element arrays were composed of a fairly limited range of options; for instance, the cover material design element consisted only of a single polyethylene (PE) film, double PE film and single glass. Their optimization algorithm was applied to design a greenhouse in two locations: Spain and the Netherlands. The effects of including thermal energy storage systems in greenhouses are not considered in their model.

2.2 Efficient operation of solaria/greenhouses

Equally important as a good design, efficient operation of greenhouses and solaria is essential to achieve low energy consumption and good thermal comfort. Control considerations may be rather different for a small solarium than for a large greenhouse; nevertheless, they are based on the same physical processes which govern temperature, humidity, CO_2 and solar radiation variations. In particular, the ventilation strategy, heating set point and shade operation have a significant impact on the indoor conditions and heating consumption. This section presents a selection of relevant work concerning the efficient control of temperature, humidity, CO_2 concentration and solar radiation.

2.2.1 Temperature control

2.2.1.1 Temperature set points

According to Kesik and Simpson (2002), a conditioned solarium is subjected to more heat gains and losses than a house and therefore requires more heating and cooling energy (per floor area). In other words, a house provides more energy efficient habitable space that a

solarium, regardless of its orientation or insulation level. This is of paramount importance when designing attached solaria; even with an energy efficient design, a solarium should not be conditioned like a house if a low energy consumption is an important design objective. In this case, temperature fluctuations wider than in a normally conditioned building must be accepted.

When auxiliary heating systems are used, many operating strategies can be employed for reducing their energy consumption. In most cases, requirements for optimum plants environment and minimum energy use are contradictory (Garzoli, 1989). Yet it is essential for an energy efficient climate control to allow temperature fluctuations within a certain range and create fluent set-points transitions (Dieleman and Hemming, 2011). In the long term, it would be possible to breed low temperature tolerant crops, but in the short term temperature integration is a more appropriate option (Bakker et al., 2008). As another alternative, Tantau et al. (2011) suggested to select a cropping sequence with wintertime crops that have lower temperature requirements to reduce the heating energy consumption of greenhouses.

The concept of *temperature integration* is based on the ability of plants to tolerate temperature deviations from an average set point. With the typical set points for heating and ventilation that lie between a narrow bandwidth of 1-2 °C, heating and ventilation may alternate many times per day, leading to high energy consumption (Körner and Challa, 2003). When temperature integration is applied, temperatures are allowed to fluctuate within a certain bandwidth over a predefined time period during which the average temperature must respect a chosen set point. This strategy may lead to energy savings of 3% for a bandwidth of 2 °C and to 13% at a bandwidth of 10 °C without impairing crop growth (Dieleman and Hemming, 2011). The most common temperature integration strategy employed is to use a higher set point for ventilation to increase heating due to solar gains and to compensate by selecting a lower set point at night or on cloudy days, which may yield energy savings of up to 16% (Bakker et al., 2008).

According to Garzoli (1989), temperature stratification is a major problem in greenhouses. To alleviate this problem, he suggested to supply heat directly to the roots of plants which would allow to reduce the air temperature by 4 °C or 5 °C.

2.2.1.2 Ventilation

Greenhouses are usually ventilated to prevent high temperatures and humidity levels (Seginer, 1997), as well as to avoid carbon dioxide depletion (Garzoli, 1989). This section is treating

ventilation-related aspects for temperature control, while ventilation for humidity and carbon dioxide control is treated in sections 2.2.2.1 and 2.2.3.1

Evaporative cooling may be employed when the outside temperature exceeds the maximum desired temperature inside the greenhouse. Evaporative cooling reduces the temperature of incoming outside air by increasing its humidity content. Both natural and forced ventilation is common in greenhouses, but if evaporative cooling is to be employed, forced ventilation systems are necessary. Desired ventilation rates for summer conditions are about 45-60 air changes per hour to provide adequate temperatures for proper plant growth. Reducing the solar radiation entering in greenhouses, by applying white paint on the glazing for instance, lowers the ventilation rate needed for temperature control. In addition, a fully cropped greenhouse has reduced ventilation needs for temperature control than an uncropped greenhouse because of the evapotranspiration of plants, which acts as evaporative cooling (Hellickson and Walker, 1983). Design strategies to achieve good natural ventilation are summarized in section 2.1.1.2.

A simple equation can be used to roughly estimate the ventilation rate needed to maintain a specific air temperature inside a greenhouse (Hellickson and Walker, 1983)

$$\tau I A_f (1 - E) = (T_{in} - T_o)\big(U A_g + \frac{Q_f}{v} c_p\big) \tag{2.11}$$

where τ is the transmittance of the glazing, I is the solar intensity on a horizontal surface, A_f is the floor area, E is the ratio of evaporation to solar radiation (a value of 0.5 is recommended), U is the heat transmission coefficient, T_{in} and T_o are the indoor and outdoor temperatures, Q_f is the ventilation air flow, v is the specific volume of indoor air and c_p is the specific heat of dry air.

For an indoor temperature of 20 °C and a relative humidity of 70%, the specific volume is 0.844 $m^3/kg_{\text{ dry air}}$. As an example, a greenhouse with floor and glass areas of 1000 m^2 and 1600 m^2 and a volume of 3000 m^3 is considered, which is subjected to a solar radiation of 600 W/m^2 with no infiltration. Inserting these values into equation 2.11 yields

$$0.84 \cdot 600 \cdot 1000(1 - 0.5) = (20 - T_o)(6.3 \cdot 1600 + \frac{Q_f}{0.844} 1000) \tag{2.12}$$

The relationship between the outdoor temperature and the required ventilation rate to maintain 20 °C inside a single and double glazed greenhouse is depicted in figure 2.7 (with U values of 6 and 2.8 W/°C-m^2 and transmittance values of 0.84 and 0.71 respectively). It can be seen that a single glazed greenhouse with no ventilation nor infiltration would require heating

at temperatures below -6 °C while a double glazed greenhouse would require heating only at temperatures below -27 °C. At one ACH, a single glazed greenhouse would need heating below -4 °C and a double glazed greenhouse below -19 °C. This analysis shows that even on cold bright days in the middle of winter, a greenhouse may need ventilation to prevent high temperature (Hellickson and Walker, 1983).

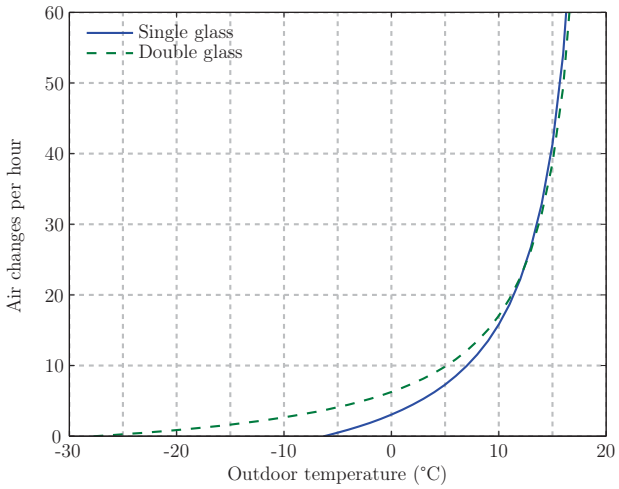

Figure 2.7: Ventilation rate for maintaining inside greenhouse air temperature at 20 °C

As seen in section 2.1.1.2, achieving natural ventilation rates of 45-60 ACH for temperature control in summer is not always possible, especially at low wind speed. In addition, such high ventilation rates are not always desirable, especially when the outdoor relative humidity is low, because it would induce a low relative humidity inside the greenhouse which could lead to increased evapotranspiration and water stress (Perdigones et al., 2008) (c.f. section 2.2.2). Solar shading materials can be used to reduce solar heat gains and therefore the ventilation rate needed for temperature control.

2.2.1.3 Shading system

The solar radiation entering a greenhouse can be reduced by using shading compounds sprayed on the glass or by using screening or shade materials. A description of different shading types based on their main function is presented in section 2.1.2.4. Plants need solar radiation between 400-700 nm, the photosythetically active radiation (PAR), as well as some near infrared (NIR) radiation, 700-1000 nm, for morphogenesis (Kittas et al., 1999). Too much PAR is not an issue for most plants, except for shade loving plants (Kempkes, 2008). As noted by Nijskens et al. (1985), the ideal solar screen should have a high visible transmittance and a high infrared reflectance. A low far infrared transmittance would also be

beneficial so that it can also be used as a thermal screen at night. The measurement of the radiation properties of twelve shading materials revealed that all of them tend to reduce the solar radiation the most in the visible range instead of the infrared. On the other hand, the majority of shades showed a far infrared transmittance below 15%, indicating their suitability to be used as night thermal screen (Nijskens et al., 1985).

The application of white paint on glass, often called whitewash, may provide about 35% shading and does not interfere with ventilation like shading nets which negatively affect the performance of natural ventilation (Kittas et al., 1999). However, it reduces the transmitted PAR as well as NIR and it is applied seasonally. As a result, once applied, it always reduces the PAR, even on overcast days where it would be needed for plants growth. The application of the whitewash must be adapted to the outdoor weather and the optimal timing for application and removal is not easy to identify (Kempkes, 2008).

Screens can be installed inside or outside greenhouses. Outdoor screens are more efficient for reducing solar gains and do not interfere as much with natural ventilation. However, they need a heavy permanent structure and are more susceptible to be damaged by weather conditions (Kempkes, 2008). Hemming et al. (2006a) pointed out that NIR filtering multilayer coating can be applied to glass and plastic covers, but that this is not desirable in the winter period in most climatic regions. They estimate that NIR filtering moveable screens could be an alternative in the future, but that adequate NIR filtering materials are still not available.

Moveable solar shades are typically controlled to be activated when the indoor temperature and/or solar radiation exceed a certain level. Lorenzo et al. (2003, 2004) have been activating an external shade (with 49% light transmittance) when the air greenhouse temperature reached 27-29 °C and when outside global solar radiation exceeded 650-800 W/m^2. With these set points, the global radiation incident on the crop was reduced by 20.5-36.4%, but similar marketable yields were obtained, due to improved thermal and hygrometric conditions provided by the screen. This may also be partly explained by the diffusion of light created by employing shades: simulations predicted that reducing the PAR transmittance of a clear greenhouse cover from 90% to 85% could not negatively affect yields if the 85% transmittive cover diffuses 80% of incoming light (Hemming et al., 2006b). Simulations from Aikman (1989) estimated even higher benefits: the redistribution of solar radiation in a crop, which can be obtained by using screens, could give an increase of 22% in annual productivity.

Simulations conducted by Montero (2006) have shown that while evaporative cooling may be more effective than shading for reducing indoor temperature, shading achieves greater water

use efficiency. It was also shown that the use of movable shading is more effective at low ventilation rates: their contribution becomes almost negligible at ventilation rates greater than 40 ACH, where the indoor temperature of a shaded greenhouse becomes practically identical to an unshaded greenhouse.

A thermal screen, unlike a solar screen, should have a high solar transmittance to take advantage of solar gains to reduce heating loads. The operating conditions of thermal screens have a significant impact on the energy consumption. Control strategies for operating thermal screens in greenhouses can be based on several approaches such as:

- Time clock operation;
- A fixed value of solar irradiance;
- A linear correlation between solar irradiance and outside temperature;
- An economic criteria based on energy saved versus crop lost;
- An energy balance on the glazing.

It was found that energy savings can be increased by 6% when the screen is controlled based on radiation level compared to time clock operation (Seginer and Albright, 1980). Marsh et al. (1984) measured an energy saving of 3.3% when the opening of thermal screens was based on an inside light level of 30 W/m^2 compared to time clock operation. They also concluded that using a more complicated control strategy based on a light level that is a linear function of the outside temperature is not justified because no additional savings were observed compared to a fixed light level control.

Simulations carried out by Dieleman and Kempkes (2006) have shown that by operating a thermal screen opening based on outside radiation level from 1 W/m^2 to 25, 50 and 150 W/m^2, additional energy savings of 2%, 3% and 4% can be achieved. They also found that operating a screen based on correlations of outside temperature and radiation can achieve a similar energy reduction of up to 4% compared to an operation strategy based on a fixed outside radiation level of 1 W/m^2.

2.2.2 Humidity control

Plants absorb solar energy and CO_2 which are converted into chemical energy by photosynthesis. In addition to this process, transpiration occurs through stomata in leaves, which serves to evaporatively cool plants. Transpiration rates depend mainly on the degree of stomatal opening, the water vapor pressure deficit between plant leaves and air as well as air turbulence (Hellickson and Walker, 1983).

The majority of plants grow best between a fairly narrow range of relative humidity levels; typically 70% to 85% is suitable for most species. Low humidity levels increase the evaporative demand on the plants which could lead to moisture stress, even if there is no shortage of water in the rooting media. Very high humidities may induce condensation on the glazing and can depress the evaporative demand on the plant and reduce nutrients uptake, which could impair cell formation. Maintaining the RH below 85-90% could be sufficient to avoid these problems (Garzoli, 1989).

This section covers three techniques that can be used for humidity control: conventional ventilation, ventilation with heat recovery and the use of a solar regenerated desiccant. Other systems such as heat pumps coupled with heat exchangers (Bakker et al., 2008) are not covered here.

2.2.2.1 Ventilation

The traditional way of reducing the relative humidity in greenhouses is with ventilation, thus exchanging warm and moist indoor air with cool and and dry outdoor air, which is energy intensive (Bailey, 1984). The moisture removed by ventilation is equal to

$$M_{\text{water}} = \frac{Q_f}{v}(W_i - W_o) \tag{2.13}$$

where M_{water} is in kg_{water}/s and W_i and W_o is the humidity ratio of the indoor and outdoor air. The mass of water added into the air by transpiration is given by

$$M_{\text{water}} = \frac{EF\tau IA_f}{h_{fg}} \tag{2.14}$$

where F is the portion of the floor area covered by plants and h_{fg} is the latent heat of vaporization of water. The total ventilation rate Q_f is equal to the ventilation rate plus the infiltration rate:

$$Q_f = Q_{f,\text{vent}} + Q_{f,\text{inf}} \tag{2.15}$$

When assuming there are no condensation on the greenhouse cover, the ventilation rate for humidity control can be calculated with

$$Q_f = \frac{EF\tau IA_f}{\rho\, h_{fg}(W_i - W_o)} - Q_{f,\text{inf}} \tag{2.16}$$

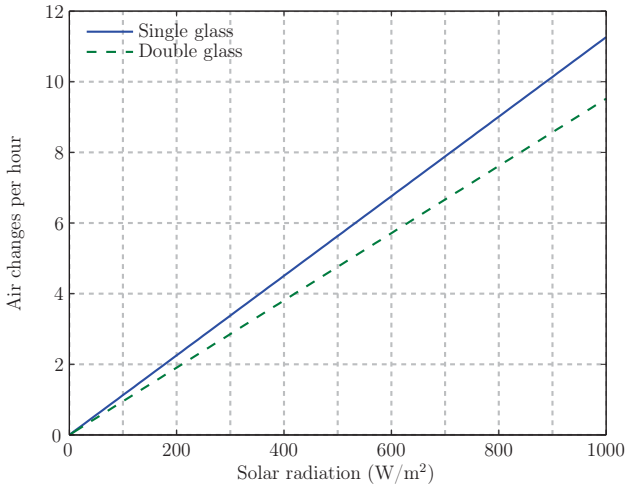

Figure 2.8: Ventilation rate for maintaining inside greenhouse air at 75% RH at outdoor condition of -20 °C and 70% RH

For the same single and double glazed greenhouses of 1000 m^2 as described in section 2.2.1.2, the ventilation rate needed to maintain 75% RH as a function of incident solar radiation is depicted in figure 2.8 (where F=0.8). It can be seen that with T_o =-20 °C, the number of air changes per hour required for humidity control is approximately 100 times less than the incoming solar radiation. For instance, a single glazed greenhouse would require about 6 ACH when subjected to a solar radiation level of 600 W/m^2. The maximum ventilation rate for humidity control is set to 10 ACH for most growers (de Halleux and Gauthier, 1998).

There are many ways to reduce the ventilation rate required for humidity control, such as selecting a higher indoor humidity set point, reducing the transpiration level of plants and dehumidifying with heat recovery. While higher humidity levels may increase the risk of fungal diseases, it may also favor crop production and quality. It was estimated that an increase of 5% of the RH level can reduce the energy consumption by 5 to 6% (Bakker et al., 2008) and increasing the maximum humidity level from 80% to 85% reduces the dehumidification needs by 30% (Campen, 2009). The transpiration rate can be decreased by a controlled reduction of the leaf area for crops with a high leaf area index. An experiment conducted with tomatoes revealed that when halving the leaf area by removing old leaves, the transpiration rate was reduced by 30% without affecting crop yield.

2.2.2.2 Ventilation with heat recovery

Typical dehumidification is achieved by cooling air below its dew point temperature, thereby condensing moisture until the desired humidity level is reached. However, air is frequently overcooled and then must be heated to meet thermal comfort, which lead to inefficiencies and high energy consumption.

Ventilation with heat recovery might be more appropriate than typical dehumidification for solaria and greenhouses. In cold weather, the ventilated air must be heated, which represents a significant fraction of heating costs: about 13-18% of heating costs of standard greenhouses are due to ventilation for humidity control. Heat exchangers can be used to recover some of the exhausted heat. Typical efficiencies of air-to-air commercial exchangers used in Canadian agriculture are about 40%. However, they are expensive and prone to problems at temperatures below 0 °C (Rousse et al., 2000).

Simulations conducted by de Halleux and Gauthier (1998) estimated the return on investment for such heat exchangers to be between for 4.8-8 years and to save CDN $ 6250 per hectare per year. Rousse et al. (2000) designed a simple air-to-air counter-flow multi-tube heat exchanger for greenhouses located in cold climates. The experimental heat exchanger, buried in the ground, operated at 0.5 and 0.9 ACH and reached efficiencies of 78-84%. The heat exchanger was inexpensive, easy to assemble and maintain, could resist corrosion and mold propagation and could operate satisfactorily even at sub zero temperatures.

A similar study conducted by Speetjens in 2001 used a heat exchanger installed in the gutter of a greenhouse were 60-70% of sensible heat was recovered (Campen et al., 2003). A study carried by Campen et al. (2003) about different methods for dehumidifying greenhouses in cold climates simulated the use of an ideal heat exchanger with 100% efficiency. They found that, depending on the crop, 108-190 MJ/m^2 can be saved for a single layer greenhouse and between 145-278 MJ/m^2 for a double layer greenhouse. The energy cost reduction ranged from 0.31-0.84 € /m^2 to 0.44-1.33 € /m^2. They concluded that forced ventilation with heat exchange is the most promising dehumidification method for cold climates, but that a low cost and efficient system need to be developed.

2.2.2.3 Solar regenerated desiccant

Dehumidification can also been achieved using solid or liquid desiccants. In this case, moisture contained in the air is absorbed/adsorbed by the desiccant, which then must be regenerated with a source of heat to evacuate moisture.

Solid desiccants can typically provide a higher degree of dehumidification; they are usually made of stationary beds or rotary wheel beds. Solar air heaters are well suited for providing heat to these systems because air is the regeneration medium (Ahmed, 2005). Liquid desiccants require lower regeneration temperatures which facilitates their coupling with low temperature sources like flat plate solar collectors. In addition, liquid desiccant systems have the potential to use the desiccant solution for energy storage (Mesquita et al., 2006).

Mathematical and numerical models of solid desiccant systems are presented by Bourdoukan et al. (2006) and Ahmed (2005), while models for liquid desiccant systems are presented by Mesquita et al. (2006), Yutong and Hongxing (2008) and Andrusiak and Harrison (2009). Lychnos and Davies (2008) studied the potential of a solar powered liquid desiccant system for greenhouses. Preliminary simulation results with a solution of magnesium chloride indicated that a reduction of the average wet-bulb temperature of 2.2-3°C is possible.

The optimum regeneration temperature of a solar desiccant system is a tradeoff between high solar collector efficiencies, which occur at low temperatures, and high desorption rates, which occur at higher temperatures (Andrusiak and Harrison, 2009). The solar regenerated liquid desiccant system studied by Yutong & Hongxing showed a higher performance under higher latent loads, which is of particular interest for greenhouses where latent loads are high. Lychnos & Davies estimated that solar powered liquid desiccant systems are of potential interest for cooling and dehumidifying greenhouses, but that future work is needed to optimize heat and mass transfers.

2.2.3 Control of CO_2 concentration

The atmospheric concentration of carbon dioxide reached 390 ppm in 2010 (Lacis et al., 2010). Many crops, such as vegetables and flowers, have shown increased growth when subjected to elevated carbon dioxide levels of 700-1000 ppm. In a closed environment with plants like a greenhouse, the CO_2 level may be quickly depleted and reach concentration below 200 ppm. «At such levels plant growth virtually ceases, irrespective of how ideal is the control of all other climatic parameters. In order to maintain the concentration at or near atmospheric concentration it is necessary to ventilate the greenhouse with outside air [...] »Garzoli (1989). It is also possible to inject carbon dioxide in greenhouses at or above atmospheric concentration. CO_2 enrichment is a common practice which enhances photosynthesis and thus increases yield and income (Dion et al., 2011).

2.2.3.1 Ventilation

The CO_2 balance of the greenhouse air is given by (Ioslovich, 1995)

$$\rho h \frac{dC_i}{dt} = C_g - C_v - G \tag{2.17}$$

where ρ is the air density, h is the effective greenhouse height, C_i is the indoor CO_2 concentration, C_g is the CO_2 enrichment flux, C_v is the CO_2 exchanged by ventilation and G is the net photosynthesis flux (in kg_{CO_2}/m^2-s). The CO_2 exchanged by ventilation is proportional to the ventilation rate Q_f:

$$C_v = \rho Q_f (C_i - C_o) \tag{2.18}$$

G from equation 2.17 characterizes the CO_2 assimilation by the crop and depends on its photosynthetic activity and respiration rate. It can be calculated with

$$G = \frac{\epsilon I_{PAR}\, g_s C_i}{\epsilon I_{PAR} + g_s C_i}\Big(1 - \delta_P (T_x - T_{in})^2\Big)\Phi - M_{\text{crop}} R_r\, e^{\nu_r (T_i - T_r)} \tag{2.19}$$

where ϵ is the photosynthesis efficiency (in kg_{CO_2}/J_{PAR}), I_{PAR} is the photosynthetically active radiation, g_s is the leaf conductance to CO_2, δ_P is an empirical coefficient representing the photosynthesis temperature response and T_x is the temperature at which the gross photosynthesis is maximal. In addition, M_{crop} is the areic dry weight of the crop, R_r is the respiration rate, ν_r is a respiration exponent and T_r is the environmental temperature. Φ is given by

$$\Phi = 1 - e^{-K\, LAR\, M_{\text{crop}}} \tag{2.20}$$

where K is a light extinction coefficient in the canopy and LAR is the leaf area ratio. I_{PAR} is simply calculated from the horizontal outdoor solar radiation I_{ho}, the average glazing transmittance τ and the ratio of PAR to solar radiation ζ:

$$I_{PAR} = \tau I_h o \zeta \tag{2.21}$$

For the same single and double glazed greenhouses of 1000 m^2 described in section 2.2.1.2, the ventilation rate needed to maintain 350 ppm inside the greenhouse as a function of incident solar radiation is depicted in figure 2.9. It can be seen that the photosynthetic activity (and therefore CO_2 assimilation and ventilation needs) increases almost linearly at low solar radiation level but a saturation effect occurs and it becomes difficult to increase plants growth by increasing radiation at higher intensities.

The values of the parameters used in equation 2.19 are presented in table 2.5. The ratio of I_{PAR} over I, ζ, was observed to vary between 0.43 to 0.48, depending on the sky conditions and time of the year (Aguiar et al., 2009); an average value of 0.46 was selected.

ϵ	10^{-8}	kg_{CO_2}/J_{PAR}
g_s	$2{\cdot}10^{-3}$	kg_{air}/m^2-s
δ_P	$2{\cdot}10^{-3}$	K^{-2}
T_x	30	°C
M_{crop}	0.1	kg/m^2
R_r	$0.4{\cdot}10^{-6}$	$kg_{CO_2}/kg_{crop\,CO_2}$-s
ν_r	0.0693	K^{-1}
T_r	25	°C
K	0.8	m^2_{ground}/m^2_{leaf}
LAR	19	$m^2/kg_{crop\,CO_2}$

Table 2.5: Photosynthesis and crop parameters for the calculation of CO_2 assimilation, from Ioslovich (1995)

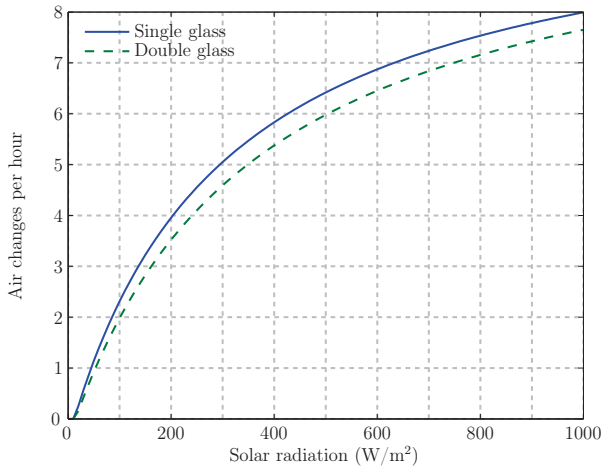

Figure 2.9: Ventilation rate for maintaining an inside greenhouse CO_2 concentration of 350 ppm

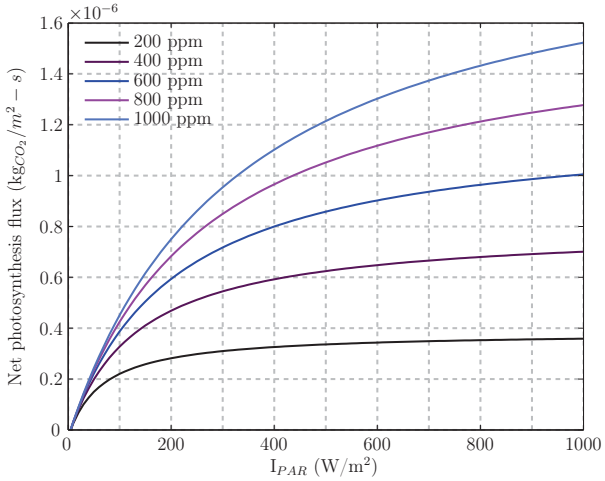

Figure 2.10: Net photosynthesis flux as a function of PAR radiation at varying CO_2 concentrations

2.2.3.2 CO_2 enrichment

If ventilation is the only way to control CO_2 concentration in greenhouses, the indoor concentration cannot exceed the ambient concentration. Since many crops have shown increased growth when subjected to elevated CO_2 levels, CO_2 enrichment is now common practice in commercial greenhouses. When practicing CO_2 enrichment, ventilation becomes then a CO_2 sink, wasting the added CO_2 through air exchange. To alleviate this problem, some growers practice intermittent enrichment, where ventilation and enrichment alternate many times per hour. In hot climates where ventilation is needed for temperature control, enrichment is stopped to conserve gas and expenses (Ioslovich, 1995).

Figure 2.10 shows the net photosynthetic flux, as defined by equation 2.19, as a function of the incident PAR radiation. At a CO_2 concentration of 200 ppm, increasing light levels only marginally increases the photosynthetic activity; this low CO_2 concentration is a limiting factor.

Carbon dioxide enrichment is particularly useful in winter, when low light levels limit the development of crops. During wintertime, CO_2 enrichment can boost photosynthesis up to 50% and increase crop yields by 20-40% (Hand, 1984). Critten (1991) developed analytical relationships for optimal CO_2 concentration for a commercial lettuce crop. Ioslovich (1995) developed a sub-optimal CO_2 enrichment method which balances ventilation and enrichment.

Conventional CO_2 enrichment is practiced with pure CO_2 in bulk or from combustion of natural gas or propane. Usually these fuels are used in burners dedicated for CO_2 enrichment, distinct from the main heating system. Performing CO_2 recovery from the exhaust gas of biomass heating systems is also possible, but future research is needed to optimize safe and clean CO_2 enrichment (Dion et al., 2011).

Combining greenhouses with animal barns could be beneficial for raising the interior CO_2 level. Animals can provide not only useful heat (see section 2.1.4), but are also a source of CO_2. There is a natural complementarity in a plant-animal system: animals are producing CO_2 when breathing and plants absorb CO_2 and produce oxygen. In such a system, animals are stimulating plants growth and plants are improving the indoor air quality, which allow to lower ventilation needs - and associated heat losses in winter (FAO, 1994).

As seen in section 2.1.4, compost can be used in greenhouses to provide supplementary heat; in addition, compost also produces CO_2 emissions. In an experimental cultivation of cucumbers grown on composting waste, elevated CO_2 levels were recorded in the composting media, more then 10 times higher than in the control media before planting, and 3 to 5 times higher at the final production stage (Kostov, 1995). Their results suggest that elevated CO_2 levels and higher temperatures of the rooting media significantly increased yields: a 28-78% yield increase was observed compared to the control, for different composting media.

Diver (2001) notes that composting operation in greenhouses should be sized based on carbon dioxide needs, not on heating needs. When based on heating needs, the volume might be too large to be practical and the indoor air quality could be impaired by having 6 times the optimum CO_2 concentration. Nitrogen (ammonia) emitted during the decomposition process can be a serious issue and damage some crops, but new design features that solve this problem are now available.

2.2.4 Lighting control

At high latitudes, the lack of light becomes a limiting factor in the darkest months. Growers have to choose between interrupting their operation during such conditions or using supplemental lighting. The following sections describe the light requirements for adequate plants growth, present the artificial light types most appropriate for horticulture and some control strategies for selecting lighting levels.

2.2.4.1 Light requirements of plants

The amount of photosynthetically active radiation (PAR) is usually defined as being between 400 and 700 nm and is measured with quantum sensors that express the PAR level in μmol/m^2-s, where mol here refers to one mole of photons. For natural light, 1 μmol/m^2-s is equal to 56 lux or 0.217 W/m^2 of PAR. Visible light is comprised in a larger waveband between 380 and 770 nm.

Plants need light in three distinct spectral ranges for adequate development triggered by photosynthesis, phototropism and photomorphogenesis. The most important photosynthetic pigments are chlorophylls a and b with peaks at 662 and 642 nm respectively. Phototropism, which regulates the control of plant organs and influence the orientation of plants in response to light, is triggered by light between 400 and 500 nm. Morphogenesis, which is responsible for healthy plant development and processes like shooting and pigment synthesis, needs far red radiation at about 730-735 nm (Tamulaitis et al., 2005). Another study estimated that plants also need radiation in the 700-1000 nm range for morphogenesis (Kittas et al., 1999).

In general, plants development depends on both the quantity and spectral quality of light that is available. The daily light integral is defined as the number of photons intercepted per square meter per day and represents the cumulative light level impinging on a crop over a day. The use of artificial light of 100 μmol/m^2-s 16 hours per day adds 5.8 mol/m^2-d to natural light. Since the daily light integral may vary between 1 and 35 mol/m^2-d throughout the year (Dorais, 2003), supplemental lighting may be necessary to maintain a more uniform plant development all year round.

2.2.4.2 Artificial light

The most commonly used artificial light source in greenhouses is high-pressure sodium (HPS) lamps. HPS lamps emit a wide peak at green-yellow wavelengths, but emit very little blue

and violet light. They have a high efficiency for converting electricity to PAR of about 26-30%. Metal halide lamps have a wider spectrum, but a 25% lower efficiency for converting watts to PAR and a reduced lifetime (Dorais, 2003).

Light emitting diodes (LED) have many advantages over conventional HPS lamps, such as increased energy efficiency and durability. The high cost of LED restricted their use to specific applications like space-based plant growth facilities, but rapidly decreasing prices indicate that using LED in greenhouses may be feasible in the coming decades. Plants grown under advanced high power AlGaInP LED exhibited better photosynthesis activity and morphology then plants grown with conventional HPS lamps (Tamulaitis et al., 2005).

2.2.4.3 Radiation control

It is possible to maintain plant production if a decreasing light level is compensated by an elevation of the carbon dioxide concentration. Such a practice could lead to significant savings since carbon dioxide enrichment is cheaper than supplemental lighting (Both, 2000), which would be also beneficial from en environmental point of view since it would favor carbon sequestration over electricity consumption.

As mentioned in section 2.2.1.3, high levels of PAR are not an issue for most plants, except for shade loving plants (Kempkes, 2008). A solar shade can be used for such crops if it is desired to reduce the PAR level in the greenhouse.

Although artificial lighting obviously increases the electrical consumption of greenhouses, it also reduces their heating needs. It was estimated that supplemental lighting can provide 25-41% of the heating requirements of a double plastic greenhouse in Quebec city (Dorais, 2003). Since canadian greenhouses are most frequently heated with natural gas (Statistics Canada, 2010), displacing natural gas by electricity may reduce carbon dioxide emissions (Dorais, 2003), especially when hydroelectricity is used.

The lighting intensity should be adapted for each crops. Light integrals of 12 mol/m^2-d or higher are generally needed for lettuce production and obtained with supplemental lighting of 50-100 μmol/m^2-s. For cucumber, it was estimated that the maximum income would occur when using 120-150 μmol/m^2-s of supplemental light. Tomato has higher light requirements: 30 mol/m^2-d or higher is often reported for tomato culture (Dorais, 2003). When subjected to the same daily light integral, radish and Chrysanthemum have shown higher dry matter accumulation under a 18 hours lighting regime than under 12 and 24 hours. However, corn and cucumber exhibited the same dry matter accumulation under a photoperiod of 12, 18

and 24 hours while, for all four species, the dry matter development was lowest with a 8 hours photoperiod (Warrington and Norton, 1991).

The installed lighting capacity is usually between 100-200 W/m^2. Lamps are usually turned off when the solar radiation level reach 240-300 W/m^2 and when the daily light integral reach 55 mol/m^2-d. Photoperiods of 12-18 hours are frequently adopted, depending on the crops (Dorais, 2003). It is generally better to have lower lighting levels during an extended period of time up to 18-20 hours, while continuous lighting should be avoided because of the apparition of growth abnormalities observed with some species (Warrington and Norton, 1991).

The use of artificial lighting in greenhouses may be an issue especially in urban areas because of the light pollution they may produce (Pearson et al., 2010). In the Netherlands, legislation requires the installation of opaque screens to reduce light transmission through greenhouse cover by 95% and the limitation of the lighting regime to 180 μmol/m^2-s, unless light pollution is totally prevented (Van Ooster et al., 2008). Light pollution is linked to diverse ecological impacts such as influences on organismal movements, foraging, interspecific interactions, communication, reproduction and mortality (Gaston et al., 2012).

The use of artificial lighting in greenhouses may increase yields significantly, but is energy and capital intensive. Therefore, high yield must be maintained to justify its use. All greenhouse parameters must be carefully controlled, including CO_2 levels, temperature and humidity, daily temperature evolution, crop schedule and pest management (Dorais, 2003). As depicted in figure 2.10, practicing CO_2 enrichment allows to make a better use of increased PAR radiation.

2.2.5 Greenhouse climate control models

The main variables affecting plants growth inside a greenhouse are the air temperature, humidity, CO_2 concentration and solar radiation level. These parameters can be controlled via various systems such as heating systems, ventilation (natural or forced) systems, dehumidification or evaporative cooling systems, artificial lights, CO_2 injection equipment and thermal/solar screens. The state of these variables will determine crop yields, energy consumption and net profits.

The modification of one system element often impact more than one variable. Sometimes, modifying a system will improve some variables while impairing others. For instance, artificial lighting in winter increases radiation level and interior temperature, effects which are

both beneficial for increasing yields. However, artificial lighting in summer is beneficial for increasing yield, but the associated temperature rise is detrimental.

One climate control strategy is to control the processes rather than the state of the variables. Partial optimization can also be used to improve indoor climate when considering parameters individually (Trigui, 2000).

Many different climate control strategies, models and programs have been developed and published. A list of some greenhouse models developed in 1988 and before is presented in de Halleux (1989). The simpler models consider only the energy balance of the indoor air, but more complex models also carry out the energy balance of other elements like the glazing cover, soil and plants. Multi elements models can be either static or dynamic. Only dynamic models can adequately represent indoor conditions on a short time scale and are therefore preferred (de Halleux, 1989).

Models for determining optimal temperature set points (Seginer et al., 1991), crop transpiration rate (Jolliet and Bailey, 1992; Stanghellini and Van Meurs, 1992), humidity levels (Jolliet, 1994; Korner, 2003), CO_2 concentration (Critten, 1991; Ioslovich, 1995) and ventilation rates (Seginer, 1997) have been developed. Models for predicting climate inside greenhouses have been developed by Zhang (1997), Wang and Boulard (2000) and Salazar and Rojano (2008), while others have used existing building energy simulation software for predicting indoor climate like TRNSYS (Carlini and Castellucci, 2010). Crop transpiration models have been developed by Jolliet (1993) and Sánchez et al. (2009).

The indoor climate should be controlled such as to maximize crop production and minimize energy use. However, these two objectives are often conflictive, therefore climate control becomes an optimization problem. Ioslovich and Seginer (1998) developed a sub-optimal method for climate control which was solved with an optimization routine. Trigui (2000) developed a control strategy based on the maximization of an objective function to maximize the net profit, estimated as the harvest value minus the cost of maintaining the climatic conditions.

Aaslyng et al. (2003) developed a climate control system based on a combination of control methods. Thermal screens were controlled to maximize profit which was calculated as a tradeoff of the energy saved with screens on versus the production loss caused by decreased irradiance. The allowable temperature fluctuations were considerably higher than usual; the temperature set point was lower on cloudy days were growth is reduced and higher on sunny days to increase production. Temperature and CO_2 set points are selected in order to achieve a desired photosynthetic level for a given irradiance and minimize heat and CO_2 inputs. The

model is divided into components which contain mathematical models for the control of biological phenomena or processes. Field trials showed significant energy savings with only small changes in plant production.

2.2.6 Closed, semi-closed and open Greenhouses

As explained in the previous sections, most greenhouses rely on ventilation through the opening of windows to control humidity, temperature and CO_2 levels. However, such practices result inevitably in sub-optimal conditions for either temperature or humidity (de Zwart, 2008). When CO_2 enrichment is practiced, its efficiency is seriously altered by the opening of windows. In addition, during the cold season, opening windows for temperature control results in wasted solar heat which would be needed later on at night.

These observations led to the development of a new concept in the Dutch greenhouse industry: the so-called closed greenhouse. Such greenhouses are equipped with a heat pump, air treatment units with heat exchangers, air distribution ducts, daytime thermal storage and an underground aquifer for seasonal storage. The temperature is controlled by active cooling instead of ventilation. Energy savings of up to 30% and production increases by up to 20% have been reported. The production increase is mainly explained by the elevated CO_2 levels that can be achieved in closed greenhouses. The economic feasibility of this concept depends highly on the production increase that can be obtained, since typically a 10% increase in yield represents much more money than a 10% energy savings (Heuvelink and Bakker, 2008).

In closed greenhouses, the air is cooled and dehumidified by air treatment units. A semi-closed greenhouse has a smaller cooling capacity than a closed greenhouse, where in this case ventilation through windows is used when the temperature is too high to be controlled by the cooling system only. Yield increase occurs mainly during the summer, where the combination of high solar radiation and high CO_2 is possible only in closed greenhouses (Qian et al., 2011). Experimental yields of a closed greenhouse compared to simulated yields of conventional open greenhouses estimated a primary energy use reduction of 19% for a stand-alone closed greenhouse and of 33% when coupled to open greenhouses covering twice the area (Opdam et al., 2005).

Besides energy savings and increased production, closed greenhouses have a high water efficiency (no water loss), offer a better temperature control and could reduce or eliminate the need for pesticides (Gelder et al., 2005). However, in 1995, an entirely closed greenhouse

was not considered economically feasible because of the high investment cost and electricity prices (Opdam et al., 2005).

The production increase is challenged particularly by the apparition of botrytis infection, which has been noticed in many field trials of closed greenhouses (Heuvelink and Bakker, 2008; Qian et al., 2011). This infection is mainly linked to high relative humidities. Another disadvantage of closed greenhouses is the presence of a high vertical temperature gradient, due the the presence of the cooling ducts at the bottom and the buoyancy effect (Qian et al., 2011).

On an annual basis, a greenhouse in the Netherlands receives an average of 2800 MJ/m^2, which corresponds to about three times its annual heating requirements. There is a seasonal imbalance: excess of solar energy is available in summer and high heating requirements occurs in winter. More heat can thus be stored in the aquifer than what is needed for the heating requirements. Since the Dutch government requires temperature neutrality, about 1 hectare of closed greenhouses must be coupled with 3 hectares of open greenhouses, or the extra heat has to be used in another way (Heuvelink and Bakker, 2008).

An interesting concept of a closed greenhouse equipped with a cooling tower and a solar collector has been suggested by Buchholz et al. (2005). This concept allows the cooling and dehumidification of the greenhouse air and the production of distilled water. If salty water is used for the evaporation process, water desalination can be achieved.

2.3 Building-integrated solaria/greenhouses

Sunspaces can be integrated to any type of buildings: residential, commercial or institutional buildings, existing or new constructions. For a single-family house, the most practical way to integrate a sunspace is by adding an adjacent solarium. For multi-dwelling units, a solarium/greenhouse could be integrated to the building as a common space localized either on the ground or on the roof or as a private space on balconies. For larger buildings, like offices or schools, a large greenhouse could be installed on the roof. This last application is very innovative and promising.

Astee and Kishnani (2010) found that by using rooftops of public housing estates for hydroponic crop production, the local food production of Singapore could be raised from 5% to 35.5%, which would enhance food security and reduce GHG simultaneously. With 14,000

acres of unshaded large rooftops, New York City could produce enough vegetables to feed over 30 million people, more than 3 times its population (Droege et al., 2009).

Caplow is the first researcher to use the term *building-integrated greenhouse* in a conference paper published in 2007 (Caplow and Nelkin, 2007). Only a few experimental and commercial rooftop greenhouses have been built so far. Montreal is hosting the first commercial rooftop greenhouse, which began its operation in 2011 (Rifkin, 2011). A few months later, another company built and started to operate a rooftop greenhouse in Brooklyn, New York (Foderado, 2012). Some other young companies have been created recently and are planning to buid a first rooftop greenhouse in the near future. Others companies developed another concept allowing to grow food in buildings, but without a greenhouse. It is possible to grow leafy vegetables in a box, vertically to enhance density, where artificial light and all other climatic parameters are carefully controlled (The Produce News, 2011).

Although the first commercial rooftop greenhouses of Montreal and Brooklyn are siting on top of a building, they are not truly integrated. The greenhouse structure literally sits over the roof, on which rubber mats have simply been added in Montreal. The heating system of the greenhouses is totally disconnected from the heating and cooling systems of the building beneath. These greenhouses are typical of good quality new greenhouses that are built in North America, but are not as efficient as the best commercial greenhouses in northern Europe like the Netherlands. They are equipped of some energy saving features, like thermal screens, but they have no special features compared to stand alone greenhouses. At the Montreal site, the growers estimate a reduction of 50% of their heating needs thanks to the heat losses of the building beneath (Hage, 2011). When greenhouses are overheating, windows simply open, which happen even in winter. The potential of using extra heat from the greenhouse to supply auxiliary heating to the building beneath has not been investigated.

Structural considerations have to be taken into account when adding greenhouses above existing buildings. Some buildings would require structural reinforcement to carry the added load, which would add significant cost to a project, but some existing buildings have the capacity to support such an additional load. Snow loads are not an issue with single glazed greenhouses because the snow melts very quickly upon contact with the warm glass. However, energy efficient greenhouses with double glazing and/or thermal curtains are slowing down snow melting. Some greenhouses equipped with thermal curtains usually supply heat only to the space below the curtains, to reduce heat loads, but have dedicated heat pipes above the curtains used only for melting snow. Structural loads due to snow must be considered in cold climates and especially for energy efficient rooftop greenhouses.

Figure 2.11: The world's first commercial rooftop greenhouse, located in Montreal

Solaria are popular additions to homes since many years. However, these spaces are usually built for agreement, not for energy purpose. In Canada, they are often categorized as three season or four season solaria. The main difference between a three and four season solarium lies in the presence of a heating system: a three season solarium is usually single glazed and does not have a heating system, while a four season solarium is equipped with double glazing and a heating system. Municipal laws are often different depending on the type of solarium. A four season solarium is considered as part of the house, and therefore must comply with buildings codes, whereas a three season solarium is considered as an annex to the house and is sometimes governed by different construction standards.

Conventional three season solaria technically do not consume energy and could lead to small energy savings by reducing heat losses through the common wall. However, if badly connected with the house (for instance, with a drafty integration), they could also increase the house heat losses. Typical four season solaria need significant heating which could easily represent 500 CAN $ per year (Protégez-vous, 2012). As noted by Kesik and Simpson (2002), a house provides more energy efficient habitable space than a conditioned solarium, either conventional or highly performant. The integration of solaria to existing houses is often problematic. Insufficient air and water tightness is frequently reported (Protégez-vous, 2012).

Solaria/greenhouses can also be integrated to multi-dwelling buildings. Montreal hosts a net-zero condominium building that performed a deep retrofit of an existing building. These condos feature individual garden plots and a rooftop greenhouse available to the owners. The greenhouse is heated only with surplus and waste heat coming from individual dwellings and the bakery located on the ground floor (Dumoulin, 2009).

2.4 Summary and research opportunities

After an exhaustive review of the main factors affecting the performance of solaria and greenhouses, some knowledge gaps and needs have been identified:

1. Despite a large number of studies carried out to identify optimum solaria and greenhouse designs, there is a need for an extensive thermal and daylighting study to identify best designs for various climates.

2. Since natural ventilation flows calculated with CFD simulations are design specific, generalizations are difficult. Nevertheless, there is a need for general guidelines to identify optimum greenhouse openings to enhance natural ventilation.

3. Existing solar screen materials are efficient for removing solar heat, but they reduce the visible spectrum even more than the solar spectrum. The development of a new fabric with a high visible transmittance and a reduced solar transmittance would be highly desirable.

4. While it is recognized that the use of multiple thermal screens is an efficient way for reducing heat losses in greenhouses, there is a need for an improved method for their control.

5. No tools nor methodologies are available at the moment for analyzing the performance of glazing-shade systems at the design stage for heating dominated buildings.

6. Although many researchers advocate the inclusion of passive thermal mass in solaria and greenhouses, no sizing strategy specific to isolated-gain applications has been reported.

7. Forced ventilation with heat recovery seems the most promising dehumidifying method for greenhouses; additional research is needed to optimize the design of these systems for cold climates. The possibility of operating them in different modes, such as dehumidification and heat storage/release modes, should be explored.

8. A large number of models have been developed for controlling the indoor climate in greenhouses. Most of these models are developed for only one type of crop and have fixed control strategies. The development of new models that are more flexible and allow to choose different crops and control strategies is desirable.

9. The concept of building-integrated solaria/greenhouses is born and the first urban greenhouses are slowly appearing on rooftops. However, up to now, the energy po-

tential of the useful heat that can be collected by solaria/greenhouses and transferred to adjacent buildings has not been characterized.

10. There is a need for research on building envelope systems that will facilitate the installation of retrofitted greenhouses on rooftops, where structural loads due to snow and wind should be assessed and minimized.

11. Greenhouses can collect significant amount of additional heat that could be used by neighboring buildings. There is a need for designing an efficient mechanical system, able to transfer heat from a greenhouse to a building while dealing with potential humidity and indoor air quality issues.

As a first step, item 9 is tackled where the energy saving potential of building-integrated solaria and greenhouses is evaluated. Then the focus of this thesis is on enhancing the solar energy utilization by increasing the solar radiation collection and using performant thermal energy storage systems where items number 4, 5 and 6 are addressed.

Chapter 3

Energy Saving Potential of Solariums/Greenhouses

Based on a published paper:

Bastien, D., Athienitis, A. 2013. Evaluation of the potential of attached solaria and rooftop greenhouses in Quebec. *In: 3rd Climate Change Technology Conference.* Montreal, pp. 1-11.

3.1 Introduction

Building-integrated solaria and greenhouses can be used as solar collectors and provide supplemental heating to an adjacent building. Some jurisdictions recognized the energy saving potential of attached sunspaces and awarded grants to conduct demonstration projects.

For instance, the US Department of Energy awarded a grant in 1981 to add an experimental sunspace to an existing house in Delaware. Measured data have shown that the sunspace reduced the heating needs of the house by 40% and the domestic hot water load by 30% (Laverty, 1983). A decade later in Glasgow, UK, the CEC Energy Demonstration Program launched the Solar Energy Demonstration Project that undertook the retrofit of 36 apartment dwellings by adding a glazed veranda and a glazed conservatory/utility extension (Porteous and Ho, 1997). The effect of these two buffer spaces is estimated to have reduced the mean heating consumption by 31%.

Typical greenhouses, used to extend the cultivation season, are usually stand-alone structures located in the suburbs. With growing cities and increased reliance on imported vegetables, urban agriculture is a rising trend which is trying to bring closer farmers and consumers. The city of Montreal carried out in 2012 a public consultation about the state of urban agriculture on its territory. The first commercial rooftop greenhouses appeared in Montreal (Rifkin, 2011) and New York city (Foderado, 2012) in 2011. These structures can be thermally linked with their host building and contribute to reduce their heating requirements.

Energy efficient solaria can collect excess heat that can be used for heating an adjacent building. However, their performance is highly dependent on their design and operation characteristics (Schoenau et al., 1990). As pointed out by Kesik and Simpson (2002), regardless of their designs, solaria conditioned with the same set points as a house require more annual space heating per unit of floor area than a house. Therefore, it is essential for an energy efficient solarium to allow wider temperature fluctuations than in a normally conditioned room for reducing its heating requirements.

This chapter presents an assessment of the energy saving potential of retrofitted solaria and rooftop greenhouses in the province of Québec, Canada. Simulations during the heating season have been conducted using the building energy simulation software EnergyPlus (U.S. Department of Energy, 2012) and are presented in section 3.3. Six different case studies of houses with an attached solarium have been considered. Solariums with different sizes, orientations and envelope qualities have been studied. In addition, simulations of two rooftop greenhouses with different floor area and various levels of envelope performance have been performed.

3.2 Methodology

An approach similar to the one presented by Pelland and Poissant (2006) for the evaluation of the potential of building-integrated photovoltaics in Canada is followed. Existing single detached and single attached residential buildings and commercial buildings with a floor area greater that 929 m^2 are deemed good candidates for the retrofit of solarium/greenhouse and are thus selected for this study. Simulations are carried out during the heating season (from October 1^{st} to April 28^{th}) using EnergyPlus. All case studies have been simulated using Canadian Weather for Energy Calculations (CWEC) data for the city of Montreal.

3.2.1 Residential buildings

Table 3.1 presents the number of dwellings and total floor area of single detached and attached buildings in the province of Québec. According to the Survey of Household Energy Use (Natural Resources Canada, 2007), the average number of storeys of residential buildings in Québec is 1.37. The total ground floor area is simply calculated as the total floor area divided by the average number of storeys. Apartment buildings were excluded from this study due to the lack of data characterizing their average number of storeys.

Table 3.1: Number of dwellings, total floor area and ground floor area of residential buildings in Québec in 2010 [a]Data from Natural Resources Canada (2015)

Housing type	Nb of dwellings[a]	Total floor area[a] (km^2)	Total ground floor area (km^2)
Single detached	1 644 500	215.3	157.2
Single attached	298 500	35.6	26.0

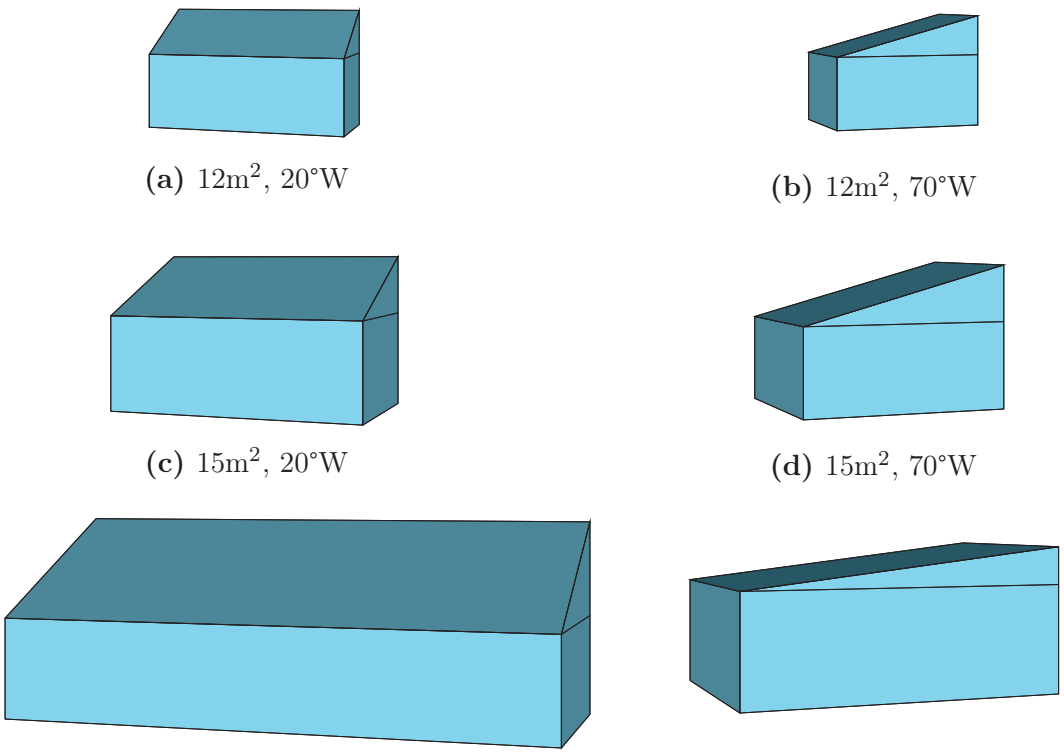

(a) 12m^2, 20°W **(b)** 12m^2, 70°W **(c)** 15m^2, 20°W **(d)** 15m^2, 70°W **(e)** 30m^2, 20°W **(f)** 30m^2, 70°W

Figure 3.1: Solarium designs — floor area and orientation

The average total area and ground floor area of a single detached building are equal to 130.9 m^2 and 95.6 m^2 respectively while the average total area and ground floor area for a single attached building are 119.2 m^2 and 87.1 m^2. The average construction year of a single detached and attached building is 1978 and 1986 respectively. In 2010, the average total energy consumption of residential buildings was 220 kWh/m^2 from which 139 kWh/m^2 was used for space heating (Natural Resources Canada, 2015).

Three different solarium sizes have been modelled: 12 m^2, 15 m^2 and 30 m^2. All solaria are retrofitted adjacent to the backyard wall of an existing house. Two back wall orientations are considered: 20°W and 70°W. One shading element parallel to the back wall with a height and width of 7 m by 8 m is located 10 meters away from the back wall, centered. This shading element represents typical shading by neighbouring houses in urban locations. The six solarium designs investigated in this study are depicted in Figure 1 and their geometrical parameters are indicated in Table 3.2. All solaria have a maximum height of 3 m and a glazed sliding door 1.8 m wide connecting to the house. Solarium façades with orientation between -90°to +90° (0° being south) are glazed while others are opaque and insulated. The selected heat balance algorithm is conduction transfer functions with a time step of 15 minutes.

Table 3.2: Geometrical parameters of the investigated solaria designs

Solarium design	Common wall length (m)	Width (m)	Roof angle (°)	South wall height (m)
12 m^2, 20°W	5	2.4	25	1.88
12 m^2, 70°W	3	4	15	1.93
15 m^2, 20°W	5	3	25	1.85
15 m^2, 70°W	3.4	4.4	15	1.82
30 m^2, 20°W	8.33	3.6	25	1.54
30 m^2, 70°W	4.5	6.66	6.6	2.23

Two different solarium envelopes have been investigated: a conventional and an upgraded envelope. The conventional solarium is constructed with regular double glazing with argon and low emissivity coating. The airtightness is moderate with a constant infiltration of 0.5 air changes per hour (ACH). The floor is made of 200 mm of exposed concrete with R5 (RSI 0.88) insulation beneath. The upgraded solarium is equipped with improved windows, with a low iron outer pane and a slightly reduced emissivity of the inner pane. An interior low emissivity shade is deployed at night when the outdoor temperature is below 20°C to further reduce heat losses. The infiltration rate is reduced to 0.1 ACH and the insulation below the concrete slab is increased to R10 (RSI 1.76). In both cases, the adjacent house is assumed to have a constant temperature of 20°C. The heating set point inside the solarium is 10°C. The

heating needs along with the excess heat inside the solarium when the temperature exceeds 28°C are presented in the next section.

Table 3.3: Solaria design characteristics

Conventional	Upgraded
Conventional db glazing with argon\low-e	Improved db glazing with argon\low-e
Constant infiltration at 0.5 ACH	Constant infiltration at 0.1 ACH
R5 insulation below the floor	R10 insulation below the floor
	Low emissivity shade deployed at night

3.2.2 Commercial buildings

The total floor area and estimated ground floor area for commercial and institutional buildings in Québec are presented in Table 4. As indicated in the Commercial and Institutional Building Energy Use Survey (Natural Resources Canada, 2002), the average number of storeys of commercial and institutional buildings is equal to 2.70. Consequently, the total ground floor area is estimated by dividing the total floor area by the average number of storey.

As presented in Natural Resources Canada (2002), the total floor area of commercial and institutional buildings greater than 929 m^2 was 63.6 km^2 in 2000, or 89.4% of the total floor area. Using this proportion and the more recent data presented in the 2008 Commercial & Institutional Consumption of Energy Survey (Natural Resources Canada, 2008), the total floor area of buildings greater than 929 m^2 is estimated to 161.7 km^2.

Table 3.4: Total floor area and ground floor area of commercial and institutional buildings in Québec in 2008 [a]data from Natural Resources Canada (2008)

Building size	Total floor area	Total ground floor area
All	180.8 km^2 [a]	67.0 km^2
>929 m^2	161.7 km^2	59.9 km^2

The average year of construction of commercial and institutional buildings in Québec is 1961 (Natural Resources Canada, 2002). In 2010, the average energy intensity was 462 kWh/m^2 from which 171 kWh/m^2 is consumed for space heating (Natural Resources Canada, 2015), which is moderately higher than for residential buildings.

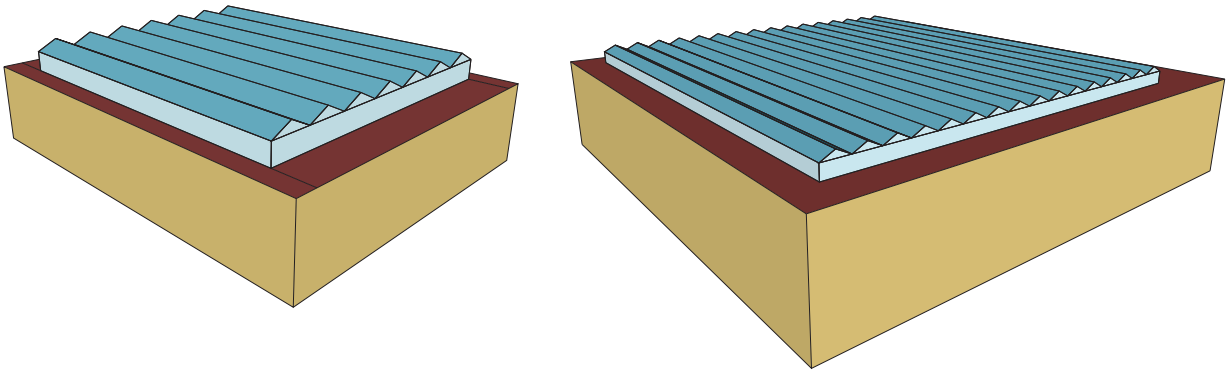

(a) 1 400 m^2, 20°W **(b)** 7 000 m^2, 20°W

Figure 3.2: Greenhouse designs — floor area and orientation

Buildings with ground floor areas of 2 000 m^2 and 10 000 m^2 have been modelled. Since roofs are often used for mechanical systems, a retrofit rooftop greenhouse covering only 70% of the roof is considered. Only one orientation at 20° west is simulated. Both are symmetrical multispan greenhouses with roof angles of 30°, wall height of 2.5 m and a span width of 5 m. The 1 400 m^2 greenhouse has seven spans while the larger 7 000 m^2 greenhouse has 16 spans, which are both depicted in Figure 2. The smaller and larger greenhouses have dimensions 40 m by 35 m and 87.5 m by 80 m respectively.

Three different greenhouse envelope designs have been considered. The conventional greenhouse design is constructed with a single pane clear glass and an interior shade with low emissivity, deployed at night. All façades/roof sections are glazed. There is a constant infiltration of 0.5 ACH and a mechanical ventilation of 5 ACH with 80% heat recovery from 9am to 4pm for humidity control during the entire heating season. The upgraded greenhouse design is equipped with high performance low iron/low emissivity/argon double-glazing. The infiltration is reduced to 0.1 ACH and the ventilation schedule remains identical. The north glazed wall is replaced with an insulated and thermally massive north wall and 100 mm of concrete is added on the floor. The high performance greenhouse design is like the previous design but with high solar gain triple glazing on the north roof sections and east/west walls. The building underneath is assumed to have a constant temperature of 20°C. The heating setpoint inside the greenhouse was set at 15°C and the excess heat above 25°C was compiled.

Table 3.5: Greenhouse design characteristics

Conventional	Upgraded	High performance
Fully glazed	North wall replaced with an insulated\massive north wall	North wall replaced with an insulated\massive north wall
Single glass	Db glass with argon\low-e	Db on south, triple elsewhere
Low-e interior shade	Low-e interior shade	Low-e interior shade
Infiltration 0.5 ACH	Infiltration 0.1 ACH	Infiltration 0.1 ACH
	100 mm of concrete on floor	100 mm of concrete on floor

3.3 Results and discussion

3.3.1 Attached solaria

The heating needs, excess heat and net energy balance of the six case studies are presented in Table 3.6. It can be seen that even conventional solaria can supply more useful heat than their heating needs with a net energy balance of 28-75 kWh/m^2 of solarium floor area. Upgraded solaria are twice as efficient and can generate a net energy balance of 118-144 kWh/m^2.

Table 3.6: Heating needs, excess heat and net energy balance of six solaria during the heating period

Design type	Conventional			Upgraded		
Solarium size and orientation	Heating needs kWh/m^2	Excess heat kWh/m^2	Net energy balance kWh/m^2	Heating needs kWh/m^2	Excess heat kWh/m^2	Net energy balance kWh/m^2
12 m^2, 20°W	33.2	108.4	75.3	15.7	158.3	142.6
12 m^2, 70°W	32.9	100.2	67.3	13.3	147.5	134.3
15 m^2, 20°W	36.9	94.3	57.5	10.3	154.5	144.1
15 m^2, 70°W	31.0	86.4	55.4	11.5	131.3	119.8
30 m^2, 20°W	29.5	82.0	52.5	5.5	141.9	136.4
30 m^2, 70°W	37.2	64.8	27.6	5.2	123.0	117.8

It is interesting to compare the energy potential of solaria per floor area, which is between 28-144 kWh/m^2, with the useful solar energy collected by water-based solar thermal panels in Montreal, which is between 150-610 kWh/m^2, depending on the size of the system (Wallin et al., 2012). The wide variation of the energy performance of solaria indicates that careful design and high quality materials must be selected in order to build a high performance solarium with the capability of collecting significant amount of heat.

Considering an average single detached house in Québec with a total floor area of 130.9 m^2 that adds an upgraded solarium, the heating consumption could be reduced by 1 612-4 092 kWh, depending on the size and design of the solarium. This would reduce the average heating requirements from 139 kWh/m^2 down to 108-127 kWh/m^2, a 9% to 23% reduction.

If 1% of all attached and detached houses in Québec would add an upgraded solarium, 31.3-79.5 GWh of solar heat could be collected.

3.3.2 Rooftop greenhouses

The heating needs, excess heat and net energy balance of the two rooftop greenhouses studied here are presented in Table 3.7. Large greenhouses used for the commercial production of vegetables must have a thermally controlled indoor climate to support satisfactory crop growth. A heating set point of 15 °C has been chosen for these simulations and the excess heat was compiled for temperatures above 25 °C. It can be seen that conventional single glazed greenhouses exhibit heating needs that exceed by far the excess heat that can be collected with a net energy balance ranging from -298 to -321 kWh/m^2.

Table 3.7: Heating needs, excess heat and net energy balance, in kWh/m^2 of greenhouse floor area, of two rooftop greenhouses during the heating period

Design	Conventional			Upgraded			High performance		
Solarium size and orientation	Heating needs	Excess heat	Net energy balance	Heating needs	Excess heat	Net energy balance	Heating needs	Excess heat	Net energy balance
1 400 m^2, 20°W	344.6	23.2	-321.4	73.2	70.4	-2.8	47.5	77.1	29.6
7 000 m^2, 20°W	320.4	22.2	-298.2	66.3	67.3	-1.0	43.2	73.9	30.7

By increasing the airtightness, adding interior thermal mass and switching to high quality double glazing, upgraded greenhouses can become fairly close to being net zero regarding their heating consumption. In other words, upgraded greenhouses have the potential to supply enough heat to adjacent buildings to compensate for their own heating consumption throughout the year and thus have a net zero heating demand.

The thermal performance of greenhouses can be further improved by converting north, east and west glazing to high solar heat gain low emissivity triple glass. Doing so allow generating a positive net energy balance of about 30 kWh/m^2. Adding a second thermal screen could be

more cost effective than selecting triple glazing and would add a lower weight. The use of two thermal screens has not been modelled here due to the inability of EnergyPlus to simulate two interior shading devices.

Covering 1% of large commercial and institutional buildings with rooftop greenhouses on 70% of their roof area would create 0.42 km^2 of cultivation area, enough to provide vegetables for about 300,000 persons.

3.3.3 Discussion

As seen from the results presented above, the heating requirements of solaria and greenhouses can exhibits large variations and are highly dependent on their design and operation. The configurations studied here have not been optimized and it is thus possible to further improve their net energy balance by doing so.

In this study, all excess heat during the heating season has been considered useful. Considering the low insulation levels and high heating requirements of the existing building stock, assuming that all excess heat would be welcome at all times in adjacent buildings is reasonable. However, for new buildings with a better envelope, this will likely not be the case and a more detailed study considering the hourly heating demand and excess heat availability would be required.

An *Ideal Loads Air System* has been selected for these simulations, which means that a 100% efficient HVAC system was assumed. Heating and cooling set points were entered in the *Thermostat* module. The ideal load assumption is realistic in the case of solaria heated with small electric baseboards, but large greenhouses are likely to be equipped with a central combustion heating system where in this case the actual efficiency of the heating system should be taken into account. The total cooling energy for a given cooling set point was interpreted in this study as the excess heat available for heating adjacent buildings during the heating season.

For the solarium models, the distribution of the solar radiation on interior surfaces is modeled by projecting the sun's ray on interior surfaces, as described in details in U.S. Department of Energy (2013) for the *Full Interior and Exterior* option. However, for the greenhouse models, the *Full Exterior* option was selected where all beam solar radiation is assumed to fall on the floor. This is a reasonable assumption in this case given the large surface of the floor compared to that of the walls.

3.3.4 Conclusion

This chapter presented an analysis of the energy saving potential of attached solaria and rooftop greenhouses for the province of Québec. Various realistic situations have been considered. A total of eighteen case studies have been simulated with the EnergyPlus building simulation software. Six different solarium designs with different sizes and orientation have been considered. Two rooftop greenhouse models with different sizes have also been simulated.

For all cases, different building envelopes have been analysed. Results indicate that the investigated solaria exhibit a net energy balance of 28-144 kWh/m^2 of solarium floor area. Retrofitting an upgraded solarium to an average house would reduce its heating consumption by 1 612-4 092 kWh, depending on the size of the solarium, which corresponds to a 9% to 23% reduction. Retrofitting an upgraded solarium to 1% of all single detached and attached houses in Québec would save 31.3-79.5 GWh annually.

Conventional greenhouses experience heating needs that far exceed their potential excess heat contribution. However, with improved air tightness, thermal load levelling and high quality double glass, net zero heating can be achieved. Surplus heat of up to 31 kWh/m^2 of greenhouse floor area can be collected when using high performance triple glazing on the northern, eastern and western orientations. Covering 1% of large commercial and institutional buildings in Québec with rooftop greenhouses could provide enough vegetables to feed 300 000 people without increasing the total energy consumption of the province.

Chapter 4

Development of a solarium model

Different solarium models have been developed in Matlab. These models are described in details in chapters 5, 6 and 7. This section presents the solar radiation models along with the convective and radiative models that are used in the three chapters cited above. The development of custom models was necessary because building simulation software currently available do not offer the flexibility and feedback (about intermediate physical parameters of interest) necessary to reach the objectives pursued in this thesis.

4.1 Solar radiation modelling

Commonly used equations for calculating the declination angle δ, the extraterrestrial radiation flux I_{on}, the hour angle H, the solar altitude α and the solar azimuth angle ϕ can be found in appendix C.

4.1.1 Solar radiation on sloped surfaces

This section presents the equations needed to calculate the direct and diffuse solar radiation incident on a surface with an arbitrary orientation from weather data. Weather files for energy calculations are available for hundreds of cities throughout the world. These weather files typically report hourly values for the direct and diffuse (or global) solar radiation.

Simple geometrical relationships can be used used to calculate the projection of the beam solar radiation on a sloped surface. The incidence angle of the beam radiation with the normal of a surface is equal to

$$\theta = \text{acos}\left(\cos(\alpha)\cos(\gamma)\sin(\beta) + \sin(\alpha)\cos(\beta)\right) \tag{4.1}$$

where γ is the solar surface azimuth which corresponds to the angle of the horizontal projection between the normal of a surface and the beam radiation. It is given by

$$\gamma = \phi - \psi \tag{4.2}$$

where ψ is the surface azimuth angle, i.e. the angle of the horizontal projection of the normal of a surface with respect to south, which is subjected to the same sign convention than ϕ. The angle β from equation 4.1 is equal to the angle between the surface and the horizontal. The beam radiation incoming on a surface with an incidence angle θ can be easily computed as the product of the direct normal radiation and the cosine of the incidence angle:

$$I_b = \text{DNR}\cos(\theta) \tag{4.3}$$

The total diffuse radiation incident on a surface is the sum of the sky diffuse and ground diffuse component:

$$I_d = I_{ds} + I_{dg} \tag{4.4}$$

The radiation reflected from the ground and hitting a surface can be calculated from the global horizontal radiation, the reflectivity of the surface ρ and the view factor between the surface and the ground:

$$I_{dg} = \text{GHR}\rho_{gr}F_{i\,gr} \tag{4.5}$$

If unavailable, the global horizontal radiation can be estimated with

$$\text{GHR} = I_{b,ho} + \text{DHR}; \tag{4.6}$$

where $I_{b,ho}$ is the direct radiation beam incident on an horizontal surface as calculated with

$$I_{b,ho} = \text{DNR}\cos(Z); \tag{4.7}$$

The Perez model (1990) presents a detailed analysis for estimating the diffuse solar radiation in the sky; this model is summarized in appendix C

4.1.2 Solar radiation distribution on interior surfaces

In most building energy simulation software, all radiation transmitted through a window is usually distributed on interior surfaces, while usually about 95% is actually retained in a room. However, for highly glazed spaces, Wall (1995) has shown that only 30%-90% of radiation transmitted through the glazing is retained in the space.

Wall (1997) also showed that simulation programs reveal important differences in the calculation of solar gains in glazed spaces. Simpler simulation programs that do not calculate accurately the solar radiation distribution overestimate significantly the absorbed solar radiation. This emphasizes the importance of using a detailed method for the calculation of solar radiation distribution in a highly glazed space.

In this model, the solar radiation transmitted through windows is distributed inside the solarium by combining ray tracing and radiosity methods. First, the transmitted beam solar radiation is distributed on interior surfaces using ray tracing techniques by calculating the area of a window illuminating directly a surface. The transmitted beam radiation directly illuminating a portion of a surface is assumed to be uniformly distributed on that surface; likewise, each surface is assumed to have a uniform temperature. The reflected component is treated as diffuse and therefore distributed with a radiosity method, along with the transmitted diffuse solar radiation.

A rectangular room with a south facing window is illustrated in Figure 4.1. It can be seen that only up to three surfaces can be illuminated directly by a beam radiation. To find the portion of the window illuminating a surface $f_{w,i}$, the coordinates of that surface need to be projected onto the window plane. $f_{w,i}$ is equal to the overlapping area between the window and the image of the surface. For instance, to find the window area illuminating the back wall $f_{w,2}$, the back wall coordinates (ABCD) are projected along the sun's ray into the window plane (A′B′C′D′).

A point P(x,y,z) can be projected into the window plane to become point P′(x′,y′) by applying the following transformation

$$x' = x + z\left(\frac{\cos(\theta_2)}{\cos(\theta_1)}\right) \tag{4.8}$$

$$y' = y + z\left(\tan^2(\theta_1) - \left(\frac{\cos(\theta_2)}{\cos(\theta_1)}\right)^2\right)^{1/2}$$

where θ_1 is the angle of incidence in the plane $z = 0$ and θ_2 is the angle of incidence on the plane $x = 0$.

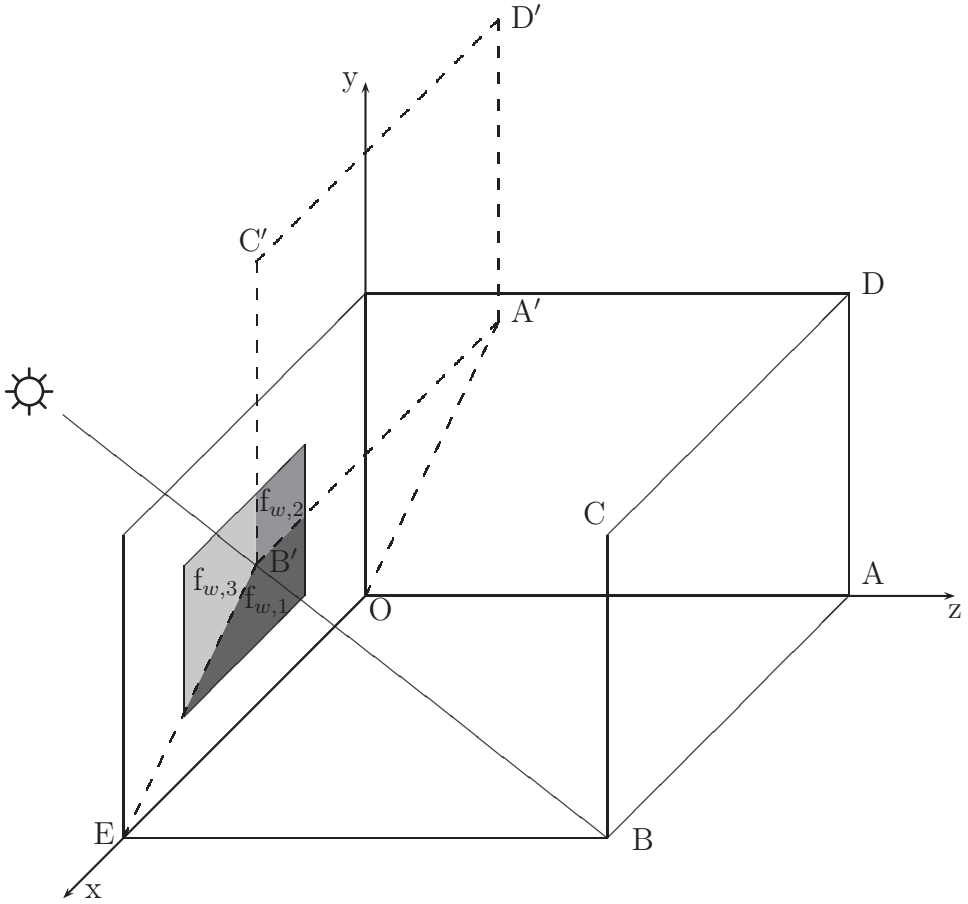

Figure 4.1: Projection of the backwall onto the window plane along a sun's ray

Once the transformation of the coordinates is performed, the overlapping area between the two polygons needs to be determined. A detailed method to compute the overlapping area between convex polygons is presented in Walton (1979). Vertices defining the overlap between two polygons A and B are either

- Vertices of A enclosed by B
- Vertices of B enclosed by A
- Intercepts of sides of A with sides of B

For a convex polygon with clockwise vertices, a point is enclosed in this polygon if it lies to the right of all sides of the polygon. For a counterclockwise polygon, a point is enclosed in the polygon if it lies to the left of all its sides. This can be determined by calculating a scalar product. Let's consider a point (x, y) represented by a three elements vector $(x, y, 1)$ and a line represented by a three elements vector (a, b, c). If $(a, b, c) \cdot (x, y, 1) > 0$, the point lies to the left of the line; similarly, if $(a, b, c) \cdot (x, y, 1) < 0$, the point is to the right of the line.

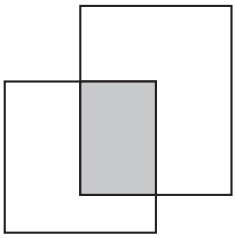

Figure 4.2: Two overlapping polygons

The intercept of lines (a_1, b_1, c_1) and (a_2, b_2, c_2) can be found with $(a_1, b_1, c_1) \times (a_2, b_2, c_2)$. However, before calculating their intercept, it should be determined if the lines intercept within their end points. Two line segments A and B intercepts if the ends of A lies to both sides of B and the ends of B lies to both sides of A. If this is the case, the dot product between line A and the two end points of B will have different signs, as well as the dot product of line B with the end points of A. Additional details on the calculation of vertices of overlapping polygons can be found in Walton (1979).

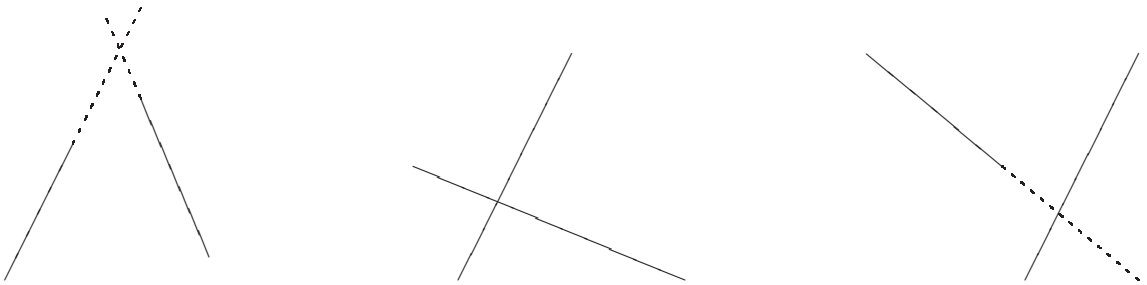

a) b) c)

Figure 4.3: Line segments

Once the vertices of the overlapped polygon are known, $f_{w,i}$ can then be computed. The solar radiation absorbed by interior surfaces in the room is calculated following the procedure presented in Athienitis and Sullivan (1985) and Athienitis and Stylianou (1991). The total beam radiation absorbed by a surface i is given by

$$S_{b,i} = \alpha_i G_b f_{w,i} + A_i \sum_j \frac{F_{ij}^d \rho_j G_b f_{w,j}}{A_j} \tag{4.9}$$

where α_i is the absorptance of surface i, G_b the transmitted beam radiation, A_i is the area of surface i, F_{ij}^d is the transfer factor and ρ_j is the reflectance of surface j. The transfer factor F_{ij}^d is the fraction of diffuse solar radiation emitted by surface j which is absorbed by surface i and is calculated with

$$F_{ij}^d = A F_{ik} M_{kj}^{-1} \tag{4.10}$$

where A is a diagonal matrix with the surfaces absorptance equal to its diagonal, F_{ik} is the view factor and M_{kj}^{-1} is the inverse of the matrix M_{kj} which is given by

$$M_{kj} = I_{kj} - \rho_k F_{kj} \tag{4.11}$$

with I being an identity matrix. Note that the first term of equation (4.9) represents the beam radiation absorbed directly by surface i while the second term represents the beam radiation absorbed as diffuse radiation after many reflections. The diffuse solar radiation transmitted through a window and absorbed by surface i is calculated with

$$S_{d,i} = A_i G_d F_{iw}^d \tag{4.12}$$

For the case of the window, one more term should be added to take into account the incoming radiation directly absorbed by the window

$$S_{d,w} = A_w G_d F_{ww}^d + A_w G_a \tag{4.13}$$

where G_a represents the incoming radiation absorbed in the glazing.

4.2 Convective heat transfer coefficients

The heat exchanged by convection between a surface i and the air is expressed as

$$Q = A_i \, h_c \, (T_{in} - T_i) \tag{4.14}$$

where h_c is a convective coefficient. The convective heat transfer between a surface and the air depends mainly on the position of the surface (horizontal/vertical) and the temperature difference between the surface and the air. Many correlations have been developed to characterize natural, mixed or forced convection. For an interior surface in a room, the air velocity is relatively low and therefore correlations for natural convection may be employed. Khalifa and Marshall (1990) developed correlations for the calculation of the heat transfer convective coefficient of interior building surfaces. They found that for a vertical glazing (with no radiator under the window), a vertical wall and an horizontal surface (facing upward), the convective heat transfer coefficient may be estimated with

Vertical glazing	$h_c = 7.61(\Delta T)^{0.06}$	(4.15)
Vertical wall	$h_c = 2.03(\Delta T)^{0.14}$	(4.16)
Horizontal surface	$h_c = 2.27(\Delta T)^{0.24}$	(4.17)

where ΔT is the temperature difference between the surface and the air. The convective coefficient representing the effect of wind on the exterior surface of a building is calculated with (Duffie and Beckman, 2006)

$$h_{c,w} = \frac{8.6 v_w^{0.6}}{L^{0.4}} \tag{4.18}$$

where L is the cube root of the solarium volume. Convective coefficients for air spaces between window panes and between windows and shading devices are calculated following the procedure outlined in ISO 15099 (2003) for thermally driven ventilation. The convective coefficient in a ventilated gap is given by

$$h_{c,v} = 2h_{c,nv} + 4v_{\text{mean}} \tag{4.19}$$

where $h_{c,nv}$ is the convective coefficient for non-vented cavities. A pressure-balance equation is used to determine the mean air velocity in the cavity and other variables of interest like the outlet air temperature in the gap. The heat balance equations are solved iteratively until they converge. The mean air velocity in the cavity is determined from

$$v_{\text{mean}} = \frac{\left[\left(\frac{12\nu\rho H_g}{L^2}\right)^2 + \frac{2\rho(1+Z_{in}+Z_{out})\rho_o T_o g H_g \sin\beta\,|T_{gap,in} - T_{gap}|}{T_{gap,in} T_{gap}}\right]^{1/2} - \frac{12\nu\rho H_g}{L^2}}{\rho(1+Z_{in}+Z_{out})} \tag{4.20}$$

where ν is the kinematic viscosity, H_g is the height of the glazing, L is the cavity width, Z_{in} and Z_{out} are the inlet and outlet pressure drop factors, β is the angle between the glazing and the horizontal, $T_{gap,in}$ is the gap inlet temperature, T_{gap} is the mean gap air temperature, the subscript $_o$ refers to a glazing height of zero and other symbols were previously defined.

Equations for calculating $h_{c,nv}$, Z_{in}, Z_{out} and T_{gap} and details about the iteration procedure are given in the Engineering Reference documentation of EnergyPlus (U.S. Department of Energy, 2013) and in ISO 15099 (2003). The equation for v_{mean} contains an error in the EnergyPlus reference; the equation above has been corrected.

4.3 Radiative heat transfer models

Long wave radiation exchanges between interior surfaces can be modeled using the Gebhart method (Gebhart, 1959; Siegel and Howell, 1981; Mottard and Fissore, 2007). In this case, the net radiation flux emitted by a surface i is calculated as

$$q_{LWR,i} = -\epsilon_i A_i \sigma \sum_{j=1}^{n} G_{ij} \left(T_i^4 - T_j^4\right) \tag{4.21}$$

where n is the number of surfaces and G_{ij} is a Gebhart coefficient. The sign is negative because the flux is leaving the surface. The n^2 Gebhart coefficients, which depend on the geometry and thermal properties of the surfaces, can be obtained by solving

$$\begin{pmatrix} (1-\rho_1 F_{11}) & -\rho_2 F_{12} & -\cdots & -\rho_n F_{1n} \\ -\rho_1 F_{21} & (1-\rho_2 F_{22}) & -\cdots & -\rho_n F_{2n} \\ -\cdots & -\cdots & \ddots & -\cdots \\ -\rho_1 F_{m1} & -\rho_2 F_{m2} & -\cdots & (1-\rho_n F_{mn}) \end{pmatrix} \begin{pmatrix} G_{1k} \\ G_{2k} \\ \vdots \\ G_{nk} \end{pmatrix} = \begin{pmatrix} F_{1k}\epsilon_k \\ F_{2k}\epsilon_k \\ \vdots \\ F_{nk}\epsilon_k \end{pmatrix} \tag{4.22}$$

Longwave radiation exchange between an exterior surface and the ground, sky and air is calculated with

$$q_{LWR,o} = A_i \big(h_{r,gnd} \left(T_{gnd} - T_i\right) + h_{r,sky} \left(T_{sky} - T_i\right) + h_{r,air} \left(T_o - T_i\right) \big) \tag{4.23}$$

where the sky temperature is calculated from the atmospheric temperature (ASHRAE, 2007) and the ground temperature is assumed to be the same as the air temperature. The linearized radiative coefficients are calculated as

$$h_{r,gnd} = \frac{\epsilon \sigma F_{gnd} (T_i^4 - T_o^4)}{T_i - T_o} \tag{4.24a}$$

$$h_{r,sky} = \frac{\epsilon \sigma F_{sky} (T_i^4 - T_{sky}^4)}{T_i - T_{sky}} \tag{4.24b}$$

$$h_{r,air} = \frac{\epsilon \sigma F_{air} (T_i^4 - T_o^4)}{T_i - T_o} \tag{4.24c}$$

Radiative heat transfer between panes of glass and window/shade cavities are calculated based on the fundamental equation for two infinite parallel plates

$$q_{LWR,1\to 2} = \frac{A_i \sigma \left(T_2^4 - T_1^4\right)}{\dfrac{1}{\epsilon_1} + \dfrac{1}{\epsilon_2} - 1} \tag{4.25}$$

Chapter 5

Methodology for selecting fenestration systems in heating dominated climates

Based on a published paper:

Bastien, D. and Athienitis, A. 2015a. Methodology for selecting fenestration systems in heating dominated climates. *Applied Energy*, 154, 1004-1019.

5.1 Chapter abstract

Selecting optimum windows in heating dominated climates is a complex task because of the inherent trade-off between their U-value and solar heat gain coefficient. In addition, the use of shades is known to reduce heat losses, but they are rarely selected for this intent and considered as an integrated fenestration system at the design stage. This paper presents a method for selecting optimum fenestration systems (windows with shades) to maximize the annual net energy balance. The method has the capability to simulate a one or two layer shading system with one exterior and/or one interior planar shade(s). This methodology generates 2D schematics indicating the net energy balance of different fenestration systems. Such schematics are useful at an early design stage when there is a need to compare different design options for different orientations on a relative basis.

Diagrams are presented for five glazings with an interior roller shade, an exterior roller shutter and a combination of both, for the four cardinal orientations for the city of Montreal, Canada. A comparison of simulated and experimental U-values of four shading devices indicates results reasonably close to each other.

5.2 Introduction

With increasing awareness to climate change and sustainable development, many studies have been conducted on improving the energy efficiency of buildings due to their important energy consumption. Indeed, in Canada, the energy consumed by the residential and commercial sectors represented 29% of the total energy use in 2012 (Natural Resources Canada, 2015), most of which used by buildings.

Virtually all previous research agree on the importance of windows and shading systems on the energy consumption of buildings (Tzempelikos et al., 2007; Ochoa et al., 2012; Lee et al., 2013; Koo et al., 2014; Huang et al., 2014; Hee et al., 2015). For instance, a Canadian study on high-rise residential buildings has reported that windows were responsible for an average of 31% of total energy loss (CMHC, 1996).

Selecting optimal windows is more complicated than opaque envelope components since the performance of windows is governed by two major variables: the solar heat gain coefficient (SHGC) and the thermal resistance. In cold climates, it is desirable to have windows with both high thermal resistance and SHGC so as to optimize utilization of solar gains. The resistance of a window may be increased by adding a supplementary pane of glass, applying a low emissivity coating and using an inert gas such as argon or krypton in the cavity. However, the former two options also reduce the SHGC, which could lead to an increased heating demand. In addition, windows are one the most expensive component in a house (on a unit area basis). As a result, the selection of windows (and their area) is one of the most problematic aspect of Net-Zero Energy Buildings (Proskiw, 2010).

Windows with different orientations are not affected by these two variables to the same extent: an equatorial-facing window (referred to as south facing in the rest of the paper) will have a better performance with a high SHGC while it is more beneficial for a north window to have a lower U-value (Karlsson and Roos, 2001). Thus selecting different windows for different orientations could reduce the energy consumption of buildings.

Moreover, the use of shading devices, and their operation if moveable, affects the performance of windows, altering their thermal performance and solar gains. An extensive study of various window attachments estimated through simulations that simple shading devices like interior roller shades and exterior solar screens could improve the U-value of a double glazed low emissivity window by 3-45% and 26-39% respectively, depending on the characteristics of the shading device (Curcija et al., 2013).

5.2.1 Background

For improving the performance of façades, it has been suggested to divide the window area into two parts: the daylighting section at the top and the view section below. Since glazing below the workplane does not contribute significantly to daylighting and is detrimental for the building energy consumption (Schumman et al., 2013), this section is better opaque, thus creating a three-section façade concept as described by Tzempelikos (2005) where ideally the view section provides diffuse light only. Schumman et al. (2013) suggested to use high transmission glass at the upper section and lower transmission glass in the view section for controlling glare, with additional forms of solar control for both sections. Tzempelikos et al. (2007) suggested to use automated venetian blinds for the upper part and manually controlled roller shade for the lower part of the window for high daylight autonomy and comfort and low energy consumption.

As noted by Tzempelikos and Athienitis (2007), cooling may be important in perimeter zones even in heating dominated climates, indicating that shading is a necessity. Because of the importance of shading devices on the performance of buildings, a few general recommendations will be reported here. For additional guidelines regarding shading strategies, one may refer to Schumman et al. (2013).

Shading type and properties should vary with orientation, since their performance indices are very sensitive to this variable (Tzempelikos and Athienitis, 2007).

Exterior shading is more effective than interior shading for blocking solar gains. Interior shading devices should be light-coloured to better reflect solar radiation. For exterior shading devices, horizontal forms should be preferred for a south façade, such as overhangs and awnings, while vertical forms should be preferred for a east, west and north façades, such as vertical fins. It is also good practice to have different shading solutions that can be managed independently for the view and daylight sections (Schumman et al., 2013).

Ochoa et al. (2012) have found that east and west windows have the highest energy consumption, Lee et al. (2013) have noted that the energy performance of east and west windows being more sensitive to changes in SHGC and visible transmittance and Huang et al. (2014) have identified east and west orientations as having the most potential for reducing the energy consumption of a building using shading devices. These observations indicate that special care must be taken when designing east and west windows and their protections.

Nielsen et al. (2011) noted that north windows with no shadings or fixed shadings are a relevant alternative, but suggests the use of automated venetian blinds for improving the daylight availability of large windows of other orientations.

Since shading devices play an important role in the energy performance of buildings, some tools have been developed to facilitate the task of selecting windows and window-shade systems (the latter being referred to as fenestration systems throughout this study).

5.2.2 Existing tools and research needs

Many tools already exist to help selecting windows and fenestration systems. Programs such as WINDOW (and its companion software THERM and RESFEN) (LBNL, 2014, 2005), WIS (WinDat, 2004) and ParaSol (Lund University, 2010) are stand-alone tools that calculate the solar and thermal properties of windows, which may be accompanied with some types of shading devices. WINDOW and WIS are mainly used for certification purposes as they carry out simulations at fixed conditions, usually chosen to match a specific standard. RESFEN and ParaSol offer the possibility of calculating annual heating and cooling loads associated with windows. There are also whole building energy simulation software with the capability of carrying detailed heat transfer calculations through windows and fenestration systems like EnergyPlus (U.S. Department of Energy, 2013), TRNSYS (Klein and al., 2010) and ESP-r (ESR U, 2011). A more detailed description of these software can be found in (Loutzenhiser et al., 2007), (Tzempelikos, 2008) and in (Rogalsky, 2011).

Nielsen et al. (2001) presented a method for comparing the energy performance of glazings or windows for heating dominated buildings. The net energy gain is calculated for the heating season and is equal to the solar gains minus the heat losses through the glazing. Following this method, diagrams presenting the net energy gain for different combinations of SHGC and U-values are generated for a specific orientation. These diagrams are useful since they allow to quickly visualize what is the optimum window for a given orientation. Heat gains can be reduced by employing a shading coefficient to represent overhangs or obstructions, but only a fixed value for the year can be simulated. This simple method can be used either with glazings or whole windows, but cannot evaluate the impact of shading devices.

For achieving low energy buildings with satisfactory indoor climate, the designers have to be aware as early as possible of the consequences of critical design decisions (Hviid et al., 2008). Tools with simplified input are needed for supporting decisions in the early design stages of a building (Nielsen, 2005).

The most accurate way of analyzing the performance of windows and shading devices is with detailed dynamic energy building simulations for a specific building and climate (Tzempelikos and Athienitis, 2007). Lee et al. (2013), among others, have identified different optimal window properties in different climates and different optimal window properties for different orientations in the same location. These results emphasize the need of evaluating different window properties when designing energy efficient buildings. However, analyzing multiple coupled variables such window size and type, shading type, properties and control, for all four orientations of a building can yield to a very large solution space.

One way to reduce the solution space of whole building simulations is to first use single space models to identify optimum shade designs and then analyze the identified optimums with whole building simulations, an approach followed by Orsi (2009).

As an alternative, the methodology described in this paper can be used first to identify optimum glazing and shading combinations as a function of orientation before carrying whole building simulations. Once implemented, the proposed methodology can be readily used at the design stage for a new project and requires significantly less effort that developing new single space building models.

5.2.3 Objectives and overview

After reviewing the existing tools, it can be seen that there is a need to develop a simple tool to be used at the preliminary design stage allowing the comparison of the net energy balance of various fenestration systems. The influence of the shades on the SHGC and U-value of the fenestration system must be accounted for in the energy balance. In addition, the control of shades should be customizable.

The goal of this paper is to present a methodology for selecting optimum fenestration systems. It has the capability of calculating the net energy gain of windows with one interior and/or one exterior shade(s), which covers most important cases. This methodology can be used independently or as an early stage design tool for identifying fenestration systems with the best performance before running whole building simulations.

The section 5.3 below presents the methodology for comparing the net energy balance of unshaded glazings, glazings with an exterior shade, glazings with an interior shade and glazings with both interior and exterior shades. It is based from (Nielsen et al., 2001), where some modifications were introduced to increase its accuracy and where the capability of analyzing shades has been integrated. Applications and limitations of this methodology are detailed

in section 5.4 along with some recommendations. Results are then presented in section 5.5, where diagrams for glazings with an interior roller shade, an exterior roller shutter and a combination of both are presented for the four cardinal orientations for the city of Montreal. Finally, section 5.6 presents a comparison of experimental and simulated U-values for four types of shading devices.

The methodology presented in this paper can be used for comparing either glazings or complete windows. For clarity, equations are presented for glazings only throughout this paper. Appendix 5.3.3 describes how to adapt the calculations for investigating complete windows.

5.3 Methodology for selecting fenestration systems

Canadian Weather for Energy Calculations (CWEC) files were used for this study. Any hourly weather data freely available on the U.S. Department of Energy (2015) website can be downloaded and serve as input. The inputs required are the time and day of the year, outdoor temperature, global horizontal radiation, direct normal radiation and diffuse horizontal radiation.

5.3.1 Unshaded glazings

5.3.1.1 Calculating net energy gain

The net energy gain (or loss) through a glazing or a window is calculated as

$$\bar{Q} = SHGC \cdot \bar{I} - U \cdot D \tag{5.1}$$

where SHGC and U are the solar heat gain coefficient and U-value of the glazing or window and $\bar{I}$ and D are given as

$$\bar{I} = \eta F_s \sum_t \left(I_b \, g_j(\theta) \Delta t' + I_d f_j \Delta t' \right) \quad \text{for } \; T_o < T_b \tag{5.2}$$

$$D = \sum_t (T_i - T_o) \Delta t' \quad \text{for } \; T_o < T_b \tag{5.3}$$

I_b and I_d are given in section 4.1.1 where the sky diffuse radiation is modeled with the Perez model (Perez et al., 1990). The angular profile g_j is used to approximate the dependency of the SHGC to the incidence angle. f_j represents the ratio of the SHGC for diffuse radiation to the SHGC at normal incidence. It is calculated with (Finlayson et al., 1993)

$$f_j = 2 \int_0^{\pi/2} g_j(\theta) sin(\theta) cos(\theta) \tag{5.4}$$

f_j and g_j are provided in table 5.1 as a function of the number of panes j. Although the angular profiles have been determined for clear glass, they have shown a mean average error of 1% and a maximum error of 5% when used with a variety of coated glass (Karlsson et al., 2001). A more detailed polynomial method presented in the work cited above can be used if a higher accuracy is required.

Table 5.1: Angular profiles, from Karlsson et al. (2001)

θ	g_1	g_2	g_3
0	1	1	1
5	0.9999	0.9998	0.9997
10	0.9994	0.9992	0.9989
15	0.9987	0.9980	0.9975
20	0.9975	0.9962	0.9954
25	0.9956	0.9936	0.9924
30	0.9928	0.9897	0.9882
35	0.9886	0.9841	0.9825
40	0.9823	0.9758	0.9743
45	0.9728	0.9636	0.9622
50	0.9585	0.9450	0.9436
55	0.9368	0.9162	0.9132
60	0.9034	0.8710	0.8625
65	0.8522	0.8003	0.7789
70	0.7740	0.6927	0.6507
75	0.6564	0.5412	0.4796
80	0.4865	0.3537	0.2905
85	0.2597	0.1592	0.1209
90	0	0	0
	f_1	f_2	f_3
Hemispherical	0.9114	0.8854	0.8748

T_{in} from equation 5.3 is the average interior temperature during the heating season. Equations 5.2 and 5.3 are computed only when the outdoor temperature T_o is below the balance temperature T_b. The balance temperature is usually defined as the value of the outdoor temperature when the internal and solar gains are equal to the building heat losses (ASHRAE, 2009, Chapter 19). However, the solar gains are actually useful for eliminating heating needs

and thus their contributions should be accounted for here. Therefore, the balance temperature used here should consider internal gains only and can be calculated from

$$Q = UA_e(T_{in} - T_b) \tag{5.5}$$

where here U is the overall building U-value, including infiltration and A_e is the total building envelope area. For residential buildings, the internal gains (in W) can be estimated with (ASHRAE, 2009, Chapter 17)

$$Q = 136 + 2.2A_{floor} + 22N_{oc} \tag{5.6}$$

The balance temperature could be 1 °C lower than T_{in} for old houses with little insulation while it could be 5 °C lower for highly insulated houses like passive houses. For non-residential buildings, internal gains should be determined accordingly to the expected building occupancy and equipment. One may refer to ASHRAE (2009, Chapter 18) for more details.

To avoid considering useful heat gains in the hot season when no heating is used, equations 5.2 and 5.3 should be computed only during the heating season and transitional periods.

F_s in equation 5.2 represents a shading factor. This factor represents shading from distant objects, window reveals and fixed exterior shadings. It is possible to use a fixed value throughout the year, or, as an alternative, monthly shading factors for various types of external shading elements can be obtained with ParaSol (Lund University, 2010). [1]

The value of the utilization factor η in equation 5.2 should be very close to 1. This method is intended for buildings in heating dominated climates aiming at a high solar utilization, in which case the solar gains as calculated with equation 5.2 are practically always useful. Please refer to section 6.6 for further details about the applications and limitations of this methodology.

5.3.1.2 Generating net energy gain diagram

Equations 6.6, 5.2 and 5.3 are then used to generate lines of constant energy gains or losses. First, an array of energy gains (or losses) is defined, in kWh/m^2 of window area. For instance, in figure 5.1, $\bar{Q}$ is an array between -300 and 500 kWh/m^2 with an increment of 50 kWh/m^2.

[1] In this software, the f(g) output variable represents the shading factor of the obstruction under consideration. The graphical output can be easily exported to a text file and then imported for use with this methodology.

Secondly, an array of possible SHGC must also be defined. Then, the user must determine the number of panes he is primarily interested in, for comparison purposes. Using the corresponding corrected incident solar radiation $\bar{I}$, from equation 5.2, an array of U-values required to achieve a specific energy performance is calculated from isolating U in equation 6.6. Plotting the SHGC array as a function of these U-values generates a diagram with lines of constant net energy gains (or losses).

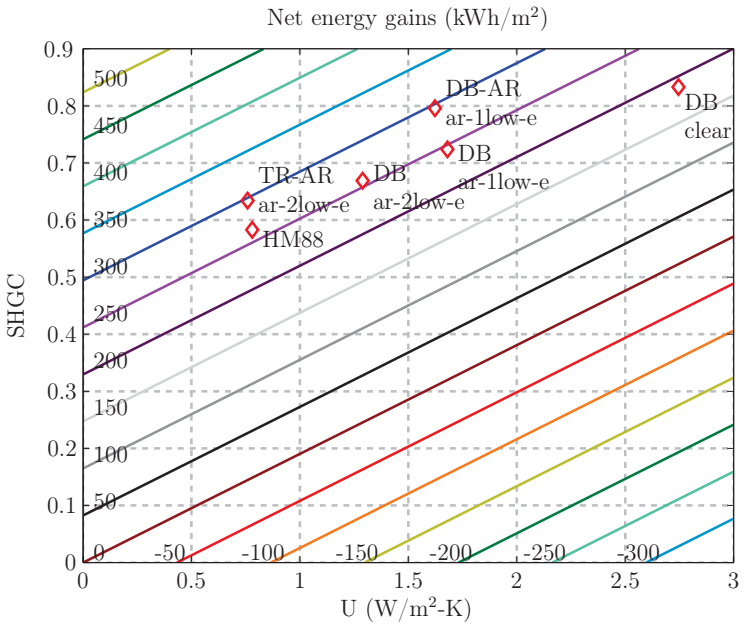

Figure 5.1: Net energy gains (in kWh/m^2) of six glazings for a south orientation in Montreal during the heating period ranging from 15/09 to 15/05 with F_s=0.9, η=1 and T_b=20°C. DB=Double; TR=Triple; AR=antireflective coating; ar=argon; low-e=low emissivity; HM88=DB glazing with suspended low-e plastic film.

After entering the U-value and SHGC of a few glazings of interest, their performance can then be easily compared for a given orientation. Figure 5.1 shows the performance of six different glazings on a south façade in Montreal.

The corrected incident radiation for single, double and triple glazings is presented in table 5.2 for Montreal for the conditions described in figure 5.1. The constant net energy gain lines in this figure have been calculated for a double glazing. Although both double and triple window products are depicted on the figure, it can be seen from table 5.2 that the difference between the corrected incident radiation for single and double glazing is 2.2% and for double and triple glazing is less than 1%. Therefore, it is possible to compare glazings with a different number of panes on the same graphic with a reasonable accuracy.

Table 5.2: Corrected incident solar radiation for a single, double and triple glazing

$\bar{I}_1$	$\bar{I}_2$	$\bar{I}_3$
621 kWh/m^2	607 kWh/m^2	602 kWh/m^2

5.3.2 Glazings with shading devices

The shade is assumed to cover the glazing only. Single, double and triple glazings can be analyzed with the presence of an exterior or interior shade, or a combination of both.

The required inputs for glazings and shades are summarized in table 5.3. Ideally, the solar transmittance and absorptance of window panes should be known. However, as an alternative, this paper presents tables to estimate these values for single, double and triple glazing where only the composition of the gas infill is required. In rare cases, if the emissivity of the outermost or innermost pane is different than 0.84, then it should be specified.

Shades can be controlled based on a hourly schedule, a solar radiation set point or on more detailed conditions determined by the user. It is also possible to use another program to perform a more complete thermal analysis to determine an annual operation schedule and import it into this methodology.

Table 5.3: Inputs parameters ([a]optional, for the analysis of windows only)

Glazing
U-value
SHGC
Solar transmittance and absorptances OR Gas infill and nb of panes
Emissivity of outermost and innermost panes, if $\neq 0.84$
Height and width of glazing (or window*)
Window U-value[a]
Window area[a]
Shade
Emissivity of both sides (typically ≈ 0.9)
Thermal resistance OR thermal conductivity and thickness
Solar absorptance
Solar transmittance
Solar reflectance of the window facing side
Cavity width between the shade and the window
Openness factor
Top/bottom/left/right opening area between the shade and glass

U-values of fenestration systems are calculated based on interior and exterior temperatures T^*_{in} and T^*_o as defined in NFRC 100-2004 (2004) (T^*_o=-18°C and T^*_{in}=21°C) for North America or in ISO 15099 (2003) (T^*_o=0°C and T^*_{in}=20°C) for Europe.

5.3.2.1 Glazings with exterior shade

First, the U-value of the window without the exterior heat transfer coefficient is calculated

$$U'_{\text{øh}_{ext}} = \frac{1}{1/U_g - 1/h_{ext}} \tag{5.7}$$

$$h_{ext} = h_{c,ext} + h_{r,ext} \tag{5.8}$$

with $h_{c,ext} = 26\,W/(m^2K)$ for north American windows (NFRC 100-2004, 2004) or $20\,W/(m^2K)$ for European windows (ISO 15099, 2003). $h_{r,ext}$ is calculated with

$$h_{r,ext} = \frac{\epsilon_{w,o}\sigma(T^4_{w,o} - T^{*4}_o)}{(T_{w,o} - T^*_o)} \tag{5.9}$$

$T_{w,o}$ is determined from an energy balance at the environmental conditions, as defined in NFRC 100-2004 or ISO 15099. $T_{w,o}$ and $h_{r,ext}$ are calculated iteratively until convergence. Secondly, the resistance of the air cavity between the shade and the window must be evaluated. The radiative coefficient exchange between the outer pane of the window and the shade is calculated with

$$h_r = \frac{\sigma(T^2_{w,o} + T^2_{s,i})(T_{w,o} + T_{s,i})}{1/\epsilon_{w,o} + 1/\epsilon_{s,i} - 1} \tag{5.10}$$

The convective coefficient in the air cavity is calculated following the procedure outlined in ISO 15099 (2003) for thermally driven ventilation. The convective coefficient in a ventilated gap is given by

$$h_{c,v} = 2h_{c,nv} + 4v_{\text{mean}} \tag{5.11}$$

where $h_{c,nv}$ represents the convective coefficient in a non vented cavity. A pressure-balance equation is used to determine the mean air velocity in the cavity and other variables of interest. The heat balance equations are solved iteratively until convergence is reached. More details about the procedure for calculating $h_{c,nv}$ and v_{mean} can be found in (ISO 15099, 2003) or in the documentation of EnergyPlus where the equations are all clearly stated (U.S. Department of Energy, 2013). The total thermal conductance of the air cavity is given by

$$h_{ExtS} = h_{c,v} + h_r \tag{5.12}$$

The exterior radiative coefficient $h_{r,ext}$ must be recalculated based on the temperature of the shade. The exterior convective coefficient $h_{c,ext}$ remains unchanged. Because the calculation of the radiative coefficient depends on the temperature of the surfaces, energy balance equations must be solved iteratively until convergence is reached. The U-value of the whole fenestration system is finally calculated as

$$U_{ExtS} = \frac{1}{1/U'_{\text{øh}_{ext}} + 1/h_{ExtS} + R_{ExtS} + 1/h_{ext}} \tag{5.13}$$

Figure 5.2 summarizes the process for calculating the equivalent U-value. The net energy gain must be calculated hourly taking into account if the shade is present or not:

if shade is absent

$$\bar{Q}'_t = SHGC_g \bar{I}_j - U_g\big(T_{in} - T_o\big)$$
$$U'_{\text{t}} = U_g$$

else

$$\bar{Q}'_t = SHGC_{ExtS} \bar{I}_j - U_{ExtS}\big(T_{in} - T_o\big)$$
$$U'_{\text{t}} = U_{ExtS} \tag{5.14}$$

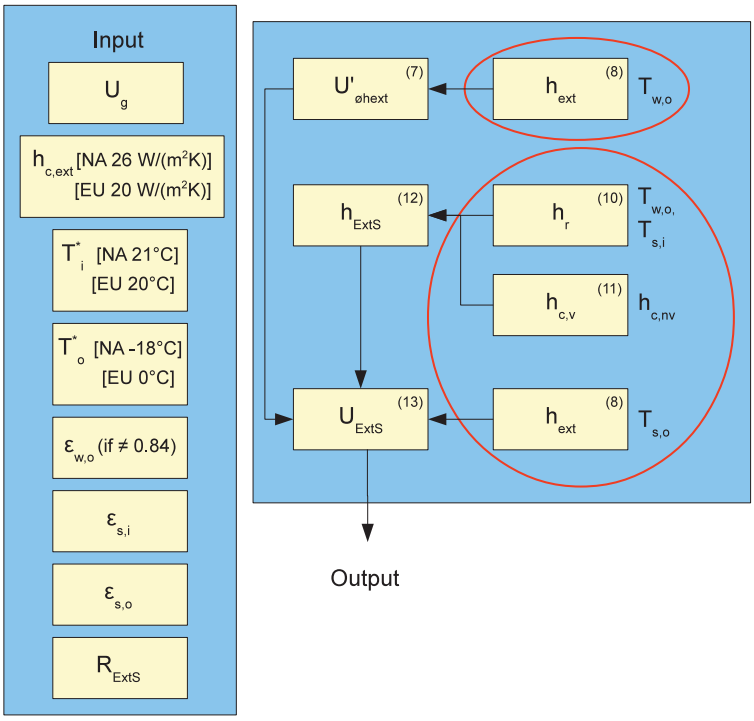

Figure 5.2: Flow chart for calculating the equivalent U-value of a fenestration system with an exterior shade. The ovals indicate that calculations are made iteratively until convergence is reached.

The effective U-value of the fenestration system is simply the average of U'_{t} and the net energy gain is the hourly sum of $\bar{Q}'_t$

$$U_{\mathrm{eff}} = \mathrm{avg}(U'_{\mathrm{t}}) \tag{5.15}$$

$$\bar{Q} = \sum_t \bar{Q}'_t \tag{5.16}$$

The effective solar heat gain is calculated with

$$SHGC_{\mathrm{eff}} = \frac{(\bar{Q} + U_{\mathrm{eff}} D)}{\bar{I}} \tag{5.17}$$

where $\bar{I}$ and D are calculated from equations 5.2 and 5.3. Situating (U_{eff},$SHGC_{\mathrm{eff}}$) on a net energy gain diagram will indicate the net energy balance of the investigated fenestration system. Note that $SHGC_{\mathrm{eff}}$ is used only to situate the net energy balance $\bar{Q}$ on the graph. While it gives an indication about how the shade and its control are reducing the equivalent solar heat gain of a fenestration system, it has no explicit physical meaning. Under some circumstances, its value can be above the SHGC at normal incidence of a bare window.

The presence of a shade affects not only the U-value of a fenestration system but also its SHGC. The SHGC of a fenestration system depends on the solar transmittance and absorptance of the different layers (ISO 15099, 2003):

$$SHGC_{1g} = \tau + \alpha_1 \frac{U}{h_{ext}} \tag{5.18a}$$

$$SHGC_{2g} = \tau + \alpha_1 \frac{U}{h_{ext}} + \alpha_2 \frac{(h_{int} - U)}{h_{int}} \tag{5.18b}$$

$$SHGC_{3g} = \tau + \alpha_1 \frac{U}{h_{ext}} + \alpha_2 U \left(\frac{1}{h_{ext}} + \frac{1}{\Lambda_{12}} \right) + \alpha_3 \frac{(h_{int} - U)}{h_{int}} \tag{5.18c}$$

$$SHGC_{4g} = \tau + \alpha_1 \frac{U}{h_{ext}} + \alpha_2 U \left(\frac{1}{h_{ext}} + \frac{1}{\Lambda_{12}} \right) + \alpha_3 U \left(\frac{1}{h_{ext}} + \frac{1}{\Lambda_{12}} + \frac{1}{\Lambda_{23}} \right) + \alpha_4 \frac{(h_{int} - U)}{h_{int}} \tag{5.18d}$$

where Λ_{ij} represents the thermal conductance of the cavity between elements i and j, as depicted in figure 5.3. The thermal resistance of the glass is always very small and therefore neglected, but the thermal resistance of the shade is accounted for since it could be significant in some cases. Layers are numbered with #1 being the outermost layer.

It is assumed that the dependency of the SHGC of the shading material with the incidence angle is identical as the glazing under investigation. This assumption seems reasonable especially with some shading materials like roller shades and insect screens where the analysis of their beam total transmittance was shown to exhibit a similar trend than glass (Kotey et al., 2009b,d). The total transmittance of a glazing with an outer shade is calculated with

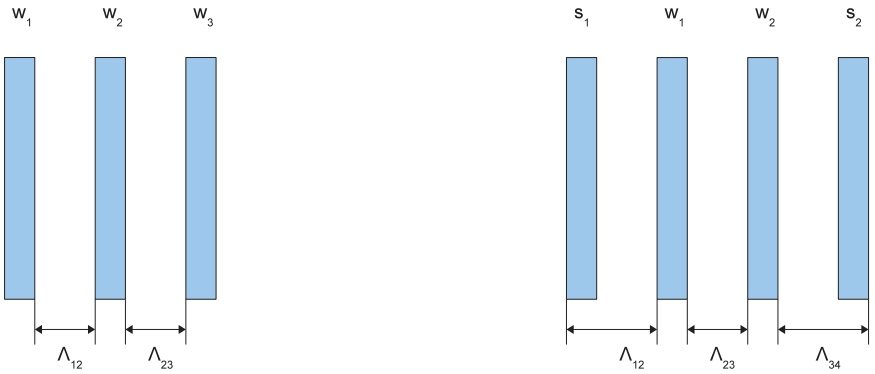

(a) Triple glazing **(b)** Double glazing with exterior and interior shades

Figure 5.3: Illustration of the thermal conductances Λ_{ij} for different configurations

$$\tau_{ExtS} = \frac{\tau_s \tau_g}{1 - \rho'_s \rho_g} \tag{5.19}$$

Glazings, either single, double or triple, are considered as a single element with their solar transmittance estimated with tables A.1 - A.3 if actual data is not available. The prime in equation 5.19 refers to the spectral reflectance measured in the opposite direction of the incident solar radiation. The typical solar reflectance of uncoated glass is 0.08.

As seen in equations 5.18, calculating the SHGC of a window with a shade requires the knowledge of the solar transmittance and absorptance of the window panes. Ideally, they should be specified as input. As an alternative, a simple method estimating the solar transmittance and absorptances of a glazing from its U-value, SHGC and gas infill has been developed and is presented in tables A.1, A.2 and A.3 in Appendix A. The absolute average and maximum associated errors and shown in table A.4.

The total SHGC of a fenestration system that consists of an outer shade and a single, double or triple glazing is calculated with

$$SHGC_{1gExtS} = \tau_{ExtS} + \alpha_s \frac{U_{ExtS}}{h_{ext}} + \tau_{ExtS}\alpha_g \frac{(h_{int} - U_{ExtS})}{h_{int}} \tag{5.20a}$$

$$SHGC_{2gExtS} = \tau_{ExtS} + \alpha_s \frac{U_{ExtS}}{h_{ext}} + \tau_{ExtS}\alpha_{g1} U_{ExtS}\left(\frac{1}{h_{ext}} + \frac{1}{h_{ExtS} + 1/R_{ExtS}}\right) + \tau_{ExtS}\alpha_{g2}\frac{(h_{int} - U_{ExtS})}{h_{int}} \tag{5.20b}$$

$$\begin{aligned} SHGC_{3gExtS} = {} & \tau_{ExtS} + U_{ExtS}\frac{\alpha_s + \tau_{ExtS}\alpha_{g1} + \tau_{ExtS}\alpha_{g2} + \tau_{ExtS}\alpha_{g3}}{h_{ext}} \\ & + U_{ExtS}\frac{\tau_{ExtS}\alpha_{g1} + \tau_{ExtS}\alpha_{g2} + \tau_{ExtS}\alpha_{g3}}{(1/h_{ExtS} + R_{ExtS})^{-1}} \\ & + U_{ExtS}\frac{\tau_{ExtS}\alpha_{g2} + \tau_{ExtS}\alpha_{g3}}{\Lambda_{23}} + U_{ExtS}\frac{\tau_{ExtS}\alpha_{g3}}{\Lambda_{34}} \end{aligned} \tag{5.20c}$$

In the case of a triple glazing with an exterior shade, the insulating value of the glass cavities, Λ_{23} and Λ_{34}, should be known to determine the SHGC of the fenestration system. This would require the knowledge of the emissivity of panes #2, #3 #4 and #5 as well as the cavity thicknesses and gas infill. If this information is known, Λ_{23} and Λ_{34} can be calculated using equation 3 from ISO 10292 (1994). Alternatively, they can be approximated with

$$\Lambda_{23} = \Lambda_{34} = \frac{1}{\left(\frac{1}{U_g} - \frac{1}{h_{ext}} - \frac{1}{h_{int}}\right)/2} \tag{5.21}$$

where h_{ext} is calculated using equation 5.8 and h_{int} can be calculated with equation 5.23 from section 5.3.2.2.

5.3.2.2 Glazings with interior shade

As a first step, the U-value of the window without the interior heat transfer coefficient is estimated from

$$U'_{\text{ø}h_{int}} = \frac{1}{1/U_g - 1/h_{int}} \tag{5.22}$$

where

$$h_{int} = h_{c,int} + h_{r,int} \tag{5.23}$$

The interior radiative coefficient $h_{r,int}$ is calculated with (ISO 15099, 2003)

$$h_{r,int} = \frac{\epsilon_{w,i}\sigma(T_{w,i}^4 - T_i^{*4})}{(T_{w,i} - T_i^*)} \tag{5.24}$$

The interior convective coefficient is calculated with

$$h_{c,int} = \frac{Nu\,k}{H_g} \tag{5.25}$$

where Nu is calculated as described in ISO 15099 (2003, section 8.2.1.1) and k is the thermal conductivity of air. Then, the resistance of the air cavity between the shade and the window must be evaluated. The radiative coefficient exchange between the inner pane of the window and the shade is calculated as in equation 5.10 where $T_{w,o}$ is replaced by $T_{w,i}$, $T_{s,i}$ is replaced with $T_{s,o}$, $\epsilon_{w,o}$ is replaced by $\epsilon_{w,i}$ and $\epsilon_{s,i}$ is replaced by $\epsilon_{s,o}$. The convective coefficient of the window/shade cavity is calculated based on equation 5.11. The total resistance of the air space between the interior shade and the window is given by

$$h_{IntS} = h_{c,v} + h_r \tag{5.26}$$

The interior radiative and convective coefficient $h_{r,int}$ and $h_{c,int}$ must be recalculated based on the shade temperature using equations 5.24 and 5.25. Again, energy balance equations must be solved iteratively until convergence is reached. The U-value of the fenestration system is then calculated as

$$U_{IntS} = \frac{1}{1/U'_{\text{øh}_{int}} + 1/h_{IntS} + R_{IntS} + 1/h_{int}} \tag{5.27}$$

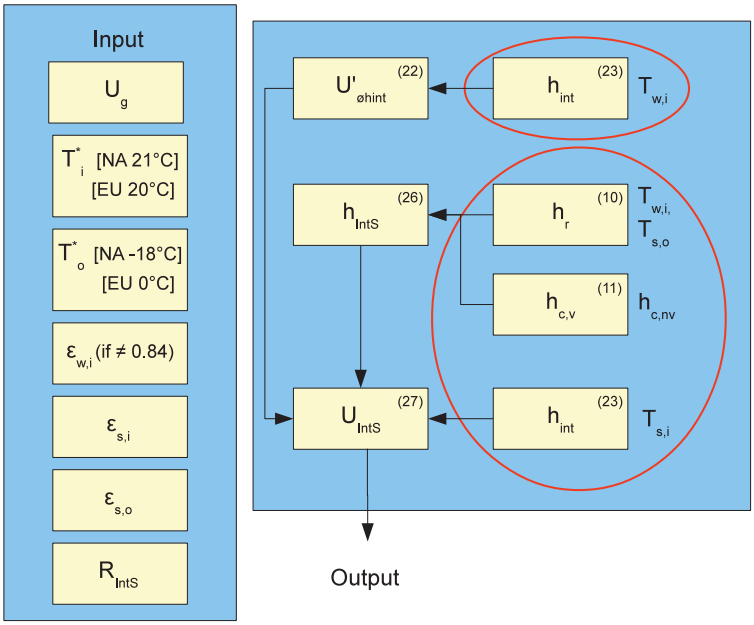

Figure 5.4: Flow chart for calculating the equivalent U-value of a fenestration system with an interior shade

The calculation procedure is summarized in figure 5.4. Finally, the effective U-value and SHGC can be calculated using equations 5.16 and 5.17 to determine graphically the net energy balance. Equations 5.36 and 5.37 must be used if windows are analyzed. If the shade is to be closed during sunny hours, tables A.1-A.3 must be used to estimate the appropriate solar transmittance and absorptance of the window (if unknown) in order to evaluate the SHGC with the shade on. The total transmittance of a glazing with an inner shade is calculated with

$$\tau_{IntS} = \frac{\tau_g \tau_s}{1 - \rho'_g \rho_s} \tag{5.28}$$

where ρ'_g is the reflectance of the innermost pane. The total SHGC of a fenestration system that consists of a single, double or triple glazing with an inner shade is determined with:

$$SHGC_{1gIntS} = \tau_{IntS} + \alpha_g \frac{U_{IntS}}{h_{ext}} + \tau_g \alpha_s \frac{(h_{int} - U_{IntS})}{h_{int}} \tag{5.29a}$$

$$\begin{aligned} SHGC_{2gIntS} =& \tau_{IntS} + U_{IntS} \frac{\alpha_{g1} + \alpha_{g2} + \tau_g \alpha_s}{h_{ext}} \\ &+ U_{IntS}(\alpha_{g2} + \tau_g \alpha_s)\left(\frac{1}{U_{IntS}} - \frac{1}{h_{ext}} - \frac{1}{h_{int}} - \frac{1}{h_{IntS}} - R_{IntS}\right) \\ &+ U_{IntS} \frac{\tau_g \alpha_s}{(1/h_{IntS} + R_{IntS})^{-1}} \end{aligned} \tag{5.29b}$$

$$\begin{aligned} SHGC_{3gIntS} =& \tau_{IntS} + U_{IntS} \frac{\alpha_{g1} + \alpha_{g2} + \alpha_{g3} + \tau_g \alpha_s}{h_{ext}} \\ &+ U_{IntS} \frac{\alpha_{g2} + \alpha_{g3} + \tau_g \alpha_s}{\Lambda_{12}} + U_{IntS} \frac{\alpha_{g3} + \tau_g \alpha_s}{\Lambda_{23}} \\ &+ U_{IntS} \frac{\tau_g \alpha_s}{(1/h_{IntS} + R_{IntS})^{-1}} \end{aligned} \tag{5.29c}$$

In the case of a triple glazing with an interior shade, Λ_{12} and Λ_{23} should be known. They can be calculated individually with ISO 10292 (1994, equation 3) if the emittance of panes is known or approximated with equation 5.21, where h_{ext} can be calculated with equation 5.8 from section 5.3.2.1.

5.3.2.3 Glazings with interior and exterior shades

Essentially, the same procedure as described in sections 5.3.2.1 and 5.3.2.2 is followed. The U-value of a glazing without the interior and exterior heat transfer coefficients is estimated from

$$U'_{\text{ø}\mathrm{h}_{ext}\&\mathrm{h}_{int}} = \frac{1}{1/U_g - 1/h_{ext} - 1/h_{int}} \tag{5.30}$$

where h_{ext} and h_{int} are calculated with equations 5.8 and 5.23. The exterior radiative coefficient and the interior radiative and convective coefficients are recalculated to account for the presence of shades with equations 5.9, 5.24 and 5.25.

The convection and radiation exchanges in the window/shade cavities must be calculated with equations 5.10 and 5.11. Finally, knowing the thermal resistance of both shades, the U-value of the fenestration system is calculated with

$$U_{IntExtS} = \frac{1}{1/U'_{\text{ø}\mathrm{h}_{ext}\&\mathrm{h}_{int}} + 1/h_{IntS} + 1/h_{ExtS} + R_{IntS} + R_{ExtS} + 1/h_{int} + 1/h_{ext}} \tag{5.31}$$

The U-values of the fenestration system with only the exterior or interior shade drawn must also be calculated with equations 5.27 and 5.13 if they are to be controlled independently.

Figure 5.5 summarizes the calculation procedure for a fenestration system with interior and exterior shades.

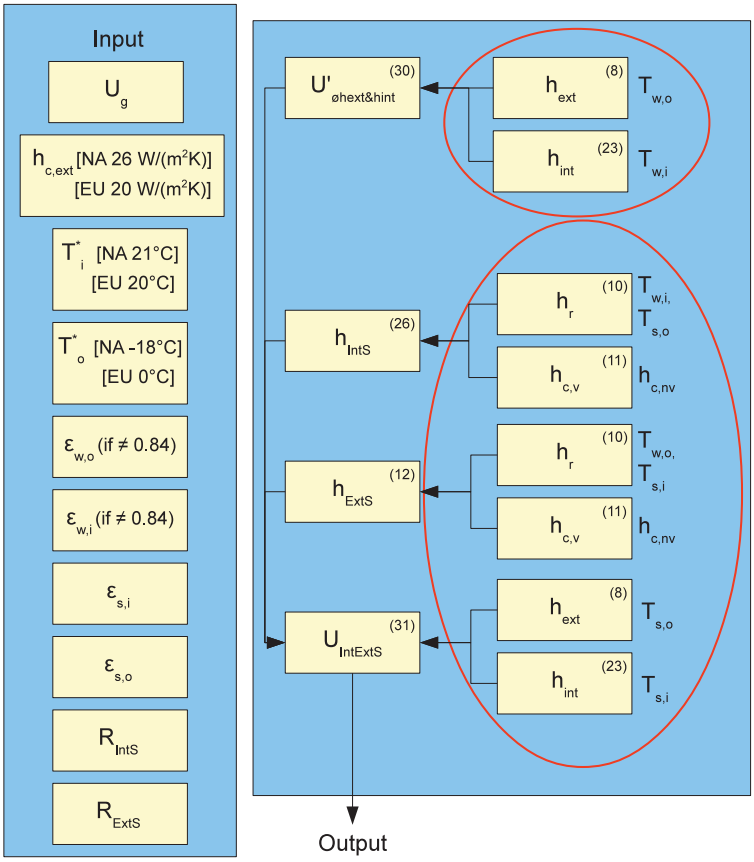

Figure 5.5: Flow chart for calculating the equivalent U-value of a fenestration system with interior and exterior shades

The total solar energy transmittance of the fenestration system is calculated with

$$\tau_{IntExtS} = \frac{\tau_{s1}\tau_g\tau_{s2}}{(1-\rho'_{s1}\rho_g)(1-\rho'_g\rho_{s2}) - \tau_g^2\rho'_{s1}\rho_{s2}} \tag{5.32}$$

where ρ_g and ρ'_g are the reflectance of the outermost and innermost pane. The effective U-value and SHGC are calculated using equations 5.16 and 5.17. Tables A.1-A.3 are used to estimate the solar absorptances and transmittance of the glazing (if unknown) if shades are to be closed during sunny hours.

The total SHGC of a fenestration system that consists of a single, double or triple glazing with an inner and outer shade is calculated with

$$SHGC_{1gIntExtS} = \tau_{IntExtS} + \alpha_{s1}\frac{U_{IntExtS}}{h_{ext}} + \tau_{s1}\alpha_g\left(\frac{1}{h_{ext}} + \frac{1}{h_{ExtS}} + R_{ExtS}\right) + \tau_{s1}\tau_g\alpha_{s2}\frac{(h_{int} - U_{IntExtS})}{h_{int}} \tag{5.33a}$$

$$\begin{aligned} SHGC_{2gIntExtS} = {} & \tau_{IntExtS} + U_{IntExtS}\frac{\alpha_{s1} + \tau_{s1}\alpha_{g1} + \tau_{s1}\alpha_{g2} + \tau_{s1}\tau_g\alpha_{s2}}{h_{ext}} \\ & + U_{IntExtS}\frac{\tau_{s1}\alpha_{g1} + \tau_{s1}\alpha_{g2} + \tau_{s1}\tau_g\alpha_{s2}}{(1/h_{ExtS} + R_{ExtS})^{-1}} \\ & + U_{IntExtS}(\tau_{s1}\alpha_{g2} + \tau_{s1}\tau_g\alpha_{s2}) \\ & \cdot\left(\frac{1}{U_{IntExS}} - \frac{1}{h_{ext}} - \frac{1}{h_{int}} - \frac{1}{h_{ExtS}} - R_{ExtS} - \frac{1}{h_{IntS}} - R_{IntS}\right) \\ & + U_{IntExS}\frac{\tau_{s1}\tau_g\alpha_{s2}}{(1/h_{IntS} + R_{IntS})^{-1}} \end{aligned} \tag{5.33b}$$

$$\begin{aligned} SHGC_{3gIntExtS} = {} & \tau_{IntExtS} + U_{IntExtS}\frac{\alpha_{s1} + \tau_{s1}\alpha_{g1} + \tau_{s1}\alpha_{g2} + \tau_{s1}\alpha_{g3} + \tau_{s1}\tau_g\alpha_{s2}}{h_{ext}} \\ & + U_{IntExtS}\frac{\tau_{s1}\alpha_{g1} + \tau_{s1}\alpha_{g2} + \tau_{s1}\alpha_{g3} + \tau_{s1}\tau_g\alpha_{s2}}{(1/h_{ExtS} + R_{ExtS})^{-1}} \\ & + U_{IntExtS}\frac{\tau_{s1}\alpha_{g2} + \tau_{s1}\alpha_{g3} + \tau_{s1}\tau_g\alpha_{s2}}{\Lambda_{23}} \\ & + U_{IntExtS}\frac{\tau_{s1}\alpha_{g3} + \tau_{s1}\tau_g\alpha_{s2}}{\Lambda_{34}} + U_{IntExtS}\frac{\tau_{s1}\tau_g\alpha_{s2}}{(1/h_{IntS} + R_{IntS})^{-1}} \end{aligned} \tag{5.33c}$$

If shades are to be controlled independently, equations 5.20 and 5.29 should also be used to calculate the appropriate SHGC with only one shade being used.

In the case of a triple glazing, Λ_{23} and Λ_{34}, can be calculated from ISO 10292 (1994, equation 3) or estimated with equation 5.21.

5.3.3 Using the methodology for windows

This methodology can be used for comparing either glazings or complete windows. In this method, it is assumed that the shade(s) (if present) covers only the glazed part of the window and is parallel to the glass. If the window has a frame, it is assumed that the shading device is not covering the frame.

For clarity, equations are presented for glazings only throughout this paper. For users interested in analyzing windows, results can be easily adapted. The window U-value is calculated from the glazing and frame U-values as well as the linear thermal transmittance Ψ:

$$U_w = \frac{\Sigma U_g A_g + \Sigma U_f A_f + \Sigma l_\Psi \Psi}{A_t} \tag{5.34}$$

where A_g is the glazing area, A_f is the frame area, A_t is the total window area and l_Ψ is the vision area perimeter. The summations in equation 5.34 refer to cases when one particular component does not have uniform properties (different glazings or head/jambs/sill properties). When analyzing windows with this method, it is necessary to know the window U-value, glazing U-value, total window area and glazing area. The contribution of the frame and linear thermal transmittance can be grouped together under the variable Ψ^*:

$$\Psi^* = \Sigma U_f A_f + \Sigma l_\Psi \Psi = U_w A_t - \Sigma U_g A_g \tag{5.35}$$

The U-value of a shaded window can then be calculated as

$$U_{wS} = \frac{\Sigma U_{gS} A_g + \Psi^*}{A_t} \tag{5.36}$$

Here it is assumed that the linear thermal transmittance is not affected by the presence of the shade. The SHGC of a bare and shaded window, $SHGC_w$ and $SHGC_{wS}$, are simply computed as follow

$$SHGC_w = \frac{SHGC_g A_g}{A_t} \tag{5.37a}$$

$$SHGC_{wS} = \frac{SHGC_{gS} A_g}{A_t} \tag{5.37b}$$

When calculating the net energy gain for windows with equation 5.14, U_g is replaced by U_w and U_{ExtS} by U_{wS}, where U_{gS} represents the U-value of the shading system under consideration. In addition, $SHGC_g$ and $SHGC_{ExtS}$ are replaced with $SHGC_w$ and $SHGC_{wS}$ from equations 5.37.

5.4 Applications, limitations and recommendations

5.4.1 Applications

This methodology is intended to be used for the design of buildings aiming at a high solar utilization. It is suitable for heating dominated buildings like solar houses and solariums/greenhouses in cold climates where maximizing the net energy balance of windows is usually an important concern. In addition, this methodology may be useful to other kinds of buildings in heating dominated climates where a *solar optimized fenestration systems* approach has been adopted.

The *solar optimized fenestration systems* concept designate a design approach where the role of windows is to maximize the net energy balance and the role of shading devices is to control overheating and glare issues as well as improving the energy balance.

As seen from the literature review, this idea is not new. Hee et al. (2015), after carrying an extensive review on static and dynamic windows, have suggested that heating dominated countries shall adopt high SHGC windows to reduce heating loads and use shading devices in summer to prevent overheating.

In heating dominated climates, the use of efficient shading devices for solar and glare control allows the adoption of high SHGC windows, which in turn yields the maximum benefits from passive solar design. With good protections, high SHGC glazings can be selected for either view and/or daylighting sections, for all orientations. Since the SHGC is closely related to the visible transmittance value (Schumman et al., 2013), a high SHGC window will generally improve daylighting as an added benefit.

Following the *solar optimized fenestration systems* design concept in heating dominated climates allows to decouple the complex issues related to glazing and shading design like solar gains/overheating and daylighting/glare. The selection of a window optimized for maximizing the energy balance and shading systems optimized for solar and glare control greatly simplifies the problem and reduces the number of possibilities to investigate. Since glazing alone cannot solve excessive heat gains and discomfort (Schumman et al., 2013), shadings must be incorporated. If well designed for solar and glare control, the glazing is now free from these constraints and can then be optimized for high solar gains and low thermal losses only, simplifying the design process and enhancing passive solar design efficiency.

Once implemented into a programming software, this methodology can be readily used during the design stage of a new building or when considering windows replacement of an existing building. It is a flexible method that can be used at any location within heating dominated countries as long as appropriate weather files are available. Diagrams for all façades orientations can be quickly generated, allowing the comparison of the net energy balance of different fenestration systems where the effect of the presence of an interior and/or exterior planar shade(s) can be analyzed.

This methodology can also be used to visualize the impact of shades on the U-value of fenestration systems, which could be useful when assessing thermal comfort and the need for perimeter heating. Tzempelikos et al. (2007) have found that windows with U$<$1.5 W/(m^{2}K) could eliminate the need for perimeter heating.

Bülow-Hübe (2001) has estimated possible annual energy savings up to 110 kWh per window for upgrading the windows of a house built in the 60's, which could lower the heating load by 6%. For a house built in 2000, energy savings of up to 50 kWh per window could be achieved, which would reduce the heating load by 9%. Since glazing type was identical for all orientations in this study and shading devices were not considered, higher savings could be obtained when using this methodology for selecting optimum fenestration systems for different orientations.

This methodology can be used for comparing either glazings or complete windows. Appendix 5.3.3 describes how to adapt the calculations for investigating complete windows.

5.4.2 Limitations

As this methodology is based on steady state calculations, it is not meant to provide an accurate estimation of the yearly total energy gained or loss through a fenestration but rather to assist the design process by comparing the performance of different products on a relative basis.

A comparison of dynamic computer simulations and a simplified method based on net energy gains carried out by Bülow-Hübe (2001, Section 5.1.7) revealed discrepancies of only about 10% when comparing the savings due to a lower U-value window. However, it also points out that solar gains might be as much as 60% larger when no shading factor is used, which stresses out the importance of evaluating properly shadings from distant objects, window reveals and fixed shading devices when present.

This methodology can only evaluate the heat transfer of planar shading elements parallel to the glazing. The calculation of heat transfer due to fixed shadings such as overhangs, fins and louvres requires detailed computational fluid dynamic simulations and therefore cannot be evaluated with this methodology.

5.4.3 Recommendations

Since the operation of shades affects the energy performance, it is important that the simulation of shades is representative of their expected operation. Shades whose main purpose is to control solar gains that are used only during the warm period, such as manual exterior shutters, should not be considered when using this methodology. However, if motorized, they can also be used in the cold season to reduce night heat losses and should therefore be

taken into consideration. As experience has shown that people are rather inconsistent when operating shades (Carmody et al., 2000), motorized control is recommended.

During the design process, it is recommended to first use this methodology to help identifying the most appropriate glazing and shading combination for a given application and climate, so as to maximize the solar energy utilization from transparent components. Thereafter, it is suggested to follow passive solar principles to adequately position and size windows and select appropriate shading devices.

For instance, over-glazing should be avoided. Positioning windows mostly towards a southern exposure with overhangs and reducing window areas on east and west façades are well known passive solar techniques to reduce risks of overheating. The integration of interior thermal mass in direct gain rooms has shown to reduce temperature fluctuations appreciably and to slightly reduce heating loads (Athienitis et al., 1997; O'brien, 2011, Appendix B).

When the outdoor temperature is only a few degrees below the balance temperature, it is possible that not all solar gains are useful to reach the temperature set point. However, the extra heat can be stored, either in thermal mass or by elevating indoor air temperature, and be used later on. Therefore, by following good passive solar design practices, it is possible to utilize most of the solar gains considered useful in this method. This is why it is recommended to select a high utilization factor, typically around 0.98.

This method calculates energy gains and losses through fenestration systems for a constant interior temperature T_i. This temperature should be selected as the average interior temperature during the heating season. Interior temperature fluctuations in a house are typically small, usually less than 3 to 4 °C, while temperature fluctuations in a solarium or a greenhouse are likely to be more significant. Nevertheless, since this method is aiming to compare different design options on a relative basis, small fluctuations of the interior temperature will not significantly impact the results. If a greater accuracy is required, an average daily interior temperature profile could be easily defined for energy calculations.

5.5 Simulation results and discussion

5.5.1 Simulation results

Simulation results are presented for Montreal, with a solar shading factor of 0.9 and a solar gain utilization factor of 0.98. Figures 5.6a - 5.8d present the net energy gain per unit area for the four cardinal orientations of five different glazings with an exterior shade, an interior

shade and the combination of both. For these simulations, shades have been open when the global horizontal solar radiation is above 50 W/m^2 and closed otherwise. Two common types of shadings have been simulated: an indoor roller shade and an exterior roller shutter. Their technical specifications are shown in table 5.4.

Table 5.4: Technical properties of simulated shading devices

	Interior roller shade	Exterior roller shutter
Solar transmitance	0.26	0.01
Solar absorptance	0.34	0.19
Emissivity of outer side	0.9	0.9
Emissivity of inner side	0.9	0.9
Reflectance of outer side	0.4	-
Reflectance of inner side	-	0.8
Air cavity	0.03m	0.03m
Top opening	0.01m	0.001m
Bottom opening	0.01m	0.001m
Left opening	0.01m	0.001m
Right opening	0.01m	0.001m
Openness factor	0.14	0
Thermal resistance	0.01 Km^2/W	0.1 Km^2/W

5.5.2 Discussion

Some researchers predicted that «superwindows» with a U-value of 0.5 W/(m^2 K) and SHGC of 0.4 would be so efficient that even north facing windows could become net energy providers (Carmody et al., 2000). However, as it can be seen in figure 5.6c, the SHGC or the thermal resistance of a bare window must be significantly higher than that to generate a net energy gain in a southeastern Canadian climate like Montreal.

As expected, the presence of a shade has the biggest impact on the net energy balance of the least insulated glazing. Even when using both interior and exterior conventional shading devices, the net energy gain of a good triple glazing is only marginally improved, as illustrated on figure 5.8a-5.8d. If one wishes to significantly improve the net energy gain of high performance triple glass, special insulating devices should be considered, such as interior cellular shades or exterior insulated shutters.

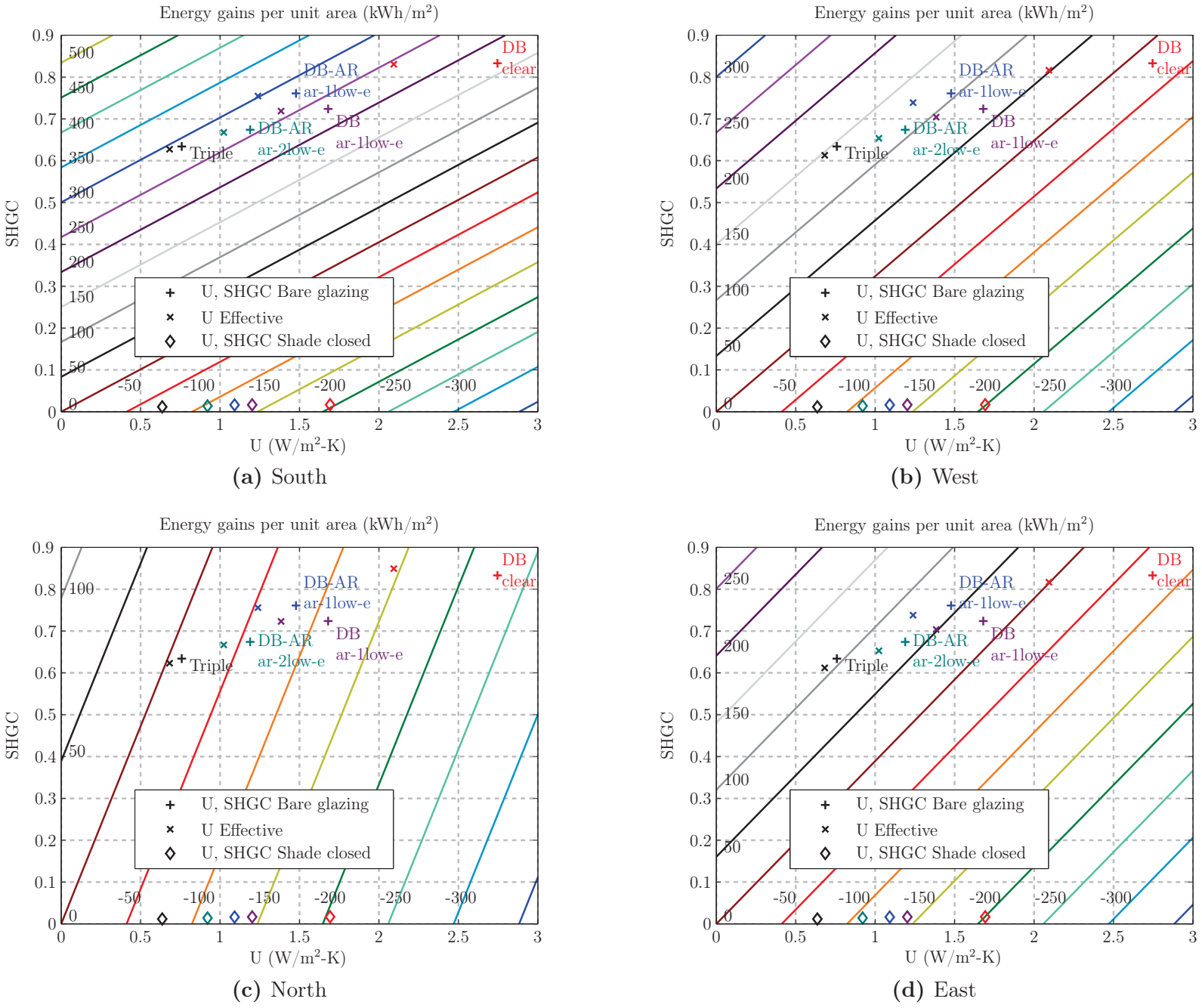

(a) South **(b)** West **(c)** North **(d)** East

Figure 5.6: Net energy gain diagrams of a fenestration system with an exterior shade

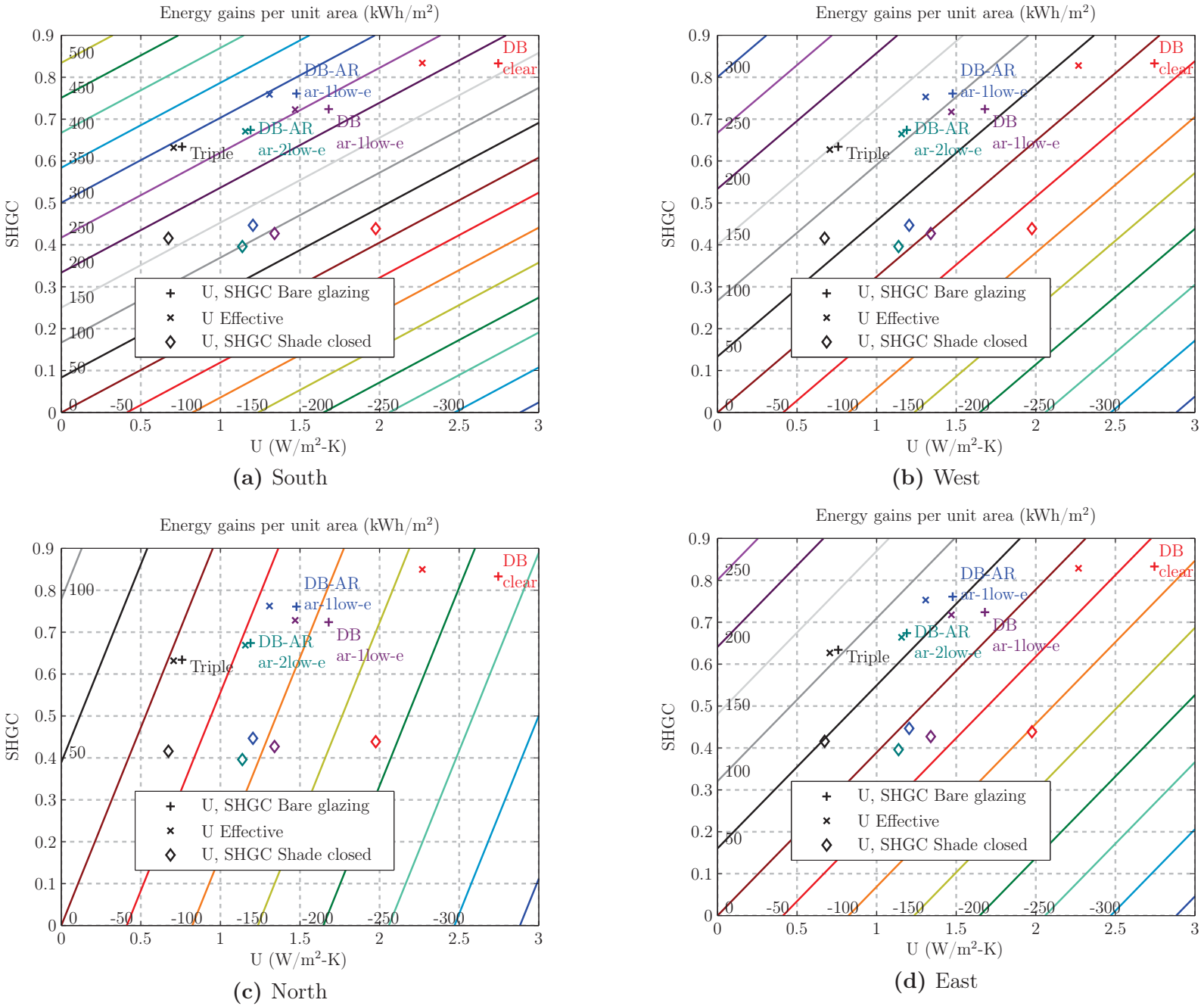

(a) South (b) West

(c) North (d) East

Figure 5.7: Net energy gain diagrams of a fenestration system with an interior shade

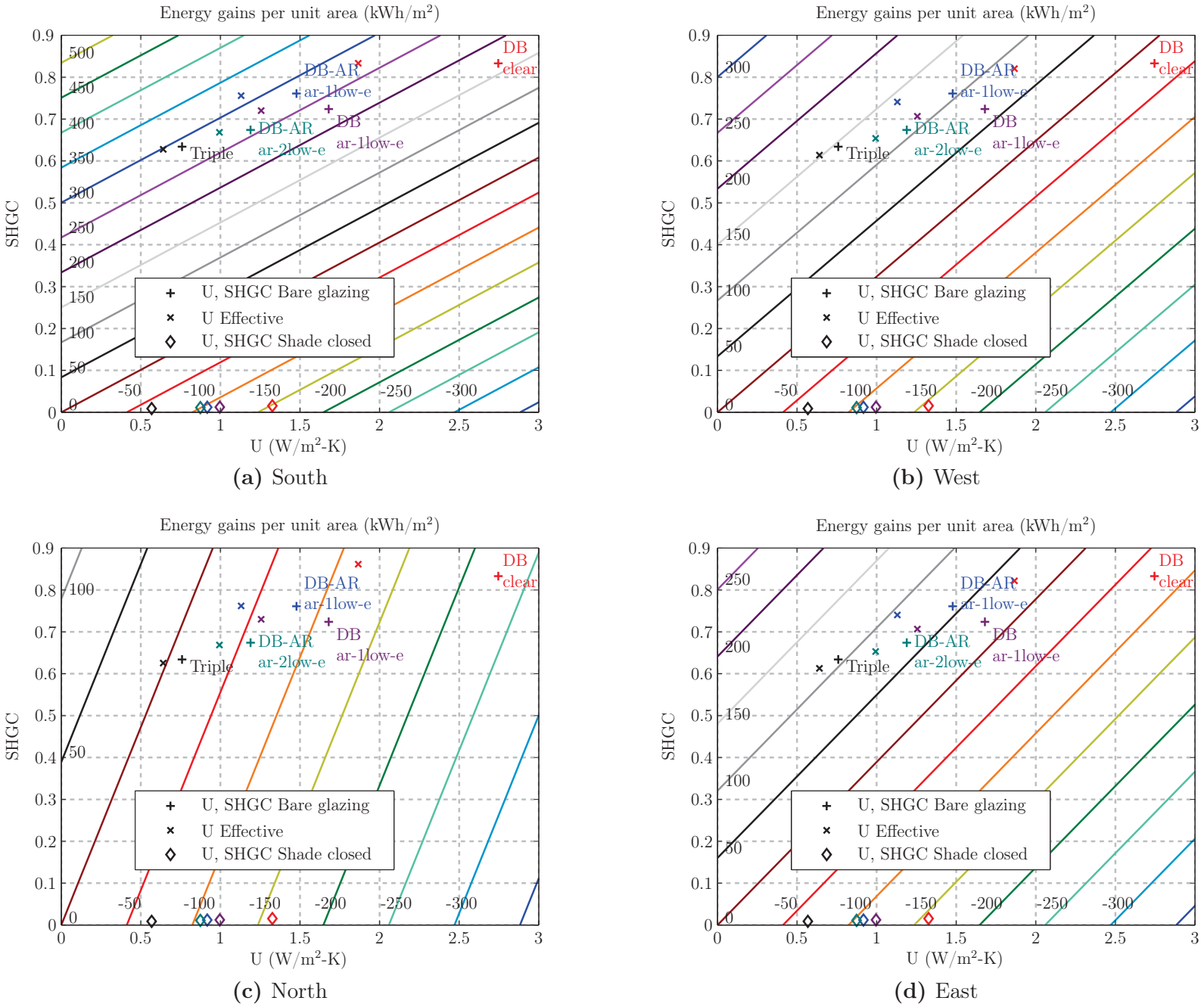

Figure 5.8: Net energy gain diagrams of a fenestration system with interior and exterior shades

It can be seen on figure 5.7a that a conventional roller shade reduces the U-value of a double glazing with argon and low-e from 1.7 to 1.3 when closed, which would significantly improve thermal comfort and could avoid perimeter heating.

5.6 Experimental comparison and discussion

An experimental test-room was built to study active heat storage with phase change materials in solariums and direct gain rooms with different combinations of interior and exterior shading devices. The purpose of this experiment was to determine experimental U-values of fenestration systems with different shading configurations and compare these values with those obtained with the methodology described in section 5.3. Since the methodology is employing fixed U-values based on interior and exterior temperatures as defined in NFRC 100-2004 (2004) or in ISO 15099 (2003), steady-state environmental conditions were provided. Therefore, the presence of thermal storage materials did not influence this specific experiment but was included for future studies about optimization of thermal storage for solariums and greenhouses.

Four different shading devices have been tested under NFRC conditions where the test-room has been installed in a cooling chamber at -18°C and the interior kept at a constant 21°C with an electric heater. Shades properties are listed in table 5.5.

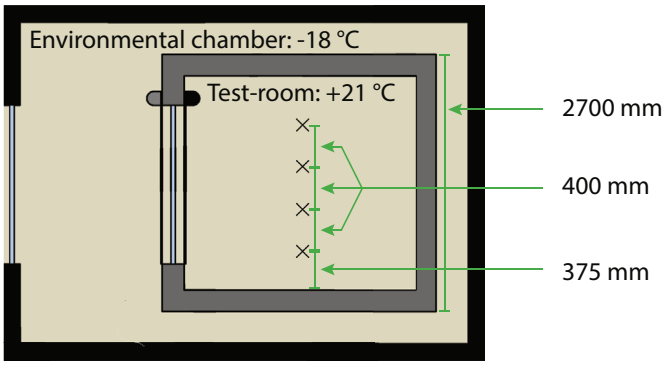

Figure 5.9: Schematic of the experimental test-room in the environmental chamber showing the configuration with interior and exterior shades. The X indicates the location of interior thermocouples.

The interior shading material 1 consists of a highly open shade with a high solar transmittance. There was a total opening area of 0.241 m^2 at the shade perimeter between the shade and the glazing. The interior shade 2 is a nonpermeable material that has been fitted tightly on the frame. The exterior shade 1 is made of commercially available polyurethane filled

aluminum slats. The exterior shade 2 is a custom made panel made of vacuum insulated panels (VIP) sandwiched between extruded polystyrene (XPS). Its thermal resistance has been evaluated at R 2.19 Km^2/W.

The test-room consists of a chamber 3 m long by 1.5 m wide and 2.7 m high simulating an attached sunspace with a 2 m by 2 m double glazed window (glazing U-value=1.314 $W/(m^2K)$ and SHGC=0.262). The glazing and framing area are 3.64 and 0.493 m^2 respectively while the U-value of the frame is 1.9 $W/(m^2K)$. The overall U-value of the window is 1.7 $W/(m^2K)$. The air tightness of the test-room has been measured at different pressure differential levels by performing blower door testing. The air infiltration at 50 Pa has been evaluated through polynomial regression as 4.1 ACH and the infiltration rate under the tested conditions (-18°C/+21°C) has been estimated as 0.2 ACH.

Four type T thermocouples (accuracy of 0.5°C) were located inside the test-room as shown in figure 5.9 and four outside in the climatic chamber. An average temperature difference between the climatic chamber and the test-room of 37.7 °C was maintained during the tests.

The electricity consumption of the heater was monitored for the unshaded test-room and the five different shading configurations described in table 5.6. The U-value of the test room attributed to the envelope (walls, ceiling and floor) has been evaluated as 0.35 $W/(m^2K)$. It was calculated from the heater electricity consumption for the unshaded test-room and by subtracting the losses due to the window and infiltration. The experimental U-value of the fenestration system in a given configuration was determined from subtracting the heat losses due to the envelope, window frame and infiltration to the heater electricity consumption. The U-values of the different shade configurations obtained experimentally are compared in table 5.6 with values that have been calculated following the methodology presented in this paper.

Table 5.5: Technical properties of tested shading devices
[a]The thermal resistance of the interior shades was too low to be measured; a value of 0.01 $W/(m^2K)$ has been selected for simulations

Description	Cavity width cm	τ_s	α_s	ϵ f/b	R Km^2/W	OP	Opening m^2
Int shade 1	15.5	0.77	0.02	0.89	0.01[a]	0.52	0.241
Int shade 2	9.4	0	0.37	0.49	0.01[a]	0	0
Ext shade 1	5.4	0	0.28	0.79/0.76	0.080	0	0
Ext shade 2	1.9	0	0.37	0.49	2.19	0	0

Table 5.6: Comparison of experimental and simulation results - U glazing = 1.314 W/(m^{2}K)

	U-value Simulated W/(m^{2}K)	U-value Experimental W/(m^{2}K)
Configuration		
Window/Int shade 1	1.09	1.18
Window/Int shade 2	0.97	1.04
Ext shade 1/Window	0.99	0.99
Ext shade 2/Window	0.31	0.45
Ext shade 1/Window/Int shade 1	0.86	0.96

As can be seen from table 5.6, simulated and experimental U-values are relatively close to each other, with simulation results having a general tendency to be lower than experimental values.

The interior shade 1 has a high openness factor of 0.52 while the interior shade 2 is totally impervious to air. It should also be noted that the interior shade 2 was installed in an airtight fashion while there were large openings around the interior shade 1. Even with such a large openness factor, openings around the shades and a relatively wide cavity, measurements are showing that the interior shade 1 improves the glazing U-value by 10%. The simulated U-value of the exterior shade 2 is significantly lower than measured. This is probably mainly due to the uncertainty related to the determination of the overall thermal resistance of the shade, which is made of a combination of VIP and EXP, arranged non uniformly in order to cover completely the glazing.

Experimental results might be indicating that the sensitivity to the openness factor and openings area is more important in reality than what is calculated with the ISO 15099 model, but a more thorough experimental validation would be needed to confirm this. It should be noted that there are no restrictions concerning the range of openness factor in ISO 15099.

The most significant uncertainty in the modelling of the heat transfer through fenestration systems probably pertains to the calculation of the convective heat transfer coefficient in the cavity between the glazing and shading layers. Although the algorithm developed in ISO 15099 has been implemented in many important building energy simulation software (EnergyPlus, WINDOW, WIS) and used to conduct comprehensive simulations of various window attachments (Curcija et al., 2013), there is a lack of experimental validation in the published literature to date. A study conducted with diffuse interior and exterior shading

screens revealed discrepancies in the ability of various building energy simulation programs to model the heat transfer in the cavity between the shading and glazing layers (Loutzenhiser et al., 2007). The development of a simple yet accurate model or correlation for the determination of the convective cavity heat transfer coefficient is an important area for future research.

The ASHWAT model (Wright et al., 2009) developed an approximate model that allows the calculation of the impact of the cavity width on the convective coefficients in the vicinity of a shade, based on the two limiting cases (where the shade is far away from a window or where the spacing approaches zero). It is acknowledged that this model is only an approximation and that future research should be conducted regarding the convective heat transfer coefficient in the glazing/shading cavity. The ASHWAT model also developed useful correlations for the determination of solar optical properties of venetian blinds, drapes, screens and roller shades (Kotey et al., 2009a,b,d,c). It should be noted that for the latter, the openness factor must not be higher than 0.2.

Although there has been significant advancement in the last decades in the evaluation of the thermal performance of shading devices, challenges remain due to the complexity of the heat transfer in complex fenestration systems (Laoudi, 2009). Should simpler validated physical models or more accurate empirical correlations be developed in the future that better describe the heat transfer through fenestration systems, they could easily replace the equations suggested in this methodology.

5.7 Conclusion

This paper presented a methodology to help in the selection of fenestration systems for buildings in heating dominated climates. The method has the capability to simulate a one or two layer shading system with one exterior and/or one interior planar shade. This method generates 2D schematics indicating lines of constant net energy gain per unit area as a function of the SHCG and U-value on which different fenestration components are situated. Such graphics are useful in early design stage to compare different design options on a relative basis for a specific orientation and climate.

The essence of the method is based on the computation of the useful solar gains through fenestration and associated heat losses when the exterior temperature is below the balance temperature. This methodology is intended to be used for the design of buildings aiming at

a high solar utilization like solar houses, solariums/greenhouses and buildings adopting the *solar optimized fenestration systems* design concept. It has the capability to evaluate the performance of either glazings or complete windows in combination with a one or two layer shading system. Once implemented, this methodology can be readily used for new or retrofit projects in different locations.

This methodology can be used independently or as a preliminary design tool to help identifying the best performing combinations of windows and shades as a function of orientation before running whole building energy simulations.

This paper presented diagrams for glazings equipped with an interior roller shade, an exterior roller shutter and a combination of both for the four cardinal orientations for the city of Montreal, Canada. A comparison of simulated and experimental U-values of four shading devices revealed results relatively close to each other, but additional research on the convective heat transfer coefficient in the cavity between the shading and glazing layers is needed.

Chapter 6

Development of a new control strategy for improving the operation of multiple shades in a solarium

Based on a published paper:

Bastien, D., Dermardiros, V. and Athienitis, A. 2015b. Development of a new control strategy for improving the operation of multiple shades in a solarium. *Solar Energy*, 122, 277-292.

6.1 Chapter abstract

This chapter presents a new control strategy for improving the performance of one interior and/or exterior planar shade(s). The control strategy is based on performing an energy balance on the fenestration system and calculating the total heat flow (i.e. solar gains + overall heat losses). The heat flow can be maximized or minimized depending on the needs of the space. A solarium model was developed in order to assess the performance of the proposed shading strategy. The solarium model can simulate passive and active thermal storage using sensible and phase change materials. A prototype solarium with motorized interior and exterior shadings has been instrumented and subjected to controlled conditions. The numerical simulations are in good agreement with experimental results.

The simulation model has then been used to perform annual simulations of an attached solarium for the location of Montreal, Canada. The year was divided in a heating mode and a mixed mode. During the heating mode (i.e. October through April), heating is provided to keep a minimum temperature of 10°C and surplus heat is considered when the temperature reaches 28°C. By using the proposed algorithm for the control of one interior and/or exterior shade(s) in the heating mode, heating requirements of the simulated solarium have been reduced by 3-9% and an additional 9-14% of surplus heat have been collected when compared to a control based on near optimum global horizontal solar radiation levels. During the mixed mode, thermal comfort can be improved significantly (+1822 hours) when the interior shade is controlled with the proposed algorithm.

6.2 Introduction

Shading devices are commonly used in various building types such as residential buildings, offices buildings, solariums and greenhouses. They are mainly used for reducing solar gains and heat losses, controlling glare and improving daylight availability.

In solariums and greenhouses, the former two objectives typically prevail. Attached solariums are one of the most popular passive solar systems (Mihalakakou and Ferrante, 2000). Integrated to either new or existing houses, they are generally built to gain additional floor space with abundant daylight. In addition, solariums also have the potential to provide adequate conditions for growing plants and vegetables, as well as collecting solar heat. With their large glazing area, the use of shades and their control may affect significantly the energy requirements and thermal comfort in a solarium.

Generally in greenhouses, a shade whose main purpose is to reject near infrared radiation for temperature control is called a solar screen, while a shade whose main purpose is to reduce heat losses is called a thermal screen. Many studies reported significant energy savings due to the implementation of thermal screens in greenhouses. For different types of greenhouses and screens, the use of a thermal screen from sunset to sunrise has been shown to reduce the energy used by 27% to 43% (Meyer, 1981), 21% to 33% (Bailey, 1988) and 16% (Dieleman and Kempkes, 2006) for greenhouses located in Germany, England and Netherlands, respectively.

The addition of shades to the windows of residential buildings has been shown to be useful for reducing heat losses. Simulations carried out by Selkowitz and Bazjanac (1979) have shown that the net annual heating requirements of a house can be reduced by 18% when R10

shutters are closed twelve hours at night for equally distributed single pane windows (with a window to floor ratio of 15% in Minneapolis). When used with clear double glass, the net annual heating requirements can be reduced by 9%.

Simulations have shown that the use of roller shades in office buildings with continuously dimmable lights could lower the source energy consumption up to 7% while improving visual comfort (Tzempelikos and Shen, 2013). The use of more sophisticated devices like an actively controlled venetian blind was estimated to reduce the energy for heating, cooling and artificial lighting by up to 22% (Nielsen et al., 2011).

6.2.1 Existing shading control strategies

Many studies have been conducted about the operation of different types of movable shading devices and their associated energy performance. Studies on office buildings generally focus on reducing heating and cooling loads, artificial lighting and glare while providing adequate workplane illuminance.

Various shading control strategies for offices buildings have been investigated such as those based on

- Time clock operation (Yao, 2014).
- Incident solar irradiance (van Moeseke et al., 2007).
- Incident total or beam radiation (Lee and Selkowitz, 2006; Wienold, 2007; Tzempelikos and Shen, 2013).
- Incident or transmitted illuminance (Galasiu et al., 2004; Tzempelikos and Shen, 2013).
- Preventing direct sunlight from falling on the workplane (Tzempelikos and Shen, 2013).
- The illuminance level at the workplane (Wienold, 2007).
- Minimizing the total heat gains when in cooling mode (with additional criteria) (Tzempelikos and Shen, 2013).
- Fixed blind tilt angle (for venetian blinds) (Carbonari et al., 2001; Galasiu et al., 2004; Huang et al., 2014).
- The cut-off angle to block beam radiation (for venetian blinds) (Wienold, 2007; Nielsen et al., 2011; Shen et al., 2014).
- Internal temperature (van Moeseke et al., 2007).
- A combination of solar irradiance and internal temperature (van Moeseke et al., 2007).
- Others (Carbonari et al., 2001; Lee and Selkowitz, 2006; Wienold, 2007; Shen et al., 2014).

Tzempelikos and Shen (2013) carried out comprehensive thermal and lighting simulations of four different shading control strategies for operating roller shades in office buildings. They mention that the transmitted illuminance is a more appropriate metric than an incident solar radiation set point for providing visual comfort with shade control, especially for spectrally selective windows with low solar gains. They note that the glazing type and shading properties have a significant impact on the performance of different shading controls, while their results indicate that the best shading control type for a specific climate and building remains essentially the same regardless of glazing type and shading properties.

Thermal conditions and requirements in solariums and greenhouses differ largely from those prevailing in office buildings; therefore appropriate control strategies for operating shading devices may also be different.

Control strategies for operating solar and thermal screens in greenhouses can be based on several approaches such as:

- Time clock operation (Seginer and Albright, 1980).
- A fixed value of solar radiation (Marsh et al., 1984; Dieleman and Kempkes, 2006).
- A linear correlation between solar radiation and outside temperature (Marsh et al., 1984; Dieleman and Kempkes, 2006).
- A combination of internal temperature and incident solar radiation (Lorenzo et al., 2003).
- An economic criteria based on energy saved versus crop loss (Aaslyng et al., 2003).

It was found that energy savings can be increased by 6% when the screen is controlled based on radiation level compared to time clock operation (Seginer and Albright, 1980). Marsh et al. (1984) measured an energy saving of 3.3% when the opening of thermal screens was based on an inside light level of 30 W/m^2 compared to time clock operation. This study also concluded that using a more advanced control strategy based on a light level that is a linear function of the outside temperature may not be justified because no additional savings were observed compared to a fixed light level control.

Simulations carried out by Dieleman and Kempkes (2006) have shown that by opening a thermal screen based on increasing the outside radiation level from 1 W/m^2 to 25, 50 and 150 W/m^2, an additional energy saving of 2%, 3% and 4% respectively can be achieved. The same study found that screen operation based on correlations of outside temperature and radiation can achieve a similar energy reduction of up to 4%.

Aaslyng et al. (2003) developed an indoor environment control system for greenhouses based on a combination of control methods. Thermal screens were controlled to maximize profit, which was calculated as a trade-off between the energy saved with screens on versus the production loss caused by decreased irradiance. The operating temperature range was considerably wider than usual; the temperature was lower on cloudy days where growth is reduced and higher on sunny days to increase production. Field tests showed significant energy savings with only small changes in plant production.

6.2.2 Benefits of thermal storage and its influence on the energy consumption of various building types

Integrating thermal mass in buildings can provide significant benefits for various building types and climates. An exterior wall with insulation on the outside and interior mass subjected to daily solar gains exhibits reduced temperature swings and a delay between the peak solar gains and the resulting peak of the room temperature (Athienitis and O'Brien, 2015).

Through simulations, Kosny et al. (2001) have evaluated that by replacing lightweight wood frame construction with massive constructions of the same R-value, annual energy savings of up to 8% can be achieved for residential buildings in cold climates and up to 18% in warm climates. To achieve these results, the thermal mass must be in good contact with the interior of the building. Wall R-values between 0.9 to 4.4 m^2 K/W (R5 to R25) have been simulated. It is interesting to note that energy savings increase with R-values in both climates; thus higher energy savings might be obtained with R-values above 4.4 m^2 K/W.

Simulations conducted by Braun (1990) on office buildings with varying properties in different climates showed possible energy cost savings between 10-50% and peak power reduction between 10-35% when the building structure is used for thermal storage. The study of 12 low-energy office buildings in Germany revealed that good thermal comfort in summer is achievable without mechanical cooling, providing that buildings are designed for low solar and internal gains, with an adequate thermal storage capacity and a sufficient heat sink (Pfafferott et al., 2007).

Thermal mass is extensively used in solariums and greenhouses. Because these spaces are subjected to greater solar gains and temperature fluctuations than residential and office buildings, greater reductions in energy requirements may be obtained by including thermal storage materials. Many different thermal storage systems have been investigated; a review

of these is presented in Sethi and Sharma (2008). In this review, earth-to-air heat exchange systems are reported to reduce heating requirements between 28 to 62% and north walls storage systems between 35 to 82%. A review of greenhouses using phase change materials (PCM) for energy storage applications has been conducted by Kurklu (1998). All studies under review suggested that PCM could be efficiently used for energy storage in greenhouses with reported energy savings from 30% to 80%.

From this brief review, it can be seen that thermal mass can be useful in virtually all buildings types and climates, although the magnitude of the energy savings is strongly affected by the building type and operation, thermal storage material and configuration and climate.

As described in the next section, this paper presents a control strategy for operating shades based on maximizing the total heat flow through fenestration systems. Maximizing the net heat flow through fenestration systems is an interesting concept whose benefits are fully realized only when solar gains are useful. The inclusion of thermal storage materials in buildings is an important element for maximizing the energy gains obtained by using the control strategy proposed here.

6.2.3 Objectives and overview

Although many studies have been conducted regarding efficient shading control, the authors are not aware of any published method for operating shades based on an energy balance on the fenestration system. The aim of this study is to develop a new control strategy for improving the performance of shades that is based on performing an energy balance on the fenestration system. In order to do so, detailed mathematical and numerical models of a solarium are developed. The best position of a shade is either totally open or totally closed; the position selected is the one that maximizes or minimizes the net heat flow of the glazing-shade system (referred to as fenestration system throughout this study). This control strategy can be used for the control of an interior shade, an exterior shade or a combination of both.

Section 6.3 presents the mathematical and numerical models of a solarium used for implementing the shading control strategy. Section 6.4 presents a comparison of the simulation model with experimental data obtained by instrumenting a solarium test-room placed in an environmental chamber under illumination provided by a solar simulator. The proposed shading control algorithm is presented in Section 6.5. Details about the applications of this methodology, its limitations and some recommendations are provided in section 6.6.

6.3 Solarium model

The solarium model can be fully glazed or be made of a combination of glazed surfaces and opaque walls. The glazed surfaces may be covered by an exterior and/or an interior shade. These shades can be used for improving the thermal resistance and thermal comfort in winter and for reflecting solar heat in summer.

The developed model consists of a detailed transient finite difference thermal network model that includes modelling of one or two thermal storages. One thermal storage is located on the floor, while the other one is located on one wall, ideally the north wall. Either conventional sensible heat storage materials or phase change materials can be modelled. Thermal storages can be made up of one layer passively charged and discharged or two layers separated by a channel with active air circulation.

The inputs of the model are read from a Canadian Weather year for Energy Calculation (CWEC) file. Any hourly weather data publicly available on the U.S. Department of Energy (U.S. Department of Energy, 2015) website can be downloaded and used as input. The required inputs consist of the global horizontal radiation, direct normal radiation, diffuse horizontal radiation, wind speed, exterior temperature and relative humidity. Hourly values are read and interpolated to fit the chosen time step.

6.3.1 Mathematical model

6.3.1.1 Solar radiation incident on sloped surfaces

Conventional equations based on geometrical relationships and the Perez model (Perez et al., 1990) are used to evaluate the diffuse and beam solar radiation incident on a surface. They are presented in section 4.1.1.

6.3.1.2 Solar radiation distribution on interior surfaces

Since it was found that only 30%-90% of radiation transmitted through the glazing is retained in a highly glazed space such as a solarium or a greenhouse (Wall, 1995), the solar radiation distribution on interior surfaces is modelled here with a detailed method combining ray tracing and radiosity techniques which is presented in section 4.1.2.

6.3.1.3 Convective heat transfer

Correlations derived by Khalifa and Marshall (1990) are used for the calculation of convective heat transfer coefficients of interior surfaces. They are presented in section 4.2, along with the exterior convective coefficient due to wind.

Convective coefficients for air spaces between window panes and between windows and shading devices are calculated following the procedure outlined in ISO 15099 (2003) for thermally driven ventilation, presented in section 4.2.

In the presence of an active thermal storage, the storage mass is divided into two layers separated by a ventilated air channel. The heat exchange in the ventilated air gap is modelled using control volumes. The air and surfaces temperature is assumed constant in each control volume. Typically three or four control volumes are sufficient to adequately capture the heat transfer. The convective coefficient in the air channel is calculated with

$$h_{c,ch} = \frac{\mathrm{Nu}\, k}{D_h} \tag{6.1}$$

where the calculation of the Nusselt number is based on the correlations developed by Candanedo et al. (2011) for the front and back surfaces separately.

6.3.1.4 Radiative heat transfer

Long wave radiation exchanges between interior surfaces are modeled using the Gebhart method (Gebhart, 1959; Mottard and Fissore, 2007), which is detailed in section 4.3.

Longwave radiation exchange between an exterior surface and the ground, sky and air is given by

$$q_{LWR,o} = q_{gnd} + q_{sky} + q_o \tag{6.2}$$

where equations for calculating q_{gnd}, q_{sky} and q_o are presented in section 4.3.

Radiative heat transfer between panes of glass and in glazing/shade cavities are calculated based on the fundamental equation for two infinite parallel plates, also presented in section 4.3. The radiative and convective coefficients of glazing and shading systems are calculated individually at every time step to take into account variations due to temperature.

6.3.1.5 Thermal Storage

The model offers the possibility to include two thermal storages: one located on the floor and one located on one wall. The wall thermal storage may be made of only one layer or two layers with active air circulation in between. The thermal storages may be composed of sensible or phase change materials (PCM). In particular, one possible design consists of PCM panels located on the north wall separated by an air channel with active recirculation. Active ventilation enhances thermal coupling between the indoor air and the thermal storage. In addition, it enables a more effective storage of excess heat and its release when needed.

Latent heat storage is accumulating or releasing heat during the phase change occurring at the phase transition temperature. The latent heat for a given mass of substance is given by

$$\dot{Q} = m\lambda \tag{6.3}$$

Heat transfer in PCM is usually modeled using finite difference or finite elements methods. The two most common modeling methods are the enthalpy method and the heat capacity method (Lamberg et al., 2004). The heat capacity method is intuitive and easy to program since the heat capacity accounts for both sensible and latent heat transfer. It allows the modeling of non-isothermal phase change, which is frequently observed for non-pure materials. The heat capacity can be estimated from results obtained by a differential scanning calorimeter (DSC) (Al-Saadi and Zhai, 2013). If not available, an effective heat capacity can be estimated with

$$c_{\text{eff}} = \frac{\lambda}{T_2 - T_1} + c_p \tag{6.4}$$

where T_1 is the temperature where melting (or solidification) begins and T_2 is the temperature at which the material is completely melted (or solidified). Hysteresis can be accounted for by calculating the effective heat capacity separately for melting and freezing or by using the heat capacity curves obtained by DSC for freezing and melting, if available.

Due to its ease of implementation and its suitability for modelling materials with gradual phase changes, the heat capacity method was chosen for this study where the latent heat transfer is simulated using empirical results obtained by DSC to approximate the heat capacity.

6.3.2 Numerical model

Numerical simulations are based on a transient lumped parameters heat transfer model; this type of model enables accurate simulation of transient effects induced by thermal mass. A finite difference thermal network formulation is used to solve equations at each node i. The temperature of a node i with and without thermal mass is calculated as

$$T_{i,t+1} = \frac{\Delta t}{C}\left(Q_{i,t} + h_{c,i}(T_{in,t} - T_{i,t}) + \sum_j (T_{j,t} - T_{i,t}) R_{ij}^{-1} + q_{LWR,i}\right) + T_{i,t} \tag{6.5a}$$

$$T_{i,t+1} = \frac{Q_{i,t} + h_{c,i} T_{in,t} + \sum_j R_{ij}^{-1} T_{j,t} + q_{LWR,i}}{h_{c,i} + \sum_j R_{ij}^{-1}} \tag{6.5b}$$

where j represents all nodes experiencing conductive exchanges with i, $Q_{i,t}$ is a heat source at node i, $h_{c,i}$ is the convective coefficient of surface i (in W/K in this case) and $q_{LWR,i}$ is the net long wave radiation emitted by surface i.

Since interior long wave radiation exchanges are modelled with non linear relationships, as expressed by equation 4.21, they are very sensitive to the temperature of interior surfaces. A relatively small change in a surface temperature causes an important change in radiation flux exchanges. An important temperature change from one time step to another might trigger instability and divergence of the simulations. Therefore, it is necessary to consider the thermal capacity of insulation materials and panes of glass, even when low and usually neglected for energy calculations, to avoid instability.

A time step of 3.6 s is used in the simulation model presented in section 6.4 where phase change materials are present and a time step of 12 mn is used in the model presented in section 6.5.

6.4 Experimental comparison

6.4.1 Description of the solarium test-room

A solarium test-room has been designed by adapting a reconfigurable mobile test-room with a PCM wall with the possibility of active charge/discharge. A schematic of the test room is presented in figure 6.1. The walls are 100 mm thick and made of interior and exterior plywood filled with fiberglass batts between wood studs. Technical characteristics of the test room are presented in table 6.1.

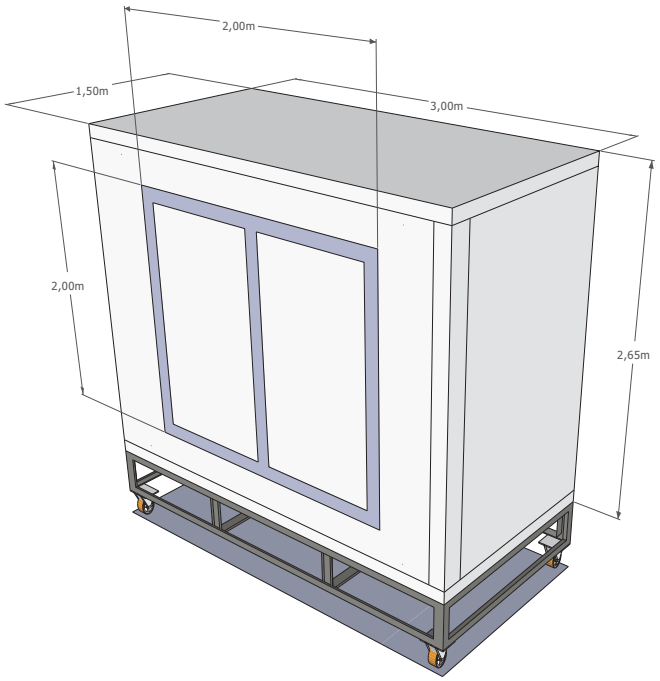

Figure 6.1: Schematic of the solarium test room with exterior dimensions

Table 6.1: Parameters of the prototype solarium [a]Could not be measured

Int room length-width-height	2.80-1.30-2.44 m
Interior shade solar transmittance	0.77
Interior shade solar reflectance	0.21
Interior shade openness factor	0.52
Interior shade emissivity	0.93
Interior shade thermal resistance	0.01 m^2K/W^a
Interior cavity width	0.155 m
Exterior shade solar transmittance	0.00
Exterior shade solar absorptance	0.28
Exterior shade openness factor	0.00
Exterior shade emissivity	0.79/0.76
Exterior shade thermal resistance	0.080 m^2K/W
Exterior cavity width	0.054 m

The fenestration system consists of a double-glazed argon-filled glazing unit with a low-emissivity coating with motorized interior and exterior shades. The interior shade is a high transmittance roller shade while the exterior shade consists of an exterior roller shutter with polyurethane filled aluminum slats. The optical and thermal properties of the shades are displayed in table 6.1. The thermal resistance of the interior shade was too low to be measured, so a value of 0.01 W/(m^2 K) has been chosen for the simulations.

The U-value and SHGC of the insulated glazing unit have been simulated with Window 6.3 (LBNL, 2014) under NFRC conditions as 1.314 W/(m^2 K) and 0.262. The U-value of the frame has been evaluated by an independent laboratory as 1.9 W/(m^2 K). The radiation emitted by the solar simulator transmitted through the window has been calculated from measurements obtained with a pyranometer mounted on a mobile arm as 0.34. Long wave radiation exchanges between the window and the hot lamps from the solar simulator had to be considered.

The air tightness has been measured at different pressure differential levels. The overall U-value of the test room with retracted shades and no PCM has been experimentally measured under steady-state conditions as 0.56 W/(m^2 K). After calibrating the model, the infiltration rate under normal conditions has been estimated as 0.25 ACH and the overall U-value of the test room for the walls, floor and ceiling (no fenestration nor infiltration) was evaluated at 0.4 W/(m^2 K).

Commercial PCM wallboards made of a mixture of an ethylene-based polymer and paraffin 60%wt were installed on the back wall. Three layers of PCM were installed on the front side and two layers on the back side with a 30 mm channel for active air circulation in between. This air channel was continuously ventilated with an air velocity of 1.5 m/s.

Four panels were necessary to fully cover the back wall and were treated as one continuous layer with uniform temperature. With five layers of PCM, the 20 installed panels are equivalent to a total latent storage capacity of about 7540 kJ (or 2.1 kWh). There were two additional layers of polystyrene insulation behind the PCM layers. Figure 6.2 shows the geometry of this active PCM wall thermal storage.

According to manufacturer's data, the melting point of this PCM is 21.7°C with a latent heat of fusion of 70 kJ/kg. For a temperature difference from 0 to 30 °C, the total heat stored per panel would be about 755 kJ or 140 kJ/kg. The properties of these PCM boards have been analyzed in other studies and their properties are summarized in table 6.2 for various sources. There are some relatively important discrepancies.

In the present study, the average mass of one panel was determined as 6.074 kg, yielding a density of 973 kg/m^3. The specific heat capacity method was implemented where specific heat capacities were evaluated from DSC curves for melting and freezing reported in Kuznik and Virgone (2009). The conductivity of the PCM was evaluated at a given temperature using the curves published in Kuznik et al. (2008).

Ten type T thermocouples were installed on the surface of each PCM layer at key locations. Results confirm that treating the 4 PCM panels as one layer with uniform temperature was a valid assumption. This was expected, since the PCM are wrapped with an aluminum sheet. Thermocouple readings of one layer were averaged and are presented in section 6.4.4.

Each layer of PCM is modeled as one control volume, centered, except for layers # 3 and 4 (layer # 1 being the innermost layer). Layers # 3 and 4 are separated by a ventilated air gap where the heat exchange was modelled using three control volumes. There was a simulated contact resistance of 0.02 m^2K/W between the panels to account for the fact that air convection pockets were probably formed in some places due to the difficulty of creating an even contact on all the surface of the PCM board.

Since it was impossible to install a thermocouple in the middle of a PCM panel, the experimental bulk temperature of one PCM was calculated as the average of the surface temperatures. These bulk temperatures have been used to calculate the amount of heat stored and are presented in section 6.4.4.

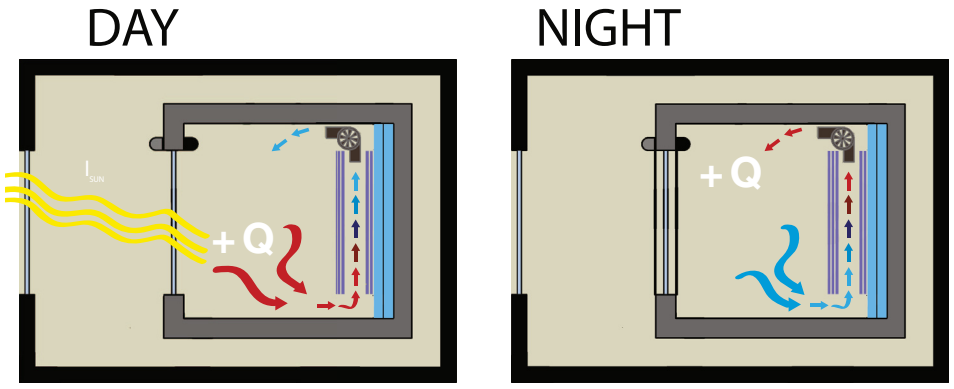

Figure 6.2: PCM wall-integrated heat exchanger (Courtesy of William Gagnon)

Table 6.2: Technical specifications of PCM panels from various sources

	Manufacturer (HR 1 °C/mn)	Kuznik et al. (2008) (HR 2 °C/mn)	Kuznik and Virgone (2009) (HR 0.05 °C/mn)	Tabares-velasco et al. (2012) (HR 0.05 °C/mn)
Mass	5.391 kg			
Dimensions	1000 x 1198 mm			
Thickness	5.2 mm			5.3 mm
Density	855.5 kg/m^3	1019 kg/m^3	$\approx$ 900 kg/m^3	855 kg/m^3
T melting	21.7°C	$\approx$ 22 °C		
T melting p		22.2 °C	22.3 °C	23.3 °C
T freezing p			17.8 °C	
Latent heat, melting	>70 000 J/kg		72 400 J/kg	
Latent heat, freezing			71 000 J/kg	
C_p - sensible	2333 J/(kg°C)			2500 J/(kg°C)
C_p - melting p		15 200 J/(kg °C)	13 400 J/(kg °C)	13 810 J/(kg °C)
C_p - freezing p			12 900 J/(kg °C)	
C_p - solid			2400 J/(kg°C)	
Conductivity - solid	0.18 W/(mK)	0.22 W/(mK)	*0.18 W/(mK)*[a]	0.18
Conductivity - liquid	0.14 W/(mK)	0.18 W/(mK)	*0.22 W/(mK)* [a]	0.14

[a]Not consistent with the author's previous study conductivity curve, values were probably inverted inadvertently

6.4.2 Experimental facility

The experimental work took place in the Solar Simulator - Environmental Chamber at Concordia University, which features two solar simulators and a climatic chamber. The environmental chamber can provide temperatures varying between -40°C and +50°C and a relative humidity between 20% and 95%. This unique facility enables accurate and repeatable testing of solar systems and advanced building envelopes under controlled conditions.

The test solarium was placed inside the climatic chamber and subjected to radiation emitted by a full-scale solar simulator. Pictures of the experimental facility are shown in figure 6.3.

(a) Solar simulator and environmental chamber

(b) Test solarium under illumination

Figure 6.3: Experimental facility

6.4.3 Testing conditions

The cyclic solar radiation profile and constant outdoor temperature selected for the experiment are illustrated in figure 6.4. The average temperature surrounding the test solarium throughout the experiment was measured as 5.7°C. The solarium was illuminated three hours per day. The average radiation incoming on the window at the first and last sunny hour was measured with a pyranometer as 502 W/m^2 while it reached 1033 W/m^2 for the peak hour.

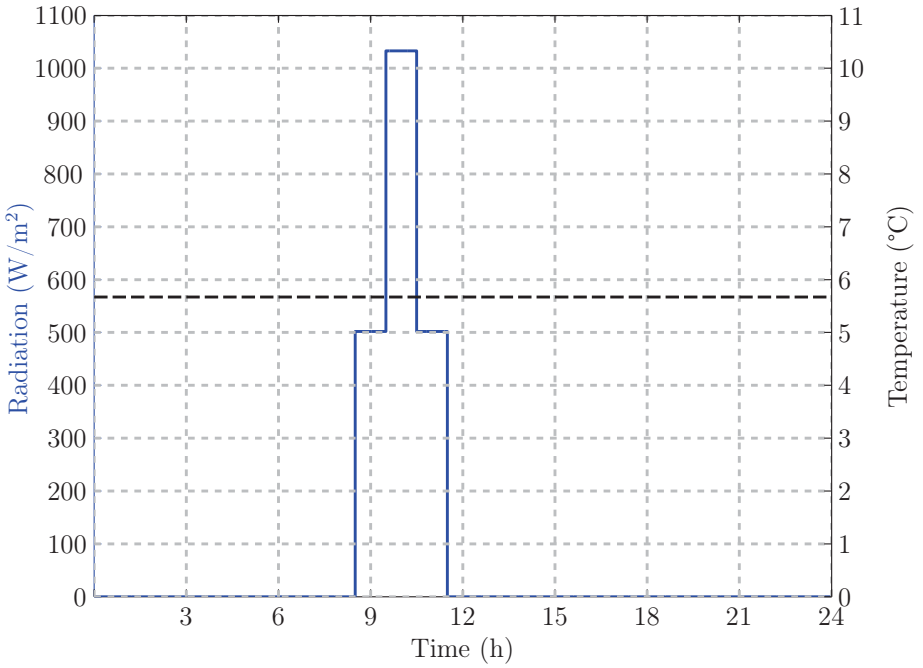

Figure 6.4: Experimental solar radiation profile incident on the window (502 W/m^2 and 1033 W/m^2) and average temperature inside the climatic chamber (5.7°C).

These cyclic conditions were provided until a steady response was observed. At the third day, the thermal response was identical to the second day with less than 1°C difference of indoor air temperature.

6.4.4 Comparison of experimental and simulated results

Simulation and experimental results are depicted in figures 6.5 and 6.6. Near cyclic conditions have been obtained after three days of both simulations and experiments; only the last day is presented.

As seen from figure 6.5, experimental and simulated temperature of bulk PCM temperature are in good agreement. The maximum temperature difference is 1.5°C and occurs for layer #2. The simulated peak temperature of the first three PCM layers tends to be lower than experimentally while the simulated peak temperature of the last two layers tends to be higher. This might indicate that the convective coefficient of the front channel surface is underestimated and the coefficient of the back surface is overestimated using Candanedo's equation (Candanedo et al., 2011).

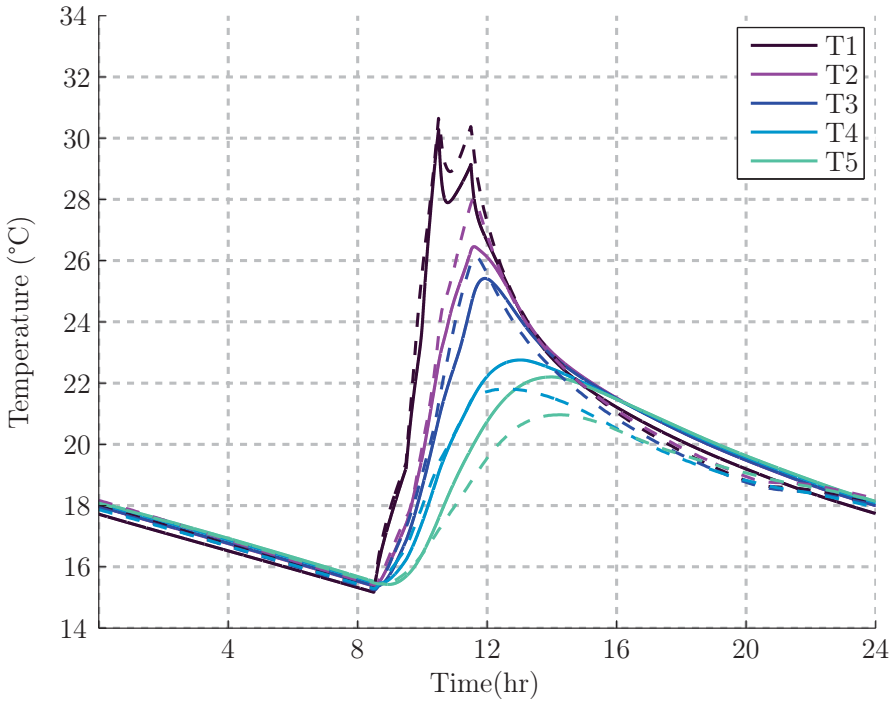

Figure 6.5: Experimental (solid) and simulated (dashed) bulk temperature of PCMs layers

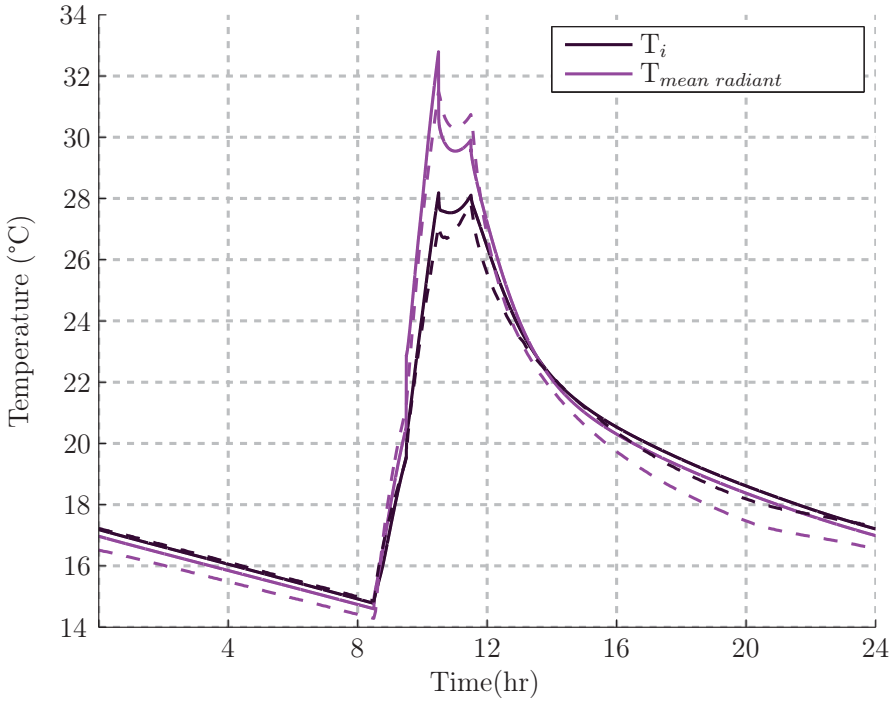

Figure 6.6: Experimental (solid) and simulated (dashed) indoor air temperature and mean radiant temperature

As depicted in figure 6.6, simulations of indoor and mean radiant air temperature are in good agreement with experimental results. The maximum absolute temperature difference is 1.0 °C for the air temperature and is 0.8 °C for the mean radiant temperature. The discontinuity of the specific heat occurring during a partial phase transition was not corrected. Using a model for transitioning inside the phase change zone such as the one suggested in Bony and Citherlet (2007) could improve the model.

The heat stored and released by each PCM layer has been calculated from the experimental bulk temperature and is presented in table 6.3. The associated uncertainty is presented in Appendix B. The heat stored per kilogram in the given experimental conditions is significantly higher than what is stated by the manufacturer. This is explained by the difficulty in evaluating the sensible specific heat of a PCM. While the reported sensible specific heat of this PCM lies between 2333 and 2500 J/(kg°C) as seen from table 6.2, it can be seen in Kuznik and Virgone (2009) that the specific heat at 5 and 30°C is respectively 3724 and 2640 J/(kg°C) for melting and 4027 and 2557 J/(kg°C) for freezing.

Table 6.3: Heat stored and released in PCMs for a diurnal cycle

	Heat stored		Heat released		Total temperature
	Per layer (kJ)	Per kg (kJ/kg)	Per layer (kJ)	Per kg (kJ/kg)	variation (°C)
Layer 1	8 260	336	7 328	298	34.1
Layer 2	7 409	302	6 507	265	25.6
Layer 3	6 971	284	6 260	255	22.2
Layer 4	4 301	175	4 974	202	13.5
Layer 5	3 453	141	4 362	178	11.6
Total	30 393	247	29 431	240	

6.5 Shading control strategy

6.5.1 Design of the simulated solarium

A south facing attached solarium has been modelled as described in section 6.3. The solarium is 10 meters long and 2.4 meters wide with a south roof angle of 35°. It is attached to a house with a thermally massive common wall made of two layers of bricks of a thickness of 200 mm each separated by a 40 mm air channel. The back side of the second layer of bricks is insulated with RSI 10.6 (R60). The temperature in the house is maintained at a constant 20°C. There is also a passive thermal storage that consists of a 200 mm concrete floor. The infiltration rate is set to 0.1 air change per hour throughout the year.

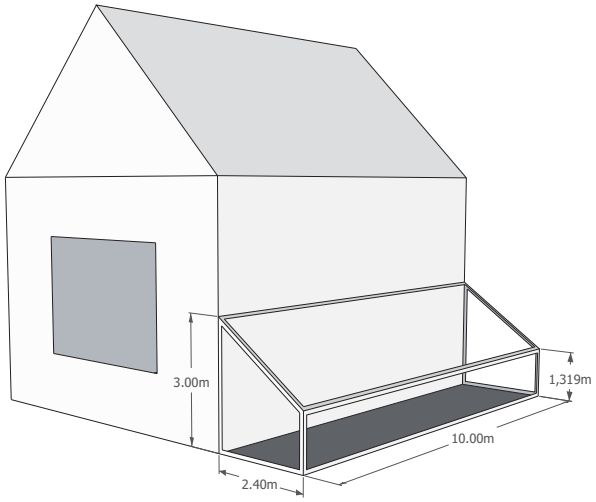

Figure 6.7: Simulated attached solarium

Simulations were conducted with clear double glass. The solarium is equipped with an interior roller blind and an exterior roller shutter, both motorized. Shades were assumed to be parallel to the glazing and to cover both glazing and framing members. For the energy control scheme, shades with different orientations can be controlled independently. The cavity between the exterior shade and the window is 50 mm while the cavity between the indoor shade and the window is 30 mm. The opaque roller shutter has a thermal resistance of 0.1 m^2K/W and an emissivity of 0.8. The interior roller blind has a solar transmittance of 0.19 and a solar reflectance of 0.71. An interior shade with such a high solar reflectance is useful both in the heating season by reflecting the solar gains from other glazed surfaces inside the space and in the warmer season by reflecting direct solar radiation outside the space.

6.5.2 Shading control algorithm

This control algorithm is based on performing an energy balance on the fenestration system. In this study, the total heat flow through a fenestration system is calculated as:

- Solar radiation transmitted through the fenestration system and absorbed by interior surfaces
- + Heat flow through the fenestration system from outdoor to the zone

To evaluate the effect of moving one shade on the solar gains from other glazed surfaces, it is necessary to consider the solar radiation gained or lost from other fenestration systems by moving the position of that shade. Therefore, when calculating the total heat flow through a fenestration system in a different state, the following term must be added:

- + Solar radiation gained or lost from other fenestration systems by moving the position of the shade

The transmitted solar radiation absorbed by interior surfaces takes into account the diffuse solar radiation that is reflected back towards the windows and transmitted outside. For multilayered surfaces (e.g. fenestrations), the optical properties are assumed to be those of the innermost layer except for the case with the exterior shade, where the optical properties are assumed to be those of the exterior shade. Conduction through the frame is also accounted for by using the parallel path heat flow method. The overall heat transfer through the fenestration system is calculated based on the convective and radiative exchanges in glass and shades cavities and the indoor and outdoor convective coefficients, as described in section 6.3.1.

More specifically, the total heat flow through a window with/without shade(s) is calculated as:

$$\text{No shade} \qquad Q_{\text{øS,i}} = S_{\text{øS,i}} - U_{\text{øS,i}} A_i (T_{in} - T_o) + \left[\mu \sum_{j \neq i} \Delta S_{\text{øS,j}} \right] \tag{6.6a}$$

$$\text{Interior shade} \qquad Q_{\text{inS,i}} = S_{\text{inS,i}} - U_{\text{inS,i}} A_i (T_{in} - T_o) + \left[\mu \sum_{j \neq i} \Delta S_{\text{inS,j}} \right] \tag{6.6b}$$

$$\text{Exterior shade} \qquad Q_{\text{exS,i}} = S_{\text{exS,i}} - U_{\text{exS,i}} A_i (T_{in} - T_o) + \left[\mu \sum_{j \neq i} \Delta S_{\text{exS,j}} \right] \tag{6.6c}$$

$$\text{Both shades} \qquad Q_{\text{in+exS,i}} = S_{\text{in+exS,i}} - U_{\text{in+exS,i}} A_i (T_{in} - T_o) + \left[\mu \sum_{j \neq i} \Delta S_{\text{in+exS,j}} \right] \tag{6.6d}$$

with the terms in brackets being needed only to evaluate the heat flow when the window is in a different state (e.g., if the interior shade is drawn, the term in brackets must be added in $Q_{\text{øS,i}}$). The coefficient μ is equal to unity most of the time, except when a shade is moved and has a different position than at the previous time step, where μ then equals 0.5. This is to reduce oscillations when the heat flow through the window in two different shading configurations is very close.

The total heat flow as described by equations 6.6 can be maximized or minimized depending on the needs of the space under consideration; by feeding the state of the HVAC system (or another variable) to the algorithm, the total heat flow can be maximized when in heating mode and minimized when in cooling mode. The control algorithm selects the best option and the shades are operated at a fully open or closed position for the entire time step.

A thermal network showing the conductive, radiative and convective heat transfers in the fenestration system considered in this study is shown in figure 6.8. Convective and radiative coefficients $h_{c,i}$ and $h_{r,i}$ are calculated individually at every time step as described in sections 6.3.1.3 and 6.3.1.4.

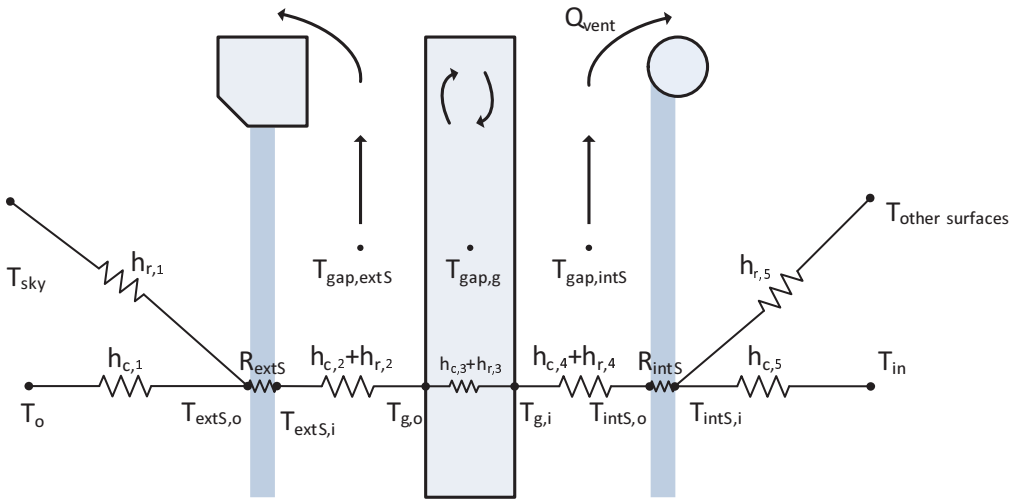

Figure 6.8: Thermal network of a fenestration system

From a physical point of view, maximizing or minimizing the total heat through a fenestration system, as described by the four discrete feasible solutions from equations 6.6, is rather straightforward. The difficulties reside in the numerical modelling, as many *what if* scenarios must be considered.

Calculating the heat flow through a bare window is simple. Calculating the heat flow through that window if a shade was drawn requires the calculation of the shade temperature if it was present because the convective and radiative heat transfer depend on it. Therefore, at all time steps, the temperature of the shade(s) must be calculated, whether present or not.

Another difficulty arises by the fact that drawing a shade of one window affects not only the solar gains through that window but also from other windows. For instance, in early morning, opening the east shade allows the solar gains inside the space and closing the west shade contributes to keeping these gains inside the space (opening the west shade would allow most beam radiation to escape the space). Therefore, at all time steps, it is necessary to calculate not only the solar radiation transmitted by surface i and absorbed with the actual shade(s) position, but also the absorbed radiation change if a shade is closed (or opened), for all glazed orientations. This is represented by the terms in brackets in equations 6.6.

6.5.3 Simulation results and discussion

The main objective of these simulations is to compare different types of controls for motorized shadings and assess their relative energy performance. An energy efficient solarium design was selected with the goal of collecting surplus heat that could be used to heat the adjacent house. Annual simulations were performed for the city of Montreal from October 1st to September 30th with a 28 days simulation warm-up period. The year is divided in two modes : a heating mode (October 1st to April 30th) and a mixed mode (May 1st to September 30th). During the heating mode, excess energy was considered when the temperature reached 28°C and heating is provided to keep a minimum temperature of 10°C. This surplus heat could be stored (with more thermal storage) or transferred to the house to partly offset its heating load.

The energy control algorithm is detailed is section 6.5.2. This type of control is compared with a control scheme based on a fixed solar radiation set-point. For the solar control scheme, shades are controlled together based on the global horizontal solar radiation level; they open when this level exceeds a predetermined value. Many simulations were run with different solar radiation levels at 25 W/m^2 increments, but only the best results are presented in table 6.4. Therefore, these radiation levels can be considered as near optimum. The solar radiation set-point judged the best was the one providing the highest average temperature during the heating mode. These set-points are presented in bold in table 6.4 and all comparisons are performed in regards to these *best* solar radiation set-points.

During the heating mode, the energy control algorithm is set to maximize the total heat flow at all time. During the mixed mode, the energy control algorithm minimizes the heat flow if the inside temperature is above 25°C or maximizes it otherwise. For the solar control in mixed mode, in addition to open when the global horizontal solar radiation level exceeds a chosen value, all shades are closed if the inside temperature is above 25°C. For all shade control types, there is no controlled ventilation in heating mode and there is 2 air change per hour if the inside temperature is above 23°C in mixed mode.

6.5.3.1 Energy consumption

As seen from table 6.4, the heating consumption of a solarium with an interior shade controlled with the energy scheme can be reduced by 3% compared to a control based on a global solar radiation level of 50 W/m^2. In addition, the excess energy (i.e. the heat stored when the temperature inside the solarium reached 28°C) can be increased by 10%.

Table 6.4: Heating requirements, excess energy, average temperature and percentage of comfortable hours of a solarium with clear double glazing and different shade configurations and controls (Set-points in heating mode: 10-28°C)

Type of control	Heating kWh	Excess energy kWh	Average temperature °C	Comfort time %	Average temperature °C	Comfort time %
			Heating mode		Mixed mode	
Solarium without shades						
No shades	3011	656	15.47	31.0	27.17	43.3
Solarium with interior shade						
Energy balance	1856	1338	17.53	35.9	26.33	63.3
Solar (25W/m^2)	1897	1184	17.38	35.8	27.43	42.5
Solar (50W/m^2)	1921	1214	17.41	35.7	27.44	42.5
Solar (75W/m^2)	1991	1234	17.39	35.7	27.44	42.6
Solarium with exterior shade						
Energy balance	1222	1216	17.61	36.1	24.25	97.7
Solar (25 W/m^2)	1324	1091	17.33	36.1	24.35	97.8
Solar (50 W/m^2)	1313	1111	17.39	36.0	24.35	97.8
Solar (75 W/m^2)	1349	1120	17.39	35.8	24.36	97.8
Solarium with interior and exterior shade						
Energy balance	670	2007	19.25	34.7	24.65	97.9
Solar (25-50 W/m^2)	767	1670	18.88	35.6	24.73	98.3
Solar (50-50 W/m^2)	735	1756	18.98	35.5	24.75	98.3
Solar (50-75 W/m^2)	780	1760	18.94	32.3	24.74	98.3

For a solarium with an exterior shade, the heating consumption can be reduced by 7% and the excess energy can be increased by 9% with the proposed control strategy compared to a radiation set-point of 50 W/m^2.

For a solarium design with both interior and exterior shades, the heating consumption can be reduced by 9% and the excess energy can by increased by 14% compared to a radiation set-point of 50 W/m^2 for both shades.

The solarium has a significantly lower heating consumption when equipped with an exterior shade compared to an indoor one. This is due to the increased thermal resistance of the exterior shade. However, the solarium equipped with an interior shade can collect more surplus heat than with an exterior shade, because of its higher solar transmittance.

6.5.3.2 Thermal comfort

A common desirable feature of a solarium is to connect its occupants with the exterior surrounding. Given the nature of this space, a wider temperature range than usual was selected for the thermal comfort range. The lowest limit for thermal comfort has been selected as 17°C, as it represents the lowest acceptable temperature (with 80% acceptance) for naturally ventilated buildings with a mean outdoor temperature of 5°C. The upper limit for comfort has been selected as 28°C. It should be remembered that the indoor air temperature was not allowed to go above 28°C when in heating mode.

The percentage of time when the operative temperature was within the comfort zone as described above is presented in table 6.4. When the exterior shade is controlled with the energy scheme, either alone or in combination with the interior shade, the comfortable period is similar to other control types. The exterior shade, which is opaque to solar radiation, is highly effective for limiting temperature rise, regardless of the control type. Controlling the interior shade with the energy scheme during the mixed mode reduces the average temperature by 1.1°C and yields 20.8% more comfortable hours, which represents 1822 hours during the simulated period.

6.6 Applications, recommendations and limitations

The shading control strategy proposed here can be used in solariums and greenhouses as well as residential and office buildings. In all cases, the presence of thermal storage materials is important for maximizing the energy gains obtained by using this control strategy, especially during the heating and shoulder periods.

One proven method of enhancing solar gain utilization is by integrating thermal storage materials in direct-gain rooms. In buildings with large glazed area, the solar gains often exceed the instantaneous heating load during the shoulder seasons; significant amounts of thermal mass are thus required to store the excess solar gains without causing large temperature swings (Athienitis et al., 1997).

This control algorithm can be used for minimizing or maximizing the total heat flow through fenestrations systems; therefore, it can be used in both heating and cooling modes. The switch from one state to another can be triggered by feeding the state of the HVAC system to the algorithm, the indoor or outdoor temperature, or other user-defined criteria.

The proposed control strategy can be employed in solariums and greenhouses in all climate types. Attached solariums and rooftop greenhouses can transfer the surplus heat to the adjacent building, thus maximizing the energy gains by making use of the excess heat. For old houses, the excess heat is likely to be useful at all time during the heating season, but this might not be the case for more recent houses with a better envelope (Bastien and Athienitis, 2013).

This control strategy is also applicable to greenhouses, where it can be particularly useful for closed and semi closed greenhouses. A closed greenhouse has no openings to bring in fresh air for humidity and temperature control. It is equipped with a seasonal thermal storage, where heat is stored during the summer for use in winter. In addition, dehumidification equipment must be present for humidity control (Vadiee and Martin, 2012). Typically, a closed greenhouse can collect about four times the heat needed for its winter operation during one year. Therefore, some are suggesting to build one closed greenhouse in combination to three normal greenhouses to fully utilize the solar gains (Vadiee and Martin, 2013a).

Closed greenhouses require a lot of mechanical equipment for temperature and humidity control, making them relatively expensive to build and operate. As a more viable alternative, the semi closed greenhouse concept has been suggested where part of the cooling and dehumidification demand is met by ventilation through windows (Vadiee and Martin, 2012).

Implementing the control algorithm presented here for maximizing the heat flow in closed greenhouses would make use of the excess heat all year round by either using it or storing it. Implementing it in semi closed and conventional greenhouses in both heating and cooling modes could reduce the heating requirements when in heating mode and reduce indoor temperature when in cooling mode.

This shading control strategy can also be applicable to residential buildings for maximizing the solar energy utilization from glazed surfaces. For applications like a solarium or a house where providing living space for occupants is important, the proposed control algorithm could be implemented as the default mode while allowing occupants override to provide for glare and privacy issues.

This control algorithm can also be included as an additional criteria in existing control strategies for office buildings based on visual comfort. Depending on the state of the HVAC system, equations 6.6 can be maximized or minimized to reduce the heating and cooling loads. The internal gains from the lighting system can be easily added to equations 6.6 so as to define a control strategy that utilizes daylight but does not allow excessive solar gains, such

as the approach suggested by Tzempelikos and Shen (2013). Optimal control algorithms such as the one presented in Kummert et al. (2001) where a cost function depending on heating consumption and thermal comfort is minimized should be developed for the optimal control of shades, lights and HVAC systems to reduce the overall energy consumption while maintaining thermal and visual comfort. The method presented in this chapter for calculating the total heat flow through fenestration systems could be useful for reaching this goal.

6.7 Conclusion

This paper presents a new control strategy for improving the control of shades based on performing an energy balance on fenestration systems. Difficulties associated with the numerical implementation of this control strategy are discussed and solutions are proposed. The presented control algorithm is generic and can be applied to any glazing type, shading properties, façade orientation and climate. It is suitable for spaces with multiple façade orientations.

The control strategy is based on analyzing the total heat flow, which can be maximized or minimized depending on the needs of the space. The presented control strategy can be used with one interior and/or one exterior planar shade.

This control method could be useful for solariums, greenhouses and residential buildings. It could also be included as an additional criteria in existing control strategies for office buildings.

A solarium model was developed in order to assess the performance of the proposed shading strategy. The simulation model has been compared experimentally with a prototype solarium equipped with indoor and outdoor motorized shadings and a ventilated thermal storage wall with phase change materials. Numerical simulations are in good agreement with experimental results.

Using this model, annual energy simulations of a solarium have been performed for the location of Montreal, Canada. The year has been divided in a heating mode (October to April) and a mixed mode (May to September). Results for heating mode indicate that the proposed control method can reduce the heating consumption by 3% and 7% for an interior and exterior shade, respectively. In addition, the excess heat collected can be increased by 10% and 9% for an interior and exterior shade, respectively. When using both an indoor and outdoor shade, the proposed control could reduce heating by 9% and increase the excess heat

collected by 14%. Results for the mixed mode show that operating the interior shade with the proposed control can significantly improve thermal comfort by increasing the comfortable period from 42.5% to 63.3%, which corresponds to 1822 hours.

Future research should include evaluating the performance of this shading control strategy for other building and shading types; developing a methodology for selecting high performing fenestration systems (i.e. combination of glazing with shades); and quantifying the benefits of different thermal mass levels in solariums and greenhouses.

Chapter 7

Methodology for sizing passive thermal energy storage in solaria and greenhouses

7.1 Chapter abstract

This paper presents a methodology for sizing passive thermal energy storage (TES) systems in solaria and greenhouses. First, potential targets for thermal mass design strategies are reviewed, along with common metrics used in the characterization of the performance of TES systems. This review exercise of targets and metrics provides the basis for the identification of the most relevant performance variables for solaria and greenhouses.

Six different solarium/greenhouse designs are investigated, which encompass the most frequent configurations. These configurations are studied with two complementary approaches: frequency response (FR) and finite difference thermal network (FD). FR models are used for sensitivity studies under short periodic design sequences while FD models are used in full-year performance assessments with real weather data.

Finally, a methodology for sizing TES in solaria and greenhouses is presented along with design recommendations. The energy balance equations for six different configurations are included, thereby the methodology is applicable to a variety of designs. The methodology is based on a FR model with a simulation design period of five cold sunny days followed by five cold cloudy days; such a design period proved to be representative of the harshest conditions in a year and thus provides a good basis for assessing design improvements. Simulation

results obtained with the FR and FD models showed a significant reduction of the daily operative temperature swing in the presence of a TES up to a thickness of 0.15-0.20 m where it remained mostly constant beyond. Increasing the thickness of a TES from 0.10 to 1 m was shown to raise the minimum operative temperature by 3 to 5 °C in unheated solaria/greenhouses. If providing comfort during the evening is an important design goal, a design with opaque north, east and west walls should be selected and include one TES on the floor or the north wall 0.05-0.10 m thick or two TES on both the wall and the floor with a thickness close to 0.06 m.

7.2 Introduction

Thermally massive elements have been present in vernacular architecture for hundreds of years; they were indeed necessary to limit temperature fluctuations and provide relative comfort in buildings before fossil fuels became largely available (Rempel and Rempel, 2013). Faced with a limited supply of fossil resources and climate change, thermal energy storage (TES) systems are still attracting interest nowadays. Storage of thermal energy is important in many applications, and especially for solar energy systems (Hasnain, 1998).

Massive materials have the ability absorb heat and release it later; the timing of the peak heat delivery should be optimized depending on the building type under consideration. For instance, Rempel and Rempel (2013) suggest 1) evening space heating for people at home; 2) afternoon space heating for people at work or at school; 3) all-night space heating for plants; 4) daytime space cooling for people, plants or equipment. They note that while passive systems cannot deliver instantly heat or cooling like mechanical systems, they are nevertheless highly adjustable by varying their material, thickness and configuration.

Many studies have been conducted about the energy saving potential of various TES designs, and a very large range of saving is reported, from being negligible up to 90% of space heating reduction (Burns et al., 1991; Kosny et al., 2001; Parameshwaran et al., 2012). This variability is caused not only by the wide design possibilities of TES systems, but also because their performance is strongly linked to their operational characteristics. While most studies identified that TES can significantly reduce the peak heating and cooling loads, a significant number of studies reported little energy savings attributed to TES (Bojic and Loveday, 1997; Aste et al., 2009; Ozel, 2014; Navarro et al., 2015).

As reported by MacCracken (2003), even if a building equipped with a TES is only shifting a portion of it's energy consumption from on-peak to off-peak hours but has the same total energy consumption, source energy savings will occur – which are 8% to 30% for two of the major California utilities. They pointed out that pollutant emissions will also be reduced, since power plants used for peak demand are the dirtiest.

The integration of TES in buildings is of particular interest for improving user acceptance (Navarro et al., 2015). Buildings integrated with TES (BITES) can be classified as active or passive systems, or a combination of both. No mechanical equipment is used in passive systems while active systems use fluids for exchanging heat with the storage media. Passive TES systems can be included in buildings at little or no cost and have the added advantages of the simplicity of design, operation and maintenance (Tiwari et al., 1988). This study is focusing on passive TES.

7.2.1 Control of passive thermal energy storage

Yu et al. (2015) presented a review of control strategies employed with active and passive BITES. They noted that buildings with passive BITES are usually equipped with HVAC systems and other equipment for regulating indoor air temperature and that an effective strategy for their control can help to maximize energy savings associated with BITES. As mentioned by Hasnain (1998), the use of inertia in building mass does not require additional HVAC equipment but special controls are required. Yu et al. (2015) noted a lack of studies on developing and evaluating control strategies for HVAC and other systems with the different types of passive BITES and concluded that future research is needed in this area.

As stated by (Bojic and Loveday, 1997), it is very important to know if the building will be heated or cooled on an intermittent or continuous basis when designing the building mass for energy savings. However, this aspect is often neglected with the majority of studies employing fixed thermostat set-points for the entire duration of the heating and cooling seasons.

An extensive study of lightweight and massive residential buildings located in various locations in the United States found that energy savings resulting from replacing light weight walls with heavy constructions are very location specific: they found reductions up to 8% of heating energy in Minneapolis and up to 18% cooling energy in Bakersfield, California (Kosny et al., 2001). Although not mentioned in the study, the set-points for heating and cooling were probably constants, indicating that further savings could be possible with different temperature controls.

A study about the impacts of thermal inertia in buildings found that the potential reduction in the energy used for heating and cooling is strongly linked to the building operation parameters such as ventilation rates and set-points for heating and cooling (Aste et al., 2009). Numerical simulations of a large building with EnergyPlus have shown that a reduction of 10% of heating energy and 20% of cooling energy is achievable in Milano by using materials with high thermal inertia coupled with appropriate operational characteristics. However, their simulations also showed that savings can be nil in the absence of adequate operational measures, like in the absence of natural ventilation at night for saving cooling energy.

According to Heier et al. (2015), sensible passive TES may pursue two objectives: either to maximize energy savings or improve thermal comfort. Since large swings of indoor temperature are beneficial for energy savings and a narrow temperature interval is key to thermal comfort, these two objectives are in conflict. This conflict may be alleviated when using phase change materials (PCM) since these materials can exchange heat effectively within a narrow temperature interval. This review identified that for residential buildings, most research have showed that only a small reduction of the heating demand is possible when using passive TES, either sensible or latent. Since TES need temperature variations to work efficiently as thermal storage, this might be the result of the strictly controlled lowest allowable temperature in residential buildings, which leaves little room for heating energy savings.

7.2.2 Design approaches

Several design approaches have been considered for the capture and release of solar heat: 1) massive exterior wall; 2) Trombe wall; 3) direct-gain space; and 4) isolated-gain space.

Massive exterior walls have been used for centuries, mainly in the form of thick adobe, cob or stone walls used in traditional architecture. Trombe walls introduced a glazed layer in front of the massive wall, mainly for reducing heat losses. Direct-gain spaces allow solar heat to enter in living spaces through windows and store that heat in interior massive elements, usually the floor or walls. Balcomb (1983) reported that it was previously thought that the thermal mass had to be exposed to direct sun to be effective, but notes that most massive surfaces enclosing a direct-gain space are quite effective as well. Isolated-gain spaces are similar to direct-gain spaces but are free of the requirement of maintaining thermal comfort for people. They may need adequate conditions for protecting plants, but their thermal requirements are more flexible than for normally conditioned spaces. This paper is focused on isolated-gain spaces such as solaria and greenhouses.

7.2.3 The use of passive storage in solaria and greenhouses: a review

Many solaria and greenhouses with various passive TES materials have been simulated and built. The most studied TES design consists of a thermally massive north wall. Since solar radiation incident from a south glazing can easily escape through the north glazing, the north wall is better opaque and insulated. Accordingly, the north wall becomes a privileged location for thermal mass. An example of the diversity of the materials and configurations selected as a north wall TES in solaria and greenhouses and their influence on the indoor climate is reported in Table 7.1.

China has a long tradition of local cultivation using so-called chinese solar greenhouses (CSG). In 2000, there were more than $2600 \cdot 10^6$ m^2 of CSG being used, providing more than 90% of the vegetables consumed in northern China in winter (Tong et al., 2009). These greenhouses have all adopted a similar design with a plastic film covering the slanted south roof, a thermal blanket deployed at night and a thermally massive north wall. These greenhouses are inexpensive and generally built with local materials. Examples of TES in CSG are reported in Table 7.1, where we can see that some earth walls can be as thick as 550 cm. Earth walls are usually rammed, either manually or mechanically, where machine rammed earth walls have a trapezoidal cross section with a smaller section at the top.

As reported by Tong et al. (2013), a few studies of massive north walls in CSG all concluded that when insulated, the best performance occurs when the insulation layer is on the outside of the massive layer; this finding is similar to studies conducted with other building types.

Wang et al. (2014) carried out simulations of CSG with different north wall designs. They mentionned that a thick earth wall can be conceptually divided into three layers: the energy-storing layer (inside), the thermally stable layer (in the middle) and the thermal insulating layer (outside). Their simulations carried out under winter conditions in northern China revealed that a 1 m wall has no thermally stable layer while this layer comprised 23% of the cross sectional area of a 1.5 m wall. From optimization calculations for minimizing the cross sectional area and maintaining a minimum temperature above 10 °C, they suggest a design of a trapezoidal wall 1.7 m thick at the base and 0.5 m thick at the top. They also conducted an analysis of the minimum air temperature as a function of the total thermal resistance and the thermal inertia index. They observed that the minimum temperature increases with both parameters, with a slower increasing rate with further increases of these two parameters.

Table 7.1: Numerical and experimental studies on the use of sensible TES north wall in solaria and greenhouses

Location	Floor area m^2	TES material	TES thickness cm	Results	Technique	Reference
Chateauroux, FR	30	Not reported	60	Heating 82% lower	Experiment	Santamouris et al. (1994b)
Ladakh, IND	20	concrete blocks	60	T_{in} 15-20 °C >T_{out}	Experiment	Santamouris et al. (1994b)
Marrakesh, MA	24	PCM	4	T_{in} 6-12 °C higher	Simulations	Berroug et al. (2011)
Elie, CA,	210	sand + ins.	15	DAT_{in} 18°C > DAT_{out}[a]	Experiment	Beshada et al. (2006)
China	300-1400	earth	80-550	Not reported	Experiment	Tong et al. (2013)
		clay brick	40-80	Not reported	Experiment	Tong et al. (2013)
		clay brick + earth	30-150	Not reported	Experiment	Tong et al. (2013)
		clay brick + ins.	45-110	Not reported	Experiment	Tong et al. (2013)
Boulder, US	9	water	5-10	Reduced T_{in} swings	Simulations	Tiwari et al. (1988)
Agrignion, GR	1000	cement, concrete + ins.	30	Heating 35% lower [b]	Exp. and sim.	Santamouris et al. (1994a)

[a] DAT = Daily average temperature

[b] The greenhouse located in Agrignion was also equipped with an earth-to-air heat exchanger which contributed to the heating reduction in combination with the north wall.

In a redesign study of a solarium located in Oregon, U.S., Rempel et al. (2013) compared the performance of integrating different levels of TES. They noticed lower air temperature peaks and warmer minimum air temperature for designs with a high level of TES. However, they also noted a slightly lower average temperature and less heat retained during the heating season than for a medium level of TES, and thus suggest to avoid the oversizing of TES. They report that occupants prioritized the experience of early evening warmth and plant protection over the supply of heat for living spaces. Interestingly, as shown later in this paper, these two priorities calls for two different thermal mass design.

Numerical and experimental studies have been conducted on the performance of greenhouses using seasonal energy storage (Vadiee and Martin, 2013b; Xu et al., 2014; Zhang et al., 2015). For efficient heat delivery and lower costs, these systems are usually equipped with a short term storage and a long term storage. Greenhouses using seasonal TES rely on active components for transferring heat from the storage media to the greenhouse air and are therefore outside the scope of this paper.

7.2.4 Objectives and overview

The aim of this contribution is to present a methodology for assisting in the design of passive TES for solaria and greenhouses. Different objectives may be pursued by incorporating TES in buildings; they are reviewed in section 7.3, along with commonly used metrics for characterizing the performance of TES. From this review, the most relevant performance metrics for isolated-gain applications are highlighted.

Six general solarium/greenhouse designs are investigated in this study and presented in section 7.4, which encompass the most frequent configurations. These configurations are analyzed with two complementary numerical modelling methods: one based on a frequency response (FR) approach for the analysis of design sequences and one based on a thermal network model solved with the finite difference (FD) method for yearly analysis.

With the FR method presented in section 7.5, different design periods are examined along with their impact on the optimal thickness of thermal storage. The effect of glazing type, varying floor area and aspect ratio, varying thermal resistance of the insulation layer, increasing thermal coupling (by raising indoor air circulation), varying thermal storage material and different design periods on the main performance variables is investigated.

The FD method, which requires spatial discretization of the thermal mass, is detailed in section 7.6. First, results obtained with the FR model are used to assist in the determination

of important parameters needed for the FD model, such as the number of nodes needed for the discretization of thermal mass. The effect of using constant, linear or non linear radiative and convective coefficients is assessed. Then, the FD method is using real weather data for analyzing the behavior of the investigated configurations for a complete year. The amount of storage needed for reaching different design goals is investigated. Both heated and unheated spaces are analyzed. The performance is evaluated for two different years and canadian cities, which allows the assessment of the sensitivity of the TES design to varying climatic conditions.

Finally, the proposed methodology for sizing TES, based on the FR model, is detailed in section 7.7 and design recommendations are presented in section 7.8.

7.3 Design intents behind thermal mass design strategies

When designing thermally massive elements in buildings, many objectives may be pursued, such as: 1) delaying the peak solar gain effect to a more favorable moment; 2) reducing the peak heat flux or the peak temperature at the room-facing layer; 3) reducing the space heating energy consumption; 4) reducing the temperature swings; 5) increasing the average space temperature; 6) increasing the minimum temperature or reducing the maximum temperature. One may focus on the processes (i.e. heat fluxes) or on the results (i.e. temperatures). Sometimes, these objectives will be in conflict with each other and call for different materials and configurations; therefore a designer must carefully select the objectives to be prioritized for a given application.

This section reviews different metrics associated to the six objectives enumerated above and discusses their relevance for passive TES in isolated-gain applications.

7.3.1 Optimal time lag

In many thermal mass design studies, the time lag is defined as the delay between the moment when the outer surface and the inner surface of an external wall reach their peak temperatures ($\tau_{[T_{\text{peak}}]}$). Many studies have analyzed the distribution and thermophysical properties of thermal mass and insulation layers of exterior walls and their impact on $\tau_{[T_{\text{peak}}]}$ and the decrement factor (the decrement factor is discussed in the next subsection). Most

studies present their analysis based on identifying the optimum distribution or properties for maximizing the peak temperature time lag and minimizing the decrement factor (Asan, 2000; Ulgen, 2002; Ozel and Pihtili, 2007; Ibrahim et al., 2013; Jin et al., 2012; Evola and Marletta, 2013). However, as explained below, these two objectives are not appropriate for isolated-gain applications.

Asan (2000) presented a numerical study on the investigation of the wall's optimum insulation position in terms of maximum peak temperature time lag and minimum decrement factor. He found that placing half the insulation in the middle of the wall and the other half at the outer surface provides both very high lag time and low decrement factor – close to optimum values.

However, as noted by Rempel and Rempel (2013), the timing of the peak heat delivery should actually depend on the building type and needs. The time lag can easily exceed 12 hours for many materials with a thickness of 30 cm and even exceed 24 hours (Asan, 2006). When the heat flux input is from solar radiation, a time lag of 24 hours in fact means no time lag at all; therefore the common conception that maximizing the time lag yields optimal performance should be reconsidered.

Some studies assumed a sinusoidal sol-air temperature over a 24 hour period (Asan, 2006). However, day length is 12 hours only at the equinox; therefore, a more realistic sol-air temperature profile should be employed for winter conditions by using Fourier series. When the sol-air temperature is calculated with more than 1 harmonic (i.e. not simply sinusoidal), the time lag of the temperature peaks and temperature crests are also different (Sun et al., 2013; Kontoleon and Bikas, 2007).

Sun et al. (2013) observed that for a massive exterior wall exposed to various periodic conditions, the average of the temperature peak and crest time lag is equal to the time lag under a sinusoidal input. The analysis of their results revealed that with a difference between the peak and crest time lag of up to 3.5 h, estimating the time lag under a sinusoidal input could induce a difference of 1.75 h with the peak time lag; this result highlights the importance of using non sinusoidal profiles as input sources.

As noted by Kontoleon and Bikas (2007), evaluating $\tau_{[T_{\text{peak}}]}$ is especially important during the cooling season for buildings that can use natural ventilation for night cooling. Gagliano et al. (2014) reported that many designers tend to increase thermal inertia without considering their limits and proper applications. They suggest that east walls should have time lags about 12-14 hours while it should be around 8 hours for west walls; longer time lags would be counter productive since that would reduce the useful time for exploiting night ventilation.

The peak temperature time lag of an exterior wall subjected to solar radiation on its exterior surface increases continuously with wall thickness (Asan, 2006). However, with massive exterior walls, heat is absorbed at the exterior surface and delivered at the interior surface, while in direct and isolated-gain applications, heat is absorbed and released from the same surface. A variable such as $\tau_{[T_{\text{peak}}]}$ cannot be employed in the latter case, since there is only one surface involved.

When using the thermal lag concept with transfer functions such a the self admittance (Athienitis and Santamouris, 2013), the input and effect can be at the same node, as captured by the self admittance time lag for instance. The self admittance is the ratio of the heat flux at one surface to the temperature of the same surface, when the temperature at the other surface is kept constant, as presented in equation 7.1.

$$Y_s = \left.\frac{Q_s}{T_s}\right|_{T_{eo}=0} \tag{7.1}$$

In frequency response models, heat sources are represented with complex Fourier series and temperatures are calculated in the frequency domain, so the self admittance is a ratio of two complex numbers (see section 7.5 for a more complete description of FR modelling).

The relationships between the heat flux, temperature and self admittance magnitude and time lag are illustrated in Figure 7.1a, for a sinusoidal heat flux input. Here the peak and crest time lags are identical, because the signal is sinusoidal. Thus, in this case, the admittance time lag can be easily interpreted as the delay between the peak heat flux and the resulting peak surface temperature.

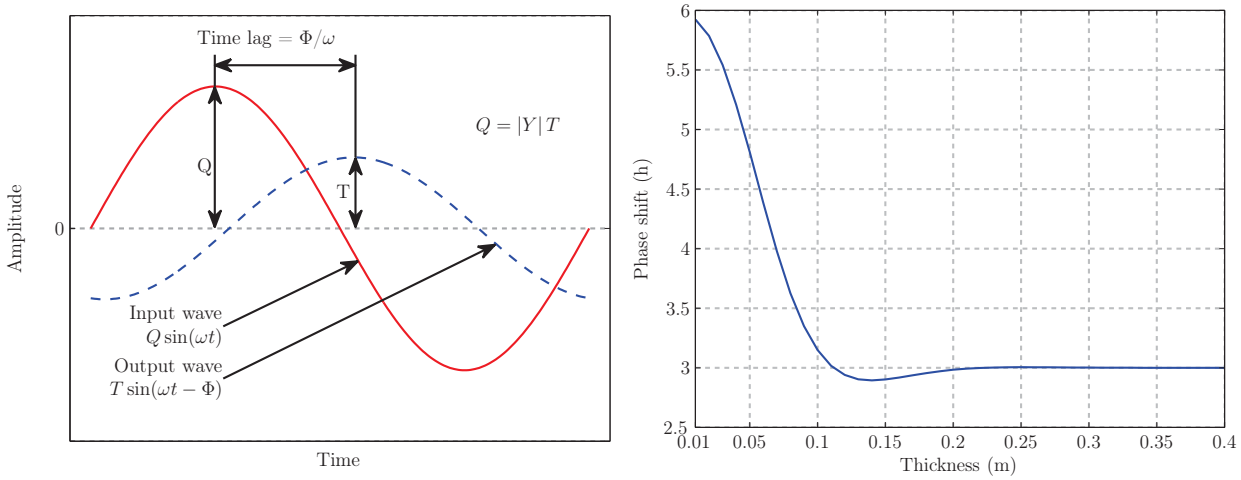

(a) Heat flux, temperature and self admittance

(b) Self admittance time lag

Figure 7.1: Heat flux, temperature and self admittance magnitude and time lag

Figure 7.1b shows the self admittance time lag of a concrete north wall in a solarium under the non sinusoidal periodic conditions of a cold sunny day at the winter solstice in Montreal (configuration N1 – more details given in section 7.4). We can see that the time lag diminishes with thickness up to a minimum of 2.9 h at 14 cm and then converges to a time lag of 3 h for thicknesses of about 20 cm and beyond, where the TES behaves like a semi infinite solid (Davies, 1994).

The operative temperature is an important parameter that closely relates to thermal comfort for both people and plants. It is defined as

$$T_{op} = \gamma_r \, T_{mrt} + (1 - \gamma_r) T_{in} \tag{7.2}$$

where T_{in} is the indoor air temperature, the radiative fraction γ_r here was set to 0.5 (a recommended value for an air velocity under 0.2 m/s (U.S. Department of Energy, 2013, section *Operative temperature control*)) and the mean radiant temperature T_{mrt} here is equal to the zone average radiant temperature (i.e. without surface temperature weighting).

For the same conditions as in figure 7.1b, figure 7.2 shows the heat flux released by the storage, the storage temperature and operative temperature for different TES thicknesses. For the three thicknesses shown, the storage temperature peak occurs earlier and the peak released heat flux occurs later with increasing thickness. It can also be seen that the released heat flux becomes more stable with increasing thickness.

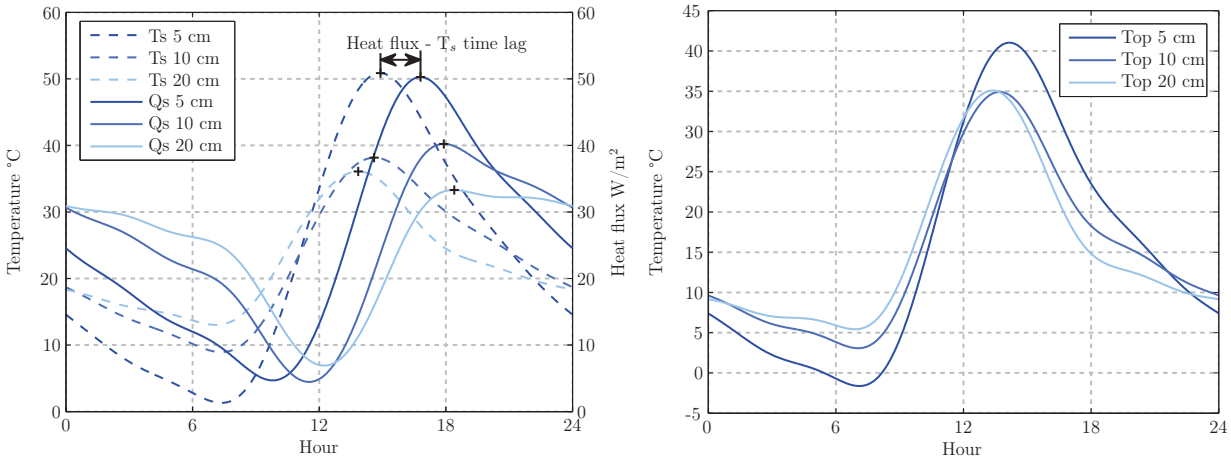

(a) Storage temperature and heat flux

(b) Operative temperature

Figure 7.2: Storage temperature, operative temperature and released heat flux for three thicknesses - configuration N1, one sunny day, winter solstice

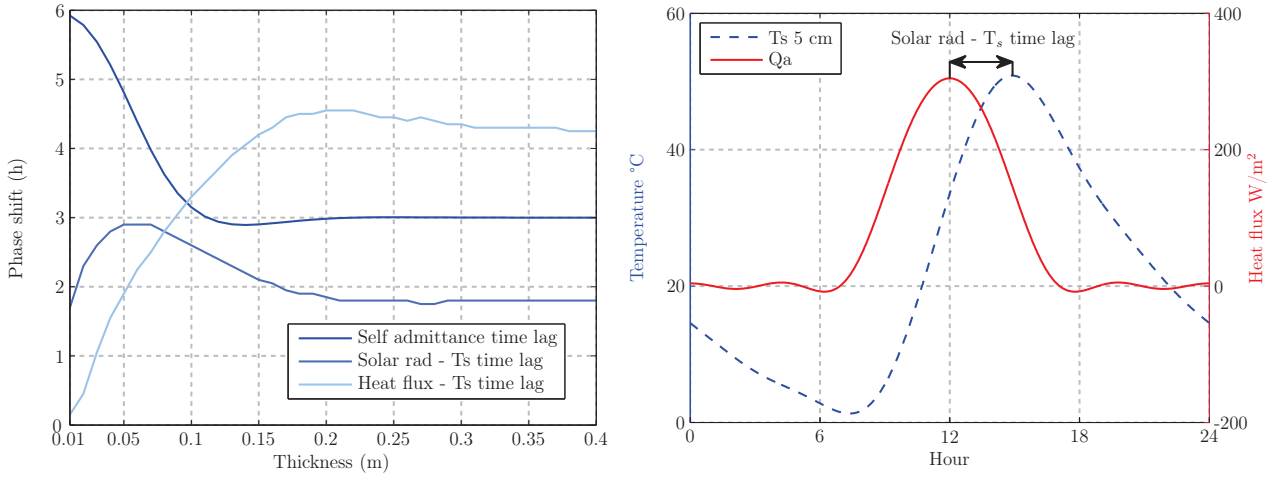

(a) Comparison of different time lags

(b) $\tau_{[Q_a - T_s]}$

Figure 7.3: Comparison of different time lags and illustration of $\tau_{[Q_a - T_s]}$ - configuration N1, one sunny day, winter solstice

The time lag between the peak released heat flux and the peak storage temperature is depicted in light blue in figure 7.3a. It increases steadily, reaches a peak at 20 cm and then converges to a slightly reduced value at greater thicknesses. Maximizing the heat flux - T_s time lag is not helpful for displacing the peak storage temperature later during the day. Furthermore, it loses significance as the released heat flux becomes smoother with increasing thickness.

7.3.1.1 New proposed metric

Therefore, here we suggest a new metric: the absorbed solar radiation heat flux - storage temperature time lag, $\tau_{[Q_a - T_s]}$. It represents the time between the peak absorbed solar radiation and the peak storage temperature, as depicted in figure 7.3b. This metric has the advantage to be easily understandable and to be relevant for thermal comfort evaluation.

As shown in Figure 7.3a, this time lag is maximum at 2.9 h for a 5-7 cm layer, is equal to 2.6 h for a 10 cm layer and converges to 1.8 h for thicknesses greater than 21 cm. With a maximum value of 2.9 h, it is not possible to delay the peak storage temperature later than 14:54 in the afternoon; thus, it is not possible to design a TES that would match the peak storage temperature with evening occupancy. It is nevertheless possible to increase the operative temperature during the evening by selecting a TES with a higher $\tau_{[Q_a - T_s]}$

As seen in figure 7.2b, the operative temperature is about 3 °C higher with a 10 cm layer and 6-8 °C higher with a 5 cm layer compared to a 20 cm layer in the period from 18:00-20:00.

This result showcases the value of $\tau_{[Q_a - T_s]}$ as an index: a higher value indicates improved thermal comfort later in the day, although at the cost of lower morning temperatures.

In light of these observations, it is clear that $\tau_{[Q_a - T_s]}$ is a valuable index for indirect-gain spaces and will therefore be one of the key output variables analyzed in this paper.

7.3.2 Optimal decrement factor and transfer admittance

In his previously introduced study, Asan (2000) defines the decrement factor of an exterior wall as the ratio of the amplitude of the temperature wave of the inner surface to that of the outer surface. As mentioned above, most studies analyzing the decrement factor adopted the position that minimizing the decrement factor is optimal. All studies investigating the decrement factor are based on the temperature decrement factor, except one that has focused on the heat flux decrement factor (Jin et al., 2012). While information regarding heat fluxes is valuable, it is the temperature of the inner wall surface that ultimately influences thermal comfort and heating loads, therefore the discussion here will focus on the temperature decrement factor only.

A low decrement factor for an exterior wall is indeed an advantage during the cooling season: reducing the temperature rise of the inner surface resulting from the sol-air temperature excitation at the outer surface will improve thermal comfort and reduce the needs for cooling. On the other hand, in winter, a temperature rise of the inner wall surface would improve thermal comfort and reduce the heating requirements and would therefore be welcome. However, some studies adopted the same objective of a low decrement factor or minimizing heat gains for both winter and summer conditions (Ozel and Pihtili, 2007; Zhang et al., 2013). Optimizing the design of an exterior wall should call for different heat transmission characteristics depending if the priority is given to minimize the cooling demand or the heating demand. Two parameters in particular should be radically different, the solar absorptivity of the outer surface and the decrement factor of the wall. An exterior wall optimized for providing heating during the cold season should have a high solar absorptivity and a balanced decrement factor. A low decrement factor would inhibit any significant heat transfer from taking place. On the contrary, an exterior wall optimized for cooling applications should have a low solar absorptivity (Kontoleon and Bikas, 2007) and a low decrement factor.

Most studies have concluded that placing the same insulation thickness as two or even three separate layers yields a lower decrement factor than as one continuous layer and should thus be preferred (Asan, 2000; Kontoleon and Bikas, 2007; Ozel and Pihtili, 2007). While

a low decrement factor might be beneficial in some applications, any layer of thermal mass not in contact with the interior will not actively participate in the heat exchanges with the indoor air and thus will see its storing potential largely unexploited. For this reason, if a low decrement factor is a design target, we suggest to reduce the decrement factor by increasing the thickness of the insulation or storage layer, but to locate all the thermal mass at the inner layer.

For isolated-gain applications, since the objective is to absorb and release the heat from the same surface, the massive layer must be reasonably insulated to avoid releasing the heat at the outer surface. Even when the thermal mass is located on the floor, it must be fully insulated; perimeter insulation only is insufficient for good performance with most soils (Rempel and Rempel, 2013).

A variable analogous to the temperature decrement factor is the transfer admittance, sometimes called the dynamic transmittance. For an external wall exposed to solar radiation from the inside, we are mostly interested in capturing the effect of the temperature variations at the inside storage layer to the resulting heat flux at the outside surface for a constant sol-air temperature:

$$Y_t = \left.\frac{Q_{out}}{T_s}\right|_{T_{eo}=0} \tag{7.3}$$

For isolated-gain applications, the transfer admittance as defined above is a more appropriate metric that the temperature decrement factor. On one hand, it explicitly involves the heat flux at the outside surface, which is a meaningful physical parameter. On the other hand, since the effects from the sol-air temperature are excluded, the analysis is simplified and it is easier to make meaningful conclusions. In fact, the decrement factor would not reveal meaningful results since both surfaces are subjected to significant excitations and it will be hard so separate the impact of the solar radiation from the impact of the outdoor temperature.

While analyzing the transfer admittance provides relevant information, results presented later in section 7.5.2.4 indicate that its value as a design parameter is rather limited and it is therefore not selected as a main output performance parameter in this study.

7.3.3 Reduction of space heating and cooling

The energy used for heating and cooling is an important quantity to evaluate when designing TES in conditioned spaces. However, many isolated-gain spaces are not conditioned, and

thermal comfort improvements in buildings are often overlooked, which highlights the need to define other metrics.

The solar saving fraction has been commonly used since the 80s to quantify energy savings associated with solar technologies like TES in passive solar houses (Rempel and Rempel, 2013). It is based on monthly heating loads using degree-days (Böer and Duffie, 1982); thus based on a constant indoor temperature. As seen in the introduction, it was found that internal temperature swings have an important effect on the performance of a TES. Therefore, the solar saving fraction is not an appropriate measure for estimating potential energy savings obtained with TES.

For isolated-gain applications, we suggest to calculate the space heating demand hourly for a daily indoor temperature profile, which allows the selection of varying temperature set-points throughout the day.

7.3.4 Minimization of temperature swings

Reducing temperature swings in a room subjected to solar gains is beneficial for improving thermal comfort. Many studies have been conducted with the objective of minimizing temperature swings. Most of these have been conducted under periodic conditions over 24 hours (Balcomb, 1983; Athienitis et al., 1986). When simulations are carried out over a longer period of time, it is possible to focus on reducing the daily average swing or the absolute swing: the daily average swing is the difference between the maximum and minimum temperature in a day, averaged over the simulation period, while the absolute swing is the difference between the maximum and minimum temperature experienced during the whole simulation period. This is an important distinction, because their optimal thickness can be significantly different.

The daily average temperature swing is an important variable that characterizes the thermal response of a space. When considering absolute temperature swings, it is more useful to report the information separately as the minimum and maximum temperature, since one important objective of TES design could be to limit the peak minimum or maximum temperature to specific thresholds.

Previous researchers have found that the optimal thickness of passive TES for reducing daily average temperature fluctuations is about 15-30 cm for concrete, when exposed to a periodic design period of one sunny day (Athienitis et al., 1986; Hadorn, 2005).

As shown on figure 7.4, the maximum self admittance magnitude does not exactly coincide with the storage temperature minimum swing. The self admittance magnitude is maximum at 0.17 m while the operative temperature swing reaches a minimum at 0.18 m and the storage temperature at 0.20 m. The authors are convinced that the most appropriate variable to optimize is the one that is closer to the desired results: a comfortable space. Therefore, the daily average operative temperature swing will be the key variable reported in the subsequent numerical analysis for characterizing temperature swings.

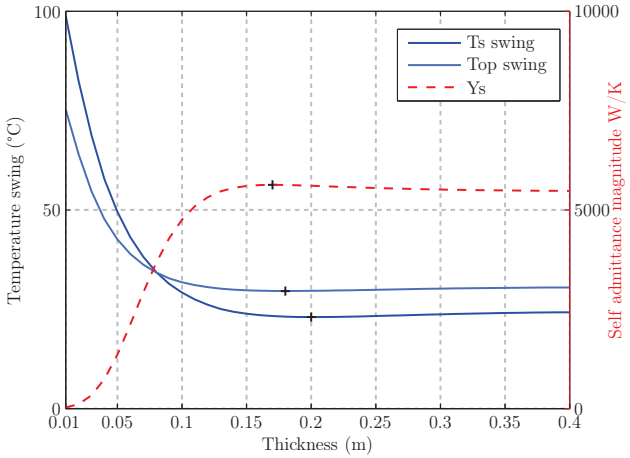

Figure 7.4: Comparison of the self admittance magnitude, storage temperature swing and operative temperature swing (for 5 harmonics).

7.3.5 Maximization of average temperature

The average operative temperature of a space is an important variable that influences thermal comfort for both people and plants. Materials with high heat capacity have the potential to affect the average temperature in a space to a small but non negligible extent. When carrying yearly simulations, the average operative temperature should be reported monthly to distinguish the effects happening in the different seasons.

7.3.6 Reduction of peak temperatures

As mentioned above, the minimum and maximum temperatures are very important variables and should thus be reported separately. For instance, if plants are grown in a solarium, avoiding temperatures below freezing may be an important design goal.

7.3.7 Performance metrics adopted for this study

After reviewing the commonly used metrics for characterizing TES, we conclude that the variables listed in table 7.2 are the most appropriate for isolated-gain applications. They are given along with the time period over which they should be calculated, assuming that simulations will be conducted either over a short design period ranging from one day to a few weeks or over a whole year.

Table 7.2: Main output performance variables selected in this study

Variable	Period
Solar radiation - storage temperature time lag	one representative sunny day
Daily average operative temperature swing	design period or monthly
Average operative temperature	design period or monthly
Minimum and maximum operative temperature	design period or annually
Space heating and/or cooling loads	design period or annually

7.4 Investigated solarium configurations

The six solarium configurations investigated in this paper are represented in figure 7.5. This research is focused on building-integrated passive TES (BITES); thus, only cases where a TES is fully covering a surface are considered. All configurations are oriented with their roof facing south. Their main characteristics are:

- F0: fully glazed, thermal mass on the floor
- F1: Insulated north wall, thermal mass on the floor
- N1: Insulated north wall, thermal mass on the north wall
- N2: Insulated north, east and west walls, thermal mass on the north wall
- FN1: Insulated north wall, thermal mass on the floor and the north wall
- FN2: Insulated north, east and west walls, thermal mass on the floor and north wall

All configurations have an RSI 20 (R 114) insulation layer behind the storage mass, a 35° sloped roof, a 3 m high north wall, a 2.4 m width and 10 m length, except otherwise specified. When insulated, east and west walls have an outer layer with a thermal resistance of RSI 20 and gypsum boards as inner layer. The rationale behind the choice of such a large value for the thermal resistance layer is explained in section 7.5.2.4.

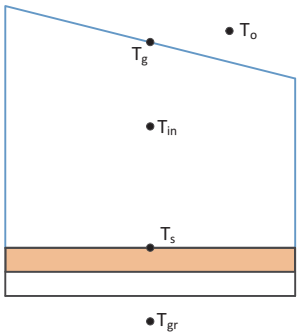

(a) Configuration F0 – TM on floor, all glazed

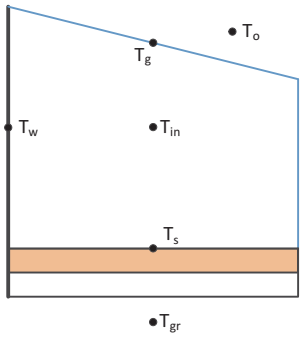

(b) Configuration F1 – TM on floor, opaque N, E/W glazed

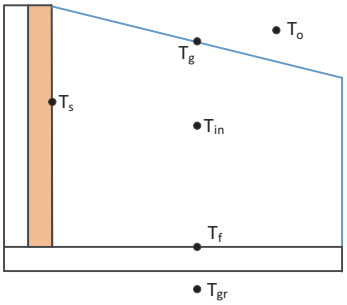

(c) Configuration N1 – TM on N, E/W glazed

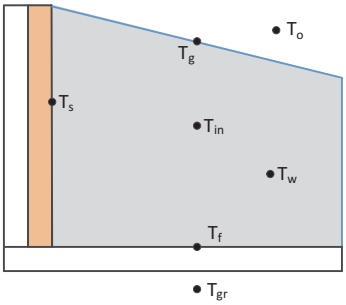

(d) Configuration N2 – TM on N, E/W opaque

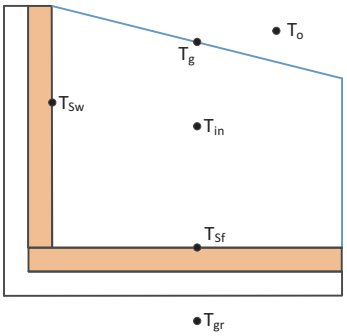

(e) Configuration FN1 – TM on floor and N, E/W glazed

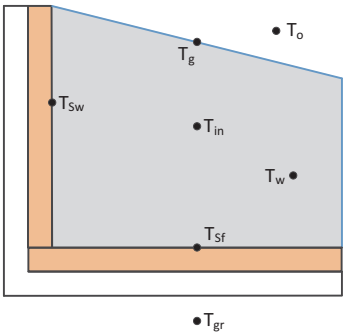

(f) Configuration FN2 – TM on floor and N, E/W opaque

Figure 7.5: Investigated solaria configurations – TM=Thermal mass, N=highest partition (north facing, on the left), E/W= East/West partitions.

7.5 Frequency response modelling

7.5.1 Model description

The first numerical method is based on fundamental network concepts used with Laplace transforms in the frequency domain. Here an analytical solution is provided: no spatial discretization is required, since the thermal mass is modelled as a two-port distributed element. The thermal network of a given configuration must first be defined, identifying all conductances and heat source elements. The admittance matrix is then defined based on this network, allowing to solve $Q = YT$ for the temperatures assuming 1D transient heat conduction.

The thermal network of configuration F0 is shown in figure 7.6a. Here we have a very simple situation with only three main nodes: T_{in} for the indoor air, T_g for the glazing and T_s for the storage mass on the floor. The floor of area A_s has a thermal mass layer of thickness L and insulation with conductance u_{gr} underneath. Infiltration and controlled ventilation exchanges are represented by u_{vent} and the total conductance between the inner glazing T_g

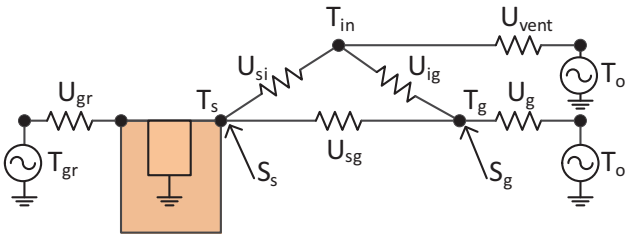

(a) Thermal network

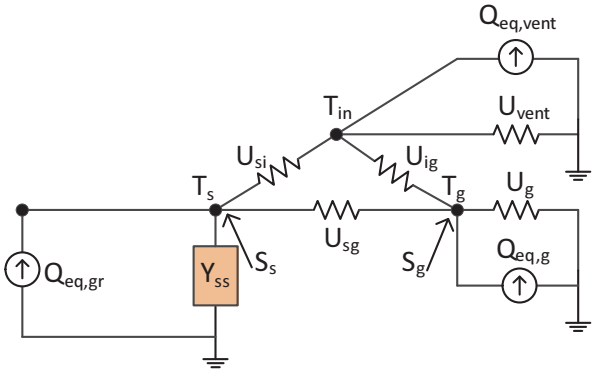

(b) Representation with a Norton equivalent

Figure 7.6: Configuration F0

and the outside air is given by u_g. With this notation, single or multiple layer glazings can be easily analyzed by providing the appropriate value for u_g with

$$u_g = \frac{A_g}{1/U_G - 1/h_{c,glazing} - 1/h_{r,glazing}} \tag{7.4}$$

where A_g is the total glazed surface area (including frame), U_G is the total U-value of the glazing material (including frame) in W/(m^{2}K) and $h_{c,glazing}$ and $h_{r,glazing}$ are the convective and radiative coefficients at the inner surface of the glazing. U represents the conductance in W/(m^{2}K) while u represents the conductance multiplied by the surface area and is thus in W/K. Convection between the floor and the air is represented by u_{si} and convection between the glazing and the air is represented by u_{ig}. Radiation exchanges between the floor and the glazing are represented by u_{sg} and the solar radiation absorbed by the storage mass and the glazing is denoted with S_s and S_g.

It is convenient to eliminate all exterior nodes and replace them with an equivalent source by building a Norton equivalent network, which consists of an equivalent heat source and a self admittance in parallel. In Figure 7.6b, the exterior node T_o connected to T_{in} has been transformed into $Q_{eq,vent}$, the ground node T_{gr} has been transformed into $Q_{eq,gr}$ and the exterior node T_o connected to T_g has been transformed into $Q_{eq,g}$. For eliminating nodes connected to materials with negligible thermal mass, the equivalent source is simply equal to the conductance multiplied by the temperature of the node to be eliminated (e.g. $Q_{eq,vent} = u_{vent}T_o$). For nodes connected to massive materials, the equivalent source is equal to the wall transfer admittance multiplied by its temperature (e.g. $Q_{eq,gr} = -Y_t T_{gr}$, with a negative sign because of the convention used).

The energy balance of this system yields $YT = Q$ and is given in equation 7.5. The elements of the admittance matrix can by obtained by inspection: diagonal entries Y_{ii} are equal to the sum of component admittances connected to node i; off diagonal entries Y_{ij} are equal to the sum of component admittances connected between i and j multiplied by -1; heat source vector elements Q_i are equal to the sum of the heat sources (actual and equivalent) connected at node i. By convention, Q_i is positive if the heat source is directed to the node.

$$\begin{pmatrix} sC_a + u_{si} + u_{ig} + u_{vent} & -u_{si} & -u_{ig} \\ -u_{si} & Y_s + u_{si} + u_{sg} & -u_{sg} \\ -u_{ig} & -u_{sg} & sC_g + u_{ig} + u_{sg} + u_g \end{pmatrix} \begin{pmatrix} T_{in} \\ T_s \\ T_g \end{pmatrix} = \begin{pmatrix} Q_{eq,vent} \\ S_s + Q_{eq,gr} \\ S_g + Q_{eq,g} \end{pmatrix} \tag{7.5}$$

sC_a and sC_g represents the lumped air and glazing capacitance; the capacitance of a an element is given by $C = \rho c_p V$, where ρ is the density, c_p is the specific heat capacity and V is the volume. The geometry, thermal network and admittance matrix of the five other investigated configurations are given in appendix D.

The self and transfer admittances are complex numbers used to represent the response of a system to a specific frequency (in the form of a predetermined design period). They can be obtained by performing a Laplace transform on the 1D heat conduction equation

$$\frac{\partial^2 T}{\partial x^2} = \frac{1}{\alpha}\frac{\partial T}{\partial t} \tag{7.6}$$

and elaborating a Norton equivalent network. A cascade matrix for a multilayer wall can be defined by specifying boundary conditions adequate for a two-port model. For a structure with two layers (i.e. mass + insulation with negligible capacitance), the cascade matrix is given by

$$\begin{pmatrix} T_1 \\ \\ Q_1 \end{pmatrix} = \begin{pmatrix} \cosh(\gamma_n L) & \dfrac{\cosh(\gamma_n L)}{u_{gr}} + \dfrac{\sinh(\gamma_n L)}{k\gamma_n} \\ \\ k\gamma \sinh(\gamma_n L) & \dfrac{k\gamma_n \sinh(\gamma_n L)}{u_{gr}} + \cosh(\gamma_n L) \end{pmatrix} \begin{pmatrix} T_2 \\ \\ -Q_2 \end{pmatrix} \tag{7.7}$$

The self and transfer admittance have been definer earlier in equation 7.1 and 7.9. From these definitions and the cascade matrix given above, the self and transfer admittance characterizing the floor in configuration F0 are given by

$$Y_s = \frac{A_s \left(U_{gr} + k\gamma_n \tanh(\gamma_n L)\right)}{\dfrac{U_{gr}}{k\gamma_n}\tanh(\gamma_n L) + 1} \tag{7.8}$$

$$Y_t = \frac{-A_s}{\dfrac{1}{U_{gr}}\cosh(\gamma_n L) + \dfrac{1}{k\gamma_n}\sinh(\gamma_n L)} \tag{7.9}$$

where k is the storage mass thermal conductivity, γ_n is equal to $(s/\alpha_{th})^{1/2}$ with s being the Laplace transform variable and α_{th} the storage mass thermal diffusivity. For the frequency domain analysis conducted here, s is equal to ωj where ω is the frequency and $j = \sqrt{-1}$. Additional details about the procedure for elaborating the Norton equivalent network and deriving the cascade matrix for multilayered walls can be obtained in Athienitis et al. (1986) and in Athienitis and O'Brien (2015).

Since the solution is obtained in the frequency domain, all elements composing the admittance matrix must remain constant in time, including the radiative and convective coefficients. Since the convective and radiative coefficients of a surface depend on its temperature, they are determined in two iterations; estimated initial values are first provided and detailed coefficients are calculated at the second iteration based on the average temperature of the surfaces obtained from the first iteration. The convective coefficients are calculated using Khalifa and Marshall (1990) correlations. Since all glazed surfaces are grouped together,

the convective coefficient of the tilted glazed roof is the same as for a vertical glazing. The radiative coefficient between two surfaces is calculated with (Duffie and Beckman, 2006, eq. 3.10.2)

$$h_{r,ij} = \frac{4\sigma T_m^3}{\frac{1-\epsilon_i}{\epsilon_i} + \frac{1}{F_{ij}} + \frac{(1-\epsilon_j)A_i}{\epsilon_j A_j}} \tag{7.10}$$

where σ is the Stefan-Boltzmann constant, T_m is the mean temperature of surfaces i and j over the investigated time sequence, ϵ represents the emissivity and F_{ij} is the view factor. Equations for the calculation of view factors can be found in Appendix C.3.

Elements composing the heat source vector must provide steady periodic conditions; therefore, the analysis with this model is focused on short design sequences. The temperature and solar radiation profiles of a specially chosen design period have to be defined for a specific location. The importance of the design sequence selection in discussed in section 7.5.2.5.

The temperature profile is based on a sinusoidal function with a maximum at 3pm. The average temperature is taken as the monthly average temperature for the month under consideration. The amplitude of the temperature profile is taken as the average monthly temperature variations divided by two.

The solar radiation incident on a surface for a sunny design day is computed using the Hottel clear sky method (Hottel, 1976) for the design day under consideration. A cloudy design day was constructed by setting the beam solar radiation to zero and multiplying the diffuse solar radiation by 1.5 from the Hottel model, which is representative of a completely overcast day. The solar radiation transmitted through the glazings of different orientations and absorbed by the interior surfaces is calculated separately with another routine that combines ray tracing and radiosity techniques. Detailed calculations are presented in Bastien et al. (2015).

Once the temperature profile and the solar radiation absorbed by the interior surfaces have been determined, complex Fourier series are required in order to calculate the time domain solution for these vectors. Five harmonics were selected for a 24 h design period. As reported in Athienitis et al. (1986), the magnitude of the self admittance Y_{sn} increases with the harmonic number while the penetration depth $(\alpha_{th}/\omega)^{1/2}$ decreases. This is further exemplified by the shift in the peak Y_{sn} magnitude, which occurs at a smaller thickness as the harmonic number increases (results not shown). However, by studying the effect of harmonics number on the storage temperature swings, Athienitis et al. (1986) reported that three to five harmonics are sufficient to ensure that the accuracy of the swings is about 0.1 °C.

Simulations with the FR model are executed with a time step of 0.05 h. A time step of 0.5 h would have been satisfying, but a smaller time step was selected in order to have a better resolution for the analysis of $\tau_{[Q_a-T_s]}$. Simulation results obtained with the FR model are presented in section 7.5.2 below. Unless indicated otherwise, simulations in this section are conducted for configuration N1 with dimensions of h=3 m, w=2.4 m, l=10 m equipped with a clear double insulated glazed unit with a concrete TES and no active air circulation for a periodic sunny day at the winter solstice for a latitude of 45°. The impacts resulting from varying these characteristics will be analyzed in the following subsections.

The analysis is focused on the main performance variables identified in section 7.3.7. In the following discussion, the word optimal refers to the extremum of one of these variables.

7.5.2 Simulation results and discussion

7.5.2.1 Main results – all configurations

As shown on figure 7.7a, under the conditions described above, the minimum operative temperature becomes fairly stable for thicknesses beyond 0.20 m for all configurations. It is significantly affected by the solarium design, and positioning the mass on the wall instead of the floor (F1→N1) raises the minimum temperature by almost 2 °C.

The observation of figure 7.7b reveals that the maximum operative temperature is also strongly affected by the design. The maximum temperature becomes relatively stable for thicknesses beyond 0.10 m for all configurations. The same observations also apply to the average temperature swing (see figure 7.7c).

The effect of the solarium design on the average temperature is very significant: having an opaque north wall instead of being glazed raises the average temperature by about 12 °C (F0→ F1). For the same thickness of thermal mass, locating the mass on the north wall instead of the floor will results in slightly higher average temperature (F1→N1).

As explained in section 7.3.1, $\tau_{[Q_a-T_s]}$ is the time lag between the peak absorbed solar radiation heat flux and the peak storage temperature. We can see in figure 7.7e that increasing the solar radiation collection of the space (by changing the north wall from being glazed to opaque, i.e. F0→F1), can increase $\tau_{[Q_a-T_s]}$ by about 0.4 h. It peaks at 5-8 cm for all configurations, and becomes fairly constant for thicknesses greater than 22 cm.

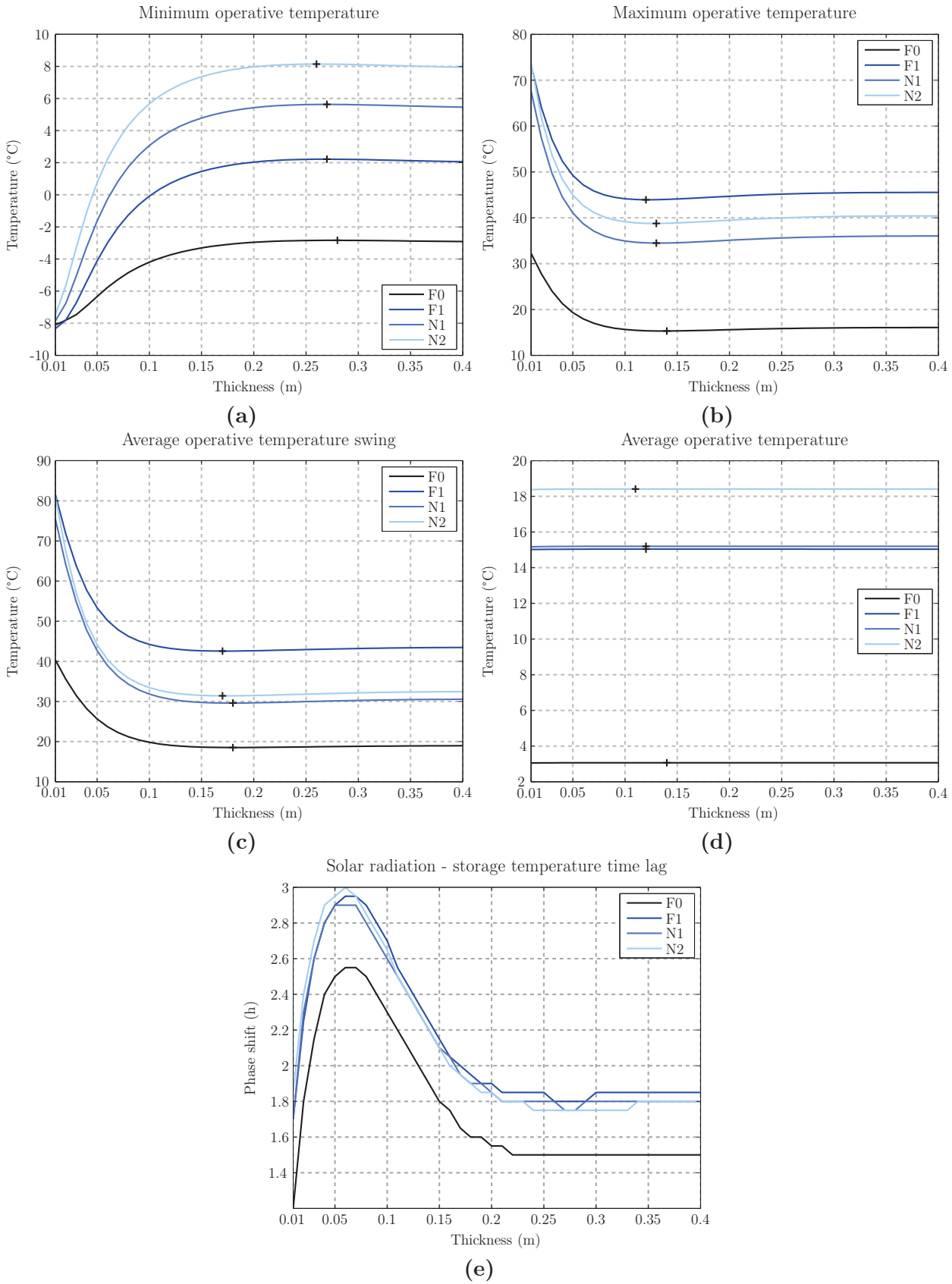

Figure 7.7: Main output performance variables – configurations F0, F1, N1 and N2

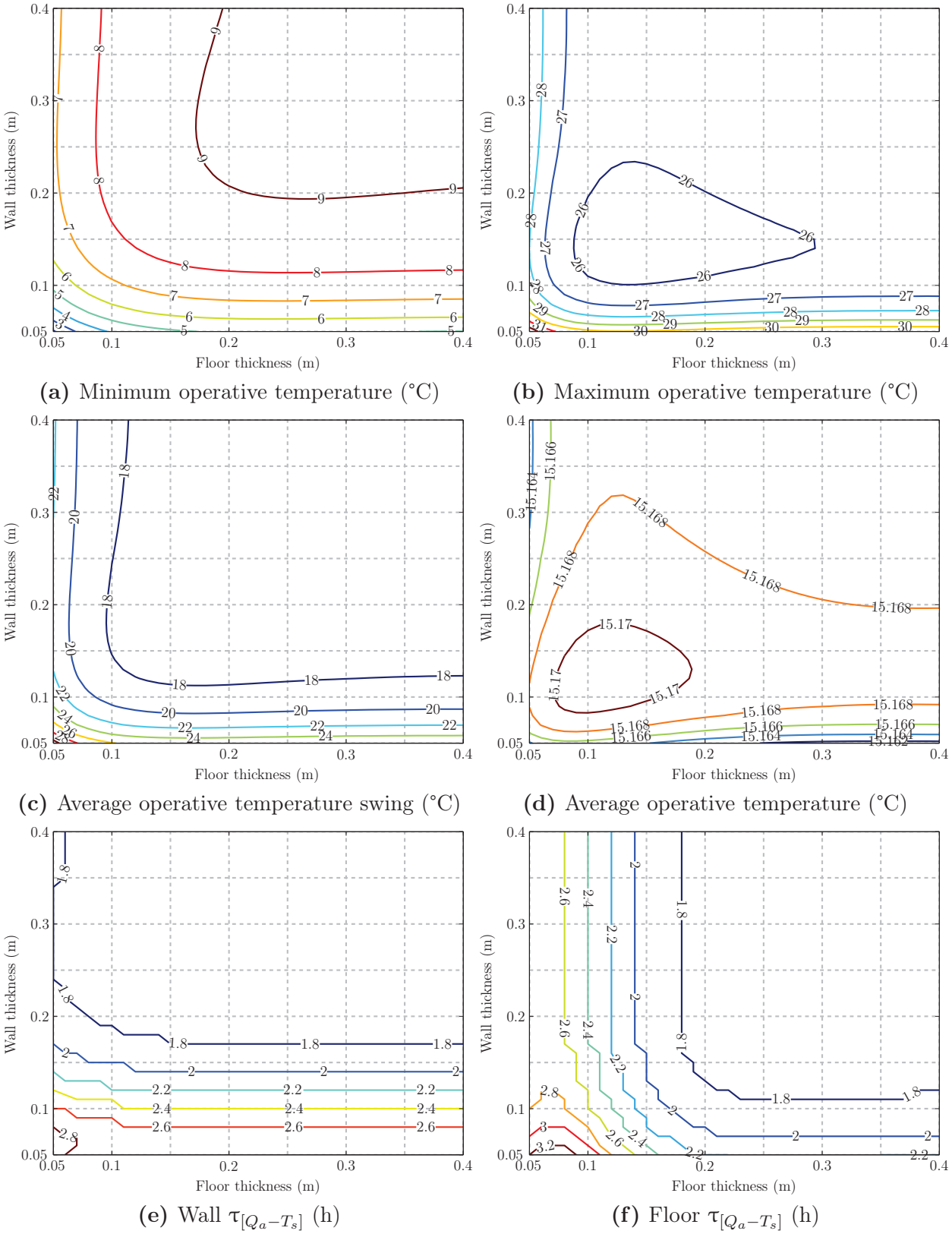

(a) Minimum operative temperature (°C)

(b) Maximum operative temperature (°C)

(c) Average operative temperature swing (°C)

(d) Average operative temperature (°C)

(e) Wall $\tau_{[Q_a - T_s]}$ (h)

(f) Floor $\tau_{[Q_a - T_s]}$ (h)

Figure 7.8: Main output performance variables – configuration FN1

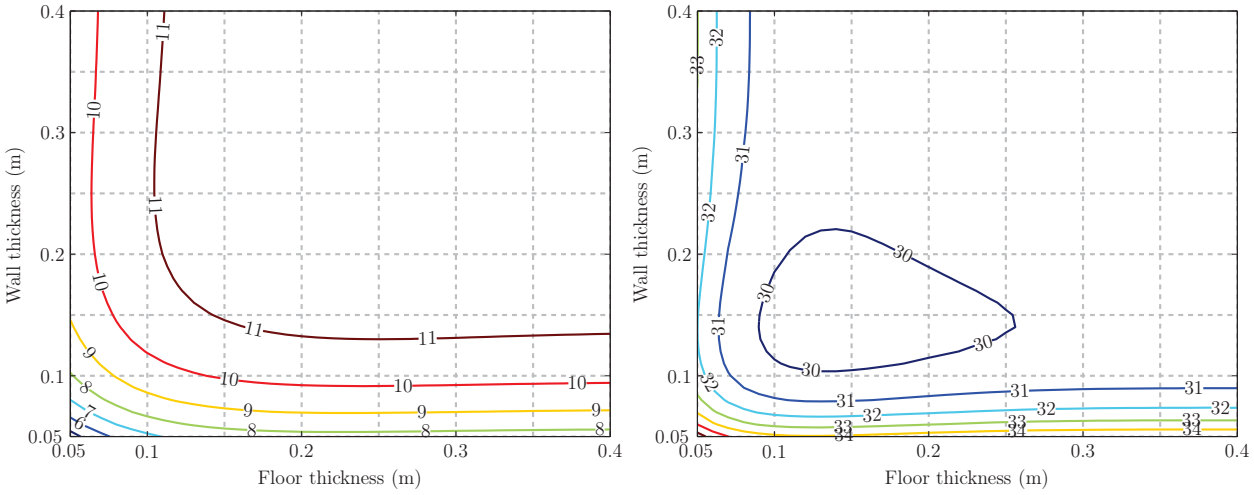

(a) Minimum operative temperature (°C)

(b) Maximum operative temperature (°C)

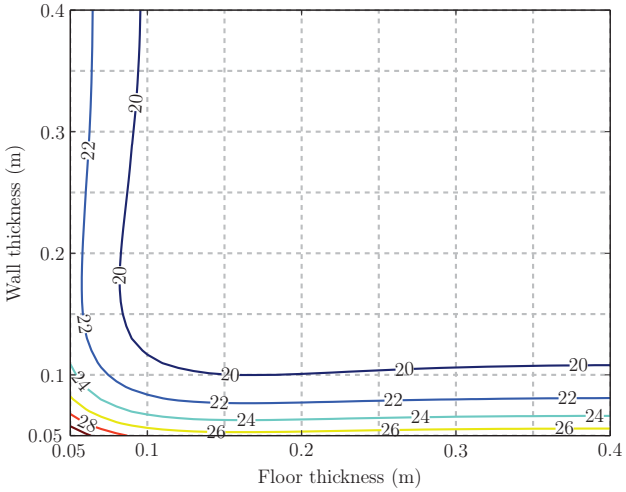

(c) Average operative temperature swing (°C)

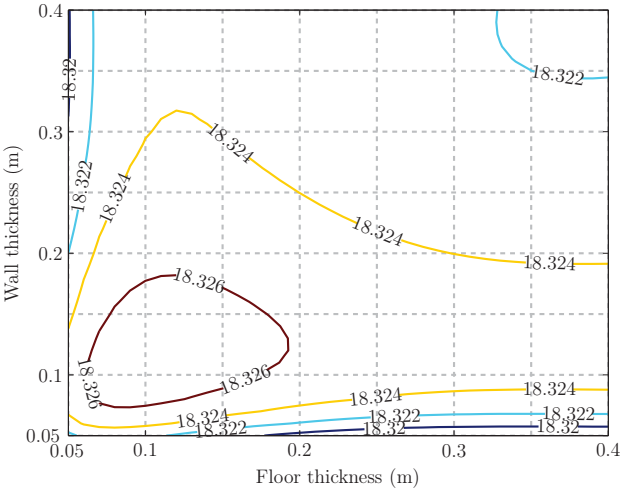

(d) Average operative temperature (°C)

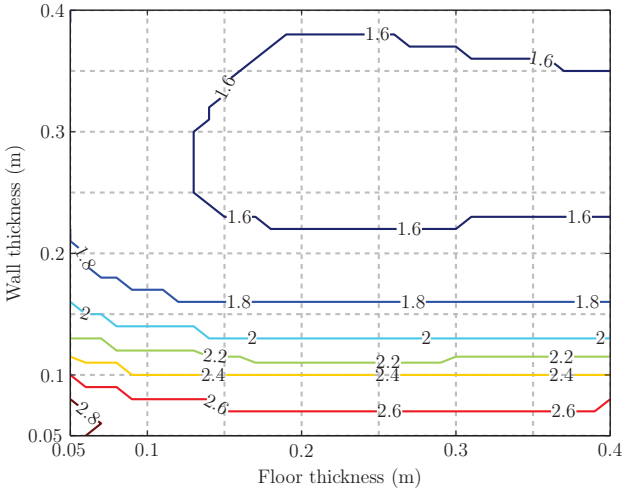

(e) Wall $\tau_{[Q_a - T_s]}$ (h)

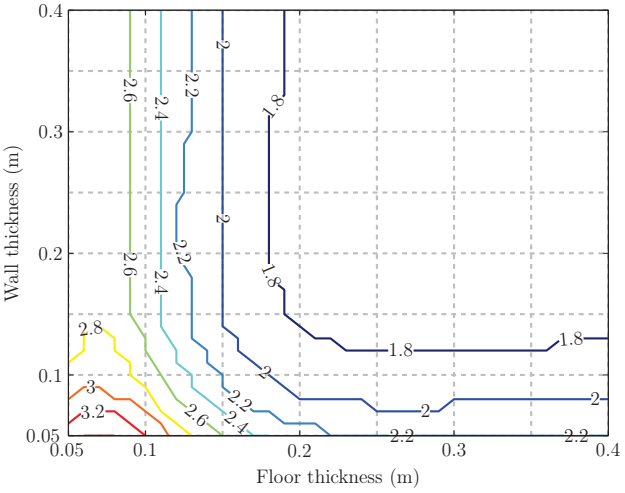

(f) Floor $\tau_{[Q_a - T_s]}$ (h)

Figure 7.9: Main output performance variables – configuration FN2

Simulation results for configurations FN1 and FN2 are shown in figures 7.8-7.9. We can see from figure 7.8a that the highest minimum operative temperature is 9.2 °C and occurs for a thickness of 0.27 m for both the floor and wall storage; it remains above 9.0 °C as long as both TES are at least 0.2 m or larger. As seen on figure 7.8c, the minimum swing is 17 °C and occurs at a thickness of 0.18 m for both TES. It remains below 18°C as long as both TES have a minimum thickness of 0.12 m.

For FN1, the maximum wall $\tau_{[Q_a-T_s]}$ is 2.8 h and occurs when both TES are 5-6 cm thick. It is greater than 2.5 h when both TES are equal or less than 10 cm. The floor $\tau_{[Q_a-T_s]}$ is maximum at 3.3 h for a 5 cm wall and a 6-8 cm floor and is above 2.8 h when both TES are between 5 and 9 cm. Therefore, implementing a 6 cm storage on both the wall and the floor maximizes $\tau_{[Q_a-T_s]}$ for both TES.

Having storage on both the wall and the floor instead of just the wall (N1→FN1) can increase the highest minimum operative temperature by up to 7 °C. As seen in figure 7.9a, the highest minimum operative temperature is 11.8 °C and occurs for a thickness of 0.24-0.29 m for both TES. It remains above 11.6 °C as long as at both TES are at least 0.20 m. Having opaque east and west walls (FN1→FN2) does not significantly impact $\tau_{[Q_a-T_s]}$ for both TES.

7.5.2.2 Impact of varying floor area dimensions, aspect ratio and orientation

Although a detailed study of design parameters and their influence on the indoor climate is beyond the scope of this work, simulation results for configurations F0 and N1 with varying dimensions are presented below. The investigated dimensions are given in table 7.3.

Table 7.3: Simulated floor area dimensions and aspect ratio

Configuration	North wall height (m)	Width (m)	Length (m)
F0-s	3	2.4	10
F0-m	4	4	10
F0-l	4	4	100
N1-s	3	2.4	4
N1-m	4	4	4
N1-l	3	2.4	10

As seen in figure 7.10, we can see that varying the floor area and aspect ratio of configurations F0 and N1 has little impact on the optimal thermal storage thickness of the main performance parameters. Varying the floor area of a fully glazed greenhouse (F0) has virtually no impact

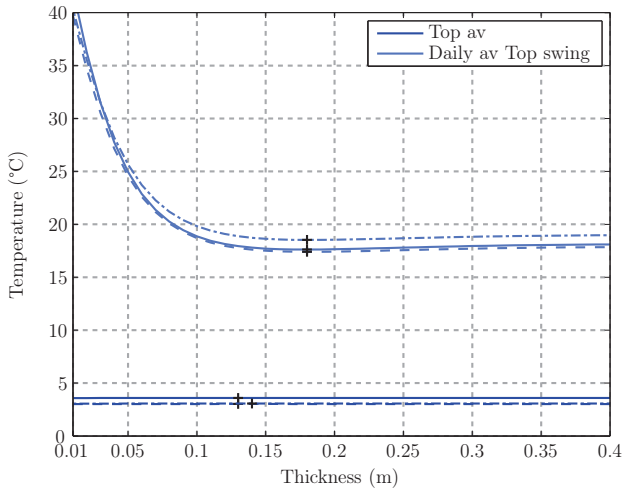

(a) Average T_{op} and its swing, F0

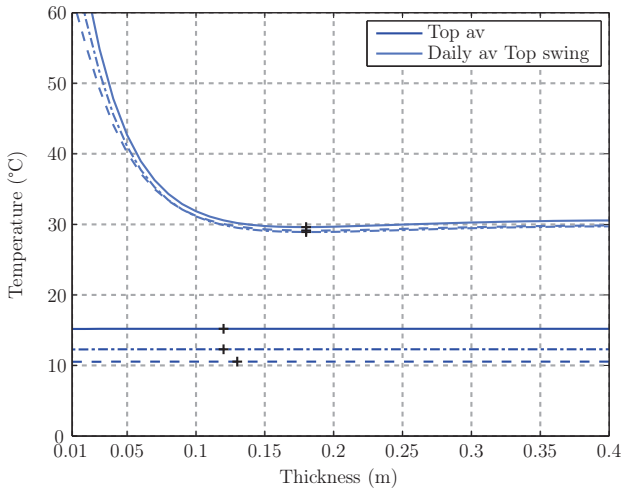

(b) Average T_{op} and its swing, N1

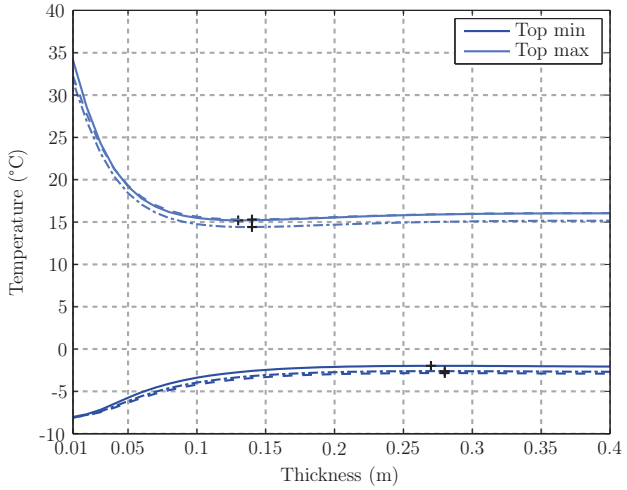

(c) Minimum and maximum T_{op}, F0

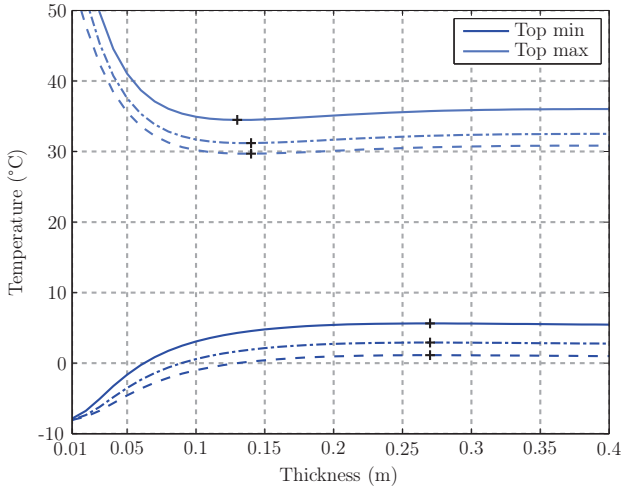

(d) Minimum and maximum T_{op}, N1

Figure 7.10: Impact of varying floor area; - - small, - - - medium, —— large

of the main performance parameters. Changes in the floor area and aspect ratio for a solarium with a massive north wall (N1) can have a small impact. From figure 7.10b, we can see that a solarium design aligned on a east-west axis with a higher aspect ratio experiences a higher average temperature, which is coherent with many studies that identified that it was most beneficial for greenhouses to have their longest side facing south (Harnett, 1975; Kozai, 1977b; Rosa et al., 1989; Gupta and Chandra, 2002). The solar radiation - storage temperature time lag is identical for the F0-s, -m and -l while it converges to a slightly higher value (0.1-0.2 h) for the N1 design with higher aspect ratios; changing the orientation from due south reduces the absorbed solar radiation, and thus lower the average and peak operative temperatures and its swing (results not shown). It can be seen that even though the main performance parameters can be affected by variations in the floor area and aspect ratio, their response to varying thermal storage thickness is similar.

7.5.2.3 Impact of TES material

In this work, the reference thermal storage material is concrete as it is a widely used material that has been studied extensively, thus facilitating comparison with the existing literature. In addition, concrete is often present in buildings for structural reasons; therefore keeping it exposed and available for thermal storage could improve indoor climate with no additional cost. However, for thicknesses greater than 0.2-0.3 m, the cost and environmental impacts of this material are likely to hinder its use in bigger volumes, making the study of inexpensive and readily available materials a necessity for large TES. This section presents a comparison of the performance of concrete TES with soil and water TES.

The thermal properties of soil are highly dependent on the soil type (i.e. the proportion of sand, silt and clay) and moisture content. In particular, changes in its thermal conductivity can significantly alter heat transfer exchanges; typical values are between 0.6-2.5 W/m^2-K, depending on the soil type and moisture content (ASHRAE, 2009, F25). Because of the variability of soil properties, two different types of soil are analyzed here: a sandy loam soil and clay loam soil. Properties representative of these two types of soil are indicated in table 7.4.

Table 7.4: TES materials properties

	k	c_p	ρ
Concrete	1.73 W/m^2-K	840 J/kg-K	2243 kg/m^3
Soil - sandy loam	0.8 W/m^2-K	800 J/kg-K	1600 kg/m^3
Soil - clay loam	1.2 W/m^2-K	900 J/kg-K	1700 kg/m^3
Water	0.59 W/m^2-K	4813 J/kg-K	998.3 kg/m^3

In the case of liquid TES such as water, convective heat transfer is present in addition to conduction. As in the case of solid TES, it is assumed here that the water temperature is uniform in a control volume. The conductivity of water is replaced by an effective conductivity $k_e = Nu\, k$ where Nu is given by (Wright, 1996)

$$Nu = 0.0674 Ra^{1/3} \tag{7.11}$$

For a fluid contained in a rectangular unit of width L with a temperature difference ΔT, the Rayleigh number is calculated with

$$Ra = \frac{g\beta_{th}\Delta T L^3}{\nu\alpha_{th}} \tag{7.12}$$

where β_{th} is the thermal expansion coefficient, ν is the kinematic viscosity and α_{th} is the thermal diffusivity of water. Here the effective conductivity is calculated at every thickness for a nominal temperature difference of 1 °C. Since the effective conductivity is proportional to $\Delta T^{1/3}$, changes is k_e are much smaller then changes in ΔT; therefore the impacts of this simplification are not very significant.

As seen from figure 7.11a, a TES made of water experiences the smallest temperature swings from the four materials investigated. In addition, a clay loam soil is significantly more efficient than a sandy loam soil for reducing temperature swings. The average temperature is very similar for these four materials.

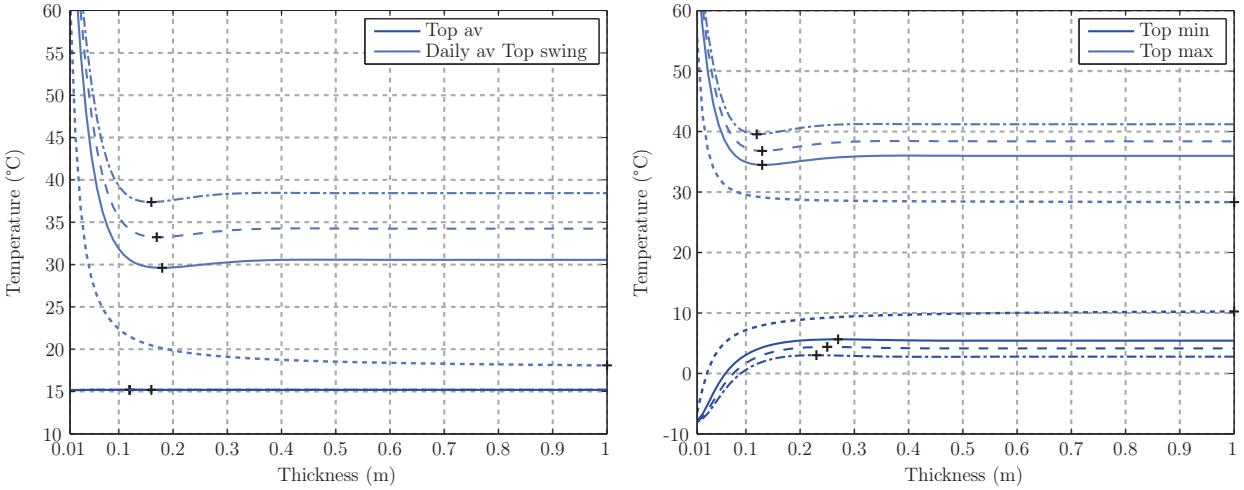

(a) Average T_{op} and it's swing

(b) Minimum and maximum T_{op}

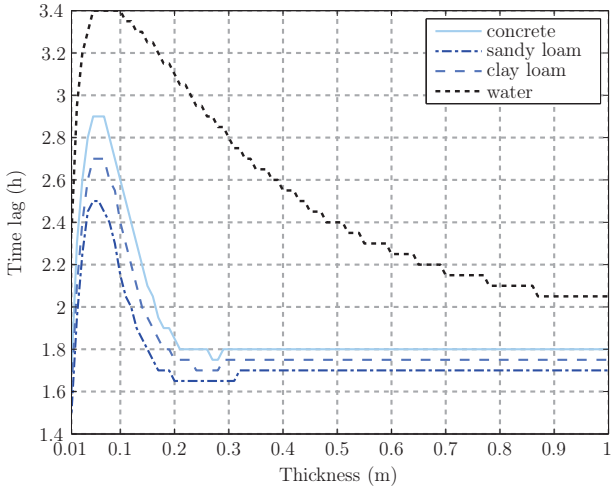

(c) $\tau_{[Q_a - T_s]}$

Figure 7.11: Impact varying of storage material; - - sandy loam, — concrete, - - - clay loam, ···· water

A TES made of water experiences reduced peak temperatures, followed by concrete and clay loam soil (see figure 7.11b). As shown on figure 7.11c, all investigated materials except water reach a constant time lag at 0.20 m and beyond. Water has s significantly wider and higher peak, with a peak time lag decreasing much more slowly than for the other materials.

7.5.2.4 Impact of varying thermal resistance of the insulation layer

So far, all simulations have been conducted with an insulation layer having a thermal resistance of RSI 20 (R 114). Such a high value was chosen with the objective of providing near adiabatic conditions at the outside storage mass layer to focus our attention on the heat absorbed and released at the inside layer.

It is well known that increased thermal resistance reduces heat fluxes with diminishing returns. Exactly how much insulation should be selected depends on economic, space and performance constraints. The sensitivity of the five main performance variables to varying insulation levels was assessed for RSI 2, 5 and 20 insulation levels. The biggest impact was observed for the minimum and average operative temperature. The average temperature was 1.0 °C lower for all thicknesses with RSI 2 compared to RSI 20 and the minimum temperature dropped by 1.0 °C for thicknesses between 0.2-1 m. Variations of the maximum operative temperature and it's swing were not significant and are therefore not presented.

The transfer admittance as a function of storage thickness is shown in figure 7.12b for the three different insulation levels. We can see that the transfer admittance approaches zero at storage thicknesses of 0.4 m and beyond for the three investigated insulation levels.

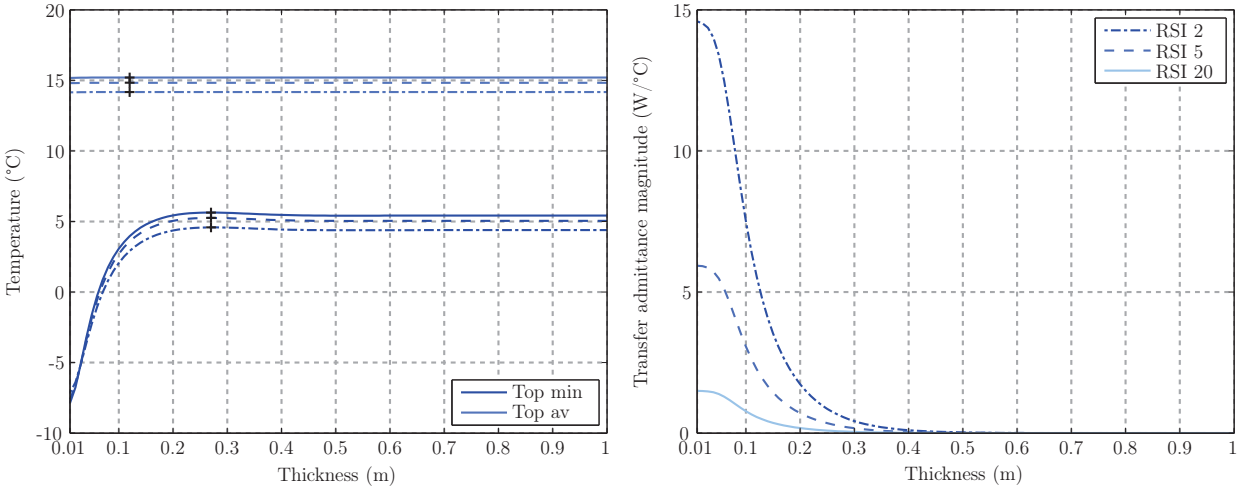

(a) Minimum and average operative temperature **(b)** Magnitude of the transfer admittance

Figure 7.12: Impact of varying thermal resistance of the insulation layer; - - RSI 5, - - - RSI 10, — RSI 20

Analyzing the transfer admittance in isolation could induce to conclude that there is no benefits to increase the insulation layer from RSI 2 to 5 or 20 for storage thicknesses beyond 0.4 m, but the observation of the minimum and average temperature reveals that the penalty for reduced insulation level is fairly constant for thicknesses between 0.1 and 1 m.

Although informative, it is not possible to extract definitive conclusions from the simulation results presented above. Therefore, the impact of varying the thermal resistance of the insulation layer will be investigated with the FD model under real weather conditions in the next section.

7.5.2.5 Impact of design sequence selection

Figure 7.13 shows the simulation results over different periodic design sequences ranging from a sunny day to seven sunny days followed by seven cloudy days. It can be seen that the optimal thickness in regards to the minimum, maximum and average operative temperatures is significantly affected by the choice of the design period.

As shown in figure 7.13a, the minimum temperature peak occurs at larger thicknesses with increasing consecutive cloudy days. Under a 7 sunny - 7 cloudy days design period, the minimum temperature for a TES thickness of 0.10 m is -5.4 °C while it reaches a minimum of -2.5 °C at 1.18 m. This is an important result that can justify the use of larger TES for applications where raising the minimum temperature is an important concern.

The maximum operative temperature exhibits a different behavior (see figure 7.13b). Under a sunny day and a 1 sunny - 1 cloudy days design periods, the extremum occurs between 0.13-0.15 m, while it occurs at thicknesses greater than 0.49 m for sequences with two consecutive cloudy days or more. As the number of consecutive cloudy days increases, two minima become visible: one around 0.10-0.15 m and a lower minima at a significantly greater thickness.

Figure 7.13c illustrates the swing of the daily average operative temperature for different design day periods. It can be seen that it is mainly independent of the design period. The minimum swing occurs between 0.17 and 0.23 m and then converges to a constant value at 0.40 m and beyond. The swing is 0.04-0.41 °C lower at the minima than the value for thicknesses greater than 0.40 m. At small thicknesses ($<$0.10 m), the temperature swing is very sensitive to the TES thickness.

As seen from figure 7.13d, the maximum average temperature occurs at a greater thickness when the number of consecutive cloudy days increases, but the overall magnitude of the variations in average temperature with thickness is very small.

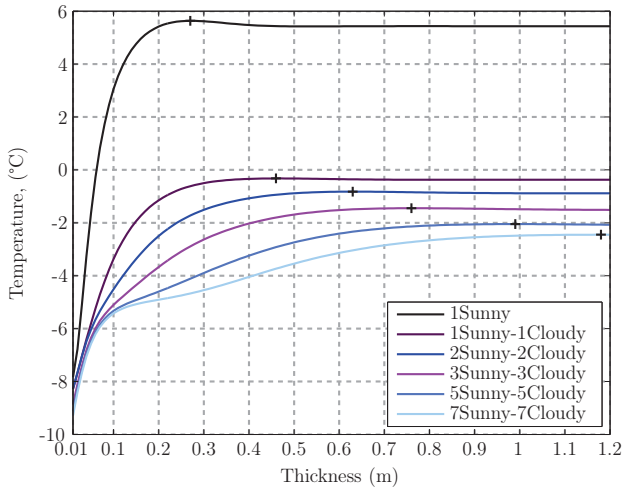

(a) Minimum operative temperature

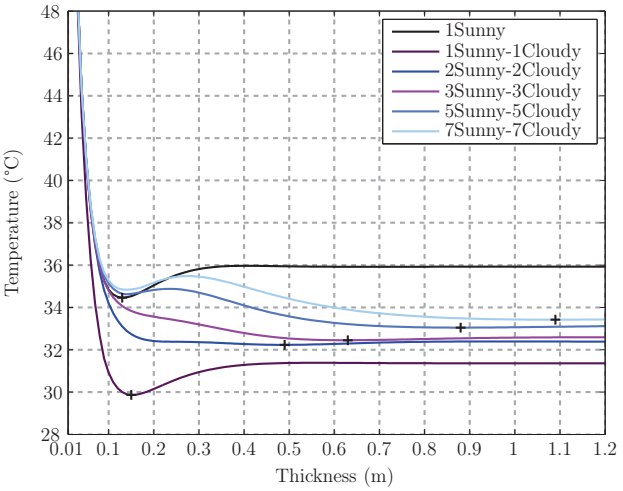

(b) Maximum operative temperature

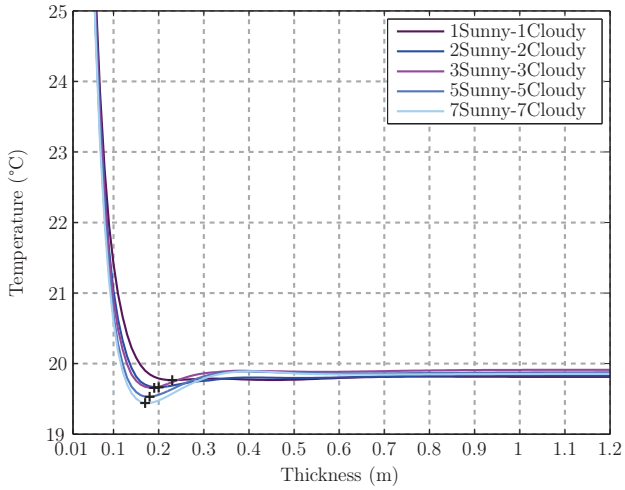

(c) Daily average operative temperature swing

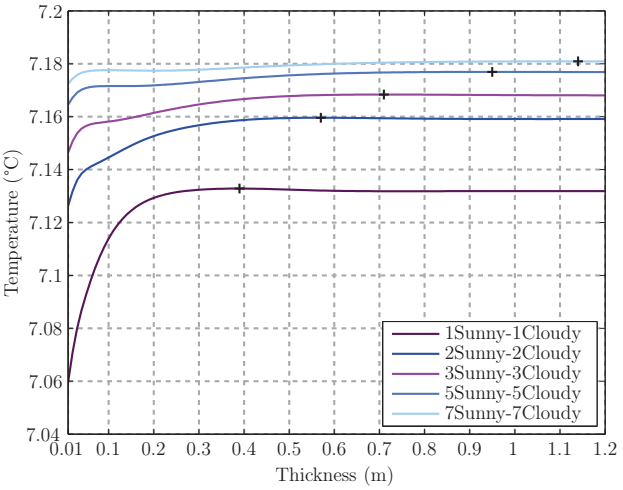

(d) Average operative temperature

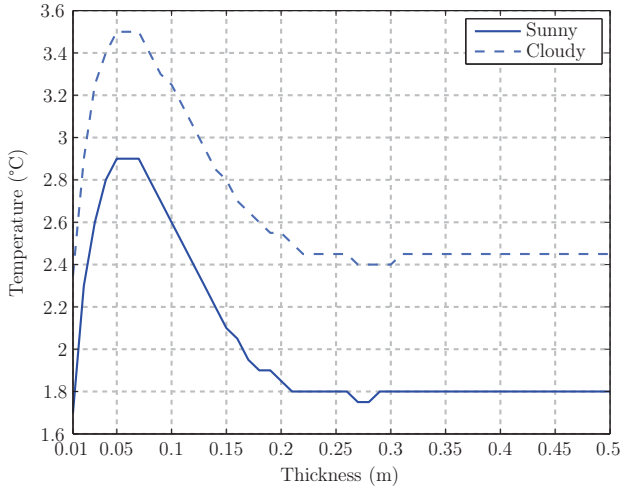

(e) $\tau_{[Q_a - T_s]}$

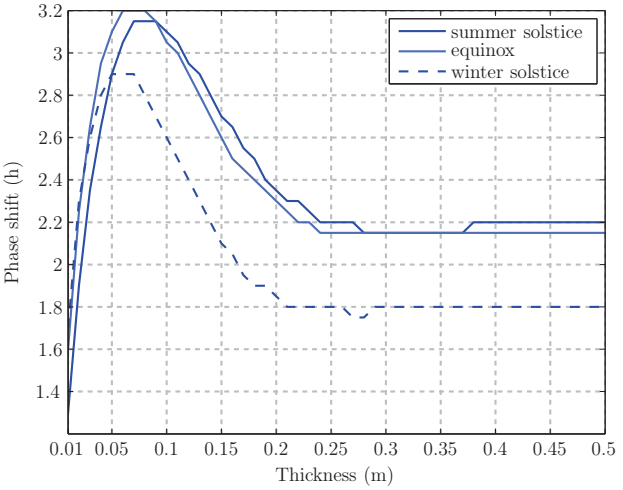

(f) $\tau_{[Q_a - T_s]}$

Figure 7.13: Impact of design sequence selection – configuration N1

The impacts of solar radiation availability on $\tau_{[Q_a-T_s]}$ are shown in Figure 7.13e, where results for a sunny day and a cloudy day at the winter solstice are compared. Although the $\tau_{[Q_a-T_s]}$ is higher for a cloudy day, its peak occurs at the same thickness whether the design period is a cloudy day or a sunny day.

Figure 7.13f shows $\tau_{[Q_a-T_s]}$ for three different moment in the year. Here simulations were conducted under the periodic conditions of a sunny day at the winter solstice, the vernal equinox and the summer solstice. Since a solarium design cannot be optimized simultaneously for different time of the year, a designer should carefully select a day representative of the moment of the year when the time lag is most desirable. However, the choice of a specific day is not of crucial importance since the behavior of $\tau_{[Q_a-T_s]}$ does not exhibit very significant variations throughout the year. It can be seen that $\tau_{[Q_a-T_s]}$ is maximum at 5-7 cm at the winter solstice while it peaks at 6-8 cm at the equinox and 7-9 cm at the summer solstice. One could choose to optimize the time lag at the winter solstice, because then solar gains are at their lowest levels and therefore more needed.

7.5.2.6 Discussion

The impacts of varying glazing type and enhanced thermal coupling have been analyzed and simulations results are presented in appendix E. It is observed that the introduction of continuous indoor air recirculation increases convective exchanges and can significantly reduces the maximum operative temperature, but reduces slightly its average and minimum temperature as well as $\tau_{[Q_a-T_s]}$. In addition, the glazing type significantly affect the average operative temperature and its peaks, but not much the optimal TES thickness.

As we can see from the results presented so far, under periodic design sequences, there seems to be three different optimal TES thicknesses for fulfilling different objectives: the optimal thickness for reducing daily average temperature swings is between 0.15-0.25 m, the optimal thickness for maximizing $\tau_{[Q_a-T_s]}$ is around 0.05-0.10 m while reducing operative temperature peaks needs a greater thickness as the number of consecutive cloudy days increases. However, the magnitude of improvement of these three performance variables is relatively small; investigating how these will translate under real weather conditions is important and will be studied in the next section.

Although frequency response modelling can be used to analyze any periodic conditions, and it is possible to create period conditions from non-periodic ones by increasing the simulation period and repeating the conditions, this modelling method is more appropriate for short

term analysis using design sequences. For accurate simulations, more harmonics are needed as the design period increases, which significantly impacts simulation time. For instance, for a one-day design period, 5 harmonics were sufficient, while 43 harmonics were necessary to analyze a 7 sunny - 7 cloudy days design period; this increased the computational time by a factor of 140. The use of a finite difference (FD) model is more appropriate for yearly simulations with real weather data.

7.6 Finite difference modelling

Here the previously developed frequency response (FR) model will be compared with a model using the finite difference (FD) method. The FR model will be progressively modified towards a finite difference thermal network model that will consider non linear radiative and convective heat transfer. The major modeling steps are presented in the first subsection where their impacts on accuracy and computational efficiency are discussed. The second subsection presents results obtained with the FD model.

7.6.1 Model parameters

All simulation results presented in this section are for configuration F0 subjected to a sunny day at the winter solstice unless specified otherwise.

7.6.1.1 Spatial discretization

The first modification introduced is the spatial discretization of the thermal mass. First, the accuracy of two different discretization schemes is analyzed. With the "3Ne" model, half of the mass is located at the center and one quarter at the edges (see Figure 7.14). With the "3Nc" model, 1/4 of the mass is in the center and 3/8 of the mass is located at 1/4 of the total thickness.

Figure 7.15a depicts the average temperature swings obtained with the FR model with distributed mass and with the "3Ne" and "3Nc" discretization schemes. It can be seen that models with thermal mass at the edges are more accurate and therefore adopted.

Figure 7.15b shows the impact of increasing the number of control volumes from three to seven. Spatial discretization with three control volumes shows good adequacy until a thick-

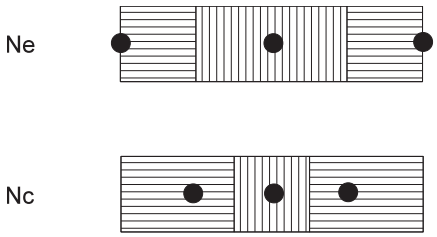

Figure 7.14: Two spatial discretization schemes

ness of about 0.2 m, but then diverges from the FR model, with the difference getting bigger with increasing thickness. As can be seen, a greater number of control volumes is needed to maintain accuracy as the thickness increases.

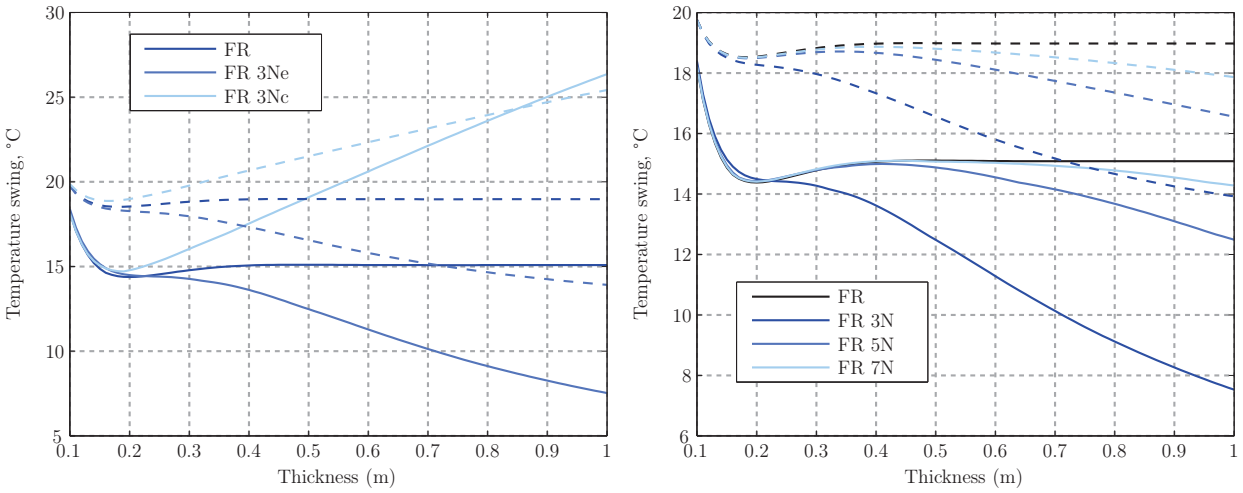

(a) Impact of spatial discretization scheme **(b)** Impact of increasing control volumes

Figure 7.15: Temperature swing as a function of TES thickness; — T_s, - - - T_{op}

Here TES with thicknesses between 0.1 and 1 m are analyzed. Analyzing smaller thicknesses would necessitate a very small time step (see next section); thus the limit was set at 0.1 m. Although TES as thick as 5.5 m have been built (as seen in the literature review), 1 m is deemed sufficient to evaluate potential benefits of large TES in solaria and greenhouses.

As seen from figure 7.16, for the aforementioned conditions and for thicknesses up to 1 m, introducing a spatial discretization scheme with thermal mass at the edges and lumping the capacitance in 23 control volumes provides a good adequacy with the FR model with distributed mass. Therefore these parameters are adopted.

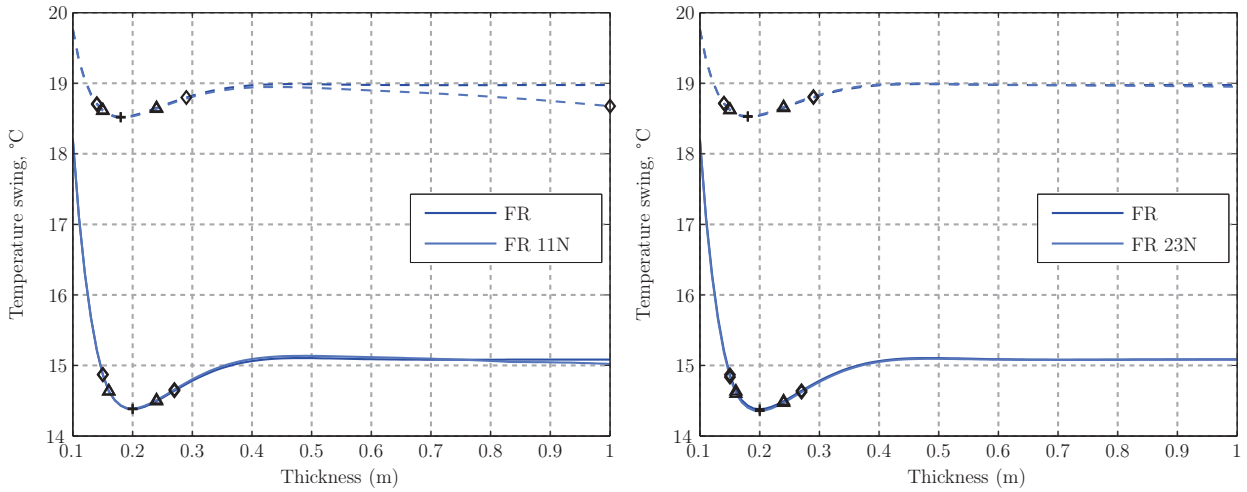

(a) 11N **(b)** 23N

Figure 7.16: Operative temperature swing as a function of TES thickness; — T_s, - - - T_{op}, + indicates extremum, △ indicates extremum ±0.15 and ◇ indicates extremum ±0.3

7.6.1.2 Temporal discretization

Developing a lumped parameter FD model requires introducing temporal discretization. The basic Euler forward method is adopted, which has a fully explicit scheme:

$$T_{i,t+1} = \frac{\Delta t}{C}\left(Q_{i,t}+h_{c,i}A_i(T_{air,t}-T_{i,t})+\sum_j (T_{j,t}-T_{i,t})R_{ij}^{-1}+A_i\sum_k h_{r,ik}(T_{k,t}-T_{i,t})\right)+T_{i,t} \quad (7.13)$$

where C is the capacitance of node i, $Q_{i,t}$ is a heat source at node i, R_{ij} is the thermal resistance between nodes i and j (in K/W), j represents nodes experiencing conductive exchanges with i, k represents nodes experiencing radiative exchanges with i and other symbols were previously defined. For comparison purposes, the convective and radiative coefficients, initial conditions and solar radiation and temperature profiles are retrieved from the FR model and used as input for the FD model in this subsection.

The Euler forward discretization scheme was adopted since it is easy to implement and computationally fast. Given the large number of control volumes required for accuracy, a time step of 0.002 h (7.2 s) is used to guarantee stability. Even with such a small time step, annual simulations can be carried out at a reasonable speed (about 40 minutes). The hourly weather data input are not interpolated to fit this time step.

The temperature swings obtained with the FR model, the FR model with discretized mass and the FD model are depicted in figure 7.17 for comparison. It can be seen for the FD

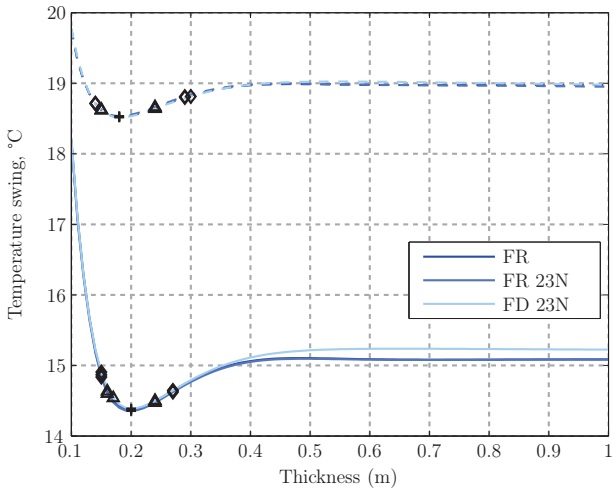

Figure 7.17: Impact of temporal discretization; — T_s, - - - T_{op}

model, a small discrepancy is introduced at a thickness of 0.4 m and beyond. Reducing the time step below 0.002 h does not reduce the discrepancy. The maximum difference of 0.13 °C between the FR and the FD 23N models is considered acceptable for the scope of this study.

7.6.1.3 Sensivity to radiative and convective coefficients

With the FR model, all parameters of the admittance matrix had to be kept constant during the simulation period, including the radiative and convective coefficients. With this model, the interior long wave radiation exchanges were calculated with a constant linearized radiative heat transfer coefficient. Here these simulations are compared with the FD model using the same linearized radiative coefficient but recalculated at every time step as a function of the temperature of surfaces. A third model is also investigated with non linear radiative coefficients calculated with the Gebhart method (Gebhart, 1959; Mottard and Fissore, 2007), where the net radiative flux emitted by a surface is calculated using the Gebhart coefficients.

In this section, the configuration under study is F0, which is fully glazed. Consequently, the radiative coefficient under study in this section is $h_{r,floor-glazing}$.

The simulation results of these three radiation models are very close to each other where only minimal variations can be observed in figure 7.18a. Mean and extreme values of the radiative coefficient obtained with different calculation methods are presented in Table 7.5. By observing Figure 7.18a, it can be seen that there is very little difference when using a

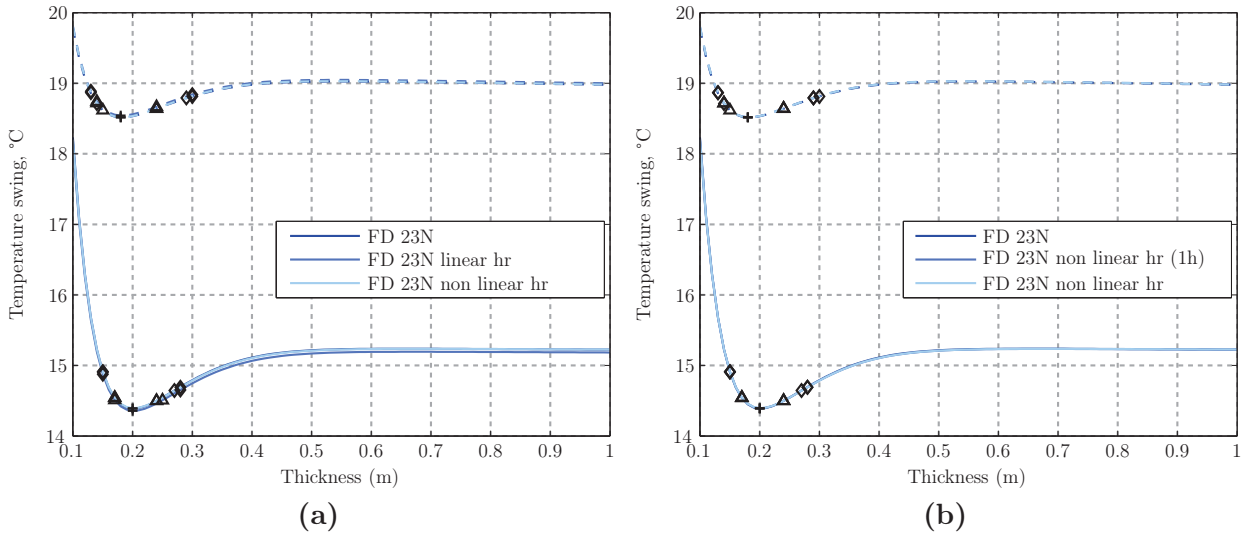

Figure 7.18: Impact of radiative coefficient calculation method; — T_s, - - - T_{op}

Table 7.5: Comparison of mean, minimum and maximum values of radiative coefficients

Method	Minimum	Mean	Maximum	Computation time
	$W/(m^2K)$			s
1 Sunny/1 Cloudy				
Constant hr	3.97	3.97	3.97	6
Variable linear hr	3.78	3.96	4.47	24
Variable non linear hr	3.96	4.15	4.69	25
Hourly non linear hr	3.96	4.15	4.69	6
5 Sunny/5 Cloudy				
Constant hr	3.97	3.97	3.97	52
Variable linear hr	3.75	3.96	4.49	299
Variable non linear hr	3.93	4.15	4.71	318
Hourly non linear hr	3.93	4.15	4.71	56

variable linear radiative coefficient comparing to a constant one, while the simulation time is are 4.0-5.8 times longer. Therefore, using a variable linear radiative coefficient is of little interest; if short simulation time is a priority, a well estimated fixed coefficient may yield fast and relatively accurate simulation results for a short sequence, and if accuracy is more important, then non linear radiative coefficients should be used.

In all models, the radiative coefficients were calculated at every time step (unless constant). Since surfaces temperature is not changing significantly for the order of magnitude of the selected time step (7.2 s), computation time can be reduced significantly without altering accuracy by updating the radiative coefficients hourly. Using non linear radiative coefficient

updated hourly yields very similar results (as shown in Figure 7.18b) with significantly less simulation time (56 s instead of 318 s); therefore this modelling approach is adopted for the subsequent simulations.

With the FR model, convective coefficients were calculated in two steps: they were estimated for the first iteration and their value was calculated using the Khalifa and Marshall correlations at the second iteration, based on the average temperature of the surfaces. With a FD model, the convective coefficients may vary during the simulation sequence. The following paragraphs presents an assessment of the impact of employing a fixed convective coefficient compared to a variable one.

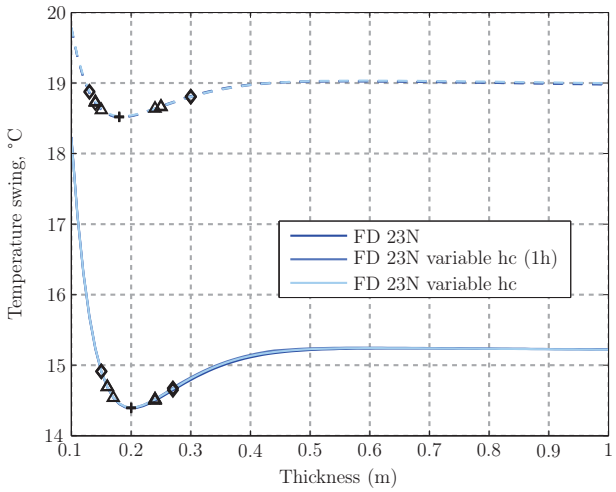

Figure 7.19: Impact of convective coefficient calculation method; —— T_s, - - - T_{op}

Simulation results using constant and variable convective coefficients are compared in Figure 7.19. There is very little differences induced by the use of a variable convective coefficient compared to a fixed one and virtually no differences at all if it is calculated at every time step or hourly.

Table 7.6 shows the minimum, mean and maximum value of the convective coefficient of the floor and glazing under a 1 sunny - 1 cloudy day and 5 sunny - 5 cloudy days sequences. The coefficients can reach much lower values when they are varying at every time step; however, since they reach such low values when the surface and air temperature are very close to each other, the impact on the magnitude of heat transfer is fairly low.

Since there is very little difference induced by updating the convective coefficients hourly instead of at every time step while the computation time is about 4 times faster, varying convective coefficients calculated hourly are adopted for the FD model.

Table 7.6: Comparison of mean, minimum and maximum values of convective coefficients

Method	Minimum	Mean	Maximum	Computation time
	$W/(m^2K)$			s
1 Sunny/1 Cloudy				
Constant hc_{floor}	3.02	3.02	3.02	6
Variable hc_{floor}	0.41	2.94	3.33	25
Hourly hc_{floor}	1.77	2.95	3.33	6
Constant $hc_{glazing}$	7.17	7.17	7.17	6
Variable $hc_{glazing}$	4.48	7.13	7.42	25
Hourly $hc_{glazing}$	6.41	7.15	7.42	6
5 Sunny/5 Cloudy				
Constant hc_{floor}	3.01	3.01	3.01	52
Variable hc_{floor}	0.20	2.93	3.43	301
Hourly hc_{floor}	1.59	2.93	3.43	58
Constant $hc_{glazing}$	7.17	7.17	7.17	52
Variable $hc_{glazing}$	3.54	7.11	7.49	301
Hourly $hc_{glazing}$	5.33	7.11	7.49	58

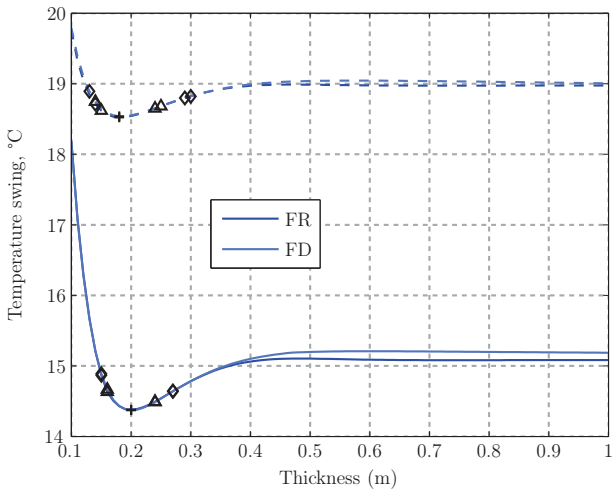

Figure 7.20: Comparison of the FR and FD models, configuration F0; — T_s, - - - T_{op}

Comparisons of the storage and operative temperature swings obtained with the FR and FD models with the parameters defined above (thermal storage divided in 23 control volumes, time step of 7.2 s, non linear h_r, variable h_c with h_r and h_c updated hourly) for a sunny day design period are depicted in Figure 7.20 for configuration F0. We can see that the two models are in good agreement with each other. Other configurations showed a similar adequacy (results not shown).

7.6.2 Simulation results and discussion

Simulations are conducted for the severe 2003-2004 winter for Quebec city and for the relatively warm 2009-2010 winter for Montreal. Weather data were obtained from the SIMEB building energy simulation software website (Hydro-Québec, 2015). Figures 7.21a show the daily average outdoor temperature and solar radiation profiles over twelve months for the 2009-2010 year in Montreal. This year was chosen because of its particularly mild winter. It can be seen that the coldest average temperature happened in January, although there is not a big difference with the daily average temperatures of December and February.

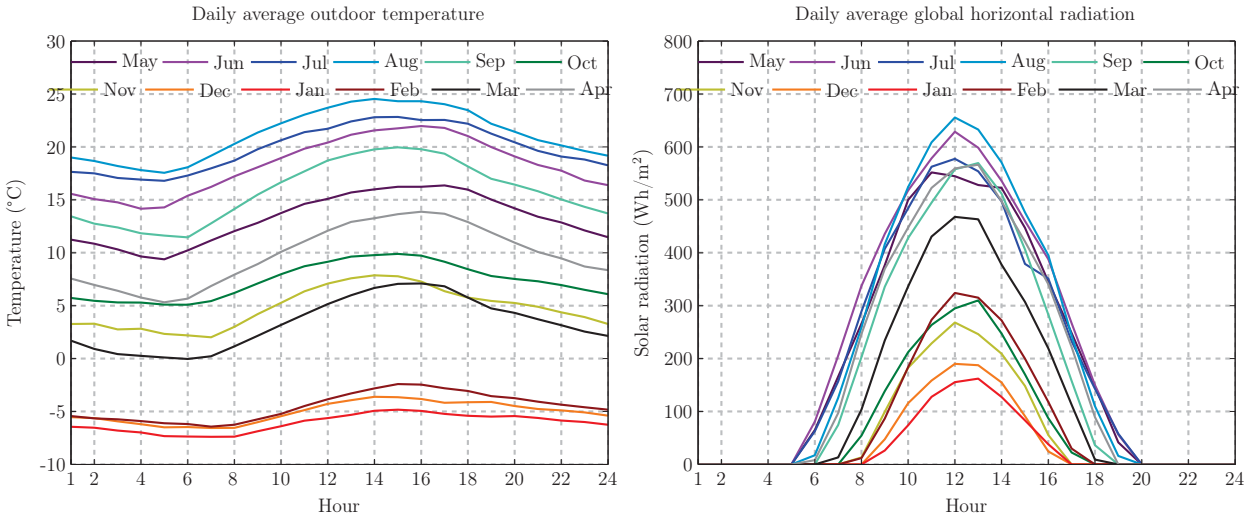

(a) Montreal weather data, year 2009-2010

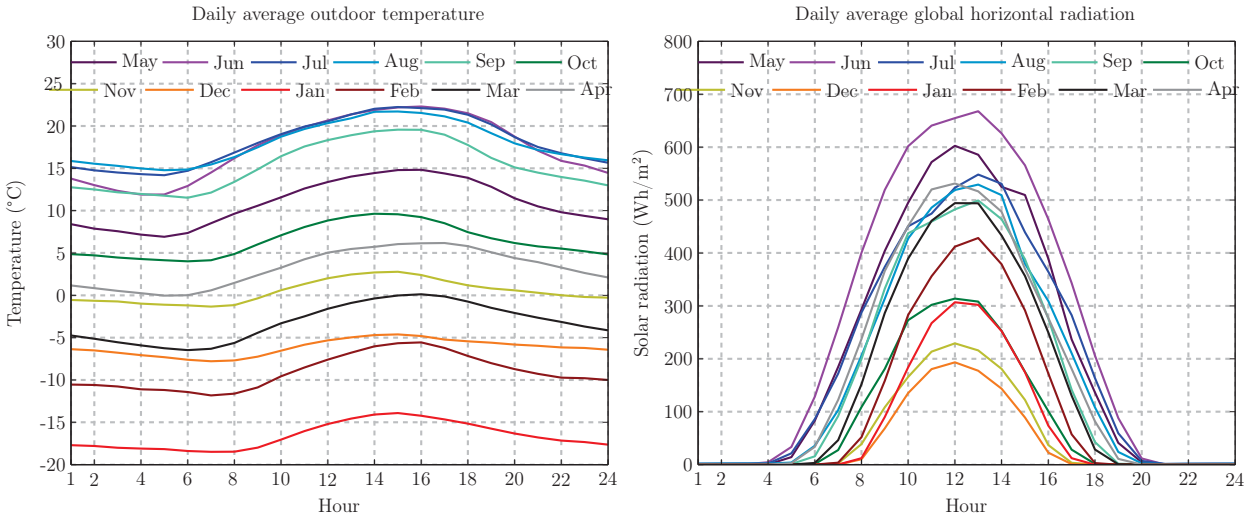

(b) Quebec weather data, year 2003-2004

Figure 7.21: Weather data employed for annual simulations with the FD model

Weather data for the year 2003-2004 in Quebec city are shown in figure 7.21b. We can see significantly lower temperatures, especially for the month of January with daily average temperatures between -19/-14 °C.

Simulations were run from April 1st to April 30th of the next year with the first month of April being used as a warm-up period. As with the FR model, the infiltration rate was constant at 0.2 ACH throughout the year. The year was divided into a cooling mode, a heating mode and a mixed mode where different ventilation rates were adopted depending on the mode. The cooling mode started in April until September, October and March were in mixed mode and the winter mode was during the months of November to February. The ventilation rules are reported in table 7.7.

Table 7.7: Ventilation rates adopted during the heating, cooling and mixed modes

Mode	T_i (°C)	Ventilation rate (ACH)
Heating	>30	0.5
	<30	0
Cooling	>24	40
	20<T_i<24	20
	<20	0
Mixed	>24	10
	20<T_i<24	5
	<20	0

Important simulation results for configuration N1 with Montreal weather data for the year 2009-2010 are presented in figure 7.22; more detailed monthly simulation results can be found in figure F.1 in appendix F. The monthly minimum operative temperature increases with thickness for all months of the year, in a small to moderate extent. The annual minimum temperature is depicted in figure 7.22b. Here we are looking at a weather sequence where there were several consecutive cloudy days followed by a temperature drop, which occurred in January. With that sequence, raising the storage thickness from 0.1 m to 1 m increases the minimum temperature from -14.0 °C to -11.4 °C.

The annual maximum temperature is depicted in figure 7.22b, where we can see a moderate reduction of the maximum temperature until a thickness of 0.15 m and a marginal reduction beyond; regardless of the storage thickness, the maximum temperature is too high and additional measures for temperature control are needed.

The daily operative temperature swings averaged annually are shown in figure 7.22c, where a reduced swing is observed at 0.18-0.20 m of storage thickness. However, the penalty for having a larger thickness is about 0.2 °C and is therefore hardly significant.

The observation of figure 7.22a reveals that December experiences an increased average operative temperature with thickness while January is relatively constant and February experiences a reduction of its average temperature. This could be explained by the seasonal character of large TES. When the average outdoor temperature is on the fall, a thicker TES can slightly increase the indoor average temperature, while with increased solar radiation availability in February, a thicker storage would stock more heat and thus the average indoor temperature would take longer to increase.

Annual simulation results under the weather of the year 2003-2004 in Quebec city are presented in 7.23 and monthly results in appendix F. As seen in figure 7.23b, at the coldest indoor conditions, which occurred in January, the minimum temperature at 0.1 m is -23.1 °C and is raised to -18.9 °C for a 1 m storage. An inflection point with a changing slope of the minimum operative temperature is visible at 0.2 m for the year 2009-2010 and at 0.3 m for the year 2003-2004.

Figure 7.23a reveals a similar behavior than in figure 7.22a: the average operative temperature for December increases with thickness, is mostly constant for January and is decreasing with thickness for February. This confirms that thick passive TES walls exhibit a seasonal behavior and are thus most advantageous in early winter than late winter for raising the average temperature.

The influence of heating was investigated and annual simulation results for configuration N1 with a heating set point of 5 °C are reported in Figure 7.24 (monthly results can be found in appendix F). The minimum temperature is still increasing with thickness, but less markedly than in the unheated case and with an inflection point at 0.25 m. As shown in figure 7.24a, increasing the storage thickness from 0.25 m to 1 m increases the minimum temperature only by 0.1 °C. The heating requirements for keeping the minimum air temperature at 5 °C are shown in figure 7.24b. A significant reduction of the heating requirements with increasing storage thickness is observed between 0.10 to 0.20 m and a more moderate reduction is observed at greater thicknesses.

Simulations of a solarium with RSI 2 instead of RSI 20 behind the storage wall have been carried out and the most important results are reported here. The minimum operative temperature dropped from -14 °C to -15°C at a 0.1 m thickness and from -11.4 °C to -11.8 °C at a 1 m thickness. The monthly average operative temperature of the three coldest months

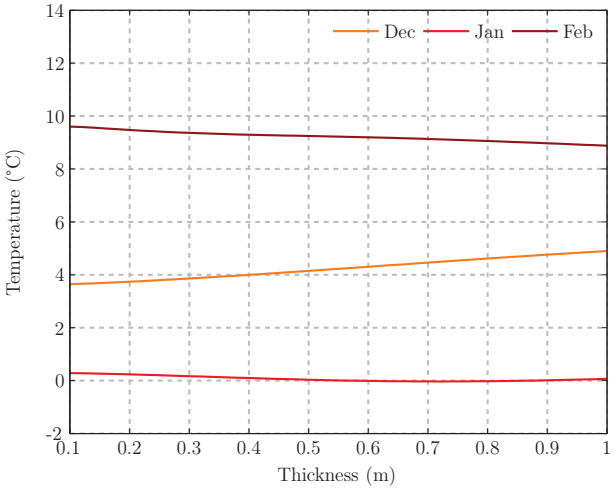

(a) Average T_{op}

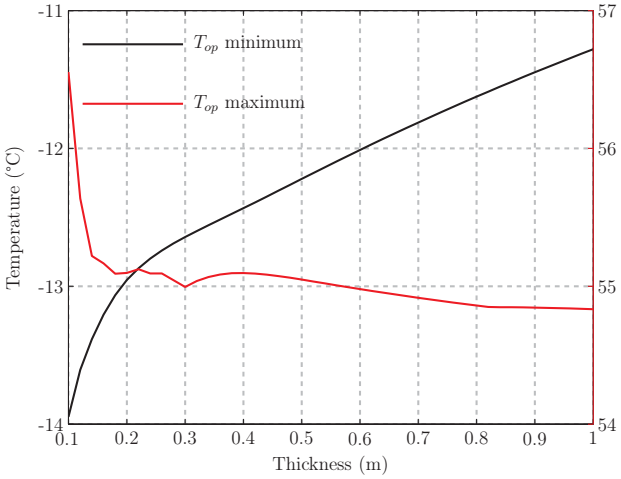

(b) Annual minimum and maximum T_{op}

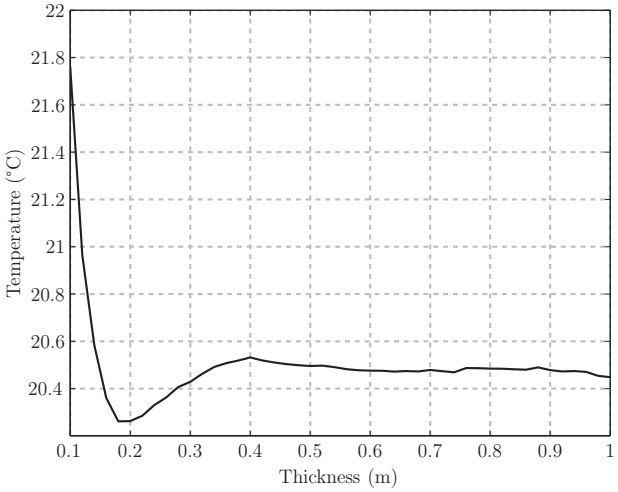

(c) Annual daily average T_{op} swing

Figure 7.22: Montreal, year 2009-2010

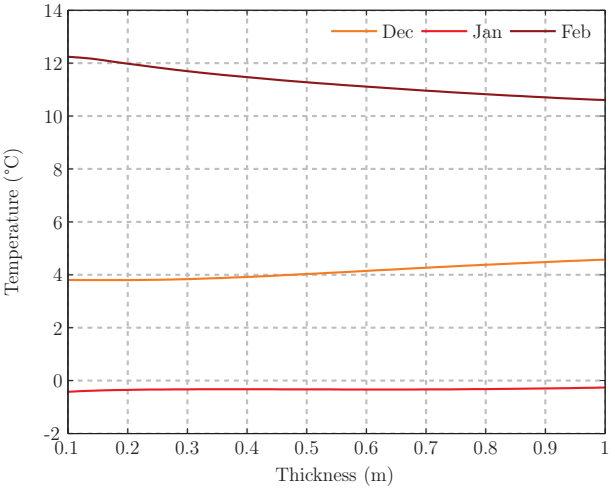

(a) Average T_{op}

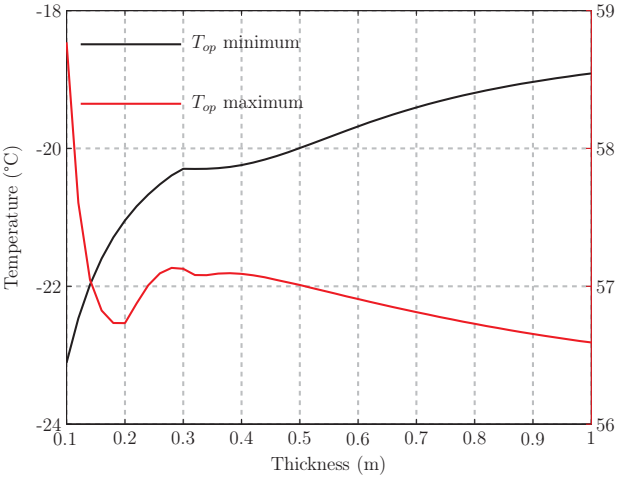

(b) Annual minimum and maximum T_{op}

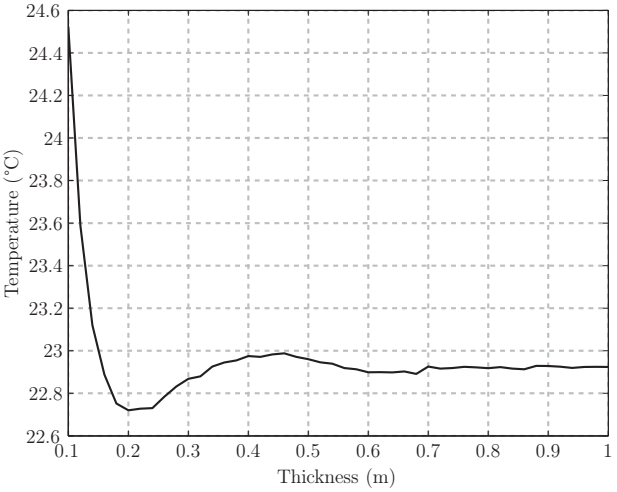

(c) Annual daily average T_{op} swing

Figure 7.23: Quebec, year 2003-2004

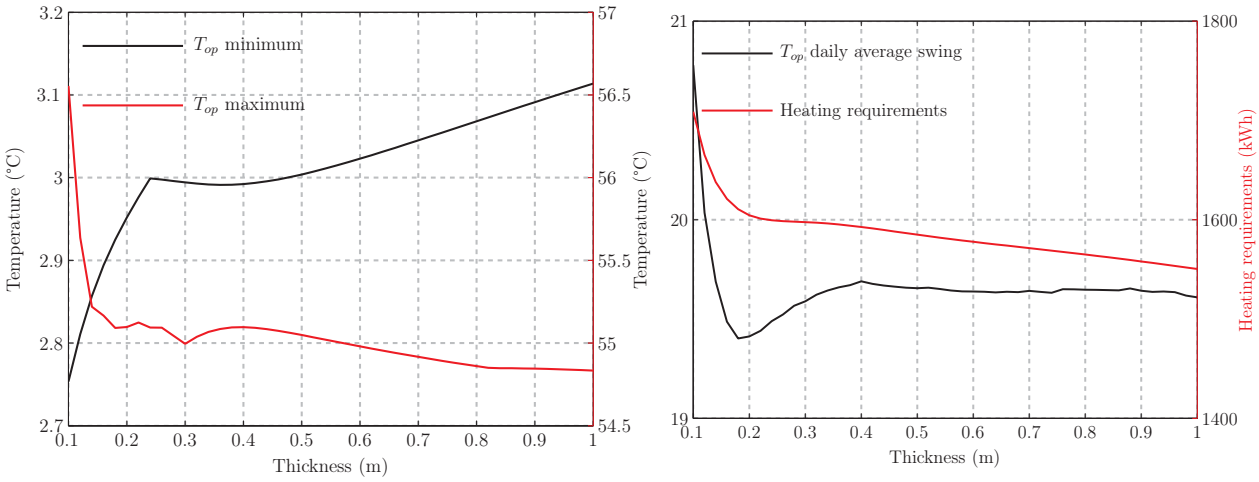

(a) Annual minimum and maximum T_{op}

(b) Annual daily average T_{op} swing

Figure 7.24: Montreal, year 2009-2010 – configuration N1 – heated ($T_{min} = 5$°C)

was about 0.5 °C lower at all thicknesses. The maximum operative temperature and average daily swing were not significantly affected. These observations are similar to those derived with the FR model. Since there are significant impacts on some of the main performance variables even at thicknesses where the transfer admittance was almost zero, we conclude that the analysis of the transfer transmittance is of little practical use and suggest to focus the attention on the main performance variables identified in section 7.3.7.

The annual minimum operative temperature is shown in figure 7.25 for configuration FN2. The minimum temperature is -11.5 °C when both TES have a thickness of 0.1 m. It reaches -8.7 °C for a 0.1 m floor storage and a 1 m the wall storage while it reaches -9.0 °C for a 0.1 m wall storage and a 1 m floor storage. This shows that locating a thick thermal storage on the north wall instead of the floor is slightly more efficient for raising the minimum temperature. The minimum temperature is raised to -6.3 °C when both storages are 1 m thick.

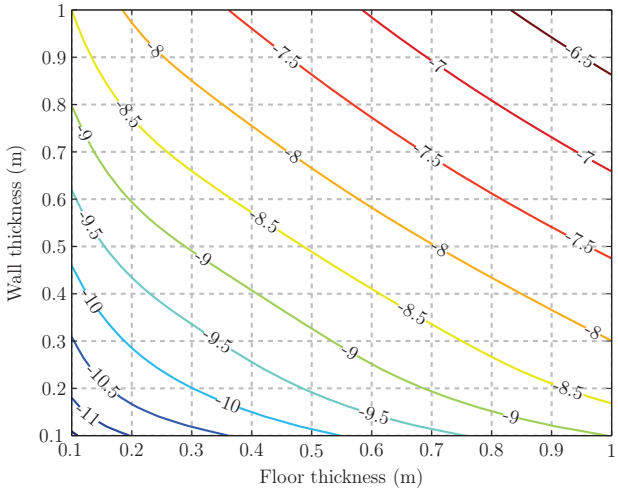

Figure 7.25: Annual minimum T_{op} (°C) – Montreal, year 2009-2010 – configuration FN2

7.7 Methodology

Numerous simulation results are presented in this chapter, which can be used to provide insight when planning the design of solaria and greenhouses in cold climates. The design of a high performance solarium or greenhouse that will provide a comfortable environment with little or no heating would benefit from carrying tailored simulations for analyzing potential design improvements. To this aim, we suggest to follow the methodology presented in this section.

Especially for a thick mass, a FR model is significantly easier to implement than a FD model because of the avoidance of spatial discretization and is thus selected for this methodology. Although annual simulations cannot be performed with this type of model, most design decisions can be made from an appropriate sequence of clear and cloudy days. Such a model requires a constant admittance matrix and therefore constant radiative, convective and conductive values. As shown in section 7.6.1.3, the use of constant convective and radiative coefficients does not significantly impact the average daily operative temperature swings. Average convective and radiative heat transfer coefficients are presented in table 7.8 for the different configurations. The main drawback of FR models would be in the case where shading devices are used, where the varying thermal resistance of the glazing will surely impact the indoor climate. In this case, an FR model could still be employed, but the sensitivity to varying glazing thermal resistance should be assessed. To assist in the design of glazing and shading systems, a methodology for selecting high performance fenestration systems can be found in Bastien and Athienitis (2015) and a control strategy for improving the operation of shades is presented in Bastien et al. (2015).

Table 7.8: Average convective and radiative coefficients, [W/m^2-K]

Configuration F0			
$h_{c,floor}$=2.9	$h_{c,glazing}$=7.1	$h_{r,floor-glazing}$=4.1	
Configurations F1, N1 and FN1			
$h_{c,floor}$=2.9	$h_{c,glazing}$=7.5	$h_{c,Nwall}$=2.3	
$h_{r,floor-glazing}$=3.0	$h_{r,floor-Nwall}$=1.3	$h_{r,Nwall-glazing}$=3.1	
Configurations F2 and FN2			
$h_{c,floor}$=2.8	$h_{c,glazing}$=7.7	$h_{c,Nwall}$=2.3	$h_{c,E/Wwalls}$=2.3
$h_{r,floor-glazing}$=2.8	$h_{r,floor-Nwall}$=1.1	$h_{r,floor-E/Wwalls}$=0.5	
$h_{r,Nwall-glazing}$=2.5	$h_{r,Nwall-E/Wwalls}$=0.5	$h_{r,glazing-E/Wwalls}$=0.5	

It is suggested to carry out simulations with a FR model over two design periods: over a period of a sunny day for analyzing $\tau_{[Q_a - T_s]}$ and over a five sunny - five cloudy days period for analyzing the other main performance variables. The analysis of $\tau_{[Q_a - T_s]}$ could be carried out at the winter solstice where solar gains are at their lowest levels or at another moment where the time lag effect would be the most desirable. We have seen that $\tau_{[Q_a - T_s]}$ is not too significantly affected by the choice of the design day.

In order to provide conditions that will be representative of the most challenging weather conditions for the five sunny - five cloudy days design period, it is recommended to model the solar radiation at the winter solstice with the Hottel model. Estimation of the average absorbed beam fractions, f_x, are provided for different conditions for avoiding tedious ray-tracing calculations; they are given in table 7.10 below for a latitude of 45°and in table G.1 in appendix G for a latitude of 55 °. The roof tilt angle does not affect much the solar radiation distribution, so f_x can be estimated to be identical to those showed in the tables even if the roof angle is different. Values can be interpolated for different width to north wall ratio, floor aspect ratio, orientation or latitude. For a glazed surface, the sum of its f_x must be equal to 1. Then, the portion of a window area illuminating directly surface i can be calculated as $f_{w,i} = f_{x,i} A_w$ where A_w is the area of the window. Finally, the beam and diffuse radiation absorbed by an interior surface is calculated following the procedure defined in Bastien et al. (2015, section 2.1.2).

For the average outdoor temperature, it is recommended to select the minimum monthly air temperature over the last 22 years for the location under consideration; this information can be readily obtained from the NASA surface meteorology and solar energy web site (NASA, 2015). The average daily temperature range can also be obtained from the same source. Any location can be specified; only the latitude and longitude have to be provided. The parameters *Air temperature at 10 m* and *Daily temperature range at 10 m* have to be selected in order to visualize only the variables of interest here.

The FR model should be used to explore design variations for improving the performance. As identified in this study, the parameters that most significantly impact the performance are the presence of a TES, its thickness and material, the glazing type and the aspect ratio of the space. The positioning of glazed and opaque surfaces also has a significant impact; however, it is very time consuming to analyze many variants with numerical simulations because this implies creating new surfaces and heat exchanges between them. It is therefore suggested to follow recommendations presented in table 7.9 to select an energy efficient design. When the positions of glazed and opaque surfaces have been selected, the energy balance equation for

the desired configuration can be found in this work with which a FR model can be readily implemented in a programming software.

Table 7.9: Design recommendations for increasing the average temperature in solaria and greenhouses

A floor area with a high aspect ratio should be selected and oriented with the longest side facing south.
South-facing surfaces should be fully glazed.
North facing surfaces should be opaque, insulated and have a thermally massive inner layer
Opaque east and west walls increase the average temperature, but also reduces the solar radiation homogeneity on the floor compared to glazed east and west walls
A glazing with a high solar transmittance and thermal resistance should be selected
Shading devices should be installed and controlled efficiently
The floor should have a thermally massive inner layer with insulation underneath
The use of water as a TES material should be considered

A high value for the thermal resistance of the insulation layers is strongly recommended during the first design exploration phase. When most of the design parameters have been decided, the impact of varying the thermal resistance should be investigated at last.

The main steps of the proposed methodology are presented in table 7.11

Table 7.10: Average absorbed beam radiation fraction at the winter solstice – $\lambda = 45°$

Floor aspect ratio	Indoor surface	Glazed surface: south wall	south roof	east	west	north	Glazed surface: south wall	south roof	east	west	north
		Longest side facing south					Longest side facing 30°west of south				
roof angle of 35°, width=north wall height											
4:1	floor	0.78	0.03	0.21	0.21	0.00	0.77	0.07	0.33	0.11	0.00
	north wall	0.12	0.89	0.79	0.79	0.00	0.11	0.77	0.65	0.89	0.00
	east and west walls	0.10	0.08	0.00	0.00	0.00	0.12	0.26	0.02	0.00	0.00
	south wall and roof	0.00	0.00	0.00	0.00	0.00	0.00	0.00	0.00	0.00	0.00
2:1	floor	0.73	0.03	0.21	0.21	0.00	0.69	0.05	0.31	0.11	0.00
	north wall	0.07	0.81	0.79	0.79	0.00	0.10	0.69	0.63	0.89	0.00
	east and west walls	0.20	0.16	0.00	0.00	0.00	0.21	0.26	0.06	0.00	0.00
	south wall and roof	0.00	0.00	0.00	0.00	0.00	0.00	0.00	0.00	0.00	0.00
1:1	floor	0.63	0.03	0.21	0.21	0.00	0.59	0.02	0.28	0.11	0.00
	north wall	0.04	0.67	0.77	0.77	0.00	0.08	0.58	0.57	0.89	0.00
	east and west walls	0.37	0.31	0.02	0.02	0.00	0.34	0.40	0.15	0.00	0.00
	south wall and roof	0.00	0.00	0.00	0.00	0.00	0.00	0.00	0.00	0.00	0.00
1:2	floor	0.49	0.02	0.20	0.20	0.00	0.45	0.01	0.23	0.11	0.00
	north wall	0.00	0.48	0.66	0.66	0.00	0.05	0.45	0.49	0.99	0.00
	east and west walls	0.51	0.50	0.14	0.14	0.00	0.50	0.54	0.28	0.00	0.00
	south wall and roof	0.00	0.00	0.00	0.00	0.00	0.00	0.00	0.00	0.00	0.00
roof angle of 15°, width=2×north wall height											
4:1	floor	0.83	0.12	0.36	0.34	0.00	0.82	0.18	0.52	0.20	0.00
	north wall	0.08	0.80	0.64	0.64	0.00	0.08	0.68	0.47	0.80	0.00
	east and west walls	0.09	0.08	0.00	0.00	0.00	0.10	0.14	0.01	0.00	0.00
	south wall and roof	0.00	0.00	0.00	0.00	0.00	0.00	0.00	0.00	0.00	0.00
2:1	floor	0.78	0.11	0.36	0.34	0.00	0.76	0.14	0.50	0.20	0.00
	north wall	0.04	0.73	0.64	0.64	0.00	0.07	0.62	0.45	0.80	0.00
	east and west walls	0.18	0.16	0.00	0.00	0.00	0.17	0.24	0.05	0.00	0.00
	south wall and roof	0.00	0.00	0.00	0.00	0.00	0.00	0.00	0.00	0.00	0.00
1:1	floor	0.68	0.10	0.36	0.34	0.00	0.66	0.08	0.46	0.20	0.00
	north wall	0.00	0.60	0.62	0.62	0.00	0.06	0.54	0.43	0.80	0.00
	east and west walls	0.32	0.30	0.02	0.02	0.00	0.28	0.38	0.11	0.00	0.00
	south wall and roof	0.00	0.00	0.00	0.00	0.00	0.00	0.00	0.00	0.00	0.00
1:2	floor	0.54	0.07	0.34	0.34	0.00	0.52	0.04	0.39	0.20	0.00
	north wall	0.00	0.44	0.53	0.53	0.00	0.03	0.43	0.38	0.80	0.00
	east and west walls	0.46	0.49	0.13	0.13	0.00	0.45	0.53	0.23	0.00	0.00
	south wall and roof	0.00	0.00	0.00	0.00	0.00	0.00	0.00	0.00	0.00	0.00

Table 7.11: Methodology for thermal mass design in solaria and greenhouses

	Step	Reference
1.	Determine the position of glazed and opaque surfaces.	Table 7.9
2.	Identify the corresponding configuration.	Section 7.4
3.	Find the heat balance equation associated to the chosen configuration.	Equation 7.5 and D.1-D.5
4.	Determine the absorbed solar radiation.	
4.1	Define the solar radiation incident on the glazed surfaces for a sunny and a cloudy day at the winter solstice with the Hottel model; for a cloudy day, $I_{beam} = 0$ and $I_{diffuse,\ cloudy} = 1.5 \cdot I_{diffuse,\ sunny}$	see Hottel (1976) or Duffie and Beckman (2006, section 2.8)
4.2	Calculate the solar radiation transmitted through the glazings and absorbed by interior surfaces.	see Bastien et al. (2015, section 2.1.2) with f_x from tables 7.10 and G.1
5.	Define the exterior temperature profile by setting $T_o = T_{av} + dT_{av}/2 \cos(\omega t + 3\pi/4)$ where $T_{av} =$ *Air temperature at 10 m*, $dT_{av} =$*Daily temperature range at 10 m* and $\omega = 2\pi/86400$.	(NASA, 2015), where T_{av} is the coldest month of the 22-year minimum
6.	Determine the conductances in the admittance matrix.	
6.1	Define the convective and radiative heat transfer coefficients.	Table 7.8
6.2	Set $U_{vent} = \text{ACH}\, V \rho_{air} C_{air}/3600$ where ACH is the infiltration + ventilation rate, in air changes per hour.	
6.3	Define $U_{gr} = A_f/R_{gr}$ and $U_o = A_s/R_o$ where $R_{gr} = R_o$=20 m^2K/W at first.	
6.4	Calculate U_g and U_w for the glazing and wall materials of interest, where $U_w = A_w/(R_w + 1/h_o)$, R_w is the total wall thermal resistance and $h_o = 20$ (W/m^2K).	Equation 7.4 for U_g
7.	Build the equivalent sources.	Section 7.5.1 and D
8.	Represent the heat sources (real and equivalent) with complex Fourier series. Use N=5 for a sunny day and N=31 for a five sunny - five cloudy days sequence.	
9.	Define the admittances and solve the heat balance equation identified in step 3 for the temperature vector.	Section 7.5.1 and D
10.	Run simulations for a sunny day and observe $\tau_{[Q_a - T_s]}$; then for a five sunny - five cloudy days design period and observe the other five performance variables.	
11.	Use the model to explore design variation for improving performance. When most design variables are identified, explore varying the R-value of the insulation layers at last.	

For the sake of exemplifying the use of this methodology, simulation results for a five sunny - five cloudy days period are presented in figure 7.26 for configuration N1 located in Montreal. For this location (45.5°N, 73.6°W), the minimum monthly air temperature is -13.7 °C and occurs for the month of January, which has an average daily temperature range of 6.5 °C. Here we can see that the minimum operative temperature is -17.5 °C at 0.01 m, -13.0 °C at 0.1 m, -10.2 °C at 0.5 m and -9.5 °C at 1 m. The average operative temperature is 0.2 °C for all thicknesses. The daily average swing drops significantly from 0.01 m to 0.1 m, reaches a minimum of 20.5 °C at 0.17 m and increases marginally for greater thicknesses. The maximum operative temperature drops significantly from 0.01 m to 0.1 m and reduces slightly for greater thicknesses. All these results are representative of those obtained with the FD model for the coldest month, presented in figure 7.22. Therefore, we can conclude that the five sunny - five cloudy design period with the conditions defined above can provide a good estimation of the behavior of a solarium during the harshest conditions in a year and thus provides a good basis for assessing design improvements.

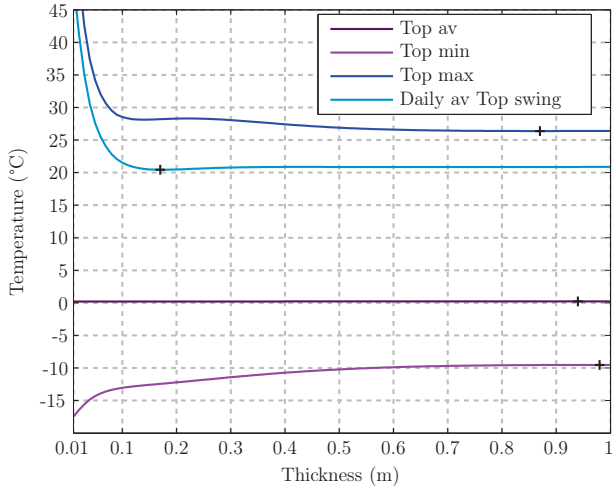

Figure 7.26: Proposed methodology – example for configuration N1 located in Montreal

7.8 Summary, design recommendations and conclusions

As seen from section 7.3, it was found that the most appropriate design variables for characterizing the performance of passive TES is isolated-gain spaces are:

- the absorbed solar radiation - storage temperature time lag ($\tau_{[Q_a - T_s]}$);
- the daily operative temperature swing;
- the average operative temperature;
- the minimum and maximum operative temperature
- the space heating requirements

The key design targets of solaria/greenhouses equipped with various passive TES systems have been analyzed with frequency response (FR) and finite difference thermal network (FD) models. Upon analysis of the simulation results obtained with these models, within the main performance parameters identified above, we can conclude that passive TES in solaria and greenhouses can most significantly impact the timing of the heat delivery (as captured by $\tau_{[Q_a - T_s]}$), the daily average operative temperature swing and the minimum operative temperature. Therefore we suggest focusing on these three design targets when designing TES in solaria and greenhouses.

As seen from figure 7.7c, the presence of a storage mass on the north wall or the floor significantly reduces the daily operative temperature swing up to a thickness about 0.10-0.20 m and becomes mostly constant beyond – under the periodic conditions of a cold sunny day. This behavior is mostly independent of the design period under consideration. Results obtained with the FD model with real weather data confirmed this observation and revealed an annual daily swing minimum around 0.20 m with minimal increase for greater thickness. Therefore, it is recommended to adopt a TES with a thickness of at least 0.15 m for reducing temperature swings.

Under periodic conditions, the minimum operative temperature is strongly affected by the design period under consideration (see figure 7.13a). Simulations with the FD model with real weather data revealed an ever increasing minimum temperature with storage thickness – at least up to 1 m. However, the slope of the minimum operative temperature changes with an inflection point at about 0.20-0.30 m; therefore the biggest contribution for raising the minimum operative temperature are made up to that point, where the minimum temperature keeps increasing beyond but less markedly. Result obtained with the FD model revealed that increasing the thickness of TES from 0.10 m to 1 m can raise the minimum temperature in unheated solaria and greenhouses by 3 to 5 °C, depending on the configuration and weather conditions. For raising the minimum operative temperature in heated solaria and greenhouses, it is recommended to select a TES thickness of about 0.25 m. For unheated solaria and greenhouses, it is recommended to select a TES with a minimum thickness of 0.3 m and even thicker if allowable by space constraints. For a fixed thickness of thermal mass, it is recommended to place about 0.10 m on the floor and the remaining on the north wall.

As seen in figure 7.7e, it is not possible to design the thickness of a passive TES system to provide a time lag appropriate for night cooling. It is however possible to improve thermal comfort in the evening by selecting a TES thickness with a high $\tau_{[Q_a - T_s]}$. If providing comfort during the evening is an important design goal, it is recommended to implement a TES on

the north wall or the floor with a thickness between 0.05-0.10 m and to select a configuration with opaque north, east and west walls. Implementing a 6 cm TES on both the north wall and the floor maximizes $\tau_{[Q_a - T_s]}$ for both TES and is thus the best option for improving evening thermal comfort.

If providing evening warmth and higher minimum temperatures are both important design goals, it is suggested to select a configuration with a massive floor and north wall and insulated east and west walls (i.e. configuration FN2) and to locate a 0.06-0.08 m TES on the floor and a TES on the north wall as thick as possible while meeting practical constraints. The use of water as TES material should be considered.

The average operative temperature under a periodic sunny day in winter remains mostly constant with thicknesses between 0.01 m and 1 m. Under real weather conditions, the monthly average temperature exhibited a seasonal behavior where the average temperature of December increased with thickness, remained mostly constant in January and reduced with thickness in February. Thus we may conclude that large passive TES tend to increase the average temperature in early winter and to decrease it in late winter. With increased solar availability in February compared to December, this could be an acceptable drawback.

As seen in figure 7.13a, increasing the storage thickness to about 0.10 m significantly reduces the maximum operative temperature under a periodic sunny winter day. The analysis under real weather conditions revealed a further reduction until a thickness of about 0.20 m for most months and varying results beyond. Regardless of the TES thickness, additional measures should be implemented to prevent overheating such as ventilation and the use of shading devices.

A reduction of the thermal resistance of the insulation layer behind the storage mass from RSI 20 to RSI 2 was found to reduce the average operative temperature of winter months by about 0.5 °C independently of the TES thickness, while a greater reduction of the minimum temperature was observed for lower thicknesses. It is recommended to analyze the effects of varying the insulation level at the end of the design process, when most of the key design variables have been selected.

The introduction of continuous indoor air recirculation increases convective exchanges and can significantly reduces the maximum operative temperature, but reduces slightly its average and minimum temperature as well as $\tau_{[Q_a - T_s]}$; it is thus recommended to use indoor fans on an intermittent basis.

It was found the use of water as TES material instead of concrete or soil can significantly reduce the daily average operative temperature swing and peak temperatures as well as increase $\tau_{[Q_a - T_s]}$. Therefore, including water in solaria and greenhouses is recommended.

Although most simulation results presented here were obtained for a 24 m^2 solarium with specific dimensions, it was shown that spaces with different dimensions have similar optimal TES thicknesses for the main output variables; thus, results presented here can be valuable for designing solaria and greenhouses with different dimensions.

This chapter presented a methodology for sizing passive TES in solaria and greenhouses that can be used for reaching different design intents. Future studies should focus on improving the efficiency of large TES in isolated-gain spaces, where the use of active ventilation and the development of efficient strategies for controlling the airflow is of particular interest.

Chapter 8

Conclusion

8.1 Summary

This Ph.D. thesis presented a wide literature review on various aspects related to the design and control of solaria and greenhouses. Relevant studies conducted on geometrical parameters and orientation, glazing and shading materials, thermal energy storage and innovative auxiliary heating systems were presented.

The four main variables governing the interior climate are the indoor temperature, relative humidity, CO_2 concentration and solar radiation level. These variables must be controlled to maintain production objectives, energy consumption targets or thermal comfort for people and plants. Different systems can be employed to modify these variables, such as shading and ventilation systems, auxiliary heating systems, dehumidification, CO_2 injection and artificial lighting systems. The impacts of these systems on the main variables have been discussed. Different climate control strategies were reviewed and the best climate control models were presented.

Based on this review of the scientific literature, the following recommendations are proposed:

- A design with a high aspect ratio must be preferred, with the longest side facing south.
- If possible, the south roof angle should be slightly higher than the latitude (+5-20°).
- The north wall should be opaque and have a thermally massive material as inner layer.
- Ventilation openings should be provided along the longest side, with both roof vents and side vents.

- Both roof and side vents should be used for summer ventilation, while only the side vents or roof vents should be used for winter ventilation.
- Due to its durability and aesthetic, glass should be the preferred glazing material for building-integrated solaria and greenhouses.
- When glass is the selected cover material, the use of anti reflecting and low emissivity coatings as well as argon filling should be considered.
- Increasing the number of layers of the glazing material is highly desirable for reducing heat losses.
- At least one shading device should be installed; two is even better.
- The floor inside layer should have appreciable thermal storage capacity and have insulation as external layer.
- Including animals or composting installations in solaria and greenhouse should be envisioned for their heat and CO_2 production, where they should be selected based on carbon dioxide needs.
- If artificial lighting is used, CO_2 enrichment should be practiced simultaneously.
- If plants are grown in the space, the use of a ventilation system with heat recovery should be considered for humidity control in winter instead of natural ventilation.

The energy saving potential of attached solaria and greenhouses has been evaluated in chapter 3 for the province of Québec, Canada. It was found that solaria can collect significant surplus heat that can be transferred to an adjacent house to partly offset its heating load. Results obtained from the different solarium configurations revealed that a net energy balance of 28-144 kWh/m^2 of solarium floor area is possible. Retrofitting an energy efficient solarium to an average house could reduce its heating demand by 9% to 23%, depending on the size of the solarium. In these simulations, the solarium was conditioned with a heating set point of 10 °C and the heat was available for the house when the temperature inside the solarium exceeded 28 °C. Simulations conducted for large rooftop greenhouses revealed that achieving net zero heating is possible and that surplus heat up to 31 kWh/m^2 of greenhouse floor area can be collected with an energy efficient design (with a heating set point of 15 °C and surplus heat when the temperature is exceeding 25°C). Covering 1% of large commercial and institutional buildings in Quebec with rooftop greenhouses could provide enough vegetables to feed 300 000 people without increasing the total energy consumption of the province.

A methodology for the design of fenestration systems in heating dominated climates has been developed and is presented in chapter 5. This methodology can be used at the early design stage for providing assistance in the selection of glazings or windows equipped with

shading devices. The solar and thermal effects resulting from the presence of an interior and/or exterior planar shade, parallel to the glass, can be simulated. Diagrams displaying the annual energy gain (or loss) per unit area as a function of the effective U-value and solar heat gain coefficient of a fenestration system are generated, for a specific surface orientation and climate. Such diagrams are useful at the early design stage when there is a need to compare various fenestration systems on a relative basis. This methodology can be used for designing buildings aiming at a high solar utilization like solaria and greenhouses, where different fenestrations systems may be selected for different surface orientation in order to increase the net energy gains of a space.

While the use of one or more shades is suggested by many researchers for reducing heat losses, the literature review revealed a need for an improved control method. A new control strategy for improving the operation of an exterior and/or interior planar shade is presented in chapter 6. The control strategy is based on performing an energy balance on the fenestration system and calculating the total heat flow (i.e. solar gains + overall heat losses). The heat flow can be maximized or minimized, depending on the needs of the space. A solarium model was developed to assess the performance of the proposed control method. Simulation results revealed that a 3-9% reduction of the heating requirements is possible and an additional 9-14% surplus heat can be collected in the heating mode, compared to a control based on global horizontal solar radiation levels (with a heating set point of 10 °C and surplus heat considered for a temperature exceeding 28 °C). During the mixed mode, it was shown that thermal comfort can be significantly improved with an additional 1822 hours within the thermal comfort range when controlling an interior shade with the proposed algorithm.

A methodology for designing passive thermal energy storage (TES) systems has been developed and is presented in chapter 7. Potential targets for thermal mass design strategies were reviewed, along with common metrics used in the characterization of the performance of TES systems. Six different solarium/greenhouse designs were investigated, which encompass the most frequent configurations. Two complementary modelling approaches were considered for analyzing these configurations: frequency response (FR) and finite difference (FD). The frequency response models were used for sensitivity studies used under short periodic conditions while FD models were used in full-year performance assessments with real weather data. Many design variations have been considered with these models, which allowed to formulate design recommendations. A methodology based on a frequency response model was presented for sizing TES in solaria and greenhouses. The methodology is applicable to various solaria and greenhouse designs with the energy balance equations corresponding to six different configurations that are provided.

8.2 Contributions

Upon reviewing the scientific literature pertaining to the design and control of solaria and greenhouses, many research opportunities have been identified and some of them were tackled. The major contributions of this thesis are:

- The evaluation of the energy potential of attached solaria and rooftop greenhouses for the province of Québec.
- The development of a methodology for selecting fenestration systems with a high solar energy utilization.
- The elaboration of a new control algorithm for improving the control of multiple shading devices that can maximize or minimize the total heat flow, depending on the needs of the space.
- The development of a methodology for sizing TES in solaria and greenhouses that is applicable to various designs and climates.

8.3 Limitations and outlook

The methodology for selecting fenestration systems is intended for the design of buildings aiming at a high solar utilization, such as solaria and greenhouses, solar houses and other kind of buildings where a *solar optimized fenestration systems* approach has been adopted. This concept designate a design approach where the role of windows is to maximize the net energy balance and the role of shading devices is to control overheating and glare issues as well as improving the energy balance. During the design process, it is recommended to first use this methodology for identifying the most appropriate glazing and shading combination for each orientation so as to maximize the solar energy utilization from the fenestration system. For ensuring a good design, it is necessary thereafter to follow passive solar design guidelines to adequately position and size windows and select appropriate shading devices to avoid overheating issues.

Since this methodology is based on steady state calculations, it is not meant to predict the yearly total energy gained or loss through a fenestration but rather to assist the design process by comparing the performance of different products on a relative basis. This methodology can only evaluate the heat transfer of planar shading elements that are parallel to the

glazing. Fixed shadings such as overhangs, fins and louvres cannot be evaluated with this methodology.

The control strategy for improving the operation of multiple shades presented in this thesis was developed to be used in solaria and greenhouses. It can also be applicable to residential buildings for maximizing the solar energy utilization from glazed surfaces, where occupants override should be allowed to provide for glare and privacy issues. The control algorithm could also be included as an additional criteria in existing control strategies for office buildings based on visual comfort. More research is needed in this area for evaluating its energy saving potential in this context. The assessment of the performance of this control strategy for other shading types is also desirable. Here again, only planar shading elements parallel to the glazing are compatible with this control strategy.

The control strategy for operating shades was developed in Matlab and its performance was assessed with simulations. To use this control strategy in real applications, it is necessary to develop an approximate model for real-time control. To this aim, transfer functions should be elaborated based on three inputs: the incident solar radiation level, the exterior temperature and the interior temperature. Developing a method for deriving these transfer functions for different designs and climates is needed for the real-time implementation of this control strategy in solaria and greenhouses.

The procedure for calculating the convective heat transfer coefficient in a ventilated cavity described in ISO15099, based on first principles physical models, is expensive to implement and lacks experimental validation. The conduction of extensive experimental studies of various shading materials and configurations and the development of simpler empirical models are needed.

Extensive simulations of solaria have been performed with frequency response (FR) and finite difference (FD) models. Comparing these simulation results with experiments would be a valuable exercise. In particular, performing an experimental comparison of two identical solaria but with different TES thicknesses and observing the differences between the main performance variables would be desirable for confirming the validity of the simulation results.

The methodology for sizing TES in solaria and greenhouses was limited to passive TES. Expanding this methodology for the design of active TES is an important research objective that should be pursued in future studies. Ventilated TES allow to increase the effective heat storage capacity of a mass by enhancing heat transfer; they have the potential to further reduce extreme temperatures in unheated solaria and greenhouses. Effective control strategies

should be developed for controlling the airflow based on various needs, such as limiting high temperatures and improving the indoor conditions for people and plants, where model predictive controls could be used to reach these goals.

Although care was taken for proposing a methodology that is accurate, yet simple to implement, the development of this methodology in a programing software will still require non negligible efforts from a designer. Integrating this methodology into a design tool that be can used for the design of solaria and greenhouses would widen its use and thus be a worthwhile effort.

Innovative greenhouse prototypes have been built with integrated photovoltaics and desalination capabilities; future research on semi transparent photovoltaics and seawater desalination specifically adapted to greenhouses would be highly valuable. Concerning materials development, further improvement of glass coatings combining very high solar and visible transmittance as well as shading materials with a high visible transmittance and low near infra red transmittance would be highly desirable for solaria and greenhouses.

8.4 Final thoughts

Many research needs were identified for improving the design and control of solaria and greenhouses, from which only a few could be addressed in this thesis. Nevertheless, with the actual state of knowledge and the existing materials available, it is already possible to build highly efficient spaces that can provide a great environment where people and plants can thrive. I believe that the work presented in this thesis can be useful for achieving this. With a little planning, it is possible to design a space that can provide a nice environment for people while capturing additional solar heat that can be used by an adjacent building and producing fresh vegetables simultaneously. Doing so is a step further for a reduced ecological footprint and increased resilience, in a very pleasant way.

References

Aaslyng, J., Lund, J., Ehler, N., Rosenqvist, E., 2003. IntelliGrow: a greenhouse component-based climate control system. Environmental Modelling & Software 18 (7), 657–666.

Aguiar, L., da Costa, J., Aguiar, R., Fischer, G., 2009. Estimates and measurements of photosynthetically active radiation and global solar irradiance in Rondonia. In: AIP Conference proceedings.

Ahmed, M., 2005. Evaluation and optimization of solar desiccant wheel performance. Renewable Energy 30 (3), 305–325.

Aikman, D., 1989. Potential increase in photosynthetic efficiency from the redistribution of solar radiation in a crop. Journal of experimental botany 40 (217), 855–864.

Al-Saadi, S. N., Zhai, Z., 2013. Modeling phase change materials embedded in building enclosure: A review. Renewable and Sustainable Energy Reviews 21, 659–673.

Alexandri, E., Jones, P., 2007. Developing a one-dimensional heat and mass transfer algorithm for describing the effect of green roofs on the built environment: Comparison with experimental results. Building and Environment 42 (8), 2835–2849.

American Society of Agricultural Engineers, 2003. Heating, ventilating and cooling greenhouses. ANSI/ASAE EP406.4 JAN03.

Andrusiak, M., Harrison, S., 2009. The modelling and design of a solar-driven liquid-dessicant air-conditioning system. In: 4th Annual Canadian Solar Buildings Conference. Toronto.

Asan, H., 2000. Investigation of wall's optimum insulation position from maximum time lag and minimum decrement factor point of view. Energy and Buildings 32 (2), 197–203.

Asan, H., 2006. Numerical computation of time lags and decrement factors for different building materials. Building and Environment 41 (5), 615–620.

ASHRAE, 2007. ASHRAE Handbook - HVAC Applications, A44. American Society of Heating, Refrigerating and Air-Conditioning Engineers, p6.

ASHRAE, 2008. ASHRAE Vision 2020 - Producing net zero energy buildings. American Society of Heating, Refrigerating and Air-Conditioning Engineers.

ASHRAE, 2009. ASHRAE Handbook - Fundamentals. American Society of Heating, Refrigerating and Air-Conditioning Engineers.

Aste, N., Angelotti, A., Buzzetti, M., 2009. The influence of the external walls thermal inertia on the energy performance of well insulated buildings. Energy and Buildings 41, 1181–1187.

Astee, L. Y., Kishnani, N. T., 2010. Building-integrated agriculture: utilising rooftops for sustainable food crop cultivation in Singapore. Journal of Green Building 5 (2), 105–113.

Athienitis, A., O'Brien, W., 2015. Modeling, design, and optimization of net-zero energy buildings. John Wiley & Sons.

Athienitis, A., Stylianou, M., 1991. Method and global relationship for estimation of transmitted solar energy distribution in Passive Solar Room. Energy Sources 13, 319–336.

Athienitis, A., Sullivan, H., 1985. Efficient method for determination of solar radiation absorbed by each room interior surface, and effects. In: International Solar Energy Society. pp. 430–434.

Athienitis, A., Sullivan, H., Hollands, K., 1986. Analytical model, sensitivity analysis, and algorithm for temperature swings in direct gain rooms.

Athienitis, A. K. ., 2007. Design of a solar home with BIPV-thermal system and ground source heat pump. In: 2nd Canadian Solar Buildings Conference. Calgary, pp. 1–9.

Athienitis, A. K., 1994. Building thermal analysis. MathSoft Inc, Cambridge.

Athienitis, A. K., Liu, C., Hawes, D., Banu, D., Feldman, D., 1997. Investigation of the thermal performance of a passive solar test-room with wall latent heat storage. Building and Environment 32 (5), 405–410.

Athienitis, A. K., Santamouris, M., 2013. Thermal analysis and design of passive solar buildings. Earthscan.

Bailey, B., 1984. Limiting the relative humidity in insulated greenhouses at night. In: III International Symposium on Energy in Protected Cultivation 148. ISHS, pp. 411–420.

Bailey, B., 1988. Control strategies to enhance the performance of greenhouse thermal screens. Journal of Agricultural Engineering Research 40, 187–198.

Bakker, J., Adams, S., Boulard, T., Montero, J., 2008. Innovative technologies for an efficient use of energy. Acta Horticulturae 801, 49–62.

Balcomb, D., 1983. Prediction of internal temperature swings in direct-gain passive solar buildings. In: Solar World Congress. Perth, Australia, p. 6.

Bastien, D., Athienitis, A., 2013. Evaluation of the potential of attached solariums and rooftop greenhouses in Quebec. In: 3rd Climate Change Technology Conference. Montreal, pp. 1–11.

Bastien, D., Athienitis, A. K., 2015. Methodology for selecting fenestration systems in heating dominated climates. Applied Energy 154, 1004–1019.

Bastien, D., Dermardiros, V., Athienitis, A. K., 2015. Development of a new control strategy for improving the operation of multiple shades in a solarium. Solar Energy 122, 277–292.

Berroug, F., Lakhal, E. K., El Omari, M., Faraji, M., El Qarnia, H., 2011. Thermal performance of a greenhouse with a phase change material north wall. Energy and Buildings 43 (11), 3027–3035.

Beshada, E., Zhang, Q., 2006. Optimizing the design of solar energy greenhouses. In: The Canadian Society for Bioengineering. Edmonton.

Beshada, E., Zhang, Q., Boris, R., 2006. Winter performance of a solar energy greenhouse in southern Manitoba. Canadian Biosystems Engineering 48, 5.1–5.8.

Böer, K. W., Duffie, J., 1982. Advances in solar energy: an annual review of research and development - volume 1. Springer US.

Bojic, M. L., Loveday, D. L., 1997. The influence on building thermal behavior of the insulation / masonry distribution in a three-layered construction. Energy and Buildings 26, 153–157.

Bony, J., Citherlet, S., 2007. Numerical model and experimental validation of heat storage with phase change materials. Energy and Buildings 39, 1065–1072.

Bot, G., van de Braak, N., Challa, H., Hemming, S., Rieswijk, T., Straten, G., Verlodt, I., 2005. The solar greenhouse: state of the art in energy saving and sustainable energy supply. Acta Horticulturae 691, 501–508.

Bot, G. P. A., 1983. Greenhouse climate: from physical processes to a dynamic model. Ph.D. thesis, Wageningen University.

Both, A., 2000. Some thoughts on supplemental lighting for greenhouse crop production. Center for Controlled Environment Agriculture.

Boulard, T., Baille, A., may 1995. Modelling of air exchange rate in a greenhouse equipped with continuous roof vents. Journal of Agricultural Engineering Research 61 (1), 37–48.

Boulard, T., Haxaire, R., Lamrani, M. A., Roy, J. C., Jaffrin, A., 1999. Characterization and modelling of the air fluxes induced by natural ventilation in a greenhouse. Journal of Agricultural Engineering Research 74, 135–144.

Bourdoukan, P., Wurtz, E., Spérandio, M., Joubert, P., 2006. Evaluation du potentiel solaire appliqué à un système desiccant cooling. In: IBPSA. Ile de la Réunion, pp. 1–7.

Braun, J. E., 1990. Reducing energy cost and peak electrical demand through optimal control of building thermal storage. ASHRAE Transactions 92 (2), 264–273.

Briassoulis, D., Waaijenberg, D., Gratraud, J., von Eslner, B., 1997. Mechanical properties of covering materials for greenhouses: part 1, general overview. Journal of Agricultural Engineering Research 67 (2), 81–96.

Buchholz, M., Jochum, P., Zaragoza, G., 2005. Concept for water, heat and food supply from a closed greenhouse - the watergy project. Acta Horticulturae 691, 509–516.

Bülow-Hübe, H., 2001. Energy-efficient window systems: effects on energy use and daylight in buildings. Phd thesis, Lund University.

Burns, P. J., Han, K., Winn, C., 1991. Dynamic effects of bang-bang control on the thermal performance of walls of various constructions. Solar Energy 46 (3), 129–138.

Butti, K., Perlin, J., 1980. Golden thread: 2500 years of solar architecture and technology. Cheshire Books.

Campen, J., 2009. Dehumidification of Greenhouses. Ph.D. thesis, Wageningen University.

Campen, J. B., Bot, G. P. A., de Zwart, H. F., 2003. Dehumidification of greenhouses at northern latitudes. Biosystems Engineering 86 (4), 487–493.

Candanedo, L. M., Athienitis, A., Park, K.-W., 2011. Convective heat transfer coefficients in a building-integrated photovoltaic/thermal system. Journal of Solar Energy Engineering 133 (2), 14.

Caplow, T., Nelkin, J., 2007. Building-integrated greenhouse systems for low energy cooling. In: 2nd PALENC Conference and 28th AIVC Conference on Building Low Energy Cooling and Advanced Ventilation Technologies in the 21st Century. Vol. 1. pp. 172–176.

Carbonari, A., Rossi, G., Romagnoni, P., 2001. Optimal orientation and automatic control of external shading devices in office buildings. In: 18th Conference on Passive and Low Energy Architecture. Florianópolis, pp. 1–12.

Carlini, M., Castellucci, S., 2010. Modelling and simulation for energy production parametric dependence in greenhouses. Mathematical Problems in Engineering, 1–28.

Carmody, J., Selkowitz, S., Heschong, L., 2000. Residential windows: a guide to new technologies and energy performance, 2nd Edition. W.W. Norton & Company, New York.

Cascone, G., Arcidiacono, C., D'Emilio, A., Mazzarella, R., 2005. Radiometric properties and field performances of different greenhouse plastic coverings. Acta Horticulturae 691, 693–700.

Chau, J., Sowlati, T., Sokhansanj, S., Preto, F., Melin, S., Bi, X., 2009. Economic sensitivity of wood biomass utilization for greenhouse heating application. Applied Energy 86 (5), 616–621.

CMHC, 1996. Energy Audits of High-Rise Residential Buildings. Canadian Mortgage and Housing Corporation.

CMHC, 1998. Tap the sun - Passive Solar Techniques and Home Designs. Canadian Mortgage and Housing Corporation.

Cohen, S., Fuchs, M., 1999. Measuring and predicting radiometric properties of reflective shade nets and thermal screens. Journal of Agricultural Engineering Research 73, 245–255.

Critten, D., 1985. A theoretical assessment of the transmissivity of conventional symmetric roofed multispan E-W greenhouses compared with vertical south roofed greenhouses under natural irradiance conditions. Journal of Agricultural Engineering Research 32 (2), 173–183.

Critten, D., 1991. Optimization of CO2 concentration in greenhouses: a modelling analysis for the lettuce crop. Journal of Agricultural Engineering Research (United Kingdom) 48, 261–271.

Critten, D. L., 1983. The evaluation of a computer model to calculate the daily light integral and transmissivity of a greenhouse. Journal of Agricultural Engineering Research 28, 545–563.

Critten, D. L., 1984. The effect of geometric transmission configuration on the light of greenhouses. Journal of Agricultural Engineering Research 29, 199–206.

Curcija, C., Yazdanian, M., Kohler, C., Hart, R., Mitchell, R., Vidanovic, S., 2013. Energy savings from window attachments. Lawrence Berkeley National Laboratory, DOE/EE-0969, 102.

Davies, M. G., 1994. The thermal response of an enclosure to periodic excitation: the CIBSE approach. Building and Environment 29 (2), 217–235.

de Halleux, D., 1989. Modèle dynamique des échanges énergétiques des serres: étude théorique et expérimen. Ph.D. thesis, Faculté des sciences agronomiques de Gembloux.

de Halleux, D., Gauthier, L., 1998. Energy consumption due to dehumidification of greenhouses under northern latitudes. Journal of Agricultural Engineering Research 69 (1), 35–42.

de Zwart, H. F., 2008. Overall energy analysis of (semi) closed greenhouses. Acta Horticulturae 801, 811–817.

Dieleman, J., Kempkes, F., 2006. Energy screens in tomato: determining the optimal opening strategy. Acta Horticulturae 718, 599–606.

Dieleman, J. A., Hemming, S., 2011. Energy saving: from engineering to crop management. Acta Horticulturae 893, 65–73.

Dion, L.-M., Lefsrud, M., Orsat, V., aug 2011. Review of CO2 recovery methods from the exhaust gas of biomass heating systems for safe enrichment in greenhouses. Biomass and Bioenergy 35 (8), 3422–3432.

Diver, S., 2001. Compost heated greenhouses. ATTRA.

Dorais, M., 2003. The use of supplemental lighting for vegetable crop production: light intensity, crop response, nutrition, crop management, cultural practices. Canadian Greenhouse Conference, 1–8.

Droege, P., Puri, V., Caplow, T., 2009. 100% Renewable energy autonomy in action - Chapter 12. Earthscan.

Duffie, J., Beckman, W., 2006. Solar engineering of thermal processes, 3rd edition. John Wiley & Sons.

Dumoulin, L., 2009. Les maisons d'ensemble Terre-Ciel : drôlement écolo ! La maison du 21ème siècle (hiver), 70–73.

EA Laboratory Committee, 2013. Evaluation of the uncertainty of measurement in calibration. EA-4/02.

ESR U, 2011. ESP-r 11.11. Energy Systems Research Unit, University of Strathclyde, Glasgow.

EU, 2009. All new buildings to be zero energy from 2019. Press release of European Union.

Evola, G., Marletta, L., 2013. A dynamic parameter to describe the thermal response of buildings to radiant heat gains. Energy and Buildings 65, 448–457.

Facchini, U., Marelli, G., Canzi, L., 1983. Solar greenhouses with low energy consumption. Colture Protette 12 (11), 31–35.

FAO, 1994. Integrated energy systems in China - Chapter 10. Food and agriculture organization of the United Nations, Rome.

Finlayson, E., Arasteh, D., Huizenga, C., Rubin, M., 1993. Window 4.0: Documentation of calculation procedures. Lawrence Berkeley National Laboratory, CA.

Fisher, D. E., Pedersen, C. O., 1997. Convective Heat Transfer in Building Energy and Thermal Load Calculations. ASHRAE Transactions 103.

Foderado, L., 2012. To find fields to farm in New York City, just look up. In: The New York Times. July 11 2012.

Gagliano, A., Patania, F., Nocera, F., Signorello, C., 2014. Assessment of the dynamic thermal performance of massive buildings. Energy & Buildings 72, 361–370.

Galasiu, A. D., Atif, M. R., MacDonald, R. a., 2004. Impact of window blinds on daylight-linked dimming and automatic on/off lighting controls. Solar Energy 76 (5), 523–544.

Garzoli, K., 1989. Energy efficient greeenhouses. In: III Energy Saving in Protected Cultivation. ISHS, pp. 53–62.

Gaston, K. J., Davies, T. W., Bennie, J., Hopkins, J., 2012. Reducing the ecological consequences of night-time light pollution: options and developments. Journal of Applied Ecology, pp 11.

Gauthier, C., Lacroix, M., Bernier, H., 1997. Numerical simulation of soil heat exchanger-storage systems for greenhouses. Solar energy 60 (6), 333–346.

Gebhart, B., 1959. A new method for calculating radiant exchanges. ASHRAE Transactions 65, 321–332.

Gelder, A. D., Heuvelink, E., Opdam, J. J. G., 2005. Tomato yield in a closed greenhouse and comparison with simulated yields in closed and conventional greenhouses. Acta Horticulturae 691, 549–552.

Giacomelli, G. A., Roberts, W. J., 1993. Greenhouse covering systems. HortTechnology 3 (l).

Gupta, M. J., Chandra, P., 2002. Effect of greenhouse design parameters on conservation of energy for greenhouse environmental control. Energy 27 (8), 777–797.

Gupta, R., 2004. Effect of latitude on weighted solar fraction of north partition wall for various shapes of solarium. Building and Environment 39 (5), 547–556.

Hadorn, J.-C., 2005. Thermal energy storage for solar and low-energy buildings. IEA Solar Heating and Cooling Task 32, 169.

Hage, M., 2011. Personal communication.

Halden, R. U., 2010. Plastics and health risks. Annual review of public health 31, 179–94.

Hammarberg, E., 2003. Antireflection treatment of low-emitting glazings for energy efficient windows with high visible transmittance. Thin Solid Films 442 (1-2), 222–226.

Hand, D., 1984. Crop responses to winter and summer CO2 enrichment. Acta horticulturae 162, 45–61.

Harnett, R., 1975. Study of glasshouse type and orientation. Acta Horticulturae 46, 209–216.

Hasnain, S. M., 1998. Review on sustainable thermal energy storage technologies, part I : heat storage materials and techniques. Energy Conversion and Management 39 (11).

He, K.-s., Chen, D.-y., Sun, L.-j., Liu, Z.-l., Huang, Z.-y., 2015. The effect of vent openings on the microclimate inside multi-span greenhouses during summer and winter seasons. Engineering Applications of Computational Fluid Mechanics 9 (1), 399–410.

Hed, G., Bellander, R., 2006. Mathematical modelling of PCM air heat exchanger. Energy and Buildings 38 (2), 82–89.

Hee, W., Alghoul, M., Bakhtyar, B., Elayeb, O., Shameri, M., Alrubaih, M., Sopian, K., 2015. The role of window glazing on daylighting and energy saving in buildings. Renewable and Sustainable Energy Reviews 42, 323–343.

Heier, J., Bales, C., Martin, V., 2015. Combining thermal energy storage with buildings - a review. Renewable and Sustainable Energy Reviews 42, 1305–1325.

Hellickson, M., Walker, J., 1983. Ventilation of agricultural structures.

Hemming, S., Kempkes, F., Braak, N. V. D., Dueck, T., Marissen, N., 2006a. Greenhouse cooling by NIR-reflection. Acta horticulturae (719), 97–105.

Hemming, S., Kempkes, F., Mohammadkhani, V., 2007. New glass coatings for high insulating greenhouses without light losses - energy saving, crop production and economic potentials. Acta horticulturae 893, 217–226.

Hemming, S., van der Braak, N., T, D., Jongschaap, R., Marissen, N., 2006b. Filtering natural light by the greenhouse covering using model simulations - more production and better plant quality by diffuse light. Acta horticulturae 719, 105–110.

Heuvelink, E., Bakker, M., 2008. Climate and yield in a closed greenhouse. Acta Horticulturae 801, 1083–1092.

Hong, J. H., Park, K. J., Sohn, B. K., 1997. Effect of composting heat from intermittent aerated static pile on the elevation of underground temperature. Applied Engineering in Agriculture 13 (5), 679–683.

Hottel, H., 1976. A simple model for estimating the transmittance of direct solar radiation through clear atmospheres. Solar Energy 18 (2), 129–134.

Howell, J., 1998. A catalog of radiation heat transfer configuration factors, 2nd Edition.
URL http://www.me.utexas.edu/~howell/index.html

Huang, Y., Niu, J.-l., Chung, T.-m., 2014. Comprehensive analysis on thermal and daylighting performance of glazing and shading designs on office building envelope in cooling-dominant climates. Applied Energy 134, 215–228.

Hutcheon, N., Handegord, G., 1995. Building science for a cold climate. Institute for Research in Construction, Canada.

Hviid, C. A., Nielsen, T. R., Svendsen, S., 2008. Simple tool to evaluate the impact of daylight on building energy consumption. Solar Energy 82 (9), 787–798.

Hydro-Québec, 2015. Simulation énergétique des bâtiments: Weather data.
URL https://www.simeb.ca:8443/index_en.jsp

Ibrahim, M., Achard, P., Wurtz, É., Biwole, P. H., 2013. Optimizing insulation-thermal mass wall layer distribution from maximum time lag and minimum decrement factor point of view. In: Conference of International Building Performance Simulation Association. Chambéry, pp. 870–876.

IEA, 2005. Implementing agreement on energy conservation through energy storage - Annex 17. No. International Energy Agency.

Ioslovich, I., 1995. Sub-optimal CO2 Enrichment of Greenhouses. Journal of Agricultural Engineering Research 60 (2), 117–136.

Ioslovich, I., Seginer, I., 1998. Approximate seasonal optimization of the greenhouse environment for a multi variable tomato model. American Society of Agricultural Engineers 41 (4), 1139–1149.

ISO 10292, 1994. Glass in building - Calculation of steady state U-value (thermal transmittance) of multiple glazing.

ISO 15099, 2003. Thermal performance of windows, doors and shading devices - Detailed calculations.

Jin, X., Zhang, X., Cao, Y., Wang, G., 2012. Thermal performance evaluation of the wall using heat flux time lag and decrement factor. Energy and Buildings 47, 369–374.

Jolliet, O., 1993. Modelling of water uptake, transpiration and humidity in greenhouses, and their effects on crops. In: Greenhouse crop model 328. ISHS.

Jolliet, O., 1994. HORTITRANS, a model for predicting and optimizing humidity and transpiration in greenhouses. Journal of agricultural engineering research 57 (1), 23–37.

Jolliet, O., Bailey, B., 1992. The effect of climate on tomato transpiration in greenhouses: measurements and models comparison. Agricultural and Forest Meteorology 58 (1-2), 43–62.

Kacira, M., Sase, S., Okushima, L., 2004. Effects of side vents and span numbers on wind-induced natural ventilation of a gothic multi-span greenhouse. JARQ 38 (4), 227–233.

Kacira, M., Short, T. H., Stowell, R., 1998. A CFD evaluation of naturally ventilated, multi-span sawtooth greenhouses. Transactions of the ASAE 41 (3), 833–836.

Karlsson, J., Roos, A., 2001. Annual energy window performance vs. glazing thermal emittance - The relevance of very low emittance values. Thin Solid Films 392 (2), 345–348.

Karlsson, J., Rubin, M., Roos, A., 2001. Evaluation of predictive models for the angle-dependent total solar energy transmittance of glazing materials. Solar Energy 71 (1), 23–31.

Kaygusuz, K., 1999. The viability of thermal energy storage. Energy Sources 21 (8), 745–755.

Kempkes, F., 2008. NIR-screen as an energy saving measure. FlowerTECH 11 (2), 20–21.

Kesik, T., Simpson, M., 2002. Thermal performance of attached sunspaces for canadian houses. In: esim. Montreal, p. 7.

Khalifa, A., Marshall, R., 1990. Validation of heat transfer coefficients on interior building surfaces using a real-sized indoor test cell. International Journal of Heat and Mass Transfer 33 (10), 2219–2236.

Kittas, C., Baille, A., Giaglaras, P., 1999. Influence of covering material and shading on the spectral distribution of light in greenhouses. Journal of Agricultural Engineering Research 73, 341–351.

Klein, S. A., al., E., 2010. TRNSYS 17: A transient system simulation program. Solar Energy Laboratory, University of Wisconsin, Madison, USA.
URL http://sel.me.wisc.edu/trnsys

Knight, T., 1808. A description of a forcing house for grapes; with observations on the best method of constructing houses for other fruits. Transactions of the Horticultural Society of London 1, 99.

Kontoleon, K. J., Bikas, D. K., 2007. The effect of south wall's outdoor absorption coefficient on time lag , decrement factor and temperature variations. Energy and Buildings 39, 1011–1018.

Koo, C., Park, S., Hong, T., Park, H. S., 2014. An estimation model for the heating and cooling demand of a residential building with a different envelope design using the finite element method. Applied Energy 115, 205–215.

Korner, O., 2003. Process-based humidity control regime for greenhouse crops. Computers and Electronics in Agriculture 39 (3), 173–192.

Körner, O., Challa, H., 2003. Design for an improved temperature integration concept in greenhouse cultivation. Computers and Electronics in Agriculture 39 (1), 39–59.

Kosny, J., Petrie, T., Gawin, D., Childs, P., Desjarlais, A., Christian, J., 2001. Thermal mass - energy savings potential in residential buildings. Buildings Technology Center, ORNL.

Kostov, O., 1995. Cucumber cultivation on some wastes during their aerobic composting. Bioresource Technology 53 (3), 237–242.

Kotey, N., Collins, M., Wright, J. L., Tiang, T., 2009a. A simplified method for calculating the effective solar optical properties of a venetian blind layer for building energy simulation. Journal of Solar Energy Engineering 131 (2), 9.

Kotey, N. A., Wright, J. L., Collins, M. R., 2009b. Determing off-normal solar optical properties of insect screens. ASHRAE Transactions 115 (1), 10.

Kotey, N. A., Wright, J. L., Collins, M. R., 2009c. Determining off-normal solar optical properties of drapery fabrics. ASHRAE Transactions 115 (2), 15.

Kotey, N. A., Wright, J. L., Collins, M. R., 2009d. Determining off-normal solar optical properties of roller blinds. ASHRAE Transactions 115 (1), 10.

Kozai, T., 1977a. Direct solar light transmission into multi-span greenhouses. Agricultural Meteorology 18, 339–349.

Kozai, T., 1977b. Direct solar light transmission into single-span greenhouses. Agricultural Meteorology 18, 327–338.

Kumar, S., Tiwari, G., Sinha, S., 1994. Optimization and comparative thermal evaluation of four different solarium-cum-solar houses. Energy Conversion and Management 35 (10), 835–842.

Kummert, M., André, P., Nicolas, J., 2001. Optimal heating control in a passive solar commercial building. Solar Energy 69, 103–116.

Kurata, K., Takakura, T., 1991. Underground storage of solar energy for greenhouses heating. I. Analysis of seasonal storage system by scale and numerical models. American Society of Agricultural Engineers 34 (2), 563–569.

Kurklu, A., 1998. Energy storage applications in greenhouses by means of phase change materials (PCMs) : a review. Renewable Energy 13 (1), 89–103.

Kuznik, F., Virgone, J., 2009. Experimental investigation of wallboard containing phase change material: Data for validation of numerical modeling. Energy and Buildings 41, 561–570.

Kuznik, F., Virgone, J., Noel, J., 2008. Optimization of a phase change material wallboard for building use. Applied Thermal Engineering 28, 1291–1298.

Lacis, A., Schmidt, G., Rind, D., Ruedy, R., 2010. Atmospheric CO2: principal control knob governing Earth's temperature. Science 330, 356–359.

Lamberg, P., Lehtiniemi, R., Henell, A.-M., 2004. Numerical and experimental investigation of melting and freezing processes in phase change material storage. International Journal of Thermal Sciences 43 (3), 277–287.

Laoudi, A., 2009. Thermal modeling of shading devices of windows. ASHRAE Transactions 115 (2), 1–20.

Laverty, C. C., 1983. Multi-purpose energy conserving sunspace. NTIS.

Lawand, T. A., Alward, R., Saulnier, B., Brunet, E., 1975. The development and testing of an environmentally designed greenhouse for colder regions. Solar Energy 17, 302–312.

Lawrence, W., 1963. Science and the glasshouse, 3rd Edition. Olivier and Boyd.

LBNL, 2005. RESFEN 5.0 User's Manual. Lawrence Berkeley National Laboratory.

LBNL, 2012. International glazing database - IGDB v 23.0.

LBNL, 2014. THERM 6.3 / WINDOW 6.3 NFRC Simulation Manual. Lawrence Berkeley National Laboratory, CA.

Lee, E. S., Selkowitz, S. E., 2006. The New York Times headquarters daylighting mockup: monitored performance of the daylighting control system. Energy and Buildings 38 (7), 914–929.

Lee, I., Lee, S., Kim, G., Sung, J., Sung, S., Yoon, Y., 2005. PIV verification of greenhouse ventilation air flows to evaluate CFD accuracy. Transactions of the ASAE 48 (5), 2277–2288.

Lee, I.-b., Short, T. H., Sase, S., Okushima, L., 2000. Evaluation of structural characteristics of naturally ventilated multi-span greenhouses using computer simulation. Japan Agricultural Research Quarterly 34 (4), 247–256.

Lee, J. W., Jung, H. J., Park, J. Y., Lee, J. B., Yoon, Y., 2013. Optimization of building window system in Asian regions by analyzing solar heat gain and daylighting elements. Renewable Energy 50, 522–531.

Lorenzo, P., Sanchez-Guerrero, M., Medrano, E., Garcia, M., Caparros, I., Coelho, G., Gimenez, M., 2004. Climate control in the summer season - a comparative study of external mobile shading and fog system. Acta horticulturae 659, 189–194.

Lorenzo, P., Sanchez-Guerrero, M., Medrano, E., Garcia, M., Caparros, I., Gimenez, M., 2003. External greenhouse mobile shading: effect on microclimate, water use efficiency and yield of a tomato crop grown under different salinity levels of the nutrient solution. Acta horticulturae 609.

Loudon, J., 1817. Remarks on the construction of hothouses: also, a review of the various methods of building them in foreign countries as well as in england. J Taylor, London.

Loutzenhiser, P., Manz, H., Maxwell, G., 2007. Empirical validations of shading/daylighting/load interactions in building energy simulation tools. IEA SHC Task 34/ECBCS Annex 43 Project C, 177.

Lund University, 2010. ParaSol 6.6.
URL http://www.ebd.lth.se/program/parasol/

Lychnos, G., Davies, P. A., 2008. A solar powered liquid-desiccant cooling system for greenhouses. Acta horticulturae 797, 95–102.

MacCracken, M. M., 2003. Thermal energy storage myths. ASHRAE Journal September, 36–43.

Mackenzie, G., 1815. On the form which the glass of a forcing-house ought to have, in order to receive the greatest possible quantity of rays from the sun. Transactions of the Horticultural Society of London 2, 171–177.

Malquori, L., Pellegrini, P., Tesi, R., 1993. Determination of solar energy transmitted by different greenhouse geometries. In: Colture Protette. pp. 81–85.

Marsh, L., Albright, L., Langhans, R., 1984. Strategies for controlling greenhouse thermal screens. Acta Horticulturae 148, 453–460.

Mccree, K. J., 1971. The measurment of photosynthetically active radiation. Solar Energy 15, 83–87.

Mesquita, L., Harrison, S., Thomey, D., 2006. Modeling of heat and mass transfer in parallel plate liquid-desiccant dehumidifiers. Solar Energy 80 (11), 1475–1482.

Meyer, J., 1981. Energy saving with mobile thermal screens. Acta Horticulturae 115, 677–684.

Meyer, J., 2011. Extremely insulated greenhouse concept with non fossil fuel heating system. Acta horticulturae 893 (201-208).

Mihalakakou, G., Ferrante, A., 2000. Energy conservation and potential of a sunspace: sensitivity analysis. Energy Conversion and Management 41 (12), 1247–1264.

Mistriotis, A., Bot, G., Picuno, P., Scarascia-Mugnozza, G., 1997. Analysis of the efficiency of greenhouse ventilation using computational fluid dynamics. Agricultural and Forest Meteorology 85 (3-4), 217–228.

Montero, J., 2006. Evaporative cooling in greenhouses: effect on microclimate, water use efficiency and plant response. Acta horticulturae 719, 373–383.

Mottard, J., Fissore, A., 2007. Thermal simulation of an attached sunspace and its experimental validation. Solar Energy 81 (3), 305–315.

NASA, 2015. Surface meteorology and solar energy data set.
URL http://eosweb.larc.nasa.gov/cgi-bin/sse/grid.cgi?uid=3030

Natural Resources Canada, 2002. Commercial and institutional building energy use survey. Office of Energy Efficiency.

Natural Resources Canada, 2007. Survey of household energy use. Office of Energy Efficiency.

Natural Resources Canada, 2008. Commercial & institutional consumption of energy survey. Office of Energy Efficiency.

Natural Resources Canada, 2015. Comprehensive energy use database.
URL http://oee.nrcan.gc.ca/corporate/statistics/neud/dpa/menus/trends/comprehensive_tables/list.cfm

Navarro, L., de Gracia, A., Niall, D., Castell, A., Browne, M., McCormack, S. J., Griffiths, P., Cabeza, L. F., 2015. Thermal energy storage in building integrated thermal systems: A review. Part 2. Integration as passive system. Renewable Energy.

NFRC 100-2004, 2004. Procedure for determining fenestration product U-factors. National Fenestration Rating Council, 81.

Nielsen, M. V., Svendsen, S., Jensen, L. B., 2011. Quantifying the potential of automated dynamic solar shading in office buildings through integrated simulations of energy and daylight. Solar Energy 85 (5), 757–768.

Nielsen, T., Duer, K., Svendsen, S., 2001. Energy performance of glazings and windows. Solar Energy 69 (1), 137–143.

Nielsen, T. R., 2005. Simple tool to evaluate energy demand and indoor environment in the early stages of building design. Solar Energy 78 (1), 73–83.

Nijskens, J., Deltour, J., Coutisse, S., Nisen, A., 1984. Heat transfer through covering materials of greenhouses. Agricultural and forest meteorology 33, 193–214.

Nijskens, J., Deltour, J., Coutisse, S., Nisen, A., 1985. Radiation transfer through covering materials, solar and thermal screens of greenhouses. Agricultural and forest meteorology 35, 229–242.

O'brien, W., 2011. Development of a solar house design methodology and its implementation into a design tool. Phd, Concordia University.

Ochoa, C. E., Aries, M. B. C., van Loenen, E. J., Hensen, J. L. M., 2012. Considerations on design optimization criteria for windows providing low energy consumption and high visual comfort. Applied Energy 95, 238–245.

Opdam, J. J. G., Schoonderbeek, G. G., Heller, E. M. B., 2005. Closed greenhouse : a starting point for sustainable entrepreneurship in horticulture. Acta Horticulturae 691, 517–524.

Orsi, A., 2009. An exploration of the impact of fixed shading device geometry on building energy performance. Master, Michigan State University.

Ould Khaoua, S., Bournet, P., Migeon, C., Boulard, T., Chassériaux, G., 2006. Analysis of greenhouse ventilation efficiency based on computational fluid dynamics. Biosystems Engineering 95 (1), 83–98.

Ozel, M., 2014. Effect of insulation location on dynamic heat-transfer characteristics of building external walls and optimization of insulation thickness. Energy and Buildings 72, 288–295.

Ozel, M. Ã., Pihtili, K., 2007. Optimum location and distribution of insulation layers on building walls with various orientations. Building and Environment 42, 3051–3059.

Öztürk, H. H., 2005. Experimental evaluation of energy and exergy efficiency of a seasonal latent heat storage system for greenhouse heating. Energy Conversion and Management 46 (9-10), 1523–1542.

Papadakis, G., Briassoulis, D., Scarascia Mugnozza, G., Vox, G., Feuilloley, P., Stoffers, J., 2000. Radiometric and thermal properties of, and thesting methods for, greenhouse covering materials. Journal of Agricultural Engineering Research 77 (1), 7–38.

Parameshwaran, R., Kalaiselvam, S., Harikrishnan, S., Elayaperumal, A., 2012. Sustainable thermal energy storage technologies for buildings: A review. Renewable and Sustainable Energy Reviews 16 (5), 2394–2433.

Parekh, A., Platts, R., Scanada Consultants, 1990. Passive solar potential in Canada: 1990-2010. Efficiency and Alternative Energy Technology Branch, Energy, Mines and Resources Canada.

Pearson, L. J., Pearson, L., Pearson, C. J., 2010. Sustainable urban agriculture: stocktake and opportunities. International Journal of Agricultural Sustainability 8 (1-2), 7–19.

Pelland, S., Poissant, Y., 2006. An evaluation of the potential of building integrated photovoltaics in Canada. 31st Annual Conference of the Solar Energy Society of Canada, 1–8.

Perdigones, A., Garcia, J., Romero, A., Rodriguez, A., Luna, L., Raposo, C., de la Plaza, S., 2008. Cooling strategies for greenhouses in summer: control of fogging by pulse width modulation. Biosystems Engineering 99 (4), 573–586.

Perez, R., Ineichen, P., Seals, R., Michalsky, J., Stewart, R., 1990. Modeling daylight availability and irradiance components from direct and global irradiance. Solar Energy 44 (5), 271–289.

Pfafferott, J., Herkel, S., Kalz, D., Zeuschner, A., 2007. Comparison of low energy office buildings in summer using different thermal comfort criteria. Energy and Buildings 39 (7), 750–757.

Porteous, C., Ho, H., 1997. Do sunspaces work in Scotland? Lessons learnt from a CEC solar energy demonstration project in Glasgow. International Journal of Ambient Energy 18 (1), 23–35.

Proskiw, G., 2010. Identifying affordable net zero energy housing solutions. CanmetENERGY, Natural Resources Canada.

Protégez-vous, 2012. Ce qu'il faut savoir. Mars.
URL http://www.protegez-vous.ca/maison-et-environnement/solariums-2012/ce-quil-faut-savoir.html

Qian, T., Dieleman, J. A., Elings, A., 2011. Comparison of climate and production in closed, semi-closed and open greenhouses. Acta Horticulturae 893, 807–814.

Rempel, A. R., Gates, K., Rempel, A. W., Shaw, B., 2013. Oregon sunspace redesign / build : new priorities for thermal mass. In: Proceedings of the American Solar Energy Society National Conference. Baltimore, pp. 1–8.

Rempel, A. R., Rempel, A. W., 2013. Rocks, clays, water, and salts: highly durable, infinitely rechargeable, eminently controllable thermal batteries for buildings. Geosciences (3), 63–101.

Rifkin, G., 2011. Cash crops under glass and up on the roof. In: The New York Times.

Roberts, W., Mears, D., Simpkins, J., Cipolletti, J., 1981. Movable thermal insulation for greenhouses. In: Proceedings of the National Agricultural Plastics Congress (USA).

Rogalsky, C., 2011. Application of a network solution to complex fenestration systems. Master thesis, University of Waterloo.

Rosa, R., Silva, A. M., Miguel, A., 1989. Solar irradiation inside a single span greenhouse. Journal of Agricultural Engineering Research 43, 221–229.

Rosencrantz, T., Bulowhube, H., Karlsson, B., Roos, A., 2005. Increased solar energy and daylight utilisation using anti-reflective coatings in energy-efficient windows. Solar Energy Materials and Solar Cells 89 (2-3), 249–260.

Rousse, D., Martin, D., Thériault, R., Léveillée, F., Boily, R., 2000. Heat recovery in greenhouses: a practical solution. Applied Thermal Engineering 20, 687–706.

Salazar, R., Rojano, A., 2008. A neural network model to predict temperature and relative humidity in a greenhouse. Acta horticulturae 801, 539–545.

Sánchez, J., Rodríguez, F., Guzmán, J., Ruiz Arahal, M., Fernández, M., 2009. Modelling of tomato crop transpiration dynamics for designing new irrigation controllers. Acta horticulturae 893, 729–737.

Santamouris, M., Argiriou, A., Vallindras, M., 1994a. Design and operation of a low energy consumption passive solar agricultural greenhouse. Solar energy 52 (5), 371–378.

Santamouris, M., Balaras, C. A., Dascalaki, E., Vallindras, M., 1994b. Passive solar agricultural greenhouses: A worldwide classification and evaluation of technologies and systems used for heating purposes. Solar Energy 53 (5), 411–426.

Santamouris, M. I., 1993. Active solar agricultural greenhouses. The state of the art. International Journal of Solar Energy 14 (1), 19–32.

Schoenau, G., Lumbis, A., Besant, R., 1990. Thermal performance of four sunspaces in a cold climate. Energy and Buildings 14, 273–286.

Schumman, J., Lee, E. S., Rubinstein, F. M., Selkowitz, S. E., Robinson, A., 2013. Tips for daylighting with windows: The integrated approach, 2nd Edition. Lawrence Berkeley National Laboratory.

Seginer, I., 1997. Alternative design formulae for the ventilation rate of greenhouses. Journal of Agricultural Engineering Research 68 (4), 355–365.

Seginer, I., Albright, L., 1980. Rational operation of greenhouse thermal curtains. Transactions of the ASABE 23 (5), 1240–1245.

Seginer, I., Shina, G., Albright, L., Marsh, L., 1991. Optimal temperature setpoints for greenhouse lettuce. Journal of Agricultural Engineering Research 49, 209–226.

Selkowitz, S. E., Bazjanac, V., 1979. Thermal performance of managed window systems. In: ASHRAE / DOE Conference on Thermal Performance of the Exterior Envelopes of Buildings. Orlando, p. 19.

Sethi, V., 2009. On the selection of shape and orientation of a greenhouse: Thermal modeling and experimental validation. Solar Energy 83 (1), 21–38.

Sethi, V. P., Sharma, S. K., 2008. Survey and evaluation of heating technologies for worldwide agricultural greenhouse applications. Solar Energy 82, 832–859.

Shen, E., Hu, J., Patel, M., 2014. Energy and visual comfort analysis of lighting and daylight control strategies. Building and Environment 78, 155–170.

Siegel, R., Howell, J. R., 1981. Thermal radiation heat transfer, 2nd Edition. Hemisphere Publishing Corporation.

Singh, R., Tiwari, G., 2000. Thermal heating of controlled environment greenhouse: a transient analysis. Energy Conversion and Management 41 (5), 505–522.

Soriano, T., Montero, J., Sánchez-Guerrero, M., Medrano, E., Antón, A., Hernández, J., Morales, M., Castilla, N., 2004. A study of direct solar radiation transmission in asymmetrical multi-span greenhouses using scale models and simulation models. Biosystems Engineering 88 (2), 243–253.

Stanghellini, C., Van Meurs, T., 1992. Environmental control of greenhouse crop transpiration. Journal of Agricultural Engineering Research 51, 297–311.

Statistics Canada, 2010. Greenhouse, sod and nursery industries. 22-202-X.

Sun, C., Shu, S., Ding, G., Zhang, X., Hu, X., 2013. Investigation of time lags and decrement factors for different building outside temperatures. Energy & Buildings 61, 1–7.

Tabares-velasco, P. C., Christensen, C., Bianchi, M., 2012. Verification and validation of EnergyPlus phase change material model for opaque wall assemblies. Building and Environment 54, 186–196.

Takebayashi, H., Moriyama, M., aug 2007. Surface heat budget on green roof and high reflection roof for mitigation of urban heat island. Building and Environment 42 (8), 2971–2979.

Tamulaitis, G., Duchovskis, P., Bliznikas, Z., Breive, K., Ulinskaite, R., Brazaityte, A., Novičkovas, A., Žukauskas, A., 2005. High-power light-emitting diode based facility for plant cultivation. Journal of Physics D: Applied Physics 38 (17), 3182–3187.

Tantau, H.-J., Meyer, J., Schmidt, U., Bessler, B., 2011. Low energy greenhouse - a system approach. Acta horticulturae (893), 75–84.

Taylor, W., 1995. Living in glasshouses: vegetality and the curvilinear forcing houses of the early nineteenth century. Journal of Garden History 15 (4), 206–220.

The Produce News, 2011. Big Box Farms takes locally grown to a new level. September 23 2011.

Thomas, R. B., 1978. The use of specularly-reflecting greenhouses back walls in greenhouses. Journal of Agricultural Engineering Research 23, 85–97.

Tiwari, G., Gupta, A., 2002. A comparison in performance of greenhouses with various shapes: a parametric study. International Journal of Ambient Energy 23 (3), 136–148.

Tiwari, G., Yadav, Y., Lawrence, S., 1988. Performance of a solarium: an analytical study. Building and Environment 23 (2), 145–151.

Tong, G., Christopher, D. M., Li, B., 2009. Numerical modelling of temperature variations in a Chinese solar greenhouse. Computers and Electronics in Agriculture 68 (1), 129–139.

Tong, G., Christopher, D. M., Li, T., Wang, T., 2013. Passive solar energy utilization: A review of cross-section building parameter selection for Chinese solar greenhouses. Renewable and Sustainable Energy Reviews 26, 540–548.

Trigui, M., 2000. Strategy for the optimal climate control of greenhouse tomatoes. Ph.D. thesis, McGill.

Tzempelikos, A., 2005. A methodology for integrated daylighting and tharmal analysis of buildings. Phd, Concordia University.

Tzempelikos, A., 2008. A review of optical properties of shading devices. Advances in Building Energy Research 2 (1), 211–239.

Tzempelikos, A., Athienitis, A. K., 2007. The impact of shading design and control on building cooling and lighting demand. Solar Energy 81 (3), 369–382.

Tzempelikos, A., Athienitis, A. K., Karava, P., 2007. Simulation of façade and envelope design options for a new institutional building. Solar Energy 81 (9), 1088–1103.

Tzempelikos, A., Shen, H., 2013. Comparative control strategies for roller shades with respect to daylighting and energy performance. Building and Environment 67, 179–192.

Ulgen, K., 2002. Experimental and theoretical investigation of effects of wall's thermophysical properties on time lag and decrement factor. Energy and Buildings 34, 273–278.

U.S. Department of Energy, 2012. EnergyPlus 7.2.

U.S. Department of Energy, 2013. EnergyPlus Engineering Reference.

U.S. Department of Energy, 2015. EnergyPlus Energy Simulation Software - Weather Data, 2015–03–10. URL http://apps1.eere.energy.gov/buildings/energyplus/weatherdata_about.cfm

Vadiee, A., Martin, V., 2012. Energy management in horticultural applications through the closed greenhouse concept, state of the art. Renewable and Sustainable Energy Reviews 16 (7), 5087–5100.

Vadiee, A., Martin, V., 2013a. Energy analysis and thermoeconomic assessment of the closed greenhouse - The largest commercial solar building. Applied Energy 102, 1256–1266.

Vadiee, A., Martin, V., 2013b. Thermal energy storage strategies for effective closed greenhouse design. Applied Energy 109, 337–343.

van Moeseke, G., Bruyère, I., De Herde, A., 2007. Impact of control rules on the efficiency of shading devices and free cooling for office buildings. Building and Environment 42 (2), 784–793.

Van Ooster, A., Van Henten, E., Janssen, E., Bongaerts, E., 2008. Use of supplementary lighting top screens and effects on greenhouse climate and return on investment. Acta horticulturae 801, 645–652.

van Vennhuizen, R., 2006. Cities farming for the future. RUAF Foundation, IDRC and IIRR.

Vanthoor, B. H., Stigter, J. D., van Henten, E. J., Stanghellini, C., de Visser, P. H., Hemming, S., 2012. A methodology for model-based greenhouse design: Part 5, greenhouse design optimisation for southern-Spanish and Dutch conditions. Biosystems Engineering 111 (4), 350–368.

Vogel, G., mar 2008. Upending the traditional farm. Science 319, 752–753.

Wall, M., 1995. A design tool for glazed spaces. Part I: description. In: ASHRAE Transactions 101. pp. 1261–1271.

Wall, M., 1997. Distribution of solar radiation in glazed spaces and adjacent buildings. A comparison of simulation programs. Energy and Buildings 26 (2), 129–135.

Wallin, J., Bastien, D., Claesson, J., 2012. The Influence of energy conservation on the performance of solar thermal systems - a cold country case study. Energy Procedia 30, 1069–1078.

Walton, G., 1979. The application of homogeneous coordinates to shadowing calculations. In: ASHRAE Transactions 79. pp. 174–179.

Wang, J., Li, S., Guo, S., Ma, C., Wang, J., Jin, S., 2014. Simulation and optimization of solar greenhouses in Northern Jiangsu Province of China. Energy and Buildings 78, 143–152.

Wang, S., Boulard, T., jan 2000. Predicting the microclimate in a naturally ventilated plastic house in a mediterranean climate. Journal of Agricultural Engineering Research 75, 27–38.

Warrington, I. J., Norton, R. A., 1991. An evaluation of plant growth and development under various daily quantum integrals. Journal of American Society for Horticultural Science 116 (3), 544–551.

Wienold, J., 2007. Dynamic simulation of blind control strategies for visual comfort and energy balance analysis. In: Building Simulation. pp. 1197–1204.

Wilkinson, T., 1809. Observations on the form of hot houses. Transactions of the Horticultural Society of London 1, 161–164.

WinDat, 2004. WIS Version 3.0.1 Help file - converted to pdf document. Window Energy Data Network.

Wong, N., Yu, C., 2005. Study of green areas and urban heat island in a tropical city. Habitat International 29 (3), 547–558.

Wright, J. L., 1996. A correlation to quantify convective heat transfer between vertical window glazings. ASHRAE Transactions 102 (1), 940–946.

Wright, J. L., Collins, M. R., Kotey, N. A., Barnaby, C. S., 2009. Improving cooling load calculations for fenestration with shading devices. ASHRAE 1311-RP 30329 (404), 95.

Xu, J., Li, Y., Wang, R. Z., Liu, W., 2014. Performance investigation of a solar heating system with underground seasonal energy storage for greenhouse application. Energy 67, 63–73.

Yao, J., 2014. An investigation into the impact of movable solar shades on energy, indoor thermal and visual comfort improvements. Building and Environment 71, 24–32.

Yu, Z. J., Huang, G., Haghighat, F., Li, H., Zhang, G., 2015. Control strategies for integration of thermal energy storage into buildings: state-of-the-art review. Energy and Buildings.

Yutong, L., Hongxing, Y., 2008. Investigation on solar desiccant dehumidification process for energy conservation of central air-conditioning systems. Applied Thermal Engineering 28 (10), 1118–1126.

Zemanchik, N., Choinière, Y., Suchorski-Trembley, A., Munroe, J., Barrington, S., 1991. Optimum building orientation for natural ventilation. In: Agricultural Institute of Canada Annual Conference. Canadian Society of Agricultural Engineering, Fredericton.

Zhang, L., Xu, P., Mao, J., Tang, X., Li, Z., Shi, J., 2015. A low cost seasonal solar soil heat storage system for greenhouse heating: design and pilot study. Applied Energy 156, 213–222.

Zhang, Y., 1997. Predicting the microclimate inside a greenhouse: an application of a one-dimensional numerical model in an unheated greenhouse. Agricultural and Forest Meteorology 86 (3-4), 291–297.

Zhang, Y., Chen, Q., Zhang, Y., Wang, X., 2013. Exploring buildings' secrets: the ideal thermophysical properties of a building's wall for energy conservation. International Journal of Heat and Mass Transfer 65, 265–273.

Appendix A

Estimating solar transmittance and absorptance

Tables A.1-A.3 were created by selecting glazings with SHGC $>$ 0.5 from the WINDOW database (LBNL, 2014) and assembled with cavity widths of 12.7 mm. 37 glasses have been selected for Table A.1. Correlations from Table A.2 and A.3 have been derived from 16 glasses assembled in 48 and 80 configurations.

Table A.1: Estimated solar transmittance and absorptance - single glazing, $h_o = 20$ W/(m^{2}K) - glazings with U$<$4 W/(m^{2}K) have low-e on surface #2

U	SHGC	τ_s	α
U$>$ 5.7	SHGC$>$0.90	SHGC-0.0035	$\frac{h_o}{U}(SHGC - \tau_s)$
	0.80$<$SHGC$<$0.90	SHGC-0.0205	$\frac{h_o}{U}(SHGC - \tau_s)$
	0.645$<$SHGC$<$0.80	SHGC-0.1000	$\frac{h_o}{U}(SHGC - \tau_s)$
	0.5$<$SHGC$<$0.645	SHGC-0.1315	$\frac{h_o}{U}(SHGC - \tau_s)$
U$<$4	SHGC$>$0.635	SHGC-0.0239	$\frac{h_o}{U}(SHGC - \tau_s)$
	0.5$<$SHGC$<$0.635	SHGC-0.0500	$\frac{h_o}{U}(SHGC - \tau_s)$

Table A.2: Estimated solar transmittance and absorptances - double glazing, $h_i = 8$ W/(m^{2}K), $h_o = 25$ W/(m^{2}K) - when present, low-e is on surface #3

U	SHGC	τ_s	α_1	α_2
Air				
U> 2.7	SHGC>0.82	SHGC-0.0097	$\frac{SHGC-\tau_s+0.0027(h_i-U)/h_i}{U/h_o+(h_i-U)/h_i}$	-0.0027+α_o
	0.80<SHGC<0.82	SHGC-0.0285	$\frac{SHGC-\tau_s+0.0090(h_i-U)/h_i}{U/h_o+(h_i-U)/h_i}$	-0.0090+α_o
	SHGC<0.80	SHGC-0.0467	$\frac{SHGC-\tau_s+0.0167(h_i-U)/h_i}{U/h_o+(h_i-U)/h_i}$	-0.0167+α_o
1.79<U<2.7	all SHGC	SHGC-0.1173	$\frac{SHGC-\tau_s-0.0881(h_i-U)/h_i}{U/h_o+(h_i-U)/h_i}$	0.0881+α_o
1.60<U<1.79	all SHGC	SHGC-0.0813	$\frac{SHGC-\tau_s-0.0427(h_i-U)/h_i}{U/h_o+(h_i-U)/h_i}$	0.0427+α_o
Argon				
U>2.5	SHGC>0.82	SHGC-0.010	$\frac{SHGC-\tau_s+0.0025(h_i-U)/h_i}{U/h_o+(h_i-U)/h_i}$	-0.0025+α_o
	0.75<SHGC<0.82	SHGC-0.0396	$\frac{SHGC-\tau_s+0.0136(h_i-U)/h_i}{U/h_o+(h_i-U)/h_i}$	-0.0136+α_o
1.50<U<1.80	all SHGC	SHGC-0.1131	$\frac{SHGC-\tau_s-0.0878(h_i-U)/h_i}{U/h_o+(h_i-U)/h_i}$	0.0878+α_o
1.36<U<1.50	all SHGC	SHGC-0.0859	$\frac{SHGC-\tau_s-0.0488(h_i-U)/h_i}{U/h_o+(h_i-U)/h_i}$	0.0488+α_o

Table A.3: Estimated solar transmittance and absorptance - triple glazing, $h_i = 7$ W/(m^{2}K), $h_o = 26$ W/(m^{2}K) - when present, low-e is on surface #5 or on surfaces #3 and #5

U	SHGC	τ_s	α_1	α_2	α_3
Air					
U> 1.7	SHGC>0.75	SHGC-0.0157	0.0160	0.0021+α_3	$\frac{0.0157-\alpha_1 U/h_o-0.0021U(h_o^{-1}+0.1645)}{U(h_o^{-1}+0.1645)+(h_i-U)/h_i}$
	SHGC<0.75	SHGC-0.0586	0.0646	0.0104+α_3	$\frac{0.0586-\alpha_1 U/h_o-0.0104U(h_o^{-1}+0.1645)}{U(h_o^{-1}+0.1645)+(h_i-U)/h_i}$
1.15<U<1.4	all SHGC	SHGC-0.1016	0.0500	-0.0628+α_3	$\frac{0.1016-\alpha_1 U/h_o+0.0628U(h_o^{-1}+0.1645)}{U(h_o^{-1}+0.1645)+(h_i-U)/h_i}$
1<U<1.15	all SHGC	SHGC-0.1433	0.0515	0.0585+α_3	$\frac{0.1433-\alpha_1 U/h_o-0.0585U(h_o^{-1}+0.1645)}{U(h_o^{-1}+0.1645)+(h_i-U)/h_i}$
U<1	all SHGC	SHGC-0.1144	0.0515	0.0585+α_3	$\frac{0.1144-\alpha_1 U/h_o-0.0585U(h_o^{-1}+0.3154)}{U(h_o^{-1}+0.3154)+(h_i-U)/h_i}$
Argon					
U> 1.6	SHGC>0.75	SHGC-0.0160	0.0160	0.0021+α_3	$\frac{0.0160-\alpha_1 U/h_o-0.0021U(h_o^{-1}+0.1878)}{U(h_o^{-1}+0.1878)+(h_i-U)/h_i}$
	SHGC<0.75	SHGC-0.0588	0.0646	0.0104+α_3	$\frac{0.0588-\alpha_1 U/h_o-0.0104U(h_o^{-1}+0.1878)}{U(h_o^{-1}+0.1878)+(h_i-U)/h_i}$
0.96<U<1.3	all SHGC	SHGC-0.1029	0.0500	-0.0628+α_3	$\frac{0.1029-\alpha_1 U/h_o+0.0628U(h_o^{-1}+0.1878)}{U(h_o^{-1}+0.1878)+(h_i-U)/h_i}$
0.78<U<0.96	all SHGC	SHGC-0.1460	0.0515	0.0585+α_3	$\frac{0.1460-\alpha_1 U/h_o-0.0585U(h_o^{-1}+0.1875)}{U(h_o^{-1}+0.1875)+(h_i-U)/h_i}$
U<0.78	all SHGC	SHGC-0.1168	0.0515	0.0585+α_3	$\frac{0.1168-\alpha_1 U/h_o-0.0585U(h_o^{-1}+0.4185)}{U(h_o^{-1}+0.4185)+(h_i-U)/h_i}$

Table A.4: Average and maximum error.

		τ_s	α_1	α_2	α_3
Single glass	Average error	0.007	0.027	-	-
	Maximum error	0.034	0.080	-	-
Double glass	Average error	0.012	0.020	0.014	-
	Maximum error	0.070	0.046	0.051	-
Triple glass	Average error	0.012	0.023	0.018	0.013
	Maximum error	0.048	0.046	0.041	0.066

Appendix B

Measurement uncertainty for heat stored/released

The uncertainty associated with the calculation of the heat stored and released has been calculated following the recommendations presented in EA Laboratory Committee (2013).

The heat stored or released has been calculated with

$$Q = mc_p(T_{t+1} - T_t) \tag{B.1}$$

where T in equation B.1 is the bulk temperature of the PCM and the index i refers to the time interval at which data was recorded (3mn).

The standard uncertainty associated to the mass is equal to 5g. The temperature of the PCM surface was measured with an accuracy of 0.5°C. Therefore, the standard uncertainty associated with the calculation of the bulk PCM temperature is $\sqrt{0.5}$=0.71°C.

The uncertainty pertaining to the specific heat was estimated by assuming a rectangular probability distribution between the values provided for melting and freezing. Consequently, this uncertainty depends on the temperature and is calculated individually for each layer. For the tested conditions, the minimum and maximum standard uncertainties associated to the specific heat are equal to 0.66 and 2337 J/(kg°C) with an average of 908 J/(kg°C).

The combined standard uncertainty associated to the heat stored and released by one layer is calculated as

$$\Delta Q = |Q| \sqrt{2\Big(\frac{\Delta m}{m}\Big)^2 + 2\Big(\frac{\Delta c_p}{c_p}\Big)^2 + \Big(\frac{\Delta T_{t+1}}{T_{t+1}}\Big)^2 + \Big(\frac{\Delta T_t}{T_t}\Big)^2} \tag{B.2}$$

The relative standard uncertainty is comprised between 0.03 and 0.79 with an average of 0.16.

Appendix C

Solar radiation modelling and view factors calculation

C.1 Solar radiation fundamentals

The declination angle δ is calculated from the approximate equation of Cooper :

$$\delta = 23.45 \sin\left(360\left(\frac{284 + n_{\text{day}}}{365}\right)\right) \tag{C.1}$$

where n_{day} is the the day of the year. The extraterrestrial radiation flux on a given day is calculated with

$$I_{on} = I_{sc}\left(1 + 0.033\cos\left(\frac{360 n_{\text{day}}}{365}\right)\right); \tag{C.2}$$

where I_{sc} is the solar constant and equal to 1367 W/m^2. The angular displacement of the sun, known as hour angle, is given by

$$H = 15(t' - 12) \tag{C.3}$$

where t' is the time in hour. The solar altitude is calculated with

$$\alpha = \text{asin}\big(\cos(\lambda)\cos(\delta)\cos(H) + \sin(\lambda)\sin(\delta)\big) \tag{C.4}$$

where λ is the latitude. The solar azimuth angle, which represents the angular displacement from south of the beam radiation, can be calculated with

$$\phi = \text{acos}\left(\frac{\sin(\alpha)\sin(\lambda) - \sin(\delta)}{\cos(\alpha)\cos(\lambda)}\right) \tag{C.5}$$

By convention, angles east of south are negatives and west of south are positive. The zenith angle Z is simply the complement angle of the solar altitude angle:

$$Z = \frac{\pi}{2} - \alpha \tag{C.6}$$

C.2 Perez model

The diffuse solar radiation in the sky is not uniformly distributed. It can be splitted into three terms: an **isotropic** term, uniform throughout the sky dome, a **circumsolar diffuse** term, which is concentrated in the region of the sky surrounding the sun, and an **horizon brightening** term, which is concentrated near the horizon. The Perez model (1990) presents a detailed analysis which takes into account these three components. Following this method, the sky diffuse solar radiation incident on a surface can be calculated with

$$I_{ds} = \mathrm{DHR}\Big(0.5\big(1-\mathrm{F1IR}\big)\big(1+\cos(\beta)\big) + \mathrm{F1IR}a/b + \mathrm{F2IR}\sin(\beta)\Big) \tag{C.7}$$

where F1IR, F2IR, a and b are given by

$$\mathrm{F1IR} = \mathrm{F11IR}(\epsilon_{\mathrm{sky}}) + \mathrm{F12IR}(\epsilon_{\mathrm{sky}})\Delta_B + \mathrm{F13IR}(\epsilon_{\mathrm{sky}})Z \tag{C.8a}$$

$$\mathrm{F2IR} = \mathrm{F21IR}(\epsilon_{\mathrm{sky}}) + \mathrm{F22IR}(\epsilon_{\mathrm{sky}})\Delta_B + \mathrm{F23IR}(\epsilon_{\mathrm{sky}})Z \tag{C.8b}$$

$$a = \max\big(0, \cos(\theta)\big) \tag{C.8c}$$

$$b = \max\big(0.087, \cos(Z)\big) \tag{C.8d}$$

The clearness of the sky is characterized by ϵ_{sky} and can be calculated with

$$\epsilon_{\mathrm{sky}} = \frac{(\mathrm{DHR}+\mathrm{DNR})/(\mathrm{DHR}+kZ^3)}{1+kZ^3} \tag{C.9}$$

The optical air mass m_o can be calculated from

$$m_o = \big(\cos(Z) + 0.50572(96.07995 - Z)^{-1.6364}\big)^{-1} \tag{C.10}$$

where Z is in degree. The sky brightness is represented by Δ_B and is given by

$$\Delta_B = \mathrm{DHR}\, m_o / I_{on} \tag{C.11}$$

A table with the irradiance coefficients F11IR, F12IR, F13IR, F21IR, F22IR and F23IR as a function of clearness index can be found in Perez et al. (1990).

C.3 View factors

F_{ij} represents the fraction of the radiation emitted by surface i reaching surface j. Because of energy conservation constraints,

$$\sum_{j=1}^{N} F_{ij} = 1 \tag{C.12}$$

where N is the number of surfaces in an enclosure. From the reciprocity principle, it follows that

$$A_1 F_{12} = A_2 F_{21} \tag{C.13}$$

Howell (1998) published an exhaustive online catalog of configuration factors where the equations presented below can be found; they are given here for the sake of completeness. The view factor between two rectangles having a common edge perpendicular to each other is given by

$$F_{12} = \frac{1}{W\pi}\Bigg\{ W\tan^{-1}\left(\frac{1}{W}\right) + H\tan^{-1}\left(\frac{1}{H}\right) - \sqrt{H^2+W^2}\tan^{-1}\sqrt{\frac{1}{H^2+W^2}} \\ + \frac{1}{4}\ln\left[\left(\frac{(1+W^2)(1+H^2)}{1+W^2+H^2}\right)\left(\frac{W^2(1+W^2+H^2)}{(1+W^2)(W^2+H^2)}\right)^{W^2}\left(\frac{H^2(1+W^2+H^2)}{(1+H^2)(W^2+H^2)}\right)^{H^2}\right]\Bigg\} \tag{C.14}$$

with $H = h/l$ and $W = w/l$. The dimensions h, w and l as well as the other parameters used in the equations in this section are illustrated in Figure C.1. For two identical, parallel and directly opposed rectangles, the view factor is calculated with

$$F_{12} = \frac{2}{\pi XY}\Bigg\{ \ln\left(\frac{(1+X^2)(1+Y^2)}{1+X^2+Y^2}\right)^{1/2} + X\sqrt{1+Y^2}\tan^{-1}\left(\frac{X}{\sqrt{1+Y^2}}\right) \\ + Y\sqrt{1+X^2}\tan^{-1}\left(\frac{Y}{\sqrt{1+X^2}}\right) - X\tan^{-1}(X) - Y\tan^{-1}(Y)\Bigg\} \tag{C.15}$$

where $X = w/z$ and $Y = l/z$. The configuration factor for two rectangles having a common edge separated by an angle α is calculated with

$$
\begin{aligned}
F_{12} = {} & \frac{-\sin(2\alpha)}{4\pi B}\left[AB\sin(\alpha) + \left(\frac{\pi}{2}-\alpha\right)\left(A^2+B^2\right) + B^2\tan^{-1}\left(\frac{A-B\cos(\alpha)}{B\sin(\alpha)}\right) + A^2\tan^{-1}\left(\frac{B-A\cos(\alpha)}{A\sin(\alpha)}\right)\right] \\
& + \frac{\sin^2}{4\pi B}\left[\left(\frac{2}{\sin^2(\alpha)}-1\right)\ln\left(\frac{(1+A^2)(1+B^2)}{1+C}\right) + B^2\ln\left(\frac{B^2(1+C)}{C\,(1+B^2)}\right) + A^2\ln\left(\frac{A^2(1+A^2)^{\cos(2\alpha)}}{C\,(1+C)^{\cos(2\alpha)}}\right)\right] \\
& + \frac{1}{\pi}\tan^{-1}\left(\frac{1}{B}\right) + \frac{A}{\pi B}\tan^{-1}\left(\frac{1}{A}\right) - \frac{\sqrt{C}}{\pi B}\mathrm{atan}^{-1}\left(\frac{1}{\sqrt{C}}\right) \\
& + \frac{\sin(\alpha)\sin(2\alpha)}{2\pi B}AD\left[\tan^{-1}\left(\frac{A\cos(\alpha)}{D}\right) + \tan^{-1}\left(\frac{B-A\cos(\alpha)}{D}\right)\right] \\
& + \frac{\cos(\alpha)}{\pi B}\int_0^B \sqrt{1+\xi^2\sin^2(\alpha)}\left[\tan^{-1}\left(\frac{\xi\cos(\alpha)}{\sqrt{1+\xi^2\sin^2(\alpha)}}\right) + \tan^{-1}\left(\frac{A-\xi\cos(\alpha)}{\sqrt{1+\xi^2\sin^2(\alpha)}}\right)\right] d\xi
\end{aligned}
\tag{C.16}
$$

where $A = h/l$, $B = w/l$, $C = A^2 + B^2 - 2AB\cos(\alpha)$ and $D = \left(1 + A^2\sin^2(\alpha)\right)^{1/2}$. For two parallel rectangles of different size, the view factor is equal to

$$
F_{12} = \frac{1}{(x_2-x_1)(y_2-y_1)}\sum_{l=1}^{2}\sum_{k=1}^{2}\sum_{j=1}^{2}\sum_{i=1}^{2}(-1)^{i+j+k+l}G(x_i,y_j,\eta_k,\xi_l) \tag{C.17a}
$$

$$
\begin{aligned}
G = {} & \frac{1}{2\pi}\left[(y-\eta)\sqrt{(x-\xi)^2+z^2}\,\tan^{-1}\left(\frac{y-\eta}{\sqrt{(x-\xi)^2+z^2}}\right)\right. \\
& \left. + (x-\xi)\sqrt{(y-\eta)^2+z^2}\,\tan^{-1}\left(\frac{x-\xi}{\sqrt{(y-\eta)^2+z^2}}\right) - \frac{z^2}{2}\ln\left[(x-\xi)^2+(y-\eta)^2+z^2\right]\right]
\end{aligned}
\tag{C.17b}
$$

For two rectangles of different size with an angle α between them that do not share a common edge, the view factor is given by

$$
F_{12} = \frac{1}{(x_2-x_1)(y_2-y_1)}\sum_{k=1}^{2}\sum_{j=1}^{2}\sum_{i=1}^{2}(-1)^{i+j+k}G(x_i,y_j,\eta_k) \tag{C.18a}
$$

$$
\begin{aligned}
G = {} & -\frac{(\eta-y)\sin^2\alpha}{2\pi}\int_\xi\left\{\left(\frac{(x-\xi\cos\alpha)\cos\alpha-\xi\sin^2\alpha}{\sqrt{x^2-2x\xi\cos\alpha+\xi^2\sin^2\alpha}}\right)\tan^{-1}\left(\frac{\eta-y}{\sqrt{x^2-2x\xi\cos\alpha+\xi^2}}\right)\right. \\
& + \frac{\cos\alpha}{(\eta-y)\sin^2\alpha}\left[\sqrt{\xi^2\sin^2\alpha+(\eta-y)^2}\tan^{-1}\left(\frac{x-\xi\cos\alpha}{\sqrt{\xi^2\sin^2\alpha+(\eta-y)^2}}\right) - \xi\sin\alpha\tan^{-1}\left(\frac{x-\xi\cos\alpha}{\sin\alpha}\right)\right] \\
& \left. + \frac{\xi}{2\,(\eta-y)}\ln\left(\frac{x^2-2x\xi\cos\alpha+\xi^2+(\eta-y)^2}{x^2-2x\xi\cos\alpha+\xi^2}\right)\right\}d\xi
\end{aligned}
\tag{C.18b}
$$

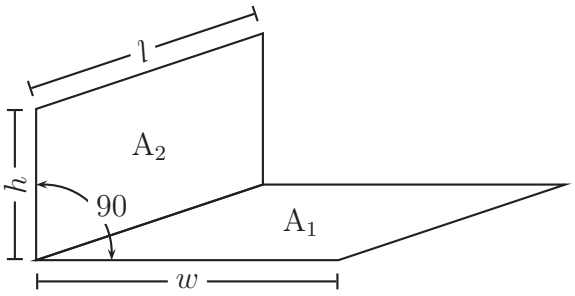

Perpendicular rectangles sharing a common edge
Equation (C.14)

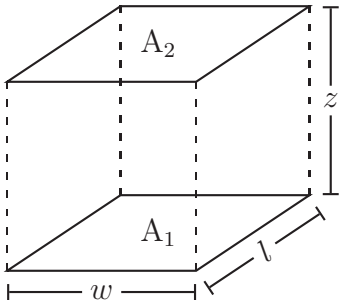

Directly opposed rectangles
Equation (C.15)

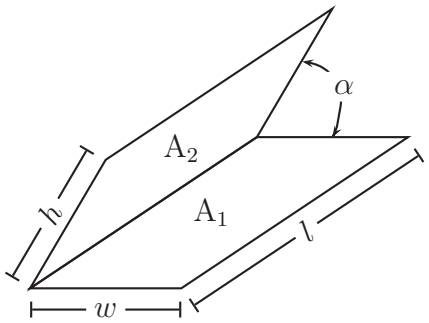

Rectangles sharing a common edge inclined at an angle α
Equation (C.16)

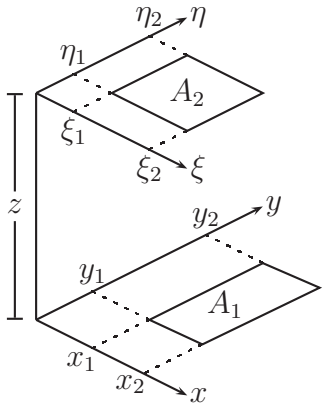

Rectangles in a parallel plane
Equation (C.17)

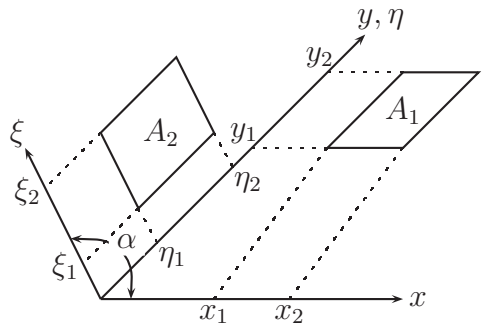

Inclined rectangles with all rectangle edges parallel or perpendicular to the line intersecting the planes
Equation (C.18)

Figure C.1: Geometries of view factors

Appendix D

Thermal networks and energy balance equations for configurations F1, N1, N2, FN1 and FN2

Figure D.1: Configuration F1 - Thermal network and energy balance equation

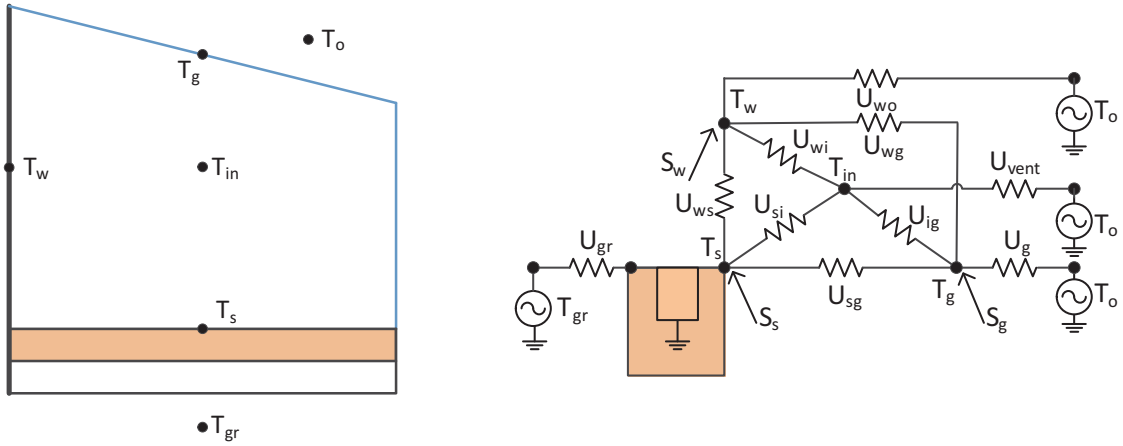

$$\begin{pmatrix} sC_a+u_{si}+u_{ig}+ & -u_{si} & -u_{ig} & -u_{wi} \\ u_{wi}+u_{vent} & & & \\ -u_{si} & Y_{s,s}+u_{si}+ & -u_{sg} & -u_{ws} \\ & u_{sg}+u_{ws} & & \\ -u_{ig} & -u_{sg} & sC_g+u_{ig}+u_{sg}+ & -u_{wg} \\ & & u_{wg}+u_g & \\ -u_{wi} & -u_{ws} & -u_{wg} & sC_w+u_{wi}+U_{ws}+ \\ & & & u_{wg}+u_{wo} \end{pmatrix} \begin{pmatrix} T_{in} \\ T_s \\ T_g \\ T_w \end{pmatrix} = \begin{pmatrix} Q_{eq,vent} \\ S_s + Q_{eq,gr} \\ S_g + Q_{eq,g} \\ S_w + Q_{eq,wo} \end{pmatrix} \quad \text{(D.1)}$$

with $Q_{eq,wo} = u_{wo}T_o$, the other equivalent sources provided in section 7.5.1 and Y_s and Y_t given in equations 7.8 and 7.9.

In equations D.2 and D.3, $Q_{eq,o} = -Y_tT_o$, $Q_{eq,gr} = u_{gr}T_{gr}$, $Q_{eq,w} = u_wT_o$, the other equivalent sources are provided in section 7.5.1 and Y_s and Y_t are given in equations 7.8 and 7.9 where u_{gr} has to be replaced with u_o.

Figure D.2: Configuration N1 - Thermal network and energy balance equation

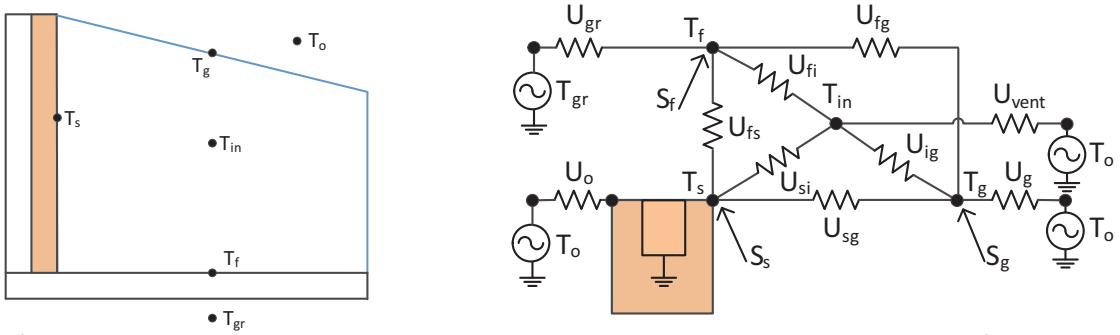

$$\begin{pmatrix} sC_a+u_{si}+u_{ig}+ & & & \\ u_{fi}+u_{vent} & -u_{si} & -u_{ig} & -u_{fi} \\ -u_{si} & Y_{s,s}+u_{si}+u_{sg}+u_{fs} & -u_{sg} & -u_{fs} \\ -u_{ig} & -u_{sg} & sC_g+u_{ig}+u_{sg}+u_{fg}+u_g & -u_{fg} \\ -u_{fi} & -u_{fs} & -u_{fg} & sC_f+u_{fi}+u_{fs}+ \\ & & & u_{fg}+u_{gr} \end{pmatrix}$$

$$\begin{pmatrix} T_{in} \\ T_s \\ T_g \\ T_f \end{pmatrix} = \begin{pmatrix} Q_{eq,vent} \\ S_s + Q_{eq,o} \\ S_g + Q_{eq,g} \\ S_f + Q_{eq,gr} \end{pmatrix} \tag{D.2}$$

Figure D.3: Configuration N2 - Thermal network and energy balance equation

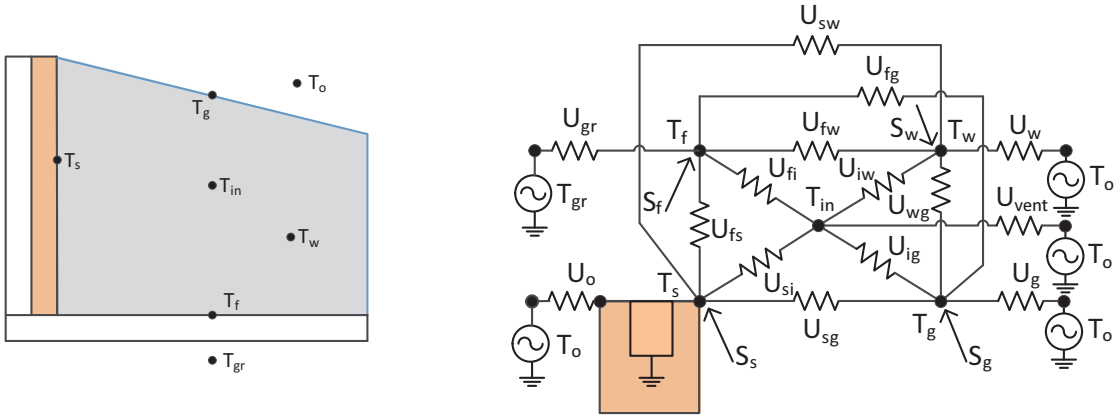

$$\begin{pmatrix} sC_a+u_{si}+u_{ig}+ & & & & \\ u_{fi}+u_{iw}+u_{vent} & -u_{si} & -u_{ig} & -u_{fi} & -u_{iw} \\ -u_{si} & Y_{s,s}+u_{si}+ & -u_{sg} & -u_{fs} & -u_{sw} \\ & u_{sg}+u_{fs}+u_{sw} & & & \\ -u_{ig} & -u_{sg} & sC_g+u_{ig}+u_{sg}+ & -u_{fg} & -u_{wg} \\ & & u_{fg}+u_{wg}+u_g & & \\ -u_{fi} & -u_{fs} & -u_{fg} & sC_f+u_{fi}+u_{fs}+ & -u_{fw} \\ & & & u_{fg}+u_{fw}+u_{gr} & \\ -u_{iw} & -u_{sw} & -u_{wg} & -u_{fw} & sC_w+u_{iw}+u_{sw}+ \\ & & & & u_{wg}+u_{fw}+u_w \end{pmatrix}$$

$$\begin{pmatrix} T_{in} \\ T_s \\ T_g \\ T_f \\ T_w \end{pmatrix} = \begin{pmatrix} Q_{eq,vent} \\ S_s + Q_{eq,o} \\ S_g + Q_{eq,g} \\ S_f + Q_{eq,gr} \\ S_w + Q_{eq,w} \end{pmatrix} \tag{D.3}$$

Figure D.4: Configuration FN1 - Thermal network and energy balance equation

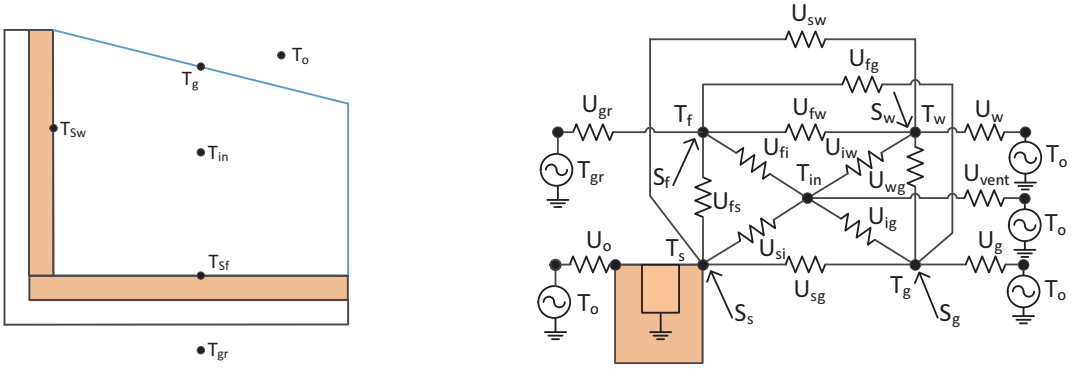

$$\begin{pmatrix} sC_a+u_{Swi}+u_{ig} \\ +u_{Sfi}+u_{vent} & -u_{si} & -u_{ig} & -u_{Sfi} \\ -u_{Swi} & Y_{s,Sw}+u_{Swi}+ \\ & u_{Swg}+u_{SfSw} & -u_{Swg} & -u_{SfSw} \\ -u_{ig} & -u_{Swg} & sC_g+u_{ig}+u_{Swg}+ \\ & & u_{Sfg}+u_g & -u_{Sfg} \\ -u_{Sfi} & -u_{SfSw} & -u_{Sfg} & Y_{s,Sf}+u_{Sfi}+ \\ & & & u_{SfSw}+u_{Sfg} \end{pmatrix}$$

$$\begin{pmatrix} T_{in} \\ T_{Sw} \\ T_g \\ T_{Sf} \end{pmatrix} = \begin{pmatrix} Q_{eq,vent} \\ S_{Sw}+Q_{eq,o} \\ S_g+Q_{eq,g} \\ S_{Sf}+Q_{eq,gr} \end{pmatrix} \tag{D.4}$$

Figure D.5: Configuration FN2 - Thermal network and energy balance equation

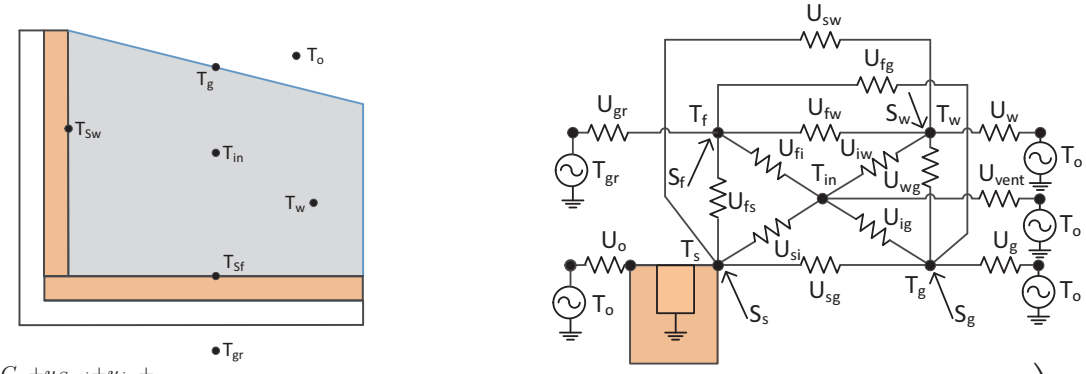

$$\begin{pmatrix} sC_a+u_{Swi}+u_{ig}+ \\ u_{Sfi}+u_{iw}+u_{vent} & -u_{Swi} & -u_{ig} & -u_{Sfi} & -u_{iw} \\ -u_{Swi} & Y_{s,Sw}+u_{Swi}+ \\ & u_{Swg}+u_{SfSw}+u_{Sww} & -u_{Swg} & -u_{SfSw} & -u_{Sww} \\ -u_{ig} & -u_{Swg} & sC_g+u_{ig}+u_{Swg}+ \\ & & u_{Sfg}+u_{wg}+u_g & -u_{Sfg} & -u_{wg} \\ -u_{Sfi} & -u_{SfSw} & -u_{Sfg} & Y_{s,Sf}+u_{Sfi}+ \\ & & & u_{SfSw}+u_{Sfg}+u_{Sfw} & -u_{Sfw} \\ -u_{iw} & -u_{Sww} & -u_{wg} & -u_{Sfw} & sC_w+u_{iw}+u_{Sww}+ \\ & & & & u_{wg}+U_{Sfw}+u_w \end{pmatrix}$$

$$\begin{pmatrix} T_{in} \\ T_{Sw} \\ T_g \\ T_{Sf} \\ T_w \end{pmatrix} = \begin{pmatrix} Q_{eq,vent} \\ S_{Sw}+Q_{eq,o} \\ S_g+Q_{eq,g} \\ S_{Sf}+Q_{eq,gr} \\ S_w+Q_{eq,w} \end{pmatrix} \tag{D.5}$$

with $Q_{eq,o} = -Y_{t,Sw}T_o$, $Q_{eq,gr} = -Y_{t,Sf}T_{gr}$, $Q_{eq,w} = u_w T_o$, the other equivalent sources are provided in section 7.5.1 and self and transfer admittances calculated with:

$$Y_{s,Sw} = \frac{A_{Sw}\left(\frac{u_o}{A_{Sw}} + k_{Sw}\gamma_{Sw}\tanh(\gamma_{Sw}L_{Sw})\right)}{\frac{u_o}{k_{Sw}\gamma_{Sw}A_{Sw}}\tanh(\gamma_{Sw}L_{Sw}) + 1}$$

$$Y_{s,Sf} = \frac{A_{Sf}\left(\frac{u_{gr}}{A_{Sf}} + k_{Sf}\gamma_{Sf}\tanh(\gamma_{Sf}L_{Sf})\right)}{\frac{u_{gr}}{k_{Sf}\gamma_{Sf}A_{Sf}}\tanh(\gamma_{Sf}L_{Sf}) + 1}$$

$$Y_{t,Sw} = \frac{-A_{Sw}}{\frac{A_{Sw}}{u_o}\cosh(\gamma_{Sw}L_{Sw}) + \frac{1}{k_{Sw}\gamma_{Sw}}\sinh(\gamma_{Sw}L_{Sw})}$$

$$Y_{t,Sf} = \frac{-A_{Sf}}{\frac{A_{Sf}}{u_{gr}}\cosh(\gamma_{Sf}L_{Sf}) + \frac{1}{k_{Sf}\gamma_{Sf}}\sinh(\gamma_{Sf}L_{Sf})}$$

Appendix E

TES design - frequency response modelling

E.1 Impact of varying glazing type

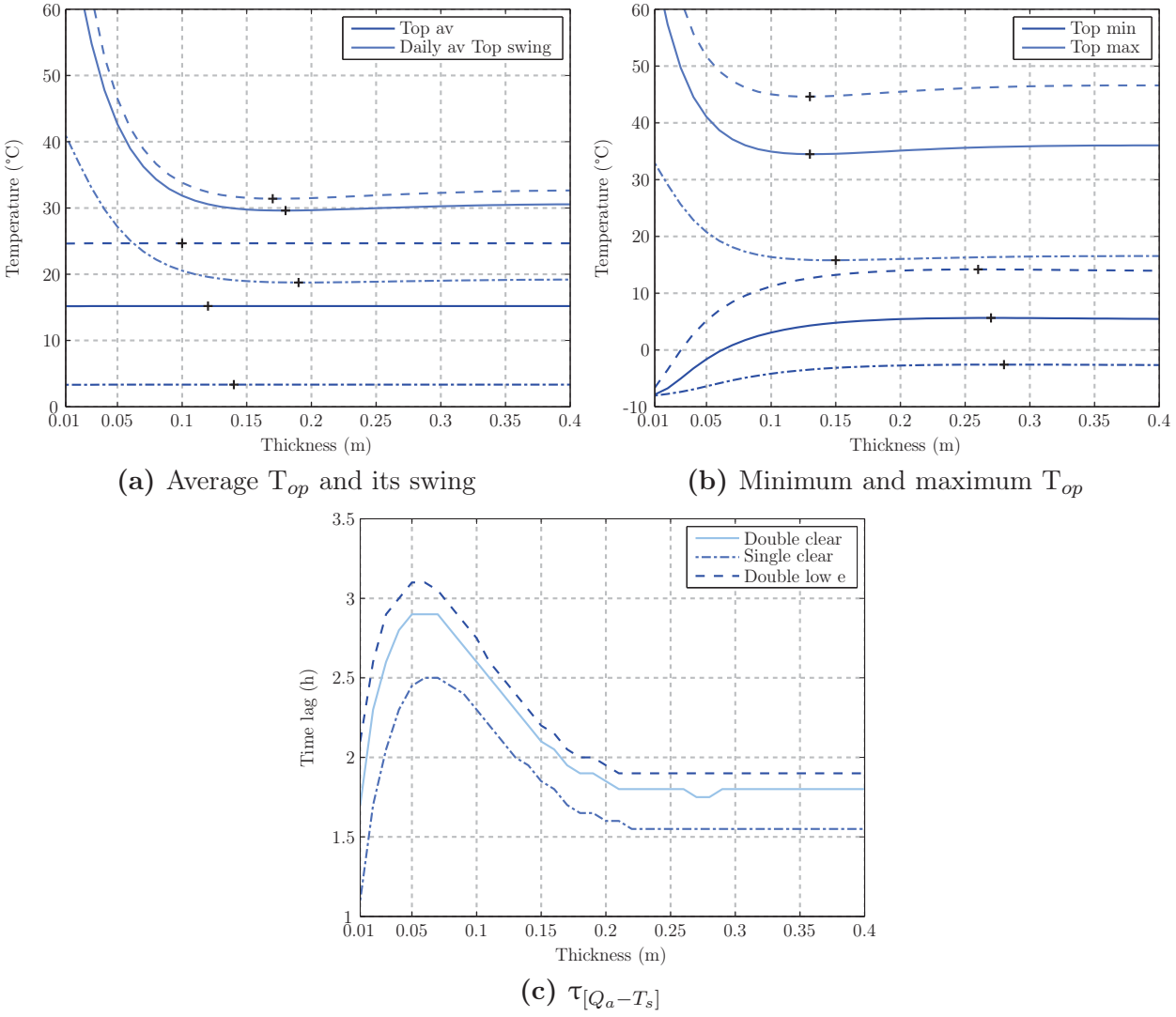

(a) Average T_{op} and its swing

(b) Minimum and maximum T_{op}

(c) $\tau_{[Q_a - T_s]}$

Figure E.1: Impact of glazing type; - - - single clear, —— double clear, - - - double low-e

As seen from figure E.1a and E.1b, the glazing type affects significantly the average operative temperature and its peaks, but not very much their optimal thickness. As depicted on figure E.1c, the peak time lag can be moderately increased by selecting a better insulated glazing: the time lag can be increased from 2.5 h to 3.1 h by changing the glazing from single clear to double with low emissivity.

E.2 Impact of enhanced thermal coupling

Ventilation in greenhouses is beneficial for minimizing temperature, moisture and CO_2 gradients. A total air flow of 0.01 $m^3/s\text{-}m^2$ of floor area is recommended (American Society of Agricultural Engineers, 2003). Using the correlation from Fisher and Pedersen (1997) for the geometry under consideration yields convective coefficients of 5.2 W/m^2-K for the floor and 11.4 W/m^2-K for the wall. The same coefficient as the wall is adopted for the glazing. The convective coefficients under natural convection were between 3.2-3.3 W/m^2-K for the floor, 2.3-2.4 for the wall and 7.3-7.6 W/m^2-K for the glazing, depending on the configuration.

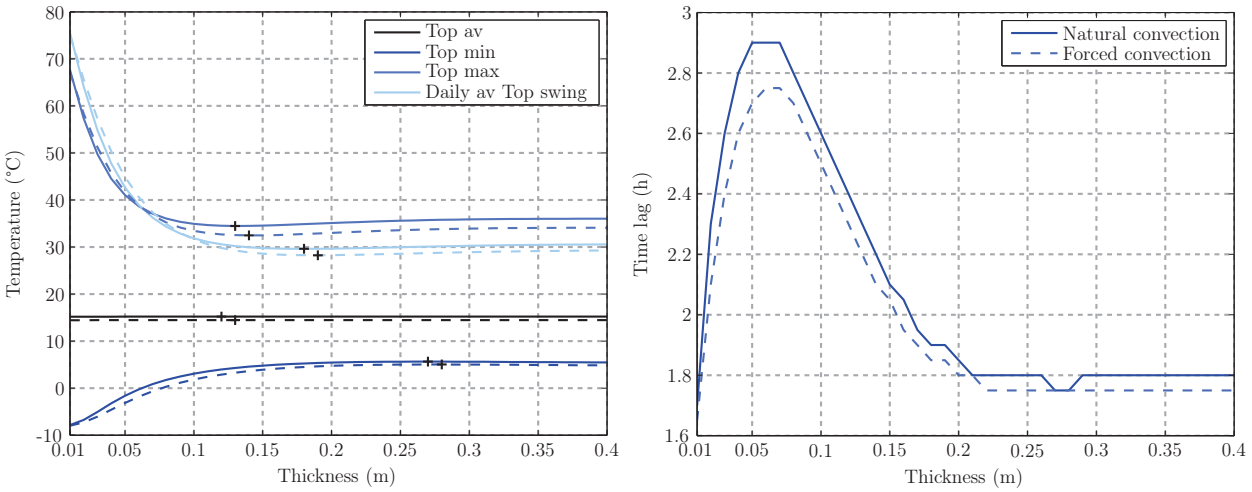

(a) T_{op} peaks, average and its swing **(b)** $\tau_{[Q_a - T_s]}$

Figure E.2: Impact of enhanced thermal coupling; — natural convection, - - - forced convection

Enhancing thermal coupling with increased ventilation yields little changes of optimum thicknesses for the main performance variables (see figures E.2a-E.2b). Increasing convective heat exchanges slightly reduces the temperature swing and maximum temperature, but has little impact on the minimum and average temperatures. It enables the effective use of a slightly thicker thermal mass: the optimal thickness is 0.01-0.02 m thicker for all configurations, with a greater impact when the mass is located on the wall (results not shown). However, introducing forced ventilation also reduces slightly $\tau_{[Q_a - T_s]}$.

Appendix F

TES design - monthly simulation results

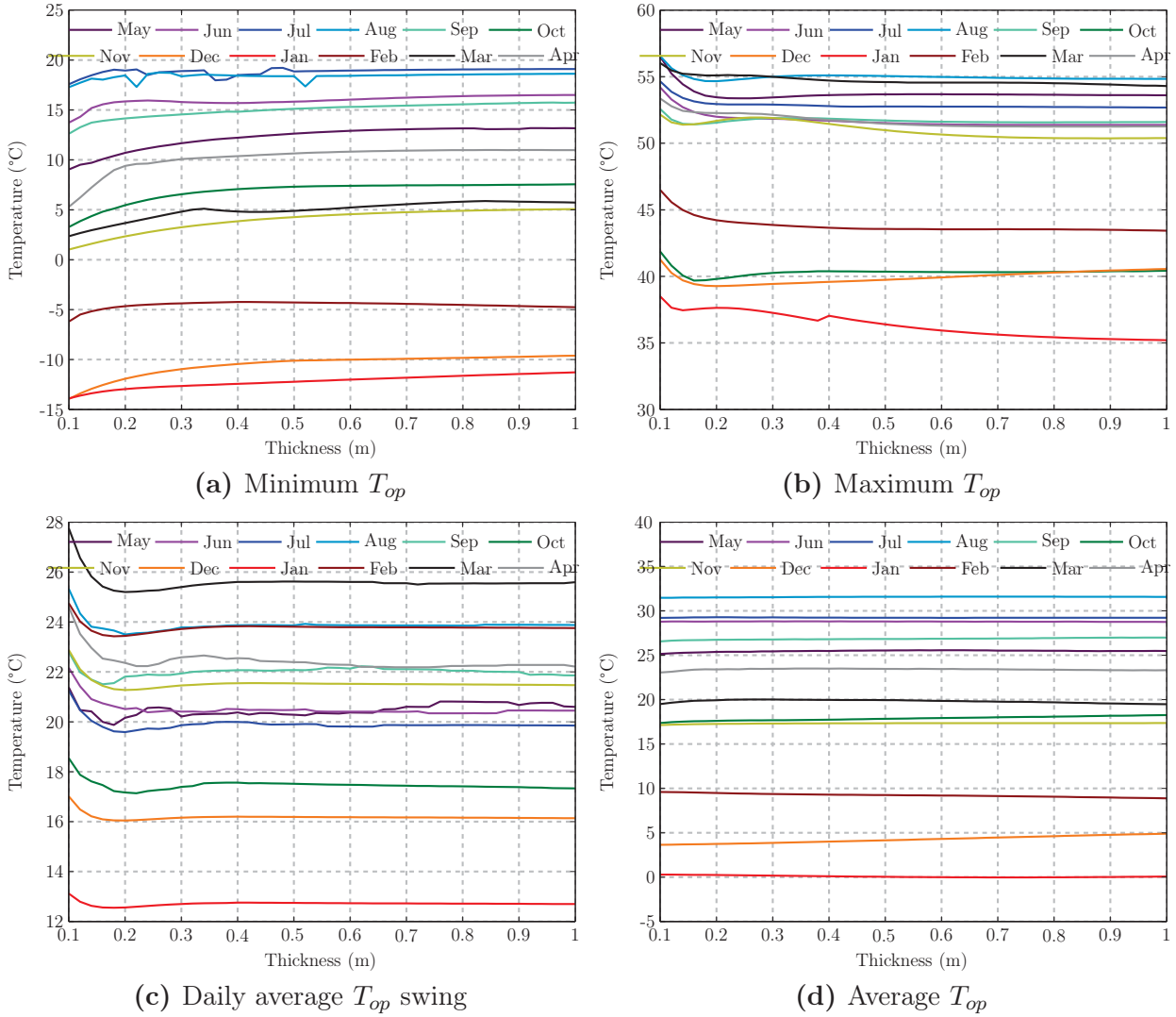

(a) Minimum T_{op}

(b) Maximum T_{op}

(c) Daily average T_{op} swing

(d) Average T_{op}

Figure F.1: Montreal, year 2009-2010 – configuration N1 – monthly minimum, maximum and average operative temperature and its daily average swing

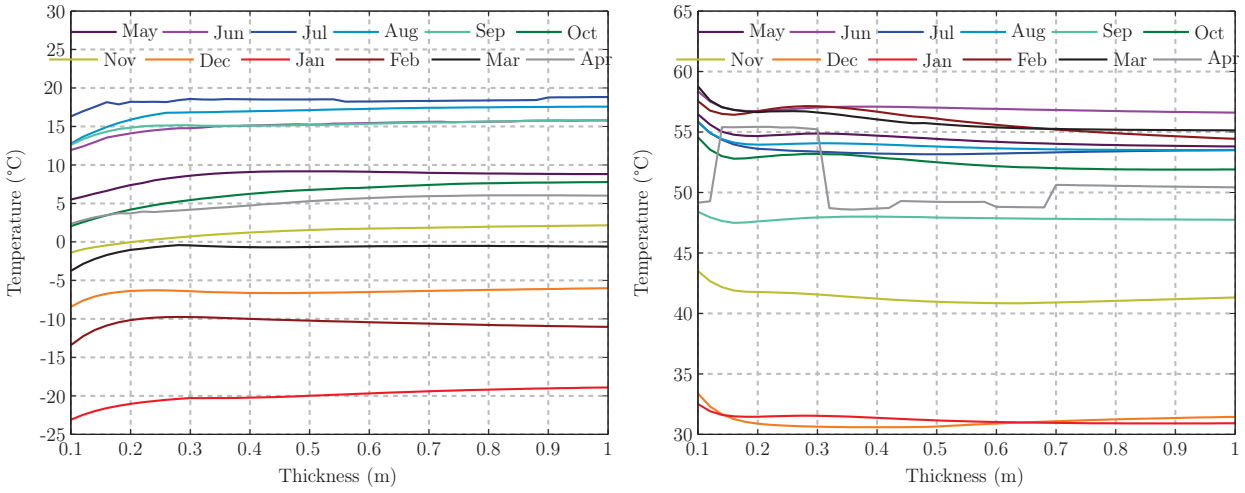

(a) Minimum T_{op}

(b) Maximum T_{op}

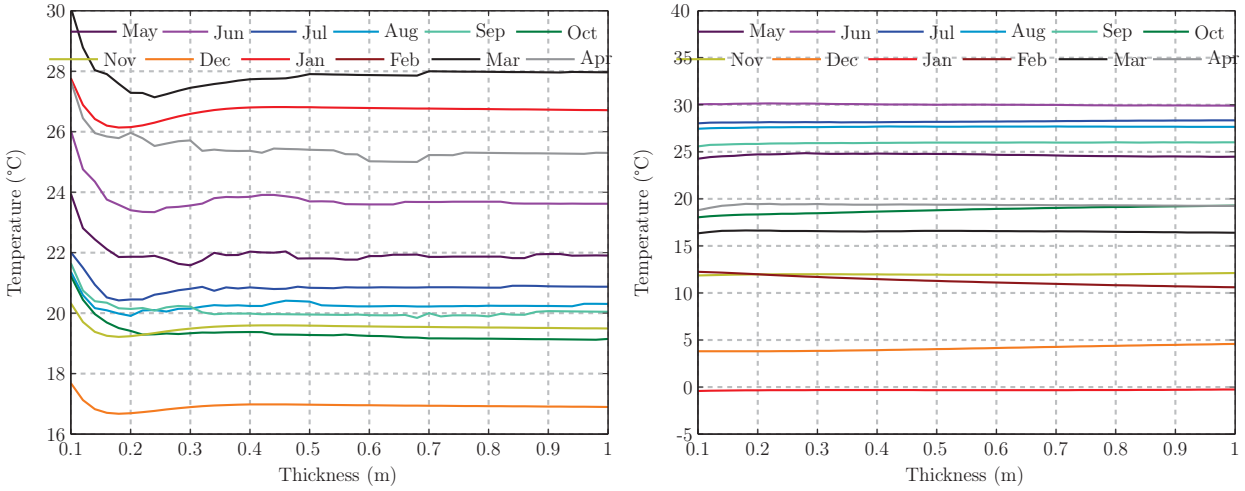

(c) Daily average T_{op} swing

(d) Average T_{op}

Figure F.2: Quebec, year 2003-2004 – configuration N1 – monthly minimum, maximum and average operative temperature and its daily average swing

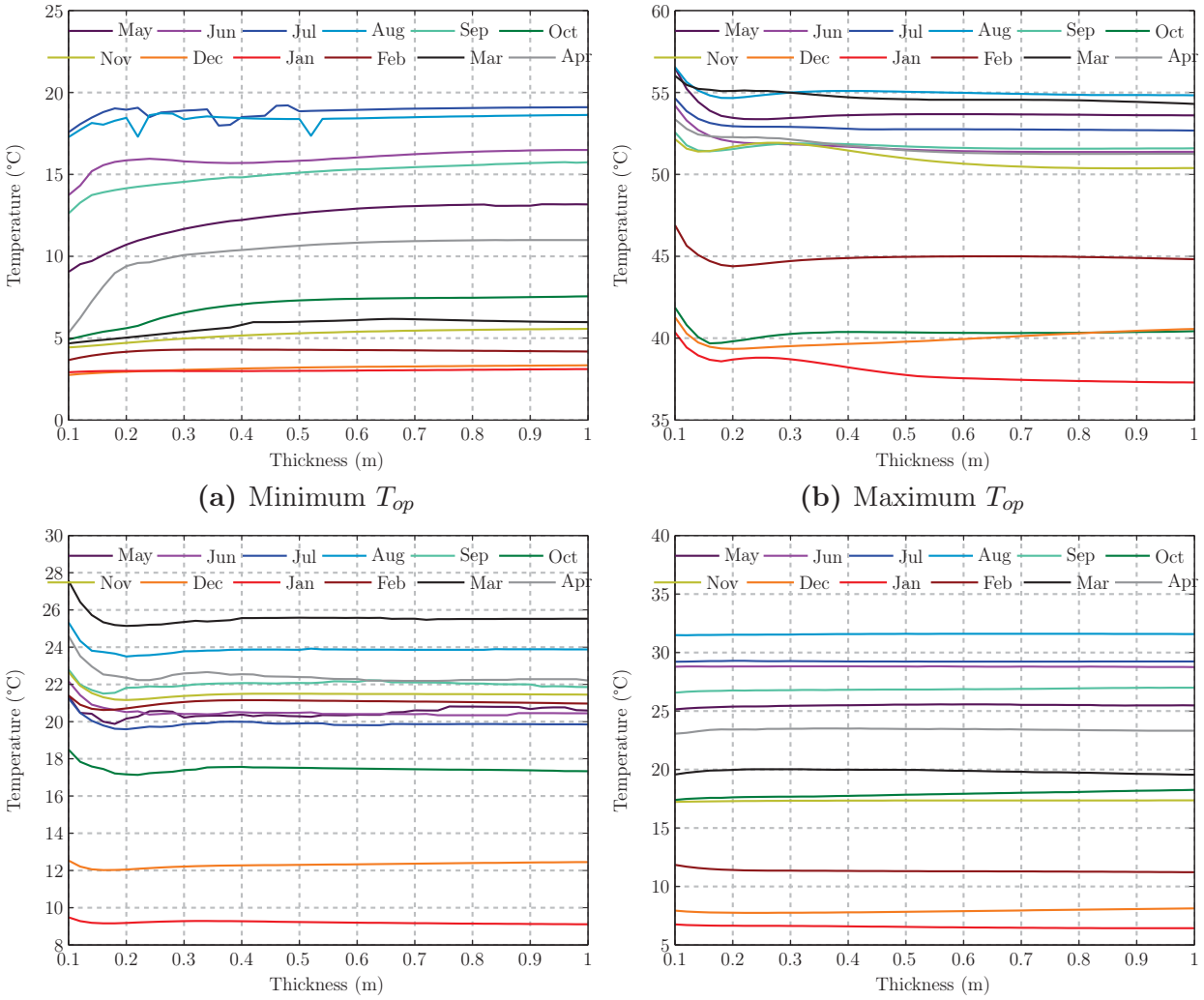

(a) Minimum T_{op}

(b) Maximum T_{op}

(c) Daily average T_{op} swing

(d) Average T_{op}

Figure F.3: Montreal, year 2009-2010 – configuration N1,heated ($T_{min} = 5$°C) – monthly minimum, maximum and average operative temperature and its daily average swing

Appendix G

Average absorbed beam radiation fraction for a latitude of 55°

Table G.1: Average absorbed beam radiation fraction at the winter solstice — $\lambda = 55°$

Floor aspect ratio	Indoor surface	Glazed surface: south wall	south roof	east	west	north	Glazed surface: south wall	south roof	east	west	north
		Longest side facing south					Longest side facing 30°west of south				
roof angle of 35°, width=north wall height											
4:1	floor	0.48	0.00	0.11	0.11	0.00	0.55	0.00	0.16	0.05	0.00
	north wall	0.43	0.95	0.89	0.89	0.00	0.31	0.89	0.84	0.95	0.00
	east and west walls	0.09	0.05	0.00	0.00	0.00	0.14	0.11	0.00	0.00	0.00
	south wall and roof	0.00	0.00	0.00	0.00	0.00	0.00	0.00	0.00	0.00	0.00
2:1	floor	0.46	0.00	0.11	0.11	0.00	0.48	0.00	0.16	0.05	0.00
	north wall	0.37	0.89	0.89	0.89	0.00	0.26	0.79	0.83	0.95	0.00
	east and west walls	0.17	0.11	0.00	0.00	0.00	0.26	0.21	0.01	0.00	0.00
	south wall and roof	0.00	0.00	0.00	0.00	0.00	0.00	0.00	0.00	0.00	0.00
1:1	floor	0.42	0.00	0.11	0.11	0.00	0.38	0.00	0.15	0.05	0.00
	north wall	0.24	0.78	0.89	0.89	0.00	0.22	0.65	0.76	0.95	0.00
	east and west walls	0.34	0.22	0.00	0.00	0.00	0.40	0.35	0.09	0.00	0.00
	south wall and roof	0.00	0.00	0.00	0.00	0.00	0.00	0.00	0.00	0.00	0.00
1:2	floor	0.34	0.00	0.11	0.11	0.00	0.26	0.00	0.13	0.05	0.00
	north wall	0.11	0.60	0.82	0.82	0.00	0.16	0.49	0.64	0.95	0.00
	east and west walls	0.55	0.40	0.06	0.06	0.00	0.58	0.51	0.23	0.00	0.00
	south wall and roof	0.00	0.00	0.00	0.00	0.00	0.00	0.00	0.00	0.00	0.00
roof angle of 15°, width=2×north wall height											
4:1	floor	0.63	0.00	0.20	0.20	0.00	0.69	0.01	0.29	0.10	0.00
	north wall	0.29	0.95	0.80	0.80	0.00	0.19	0.88	0.71	0.90	0.00
	east and west walls	0.08	0.05	0.00	0.00	0.00	0.12	0.11	0.00	0.00	0.00
	south wall and roof	0.00	0.00	0.00	0.00	0.00	0.00	0.00	0.00	0.00	0.00
2:1	floor	0.60	0.00	0.20	0.20	0.00	0.61	0.01	0.28	0.10	0.00
	north wall	0.24	0.89	0.80	0.80	0.00	0.17	0.78	0.70	0.90	0.00
	east and west walls	0.16	0.11	0.00	0.00	0.00	0.22	0.21	0.01	0.00	0.00
	south wall and roof	0.00	0.00	0.00	0.00	0.00	0.00	0.00	0.00	0.00	0.00
1:1	floor	0.54	0.00	0.20	0.20	0.00	0.48	0.00	0.27	0.10	0.00
	north wall	0.14	0.78	0.80	0.80	0.00	0.16	0.65	0.65	0.90	0.00
	east and west walls	0.32	0.22	0.00	0.00	0.00	0.36	0.35	0.08	0.00	0.00
	south wall and roof	0.00	0.00	0.00	0.00	0.00	0.00	0.00	0.00	0.00	0.00
1:2	floor	0.44	0.00	0.20	0.20	0.00	0.34	0.00	0.22	0.10	0.00
	north wall	0.05	0.60	0.73	0.73	0.00	0.13	0.49	0.56	0.90	0.00
	east and west walls	0.51	0.40	0.07	0.07	0.00	0.53	0.51	0.22	0.00	0.00
	south wall and roof	0.00	0.00	0.00	0.00	0.00	0.00	0.00	0.00	0.00	0.00